RATES OF COMBUSTION IN FLOWING STREAMS OF GASES

Thesis
submitted for the
Degree of Doctor of Philosophy
in the Faculty of Science,
University of London

By

Norman Harold Pratt, B.Sc.

lately of the Department of Chemical Engineering and
Applied Chemistry,
Imperial College of Science and Technology,
London, S.W.7.

Present Address
National Gas Turbine Establishment,
Pyestock, Farnborough,
Hants.

June, 1962

Acknowledgements

The experimental work described in this thesis was carried out in the laboratory of the late Professor Sir Alfred Egerton, F.R.S. in the Department of Chemical Engineering, Imperial College, between July, 1957 and September, 1960.

The author is greatly indebted to Sir Alfred for the initial direction of the research, for his quiet encouragement and many kindnesses. To Dr. J. H. Burgoyne the author is grateful for his undertaking to continue the supervision after Sir Alfred's death.

To the many colleagues, both at Imperial College and at the National Gas Turbine Establishment, who have contributed in discussion and in more practical ways, the author expresses his thanks.

The author is indebted to the Department of Scientific and Industrial Research for the provision of a Research Assistantship and to the National Gas Turbine Establishment for help with the reproduction of this thesis.

Finally, my lasting thanks to my wife for her tolerance and patience while this thesis was being written.

Abstract

Experimental data on local temperature, composition and gas stream velocity have been obtained from the reaction zone of very lean (0.00015 to 0.0012 mole fraction) methane-air mixtures in a cylindrical silica flow-reactor at atmospheric pressure.

Methane and air were separately preheated to the temperature range 1130 to 1190°K and then mixed. Both the mixing process and the gas sampling techniques have been examined in considerable detail. It was found that satisfactory mixing could only be achieved with the accompaniment of some turbulence. Gas sampling and probing techniques were developed so that interference with the reaction was minimised, and the sampled gas composition was frozen. The results were analysed in terms of the conservation equations for heat and species which showed that radial transport processes were an important influence in controlling the reaction. Attempts to apply radial transport correction terms were only qualitatively successful; this was partly attributed to some residual turbulence in the boundary layer.

An empirical correction term was then applied and the heat release rates examined in terms of flow rate, methane concentration and temperature. An overall activation energy of 58 kcal was obtained. The similarity of the heat release rate profiles obtained to those obtained in flames was noted.

The uncorrected specie profiles (methane, carbon monoxide, carbon dioxide) were then examined kinetically. In the induction period the results indicated a self-inhibiting mechanism second-order in methane. Later in the reaction, and at very low methane concentrations, a straight forward first-order dependence was obtained. On the basis of the assumption that carbon monoxide was oxidised via $CO + OH \rightarrow CO_2 + H$, a profile of the hydroxyl radical concentration was obtained. A rate constant deduced for the reaction $CH_4 + OH \rightarrow$ products (1.0×10^{12} at $1200^{\circ}K$) was compared with values quoted in the literature; the significant agreement suggested that the hydroxyl radical mechanism accounted for most of the methane oxidation. Examination of the low concentration intermediates (hydrogen, formaldehyde, hydrogen peroxide) indicated that the reaction tube surface had negligible chemical effect on the reaction.

The results are discussed in relation to recent relevant studies of flames, in shock tubes, in vessels, and in other high temperature flow systems.

Contents

Chapter			Page
1		Introduction	12
	1.1	Field of interest	12
	1.2	General background	14
	1.3	Immediate background to the present work	16
	1.4	High temperature methane oxidation	20
		1.4.1 The main features of the methane oxidation (flameless combustion) reaction	20
		1.4.2 Mechanism of the flameless oxidation	22
		1.4.3 Flame mechanism of methane oxidation	29
	1.5	Aims of the present work	30
2		The Apparatus (1) General Description and Procedure	33
	2.1	Introduction	33
	2.2	The gas supply and metering system	33
	2.3	The reaction system	35
	2.4	The furnace, temperature control and measurement	37
	2.5	Probes and samplers	40
	2.6	Analysis of sampled gases	42
	2.7	Method of experiment	44
Appendix 2A		Removal of oxygen from methane	46
3		The Apparatus (2) Mixing and Sampling	50
	3.1	Introduction	50
		Part I - Mixing	50
	3.2	Some theoretical considerations	50
	3.3	Practical inlets constructed	56
		Part II - Sampling	62
	3.4	Guiding principles	62
	3.5	The effects of probing	65
		3.5.1 The effect of the probe on the reaction	65
		3.5.2 The interpretation of the sample taken	68

Contents (cont'd)

Chapter			Page
3 (cont'd)			
		3.5.3 Interpretation of the temperature measured	69
		3.5.4 Interpretation of the gas stream pitot and static pressures	70
	3.6	Practical development	72
		3.6.1 The water-cooled sampler	72
		3.6.2 Silica sampler	73
		3.6.3 Pitot and static probes	73
		3.6.4 Temperature probes	74
		3.6.5 Composite probes	75
Appendix	3A	Thermal conductivities and diffusion coefficients	78
	3B	Annular flow in the sampling probe	82
	3C	A 'sonic' probe	84
4		Preliminary observations and conclusions	88
	4.1	Exploratory experiments	88
		4.1.1 The intention of the exploratory experiments	88
		4.1.2 Typical profiles	88
		4.1.3 Attempts to vary and stabilise heat release rates	89
	4.2	Phenomenological account of incidental observations	90
		4.2.1 'Ignition'	90
		4.2.2 'Blow-off' and 'flashback'	91
		4.2.3 Effects of asymmetric profiles	91
	4.3	Effectiveness and comparison of water-cooled and silica samplers	92
	4.4	Stability of reaction zone conditions	93
		4.4.1 Effect of heat input and flow fluctuation	94
		4.4.2 Effect of sample withdrawal on the reacting gas	95
		4.4.3 Stability achieved in practice	96
	4.5	Qualitative effects of certain additives	97

Contents (cont'd)

Chapter			Page
4 (cont'd)			
		4.5.1 Acetone in the methane supply	97
		4.5.2 Oxygen in the methane supply	98
		4.5.3 Methane in the air supply	99
	4.6	Qualitative tests for intermediates	99
	4.7	Preliminary conclusions	101
		4.7.1 Experimental improvements required	101
		4.7.2 Limitations of the apparatus	102
		4.7.3 Additional remarks	103
5		Experimental results and data reduction	108
	5.1	Introduction	108
	5.2	Experimental results	110
		5.2.1 Range of experimental conditions	110
		5.2.2 Composition data	110
		5.2.3 Gas velocity data	112
		5.2.4 Temperature data	113
		5.2.5 Tables	114
	5.3	Analysis of the results	115
		5.3.1 Nature of the analysis	115
		5.3.2 Steady-state conservation equations	116
		5.3.3 Initial data reduction	119
	5.4	Adequacy of the calculation and experimentation	122
		5.4.1 Adequacy of the calculation of T_c	122
		5.4.2 Adequacy of the sampling techniques	124
6		The fluid mechanics of the reaction zone	156
	6.1	Attempts to correlate $(T_c - T_e)$ with reaction zone conditions	156
	6.2	Qualitative fluid mechanical description of the flow in the reaction zone	157

Contents (cont'd)

Chapter			Page
6 (cont'd)			
		6.2.1 Flow effects attributable to the inlet geometry	158
		6.2.2 The nature of the boundary layer flow	159
		6.2.3 The nature of the core flow	160
		6.2.4 Conclusions concerning transport rates	162
	6.3	Analysis of the boundary layer transport rates	164
	6.4	Significance of radial transport fluxes computed in the boundary layer	167
7		Factors affecting the rate of heat release	170
	7.1	Typical data	170
	7.2	Calculation of the heat release rate q'''	171
	7.3	The volumetric heat release rate profiles	174
		7.3.1 Typical heat release rate profiles	174
		7.3.2 The effect of flow rate on the maximum heat release rate	174
		7.3.3 The effect of methane concentration on the maximum heat release rate	175
	7.4	An activation energy derived from the maximum heat release rate	176
8		Kinetics and Mechanism	178
	8.1	Treatment of the composition data	178
	8.2	Reaction order	179
		8.2.1 Effective order with respect to methane	179
		8.2.2 Effective order with respect to carbon monoxide and oxygen	180
	8.3	Estimation of hydroxyl radical concentration	181
	8.4	The reaction between methane and hydroxyl radicals	184
	8.5	The intermediates H_2O_2, H_2 and HCHO	186
		8.5.1 Hydrogen peroxide	187
		8.5.2 Hydrogen	189

Contents (cont'd)

Chapter			Page
8 (cont'd)			
	8.6	The effect of variation of temperature, flow rate and methane concentration on the maximum formaldehyde concentration	189
		8.6.1 The effect of surface and temperature on formaldehyde	189
		8.6.2 The effect of methane concentration on the formaldehyde maximum	190
9		Discussion and Conclusions	195
	9.1	Main features and comparisons	195
	9.2	The induction period	199
	9.3	The main propagating sequence	201
	9.4	The carbon monoxide oxidation phase	205
	9.5	Suggestions for further work	209
	9.6	Summary and conclusions	212

List of tables

Table No.	Title	
2.1	Details of furnace and associated components	48
3C	'Sonic' probe analysis	86
3.1	Typical values of a, n, z, A × n	87
4.1	Main heat input for various positions of the water-cooled sampler	105
4.2	Set 'A': Continuous fixed-location sampling (20 cm) from reaction zone with no interim correction to heat input and flows	106
	Set 'B': Variation in conditions during a typical run, as indicated at 20 cm sampling position, interim corrections applied	106
4.3	Range of conditions for which the apparatus was applicable	107
5.1(a)	Summary of heat release runs	127
5.1(b)	Notation of Tables 5.2 to 5.37	128
5.2 to 5.17	Details of heat release runs	129 to 144

List of tables (cont'd)

Table No.	Title	Page
5.18	Summary of runs concerned with intermediates	145
5.19 to 5.37	Details of runs concerned with intermediates	146 to 155
8.1	Calculated values of hydroxyl radical concentration	192
8.2	Rate constant k_4 for $CH_4 + OH \rightarrow$ products	193
8.3	Comparison of rate constants $CH_4 + OH \rightarrow$ products	194
9.1	Comparison of maximum formaldehyde concentration with theory	214
9.2	Comparison of 'overall' rates of carbon monoxide oxidation	215

List of illustrations

Fig No.	Title
2.1	Gas supply and inlet arrangement
2.2	Gas supply system
2.3	Control and analysis instrumentation
2.4	Sampled Gas analysis system
2.5	The inlet (Model 'D')
2.6	Furnace heating arrangement
2.7	Preheat 'A' control circuit
2.8	Thyratron operation (schematic)
2.9	Probes
2.10	Extraction system (formaldehyde and hydrogen peroxide)
2.11	Probe mounting and part of analysis system
2.12	CO_2 in methane after catalytic removal of O_2
3.1	Mixing efficiency of inlets
3.2	Inlet end-plate design
3.3	Methane supply and control valves
3.4	First design of probes
3.5	Some characteristics of annular flow
4.1	Reproducibility of conditions (temperature profiles)
4.2	Temperature profiles (mean of Fig 4.1(a)-(d))
4.3	Velocity profiles
4.4	Composition profiles - (a) methane, (b) carbone monoxide
4.5	Development of velocity and temperature profiles (initially symmetrical)
4.6	Development of velocity profiles (initially asymmetrical)

List of illustrations (cont'd)

Fig No.	Title
4.7	Quenching efficiency of probes (1) circular internal cross-section
4.8	Quenching efficiency of probes (2) annular internal cross-section
4.9	Locus of maximum heat release rate
5.1	Typical pitot pressure profiles
5.2	Comparison of calculated (T_c) and measured (T_e) gas temperature (Run 12)
5.3	Comparison of calculated (T_c) and measured (T_e) gas temperature (Run 25)
6.1	Comparison of measured and calculated temperature (all data)
6.2	Plot of log $(T_c - T_e)/(T_{e,f} - T_{e,o})$ versus log X_{CH_4}, log (flow rate), log $(T_c - T_e)$, log T_{mean}
6.3	Rate of temperature divergence $[\Delta(T_c - T_e)$ per cm z$]$
6.4	Comparison of temperature profiles along axis and near wall
6.5	Effect of correcting temperature profiles for radial transport
6.6	Methane mass fraction change at axis due to radial methane transport
6.7	Heat change at axis due to radial heat transport
7.1	Profiles of velocity, temperature and composition Run 10
7.2	Profiles of velocity, temperature and composition Run 21
7.3	Profiles of velocity, temperature and composition Run 25
7.4	Profiles of velocity, temperature and composition Run 12
7.5	Profiles of velocity, temperature and composition Run 20
7.6	Typical heat release rate profiles
7.7	Maximum heat release rate versus flow rate
7.8	Maximum heat release rate versus initial methane mole fraction
7.9	Activation energy from maximum heat release rate
8.1	Reaction order with respect to methane
8.2	Typical hydroxyl radical profiles (Run 10)
8.3	Intermediates and products versus reactedness
8.4	Radial distribution of CH_4, CO, CO_2, HCHO, and H_2O_2
8.5	Maximum formaldehyde concentration versus initial methane concentration

CHAPTER 1

Introduction

1.1 Field of interest

Despite the avalanche of interest in combustion which has occurred in the last decade, relatively little effort has been made to elucidate the detailed kinetics and mechanism of high temperature homogeneous gaseous oxidations. This lack of attention cannot be attributed to the insignificance or irrelevance of such studies since they have very evident application in many branches of applied science. Fast chain reactions are the concern of the combustion chamber designer, be that chamber for an aircraft or automobile engine, or for an industrial furnace, and increasingly the concern in recent years of the process engineer anxious to obtain the intermediates or products of high temperature oxidation reactions. Whilst it cannot be claimed that the temperature range used in the present investigation would interest the rocket or hypersonic ramjet engineer, there can be no doubt that, for instance, the rate and mechanism of carbon monoxide oxidation at high temperature will be of interest in the high speed flight field because of the general lack of kinetic data at high temperatures.

However, the immediate concern of the present contribution is in those reactions occurring in the temperature range 1100 to 1300°K. This temperature range is of particular interest in studies of the mechanism of flame propagation and of ignition because it covers the temperature range of near-limit flames and is a temperature range where the lack of data is particularly evident.

In the recent literature on flame structure studies (see for instance Reference 1) it has been both implied and explicitly stated that "flame structure cannot be accounted for by an overall mechanism based on reactant concentration", and "it is still not possible to say anything definite about detailed kinetics (in flames)". Levy and Weinberg[1] have also shown that the effective activation energy varies with position along the path through the flame front. Their approach, however, does not allow any detailed analysis, species-wise, of the intermediate reactions.

Friedman and his group[2,3], Fristrom and co-workers[4 to 8], Fenimore and Jones[9 to 12] and Foner and Hudson[13] in America have attempted to bridge the gap by direct sampling from a flame. This approach involves a number of assumptions which are discussed further in Chapter 3. Schlieren and spectroscopic studies[1,14,15] avoid the problems of direct sampling, but involve more deductive interpretation. Both the optical approach and the sampling approach utilise premixed systems. Due to the preheating of the mixture ahead of the flame front the kinetics will inevitably involve some proportion of the lower temperature mechanisms, which will be an additional complication in any detailed analysis of flame intermediates. The lower temperature (300 to 500°C) mechanisms of the simplest fuel/oxidant systems are currently relatively well understood from classical kinetic studies in vessels. In order to arrive at a better understanding of flame phenomena, it is evidently necessary to study the high temperature mechanisms on their own.

Ideally flame-type reactions can only be studied in flames. In practice any attempt to elucidate detailed kinetics 'in situ' is made extremely arduous by a number of factors. Among these are the large concentration, temperature and velocity gradients in the vicinity of the flame front, together with the interdependent problems associated with mass and energy transfer and also the possible attendant energy and chemical non-equilibrium.

An additional drawback is the overall interdependence of the variables. Although this has been to a certain extent circumvented by the use of cooled porous matrices as flame holders[16] or by the preheating of the reactants, the range over which the various parameters can be independently varied is strictly limited.

The half-lives of the reactions of interest at these elevated temperatures (in the microsecond to millisecond range) make the use of flow or intermittent systems essential. Intermittent methods, as exemplified by the shock tube are attractive in many ways. However it was the set purpose of the present researches to investigate phenomena in a steady-state flow system. Since the results from the two approaches should be complementary some recently reported shock tube work on methane oxidation[17] will make interesting comparison with the work to be described here.

1.2 General background

In the Chemical Engineering Department, Imperial College, the general problem of flame reactions has been tackled from two directions

(a) The development and use of theoretical and practical methods to investigate the flame reaction zone in situ. It began with the work of Weinberg[18] who used optical techniques to study the reaction zone of flames supported on the flat-flame burner[19]. This approach has proved extremely profitable, but has not revealed the detailed chemical structure of the flames used. It has led to the establishment and a considerable understanding of the general principles and physical aspects of the problems associated with 'free' flames.

(b) In parallel with (a) attempts were made to magnify the reaction zone to facilitate the detailed study of the high temperature chemistry. Techniques for studies along these lines derive from an investigation into the economic use which could be made of the 0.5 to 1.0 per cent methane in the updraft of mines' ventilation air. It proved possible to utilise the methane at these concentrations in a specially boosted turbine[20] as a result of preliminary work by Meads[21]. The flow techniques which Meads had employed were further developed by Burgoyne and Hirsch[22,23] to obtain a much broader picture of the high temperature oxidation of methane (although still confined to lean fuel/air ratios). They also extended the work towards the lower temperature (and higher concentration) region where results from static vessel studies are applicable and comparable.

As a result of this work Egerton and Ray (see Section 1.3) adopted very similar techniques, and continued to use the lean methane/air system in their investigations to establish the nature of reactions

occurring just prior to the luminous combustion zone in a flame front.

Other particularly relevant work employing flow systems has been undertaken by Lloyd[24,25] and Mullins[26,27] who investigated the ignition delays occurring in a number of hydrocarbon/air systems under a wide range of concentration, pressure and temperature conditions. The latter workers conducted their experiments on an engineering scale, however, and were not concerned with detailed kinetics. Earlier work by Sachsse[28], and Sakharov and Durynina[29] also involved flow methods and lean methane mixtures. Much more recently flow methods have been employed widely in combustion studies (see for instance References 30 to 34), particularly in the U.S.S.R. The work of Kozlov[30], on the high temperature oxidation of methane in a steady-state furnace flow system, is of particular interest because of its similarity to the present contribution.

The work, already referred to, of Fristrom and co-workers using direct sampling techniques in flames is also of special relevance to the present study, particularly as their most recent work (8th Combustion Symposium) has been concerned with the kinetics of the methane/oxygen flame. In addition, Fenimore and Jones[12] have recently reported work on the methane/air flame at atmospheric pressure.

1.3 Immediate background to the present work

The work of Egerton and Ray (Reference 35 and partly in 36 and 37 with a summary in 38) which may be considered as a necessary precursor of the present work, employed a probe sampling technique instead of the analysis of the total reaction product as had been the case in Meads'

and Hirsch's work. It led to a closer acquaintance with the combustion of methane in the temperature range 1140 to 1240°K, used separate pre-heating and subsequent mixing of the fuel and oxidant to give methane concentrations in the range 0.8 to 2.2 per cent and mean gas stream velocities in the range 238 to 928 cm/s (calculated at 1173°K).

Experimentally this was accomplished in cylindrical mullite reaction tubes of 0.8 cm and 0.45 cm I.D. A silica sampling probe was employed and the sampled gas analysed for methane and carbon monoxide, and, for part of the work, for formaldehyde and hydrogen. No attempt was made to measure the gas stream velocity profile, a mean velocity being calculated from the flow rates and furnace temperature, and the reaction was considered isothermal, the reaction temperature being the furnace temperature as measured in the packed annular space between the reaction tube and the inner wall of the furnace core.

As had become apparent from the work of Burgoyne and Hirsch[23], and Vanpée[39], the oxidation of methane at these temperatures is a two-stage process, the second stage involving the oxidation of carbon monoxide which appears as a product of the first stage. In view of this Egerton and Ray extended their own work to a preliminary study of the wet and dry oxidation of carbon monoxide under conditions similar to those encountered in the oxidation of methane. Further discussion of the relevant parts of Ray's work will be given in the subsequent presentation. Here it will be sufficient to draw attention to the purpose and to some of the objectives, limitations and conclusions of that work with a view

to clarifying the aims of the present work (see Section 1.5).

To understand the purpose of Egerton and Ray's work it must be remembered that in a 'free' flame the reactions are undoubtedly influenced by diffusion and are occurring under nearly adiabatic conditions, and that they are not chemically influenced by surfaces, whereas in vessels - conditions often chosen for ignition studies - the influence of the surface is always present and is manifested in the kinetics. Care must be taken therefore, in applying the results of vessel studies to chemical processes occurring in industrial furnace and combustion chamber flames - typified by 'free' flames - where surface plays a less significant role. The flow method, on the other hand, is applicable to the high temperature conditions, has been shown[23] to involve far less surface influence (chemically), and to enable detailed kinetic studies to be made on reactions having half-lives in the microsecond to millisecond range - the range of interest in flame structure studies. Despite the fact that the flow method involves more nearly isothermal conditions - or perhaps because of this - it could indicate the probable course of reaction in flames[40].

With this in view Egerton and Ray made a preliminary survey of the methane/air reaction in order to establish the points at which more detailed investigation was required.

The analysis of their results was limited by lack of detailed knowledge of the velocity and temperature conditions in the gas. In addition there was some doubt whether the formaldehyde and hydrogen

withdrawn for analysis were satisfactorily quenched. For the more stable species it was claimed that the withdrawal rate was adequate for satisfactory quenching.

The inability to give an adequate kinetic description of the methane oxidation under their conditions resulted in a very qualitative treatment of the measurements. It should be remembered, however, that the work was considered at the outset to be a preliminary investigation and the need for more detailed sampling in a wider diameter reaction tube was emphasised.

The work focussed attention on the following problems:-

(a) the need for an understanding of the sudden changeover from a slow reaction to an explosive ignition with no measured change in the furnace conditions. This observation should be seen in relation to the work of Mullins[26,27], who showed that for 4 per cent methane/vitiated air mixtures rather long ignition delays are obtained (30 ms. at 1193°K, 7 ms. at 1373°K) compared with other hydrocarbons

(b) the need for a more detailed assessment of the influence of surface at high temperatures

(c) the need for a better understanding of the mechanism of methane oxidation under their experimental conditions in respect of (i) the self-inhibiting effect of methane on its own oxidation, (ii) the inhibition of the oxidation of wet carbon monoxide by methane, (iii) the influence and role of formaldehyde, (iv) the mechanism of formaldehyde oxidation, (v) the place and influence of the HO_2 radical in the various reactions.

From recent flame studies[9,15,41,42] a further question arises concerning the relative place of OH and HO_2 in the mechanism, and the evidence for HO_2.

All of these problems have as their basic requirement the need for a much more detailed examination of the reaction zone under appropriate conditions.

1.4 High temperature methane oxidation

Since the early work of Bone[43] many workers have turned their attention to the mechanism of hydrocarbon oxidation, and in particular to methane. Very much of the early work on the oxidation reaction was carried out by the time-honoured pressure-time technique using static systems. This method, convenient at low temperatures, was extended to the comparatively fast high temperature reaction by Vanpée[39]. Work using flow systems has been a comparatively recent innovation brought about largely by the change of emphasis from 'chemistry' of combustion reactions (both the 'overall' kinetics and attempts to isolate all possible intermediates) to the study of flame processes (which here means the investigation of the various contributing effects in combustion studied to present a cogent picture of the whole - a tendency well illustrated in modern theories of flame propagation[44 to 47]).

1.4.1 The main features of the methane oxidation (flameless combustion) reaction

(a) Main products water and carbon monoxide, and carbon dioxide at temperatures high enough for carbon monoxide to oxidise.

(b) An induction period (ignition delay in ignition studies) followed by an increase in the rate, degenerate branching generally attributed to formaldehyde.

(c) Reaction rate and induction period highly sensitive to the nature and extent of surfaces at low temperatures.

(d) A complex rate dependence - for instance[48,30]

$$\left[CH_4\right]^2 \left[O_2\right]^{0.5} \quad \text{at } 400^\circ C$$

$$\left[CH_4\right]^{0.5} \left[O_2\right]^2 \quad > 570^\circ C$$

$$\left[CH_4\right]^{-0.5} \left[O_2\right]^{0.25} \quad 930 \text{ to } 1120^\circ C \quad \left[O_2\right] > 5\%$$

$$\left[CH_4\right]^{-0.5} \left[O_2\right]^{1.5} \quad 930 \text{ to } 1120^\circ C \quad \left[O_2\right] < 5\%$$

(e) The reaction is very sensitive to traces of foreign substances. Positive catalysts include formaldehyde, which in some circumstances completely eliminates the induction period, or even accelerates the reaction initially.

(f) At high temperatures, where carbon monoxide oxidation is occurring, small amounts of methane can accelerate, and large amounts inhibit the carbon monoxide oxidation[49].

Point (f) is of interest since it demonstrates the close similarity between the reactions occurring in the slow reaction at high temperatures and reactions occurring in flames, similar effects having been demonstrated in carbon monoxide/air flames[50].

(g) Methane (and benzene) differ from the remainder of the hydrocarbons in having no low temperature explosion region. There is evidence however that the mechanism changes in the temperature range 500 to 600°C (Reference 23 and (d) above), so that it may be true to describe it as having a 'low temperature' and a 'high temperature' mechanism. One may anticipate an additional possible change in the mechanism under flame conditions due to the ready availability of chain initiators by 'back-diffusion' along the concentration gradients in the flame front.

Convenient summaries of the various stages in the development and understanding of the mechanism of methane oxidation may be found in the literature[51 to 58]. The need for more careful definition of the physical factors involved has recently been emphasised[57].

It will be convenient to consider the mechanisms proposed as a result of the flameless oxidation studies separately from those deduced from flame studies. This will lend point to the kinetic analysis of the experimental data of the present investigation.

1.4.2 Mechanism of the flameless oxidation

(a) Initiation reactions

The reaction $CH_4 + O_2 \rightarrow CH_3 + HO_2$ ....(1)

is favoured by Walsh[53] as the initiation step, while Norrish[52] favours

$$CH_4 + O_2 \rightarrow HCHO + H_2O \quad ....(2)$$

followed by

$$HCHO + O_2 \rightarrow H_2 + CO_2 + O$$

$$O + CH_4 \rightarrow CH_3 + OH$$

Reaction (1) is at least 55 kcal endothermic according to Semenov[58], 53 kcal according to Fabian and Bryce[59]. It may be noteworthy that Kozlov[30] and Hirsch[22] obtain 60 kcal and 64 kcal respectively, for the high temperature 'overall' activation energy.

The reaction $CH_4 + OH \rightarrow CH_3 + H_2O$ ....(3)

favoured by Lewis and von Elbe[51] is consequent upon an initiation step and the reaction.

$$HCHO + O_2 \rightarrow \text{free radicals} \rightarrow OH \qquad ....(4)$$

where formaldehyde acts as the agent for degenerate branching.

(b) Chain propagation

The remainder of the scheme for the slow oxidation is, according to Lewis and von Elbe[51]

$$CH_3 + O_2 \rightarrow HCHO + OH$$

$$OH + HCHO \rightarrow H_2O + CHO$$

$$CHO + O_2 \rightarrow CO + HO_2$$

$$CHO + O_2 + M \rightarrow CHO_3 + M$$

$$CHO_3 + HCHO \rightarrow 2CO + H_2O + OH$$

and radicals $\overset{\text{wall}}{\rightarrow}$ destruction.

This scheme ignores the reactions

$$CH_4 + H \rightarrow CH_3 + H_2$$

which is admittedly unlikely in a large excess of oxygen but nevertheless should not be ignored since it is slightly exothermic ($\Delta H \sim 5$-12 kcal), and[60]

$$CH_4 + HO_2 \rightarrow CH_3 + H_2O_2$$

Consideration of the reaction

$$CH_4 + O \rightarrow \text{products}$$

is perhaps unnecessary at low temperatures. Its anticipated low activation energy (e.g., Steacie[61] E ~ 8 kcal) renders it a possible mechanism at high temperatures, as suggested by Vanpée[39].

Recent Russian isotope tracer studies[62] of a mixture containing 33 per cent methane in air at 700°C has indicated the need to consider methyl alcohol, since it was shown that

$$CH_4 \rightarrow HCHO \rightarrow CO$$
$$\searrow \quad \nearrow$$
$$CH_3OH$$

although the large concentration of methane present probably makes it unimportant from the present standpoint.

The further reactions of the intermediates must also be considered. For instance

$$CH_3 + O_2 \rightarrow CH_3OO$$

is frequently postulated[51,58]. It has zero activation energy and a frequency factor of ca 10^{11} cm^3 $mole^{-1}$ s^{-1}. The possibility of a further step involving an isomerisation ($\rightarrow H_2COOH$) has been proposed by Semenov[58], then breakdown is possible as

$$H_2COOH \rightarrow HCHO + OH$$

Everett and Minkoff[63] have invoked this methyl peroxy radical and the reaction

$$CH_3OO + CH_4 \rightarrow CH_3OOH + CH_3$$

as the source of their hydroperoxide. Kondratiev[62] has reported that

at room temperature CH_3OOH is the only product of the reaction $CH_3 + O_2$. At 100°C+ he has reported formaldehyde formation to be possible via

$$CH_3OOH \rightarrow HCHO + H_2O$$

$$CH_3OO \rightarrow HCHO + OH$$

At higher temperatures mass spectroscopic investigation[59] of the reaction $CH_3 + O_2$ for the formation of HO_2 has indicated the probable course of the reaction as $CH_3 + O_2 \rightarrow CH_2 + HO_2$. Although it is difficult to explain the presence of formaldehyde otherwise, it must be stated that the evidence for the methyl peroxide radical in methane combustion is rather flimsy. The work of Salooja[56] and recent ideas on the oxidation of other higher hydrocarbons[64] and alcohols[65] has indicated the importance of H_2O_2 as an intermediary, and has brought into question the origin of the organic peroxides. It seems possible they could be the result of secondary reactions of hydrogen peroxide.

Subsequent oxidation of formaldehyde is possible by several mechanisms.

The oxidation of formaldehyde has been studied by a number of workers. At low temperatures (e.g., Reference 66) the intermediates include relatively large molecules such as performic acid. The likelihood of the larger molecules having any significant lifetime at high temperatures is doubtful, however, and for this reason, and in order to keep the discussion as brief as possible, these entities will not be considered here. They are, in any case, markedly surface dependent.

The reaction

$$HCHO + M \rightarrow H_2 + CO + M$$

is sterically unlikely.

$$HCHO + M \rightarrow CHO + H + M$$

is ~ 80 kcal endothermic and may consequently be ignored.

$$HCHO + OH \rightarrow CHO + H_2O$$

as proposed by most workers, is exothermic (~40 kcal) and quite probable.

$$HCHO + O_2 \rightarrow HCOOH + O$$

has also been proposed[67], as have

$$HCHO + HO_2 \rightarrow H_2O_2 + CHO$$ [62]

$$HCHO + O_2 \rightarrow HO_2 + CHO$$ [68]

while

$$HCHO + O \rightarrow CO + H_2O$$

is possible at high temperatures.

The performyl radical may then react according to

(i) $CHO + OH \rightarrow CO + H_2O$ ....(A)

(ii) $CHO + M \rightarrow H + CO + M$

(iii) $CHO + O_2 \rightarrow CO_2 + OH$

(iv) $CHO + O_2 \rightarrow CO + HO_2$ [68] ....(B)

(ii) is endothermic by not less than 13 kcal[61] and probably 26 kcal[69] while (iii) is sterically improbable. Although Lewis and von Elbe[51] suggest the performyl radical may be relatively inert like HO_2, at high temperatures this need not be true. The choice would seem to lie between A and B. The importance or otherwise (in methane oxidation) of the

mechanism of breakdown of the performyl radical depends to a large extent on its lifetime. If it does not have a significant lifetime, then chain continuation may be through H atoms[54]. Some evidence for the performyl radical having a significant lifetime is available[70]. We shall not consider the role of HO_2 or H_2O_2 here.

(c) The further oxidation of the products

The mechanism for the disappearance of carbon monoxide must now be considered. It exhibits two distinct mechanisms in its oxidation, one applicable to the system in the absence of water vapour, the other applicable in the presence of water vapour (or other hydrogen containing species). Very small amounts of water vapour are sufficient to permit the second mechanism. Often sufficient water-derived radicals are present on the reaction vessel wall, despite attempts to study the dry reaction. The mechanism of the dry reaction is as yet incompletely resolved, but will not concern us since under all likely experimental conditions in this work adequate water-derived radicals will be present.

From its dependence on water vapour it may be expected that

$$CO + OH \rightarrow CO_2 + H$$

would be of major importance. This idea is supported by estimates of the rate constant[41,42,71]. Consideration of the possible alternatives supports this contention. The reaction

$$M + CO + O \rightarrow CO_2 + M$$

or if preferred

$$CO + O \rightarrow CO_2$$

violates spin conservation - ground states are CO $^1\Sigma$, O ^3P, CO_2 $^1\Sigma$, whereas CO $^1\Sigma$ + $O^3P \rightarrow CO_2{}^{*3}\Pi$ (probably), while the direct transition $CO_2{}^{*3}\Pi \rightarrow CO_2$ $^1\Sigma$ violates conservation rules. The possibility that $CO_2{}^{*3}\Pi$ may be stabilised by transition to a lower excited level has been suggested[72].

The reaction

$$CO + O_2 \rightarrow CO_2 + O$$

is acceptable mechanistically, but would not account for the pronounced effect of OH, H_2O, H_2 on the carbon monoxide/oxygen reaction.

The reaction $CO + HO_2 \rightarrow CO_2 + OH$ is possible, and if it occurs, as is suggested by Lewis and von Elbe at lower temperatures[51], it would be extremely exothermic and might result in vibrationally excited $CO_2{}^*$.

Two further features of this reaction deserve mention. A pale blue pre-ignition glow is associated with the reaction. It has been stated to be absent in the dry reaction[73]. It has been shown that formaldehyde inhibits the oxidation by the wet mechanism at high temperatures[22].

(d) Radical-radical reactions

It is not proposed to consider radical-radical interactions save in the following instance. The reaction

$$HO_2 + CH_3 \rightarrow HCHO^* + H_2O$$

has been postulated[74] to account for the formation of excited formaldehyde found in methane oxidation under engine conditions. It is evident

that excited formaldehyde cannot be formed thermally since it has 77 to 81 kcal excitation energy[74,78].

(e) Energy chains

Evidence of energy rich species raises the problem of energy chains, as distinct from simple radical and atomic (i.e., free-electron) chains, and how such chains may be treated kinetically. This problem, and the related one of non-equilibrium concentrations of radical species has attracted interest in recent years (see, for instance Shuler[75]). The likelihood of energy rich chains, and of large excess concentrations of radicals is considerably less under the conditions envisaged in the present work than under flame conditions. It is well, however, that note is taken of these possibilities and the consequent need to modify the interpretation of high temperature rate phenomena. The importance of energy chains in dry carbon monoxide oxidation must not be overlooked.

1.4.3 Flame mechanism of methane oxidation

A probable course of the flame reaction has been conveniently summarised by Westenberg and Fristrom[42]

$$CH_4 + OH \rightarrow CH_3 + H_2O$$

$$CH_4 + O \rightarrow CH_3 + OH$$

$$CH_3 + O_2 \rightarrow HCHO + OH \text{ †}$$

$$HCHO + OH \rightarrow CHO + H_2O$$

$$CHO + OH \rightarrow CO + H_2O$$

$$CO + OH \rightarrow CO_2 + H$$

† Fenimore and Jones have recently presented evidence favouring $CH_3 + O \rightarrow \ldots \rightarrow$ eventually CO, as the main propagation step.

plus a "shuffling" reaction

$$H + H_2O \rightleftarrows OH + H_2$$

and chain branching

$$O + H_2 \rightarrow OH + H$$

$$H + O_2 \rightarrow OH + O$$

and gas phase recombinations of the type

$$OH + OH \rightarrow H_2O + O$$

$$O + O + M \rightarrow O_2 + M$$

$$OH + H + M \rightarrow H_2O + M$$

$$H + H + M \rightarrow H_2 + M$$

the last 7 reactions replace the wall reactions of vessel studies. The last two may be unimportant in excess oxygen.

The equilibrium concentrations of radicals and atomic species are must greater under flame conditions and the role of the oxygen atom especially may be expected to be significant in oxygen rich conditions.

1.5 Aims of the present work

The relevance of the two extremes - the need to provide initiation in the slow reaction and the abundance of such initiating centres in the flame reaction - to the high temperature work presented here may be appreciated from the work of Egerton and Ray, where slow combustion suddenly transferred to flame type reaction.

The need for a closer acquaintance with the physical (including aerodynamic) factors affecting reactions in high temperature flow systems has already been mentioned. The two most important aspects in this respect are undoubtedly the mixing and the sampling phenomena. As will

be demonstrated, transport processes are extremely important, being particularly dependent on the inlet geometry.

To achieve a better understanding of these and of the influence of the surface - both catalytically and as a heat source or sink - a larger diameter reaction tube than that used by Egerton and Ray was employed. This was to facilitate the detailed study of conditions in the reaction zone. Questions of stability, reproducibility and accuracy had also to be investigated.

The first part of the thesis (Chapters 2 to 4) is largely concerned with the experimental arrangement, the mixing and sampling problems, and an assessment of the overall performance of the system. The second part of the thesis (Chapters 5 to 9) is concerned with the use of the apparatus to study two particular aspects of the methane oxidation reaction. Heat release rates have proved a useful method of analysis in flame structure studies. A similar analysis is attempted here. An analytical approach is envisaged, rather than the development, or redevelopment, of any theory. Some detailed knowledge of the energetics and rates of the reactions should be forthcoming from this approach which may well make useful comparison with recent flame structure studies of the methane/oxygen system[12,42].

The second aspect which will receive attention concerns the role of intermediates in the reaction. To anticipate later findings, this will involve a study of formaldehyde and hydrogen peroxide in the reaction and the factors affecting their formation and disappearance.

This will have particular point in view of the significance of hydrogen peroxide in the lower temperature mechanism as demonstrated by the careful work of Salooja[56]. As previously indicated, other recent work has demonstrated the importance of hydrogen peroxide[64,65].

CHAPTER 2

The Apparatus (1)

General Description and Procedure

2.1 Introduction

This chapter will be confined to a description of the apparatus as it emerged in its final form, and to its use in that form. Features of the work which require more critical treatment, such as the inlet and sampling problems, are considered in greater detail in the following chapter, together with some other aspects of the work better detailed separately. The range of conditions for which the apparatus proved suitable is summarised in Table 4.3.

The general lay-out of the apparatus can best be judged from Figures 2.1 to 2.4, which show the gas supply and metering systems and the analysis system. Table 2.1 lists the dimensional and constructional details of the furnace and associated components. The cylindrical reaction zone extends horizontally from the centre of the furnace and is probed from the exhaust end. The reactant gases are separately preheated to the required temperature and allowed to intermix at the beginning of the reaction zone. Samples are withdrawn through a sampling probe and analysed for residual reactant (methane), intermediates and products. Gas stream temperature and velocity are also measured. Maximum total flow rates of 11.5. $^{-1}$ (cold) were employed.

2.2 The gas supply and metering system

Methane has been used as fuel throughout the present experiments.

Originally the methane obtained from Point of Ayr colliery had a purity better than 98 per cent, but in later supplies this decreased to values in the range 75 to 85 per cent. Methane of greater purity was not readily available in sufficient quantity elsewhere. It was established by chromatographic analysis that the impurity was almost entirely air, with carbon dioxide as the only other identified contaminant, neither hydrogen nor any higher hydrocarbon being detected.

Oxygen was removed by passing the impure methane over a Nickel or Iron oxide catalyst bed (it is unimportant which is used for the present purpose - see Appendix 2.A. and ref. 76). The catalyst bed was maintained at 420 to 430°C in an auxiliary furnace, the oxygen being converted to carbon dioxide and water by reaction with some of the methane. The carbon dioxide and water were removed by passing the gas stream successively through absorbent towers containing self-indicating soda lime (carbosorb), calcium chloride and magnesium perchlorate. The methane, containing 15 to 20 per cent residual nitrogen, was then metered through a capillary flowmeter, using di-butyl phthalate as the flowmeter liquid. The flowmeter was calibrated by the soap bubble method[77] at a known total line pressure, in excess of ambient, by arranging needle valves both before and after the flowmeter. By this means the flowmeter could be used at a constant total line pressure, independent of the prevailing ambient pressure. (A similar procedure was adopted for all the flowmeters.)

Clean, dry, carbon dioxide - free air was used as the oxidant for all the experiments. It was supplied by two Bullows "Hydrovane" compressors each capable of delivering about 60 $l.min^{-1}$ at 30 p.s.i.g. These were arranged in parallel and were followed by a surge volume, oil filter and two lines of absorbent towers in parallel. Each absorbent line contained self-indicating soda lime, silica gel, activated carbon and magnesium perchlorate. It was found convenient to use duplicate purifying lines as it halved the upstream line pressure needed for a given flow and reduced the flow velocity through the cleaning agents.

2.3 The reaction system

A reaction tube of considerably greater diameter than those previously used by either Hirsch[22] or Ray[35] has been employed, for reasons given in Chapter 1. In the initial experiments a mullite tube was employed, but subsequent development of the inlet and temperature controlling device made it advisable to replace this by one made of silica, of identical dimensions.

With a mullite reaction tube it had been shown that the platinum resistance thermometer, although wound on the outside of the tube non-inductively, was picking up the strong pulse feed from the thyratron (see Section 2.4 for a description of the temperature control). It was found that this effect became dominant above about 650°C and over-ruled the controlling characteristic of the thermometer. Since the effect was temperature-dependent and there was no electrical contact

between the controlling thermometer and the controlled heating circuit (Preheat 'A'), except through the mullite reaction tube, it was concluded that the mullite was acting as a conductor, albeit a poor one, at the elevated temperatures. After consideration of a number of alternative solutions, it was decided to change the material of the reaction tube to silica, despite its lower maximum operating temperature. It was found unnecessary to shield the platinum thermometer, either thermally or electrically, in the final form of the apparatus.

The final form of the inlet (Figure 2.5) comprised a containing sheath of thin-walled transparent silica, within which was mounted an array of smaller silica tubes supported on four platinum discs. The inlet tubes were arranged symmetrically about the axis of the containing sheath, and projected beyond it in both directions. At the outlet end (i.e., the end forming the commencement of reaction zone within the furnace) they terminated in much finer silica tubes, 'inlet ports', which formed the mixing point. At the opposite end of the sheath, the inlet tubes were individually connected, via an adaptor, to the methane supply. Air was introduced through the adaptor, flowed between the methane carrying tubes along the preheater and passed into the reaction zone through a number of fine holes in the final platinum disc. (A more detailed description is given in Chapter 3.)

Sampling devices were introduced from the exhaust end of the reaction zone, parallel to the reaction tube axis; they could be positioned to probe any point in the reaction zone through the agency

of a three-way adjustable optical movement, on which they were mounted. Absolute position of the probe tip was determined by allowing the probe to contact the reaction tube wall, giving subsequent radial positions to within 0.2 mm relative to the wall. Axial position was determined from a previous measurement of the mixing point postion relative to the axial scale and a knowledge of the overall probe length. This gave an absolute accuracy of about 1 mm. Relative accuracies were considerably better; radially the probe tip position could be adjusted with an accuracy of 0.05 to 0.1 mm; axially adjustment was made to the nearest 0.1 mm.

The exhaust gases, at atmospheric pressure, were deflected into an extraction system by an asbestos shield with a mica window. The window allowed direct visual observation of the reaction zone, while the shield prevented the exhaust gases from reaching the probe mounting.

2.4 The furnace, temperature control and measurement

The furnace used by Hirsch and by Ray was suitably modified to accommodate a larger reaction tube and the heating arrangements altered to cater for the increased volume flow. The heating arrangements, shown schematically in Figure 2.6, were divided into three sections. In addition to the two previously used (see Reference 22), which in the present set-up were controlled by two 2 KVA Variacs supplied from a 7.5 KVA constant voltage transformer, a third heating circuit was added, the heating elements of which were situated in the inlet sheath. For the third heater six twin-bore silica tubes served to carry the heating

wire, supported in the platinum discs parallel to the methane inlet tubes. Thus the heating circuits comprised a main furnace heating unit 'M', a preheat unit 'B', both essentially as described in Reference 22, and a second preheat unit 'A', as just described.

Preheat 'A' was controlled by an automatic continuously varying control system (as distinct from an 'on-off' control), which served to maintain the furnace temperature conditions constant. This temperature control was sensitive to temperature changes, at the platinum resistance thermometer, of about one-tenth degree K at a working temperature of 1173°K. Maximum effectiveness was obtained with the Variac controls to 'M' and 'B' adjusted to give minimal overall temperature variation with time, the control design being intentionally most effective in obtaining compensation in the preheat for small fluctuations in gas flow. Any change in the experimental conditions greater than 1 or 2 per cent, such as large fluctuations in the gas flow, changes in the nature of the reaction in the reaction zone (e.g. 'flashback', which gave a series of diffusion flames on the inlet ports), or variation in the furnace heating rate caused by the largest fluctuations in the mains voltage, could not be accommodated by the control without totally changing the experimental heating conditions. These points are further considered in Chapter 4.

A circuit diagram of the control system is shown in Figure 2.7. It comprised an A.C. bridge, consisting of two one-volt voltage arms, the platinum resistance thermometer and a balancing arm. The balancing

arm contained three Muirhead standard decade resistances of tens, units and tenths of an ohm respectively. The output of the bridge was fed into a two-stage amplifier. The amplified output voltage of the bridge was a measure of the unbalance between resistance thermometer and the standard resistances. This was set to be zero at the desired furnace temperature. Control was obtained by referring the amplified bridge unbalance voltage to a phase-shifted reference voltage, the combined voltages constituting the control grid signal to the thyratron. The mode of operation is best understood by considering three cases:-

(a) 'Correct' condition recorded at the resistance thermometer

(b) condition 'too hot' at the thermometer

(c) condition 'too cold' at the thermometer

In case (a) the total energy input to the furnace exactly balances the total energy loss, the shaded portion on the thyratron anode voltage curve (Figure 2.8 (a)) representing the contribution required from preheat 'A' to achieve this. In this instance the bridge voltage is zero and hence the thyratron is triggered by the phase-shifted grid signal alone. In case (b) the resistance of the resistance thermometer is too great, the bridge is out of balance and the phase shift of the grid signal is modified by the amplified bridge voltage in the sense to trigger the thyratron later in the cycle (Figure 2.8 (b)). This gives a lower energy input to preheat 'A'. In case (c) a phase shift of the grid voltage in the opposite sense is achieved, resulting in earlier triggering of the thyratron and consequent increase in energy input to preheat 'A' (Figure 2.8 (c)).

By selecting suitable values of resistance in the decade balancing arm the furnace temperature could be controlled at approximately one degree K intervals throughout the temperature range of the experiments.

Measurement of the temperature was made by either two or three platinum - platinum 13 per cent rhodium thermocouples, depending on the nature of the particular experiment. The platinum resistance thermometer was not used for measuring the temperature for two reasons, (a) it was simpler to use a thermocouple and (b) the resistance seemed to be affected slightly (presumably by induction) by the current flowing in 'M' and 'B'. One thermocouple was situated immediately below the platinum resistance thermometer measuring the 'control' temperature; the second, situated in the inlet sheath approximately on the axis and 5-8 cm upstream from the mixing point, measured the temperature of the air at the end of preheat 'A'; the third, shielded from catalytic effects by a thin silica sheath, was situated in the composite probe (see Chapter 3) and was used to measure the sampled gas temperature in the manner of a suction pyrometer. At high temperatures silica is known to attack platinum, but no trouble was experienced from this cause during the experiments described here. The cold junctions of the thermocouples were maintained at $0^{o}C$ in melting ice. The thermocouple e.m.f.s. were measured on a Cambridge potentiometer which could be read to 0.005 mV ($\frac{1}{2}^{o}K$). Temperatures were obtained from the e.m.f.s using the manufacturer's tables.

2.5 Probes and samplers

Three probes were eventually developed, for two complementary aspects of the experimental work. An assessment of the physical factors

affecting the reaction rates was obtained using a composite probe and a static pressure measuring probe, while a water-cooled sampler was employed in a semi-quantitative study of the reaction intermediates. The principle features of the three probes are shown in Figure 2.9. A more detailed discussion of 'probing' appears in Chapter 3.

The composite probe was used to determine the point values of the three required parameters - gas stream composition, velocity and temperature. Strictly this probe measured only the total-head pressure, the static pressure having to be determined separately and the gas stream velocity calculated from the difference. This was considered sufficiently accurate since the static pressure was relatively insensitive to gas stream temperatures and composition. Both total-head and static pressures were measured on a Chattock manometer. This is a sensitive pressure measuring device, the pressure difference between two arms being detected by the movement of a liquid - liquid junction (water and paraffin were used) observed at low magnification. It was used as a null-point instrument by adjusting the relative heights of the two arms by means of a micrometer screw. An illustration, together with a full description of its operation, will be found in Ower: "The Measurement of Air Flow"[79].

Measurement of the pitot pressure resulted in a knowledge of the time-mean gas stream velocity to an accuracy of 1 to 2 per cent in midstream, deteriorating to 3 to 4 per cent or worse at positions close to the reaction tube wall. Temperature and composition could be measured

simultaneously, while the total-head pressure was determined consecutively. With the water-cooled sampler it was not practicable to measure temperature, as the probe perturbed the local gas stream temperature near its tip and in consequence made measurement of velocity meaningless.

2.6 Analysis of sampled gases (see Figure 2.11)

A flow diagram of the analysis system is shown in Figure 2.4. A gas sample was continuously withdrawn from the reaction zone except when the total-head pressure was being determined. In the case of the composite probe, additional cooling was obtained from a double surfaced water condenser and the sample was then passed through a three-way tap, sample trap, water absorbent tubes containing magnesium perchlorate, and into a small diaphragm pump. On the downstream side of the pump the sample passed through three infra-red gas analysers, of the type described by Hirsch[22]. These were non-dispersive instruments, selectively sensitive to carbon dioxide, carbon monoxide and methane respectively. Any carbon dioxide was removed after the first analyser since both the other analysers showed a slight response to this constituent. No such interfering effects occurred for the other gases at the concentrations handled in these experiments. Finally the sample passed through a capillary flowmeter (calibrated for air) after which a part of the gas flow was put through the test cell of a differential katharometer for the estimation of hydrogen[22]. The reference cell of the katharometer was supplied from a T-junction in the main supply line immediately prior to the furnace. By placing needle valves immediately before the

first analyser and immediately after the sample flowmeter, the analysers could always be used at a constant pressure slightly in excess of ambient, this obviating one of the difficulties experienced by Ray[35].

Analysis for low concentration intermediates, when required, was at first done by freezing out all the condensibles at -196°C and then analysing for formaldehyde and hydrogen peroxide by spectrophotometric methods in the manner described by Salooja[80]. Later a sufficiently accurate method was developed whereby formaldehyde was directly absorbed in an aqueous solution (10 ml) containing chromotropic acid (0.5 ml of 1 per cent) and sulphuric acid (80 per cent). The details of the absorption system are shown in Figure 2.10. Its mode of operation allowed sampling to be continuous. The by-pass was used except for the actual sampling period, during which the sampled gas flowed through the extraction vessel. By this means extraction times of 10 seconds were found to be sufficient at the sampling flow rates used. Even at flow rates of 1 litre per minute (considerably in excess of those used) absorption of formaldehyde in the suphuric acid solution was better than 98 per cent. This high efficiency may be attributed to the special bubbler used (Figure 2.10 - inset). It consisted of a short length of small diameter glass tubing having the end constricted and drawn out. This narrower portion was finely perforated and enclosed in a thin glass envelope having considerably larger perforations. Liquid was trapped inside the envelope and violently mixed with the gas issuing from the fine perforations.

When it was desired to determine hydrogen peroxide concentration the sulphuric acid solution was replaced by methanol cooled to -80°C, and the extraction time increased to 10 min. (By the earlier method extraction times of 20 to 30 min were required for quantitative measurement of peroxide.) Titanous sulphate reagent (1 ml) was then added and the solution made up to 10 ml. The optical density was measured at 4100 A° against a blank, the concentration being determined from a calibration curve. For the formaldehyde solutions the optical density at 5700 A° was measured. The analyses of the reaction intermediates are considered in greater detail in Chapter 4.

2.7 Method of Experiment

A run, unless otherwise stated, consisted of a sequence of point determinations of the required parameters in the reaction zone, under conditions of steady flow and temperature and of constant inlet composition. The furnace was heated to approximately the required temperature on heaters 'M' and 'B'. The air compressors were switched on, followed immediately by preheat 'A'. The air flow rate was then approximately set to the required amount, and the fuel introduced with the temperature conditions slightly below those finally required. Successive adjustments were made to the flows and heating rates until the required conditions were attained and this state was held constant (furnace temperature variation $\pm\frac{1}{2}$°C, flow variation <1 per cent) for an hour before any measurements were attempted. Failure to observe this settling down period always resulted in the experimental observations containing a

contibution from the variation in furnace conditions with time. This was especially noticeable in the runs carried out with the composite probe. Equally, with two flow rates and three heating rates capable of independent variation (quite apart from day to day variation in ambient conditions) it was important to make each run as self-consistent and independent as possible since the reaction zone conditions could never be exactly reproduced from one day to the next.

The method and experimental techniques and procedures are discussed and assessed in greater detail as an integral part of the next two chapters.

APPENDIX 2A

Removal of oxygen from methane

Gas chromatography revealed progressive contamination of the methane from Point of Ayr Colliery by oxygen and nitrogen in proportions which pointed to atmospheric air as the contaminant. This contamination was negligible up till 1958, but subsequently increased, becoming constant at about 3 per cent oxygen. This had to be removed.

Mardi[76] had shown that lean methane-air mixtures could be rapidly oxidised to carbon dioxide and water, without detectable amounts of intermediates, at temperatures in the region 400 to 450°C, using a variety of metal oxide catalysts in pellet or granular form. This seemed a promising means of removing the oxygen.

An auxiliary furnace was incorporated into the methane supply line having a vertical pyrex reaction tube (3 cm bore) which was half-filled with glass rings supporting a catalyst bed 8 to 10 cm deep. The catalysts used were either calcined nickel or iron oxides, having similar catalytic activity. Furnace and flow conditions were chosen experimentally (Figure 2.12) so that the carbon dioxide produced accounted for the oxygen originally present. Faster flows or lower furnace temperature resulted in partial removal of oxygen, but no carbon monoxide. The condition chosen was a furnace temperature of 420 to 430°C for all methane flow rates. The catalyst bed had to be replaced every 50 cu ft of methane. The residual nitrogen in the methane supply was tolerated,

whilst the carbon dioxide and water produced by catalysis were removed by carbosorb, calcium chloride and magnesium perchlorate.

Details of furnace and associated components

Item	Component	Material	Dimensions	Foot Notes
1	Main Furnace	Syndanyo construction Fosasil insulation	760 × 260 × 260 mm	
2	Preheat Furnace	Syndanyo construction Fosasil insulation	360 × 260 × 260 mm	
3	Main Heater wiring - 'M'	Nichrome	17 s.w.g. 36Ω	
4	Preheater wiring - 'A'	Kanthal 'A'	23 s.w.g. 37Ω 6 × 1600 mm	a
5	Preheater wiring - 'B'	Nichrome	20 s.w.g. 56Ω	b
6	Furnace Tube	Fused silica	Bore : 50 mm length: 1120 (760 + 360) mm	
7	Reaction Tube	Satin surfaced silica	Bore : 22.5 to 23.0 mm o.d. : 28 to 29 mm length: 1250 mm	
8	Inlet sheath	Transparent silica	Bore : 19.5 to 20.0 mm o.d. : 22.0 to 22.5 mm length: 800 mm	
9	Methane inlet tubes (19)	Satin surfaced silica	Bore : ~1 mm o.d. : ~3 mm length: 850 to 900 mm	c
10	Inlet heater tubes (6)	Satin surfaced silica	Twin bore: 1 mm o.d. : 4 to 5 mm length : 3 each 720, 740 mm	d
11	Inlet End Plate	Platinum	see Figure 3.2	
12	Inlet thermocouple Inlet thermocouple sheath	Pt/Pt 13 per cent Rh Transparent silica	32 s.w.g. Bore : 0.5 to 0.8 mm o.d. : 1.5 to 2.0 mm length: 900 mm	
13	Main thermocouple Main thermocouple sheath	Pt/Pt 13 per cent Rh Satin surfaced silica	26 s.w.g. Twin bore: 1 mm o.d. : 5 mm length : variable up to 500mm	

Item	Component	Material	Dimensions	Foot Notes
14	Resistance thermometer	Platinum	Nominal 20Ω (200 cm 40 s.w.g.)	e
15	Water-cooled sampler	Nimonic Silver steel tip	Bore : 0.48 mm o.d. : 3.2 mm length: 570 mm	f
16	Composite probe	Transparent 'AA' quality silica	Bore : 1.80 to 1.85 mm o.d. : 4.2 mm length: 640 mm	
17	Composite probe thermocouple	Pt/Pt 13 per cent Rh	40 s.w.g.	
	Composite probe thermocouple sheath	'AA' quality silica	Bore: 0.5 mm o.d.: 1.3 mm	length to suit Item 16
	Composite probe inner insulation	'X-ray' tubing	Bore: 0.15 to 0.25 mm o.d.: 0.19 to 0.32 mm	
18	Static Pressure probe	Satin surfaced silica	Bore : 1 mm o.d. : 4 mm length: 620 mm	g

NOTES

(a) Each length was bent double and threaded through the twin bores of a heater tube. The six elements thus formed were connected in series (see Figures 2.5 and 2.6).

(b) In two parts; about 80 turns on the furnace core and about 100 turns on a former at the preheat end of the reaction tube (see Figure 2.6).

(c) Tapered, and a 15 mm length of 0.25 to 0.5 mm bore, 0.8 to 1.0 mm o.d. transparent tubing fused to the tip, (see Figure 2.5).

(d) Carrying preheater 'A' wiring.

(e) Wound non-inductively - connecting leads thickened in 2 stages
(1) to 32 s.w.g. for 100 mm (2) to 22 s.w.g. for 450 mm

(f) Length dimension given is from tip to first 'shoulder'

(g) 3 x 10 thou holes situated symmetrically around circumference at 30 mm from hemispherical tip.

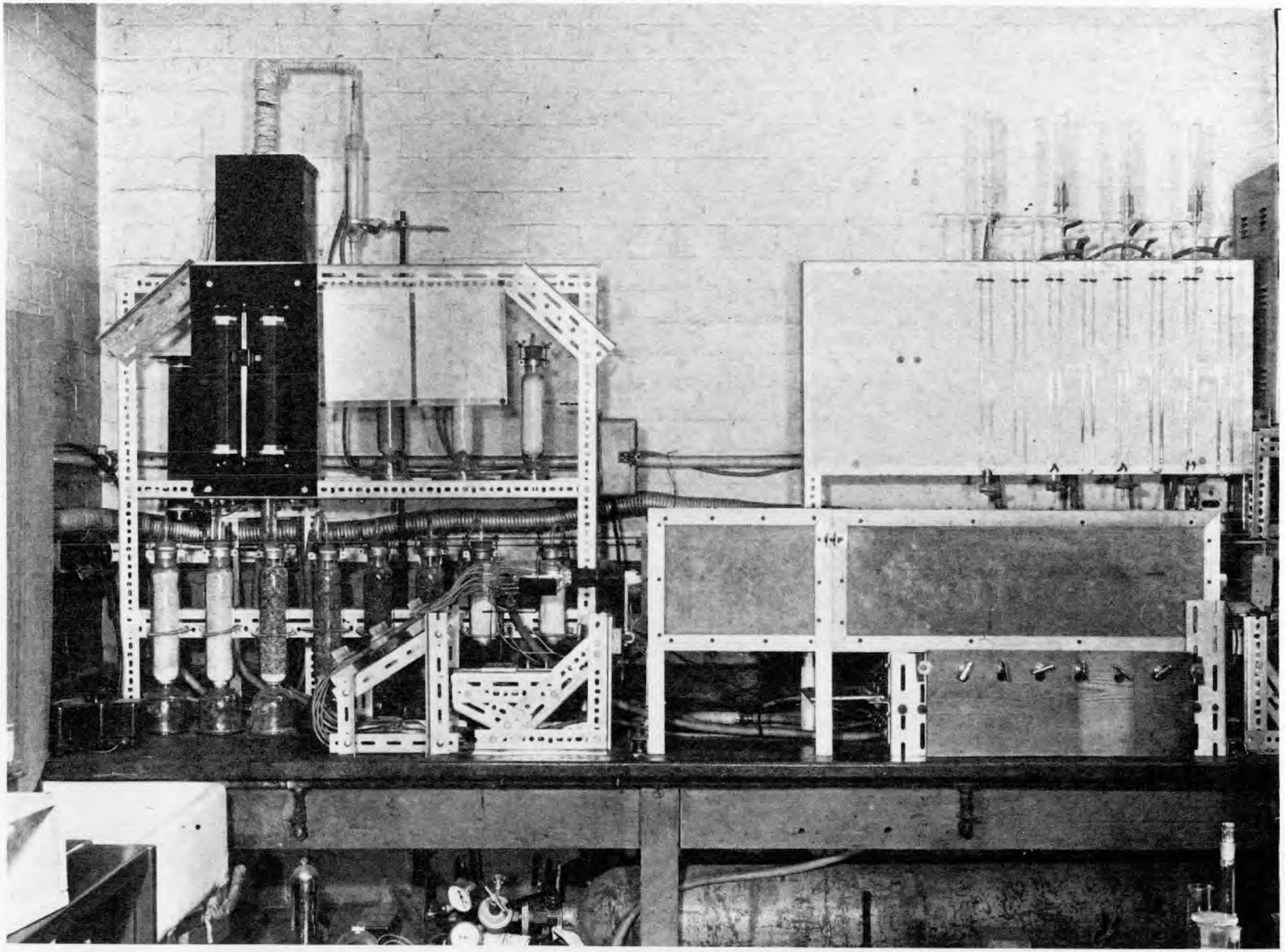

FIG.2.1. GAS SUPPLY AND INLET ARRANGEMENT

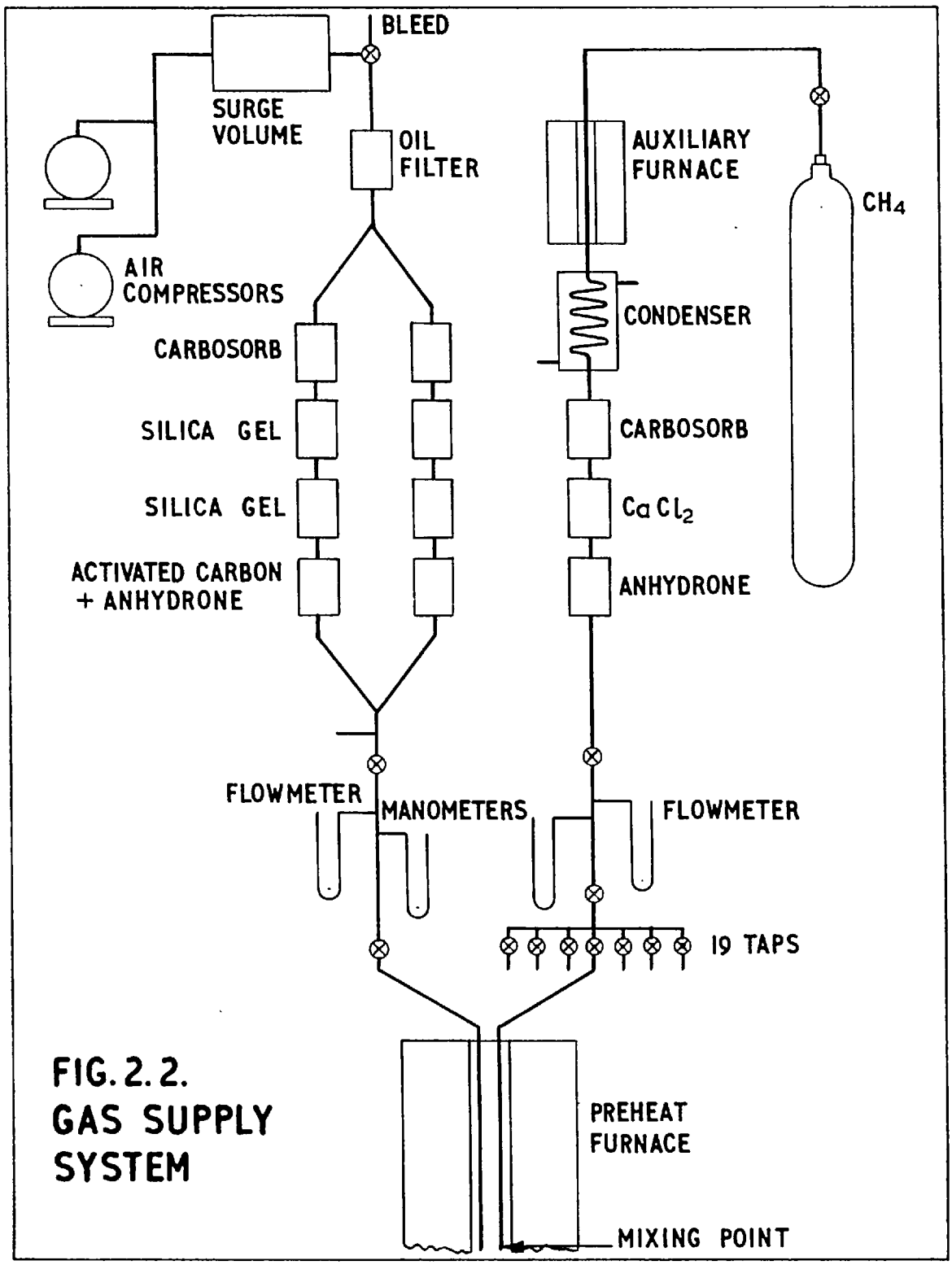

FIG. 2.2.
GAS SUPPLY SYSTEM

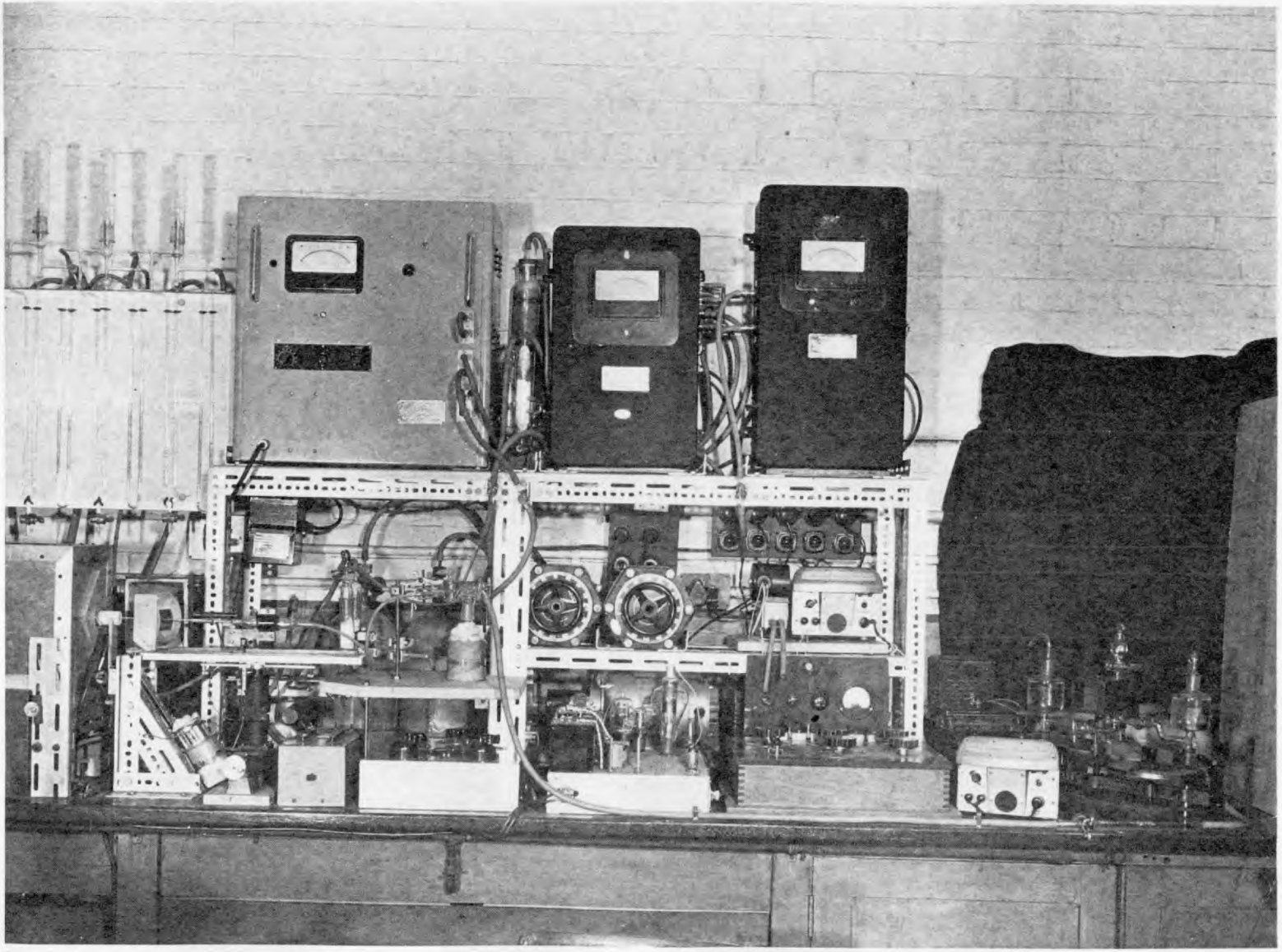

FIG. 2.3. CONTROL AND ANALYSIS INSTRUMENTATION

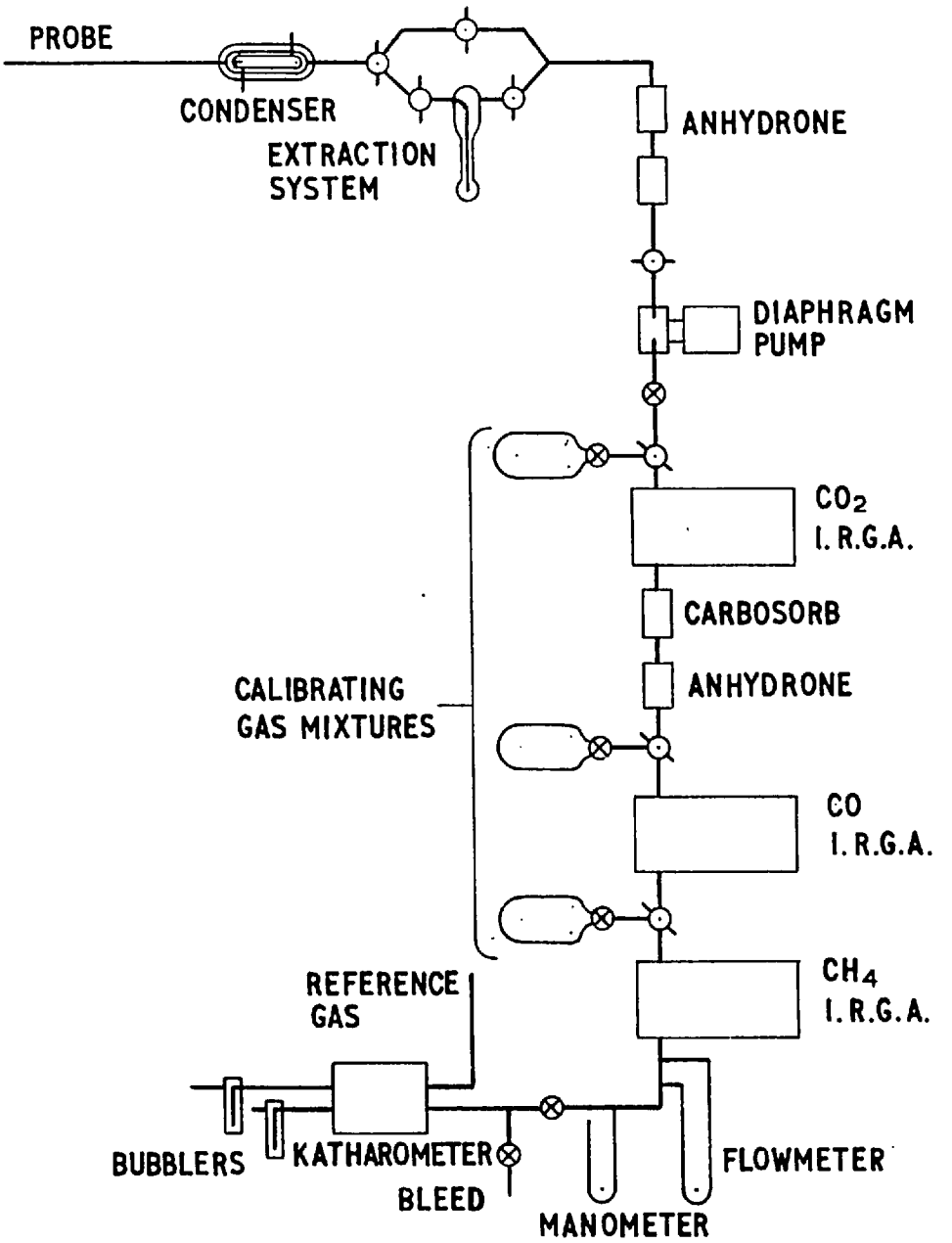

FIG. 2.4. SAMPLED GAS ANALYSIS SYSTEM

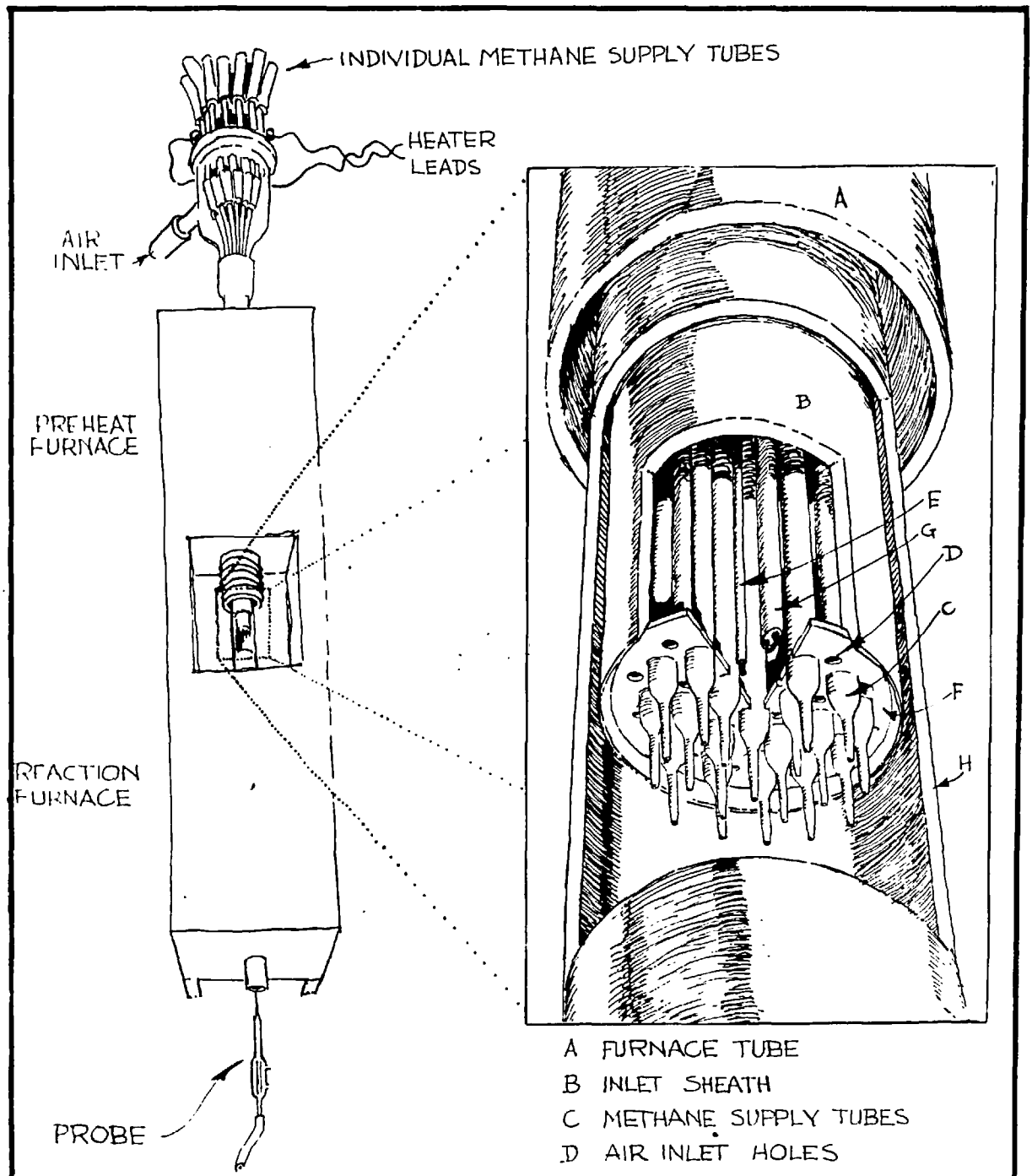

A FURNACE TUBE
B INLET SHEATH
C METHANE SUPPLY TUBES
D AIR INLET HOLES
E INLET THERMOCOUPLE
F PLATINUM END-PLATE
G HEATER ELEMENTS
H REACTION TUBE

FIG. 2.5. THE INLET (model 'D')

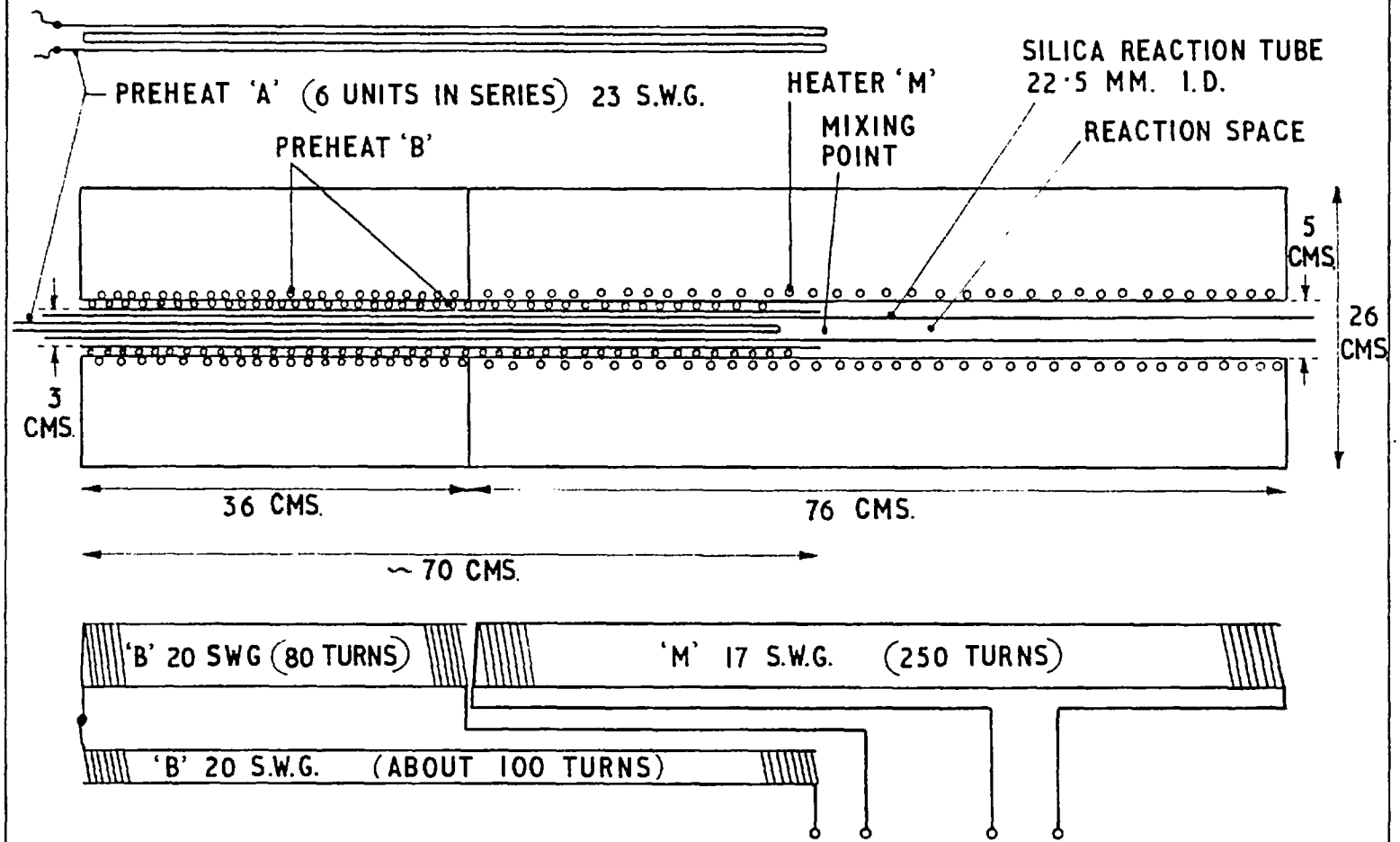

FIG. 2.6. FURNACE HEATING ARRANGEMENT

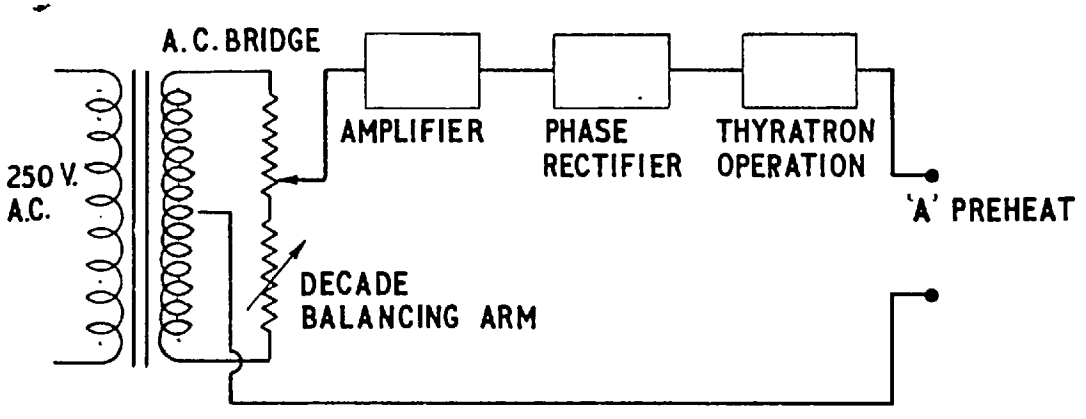

FIG. 2.7. PREHEAT 'A' CONTROL CIRCUIT

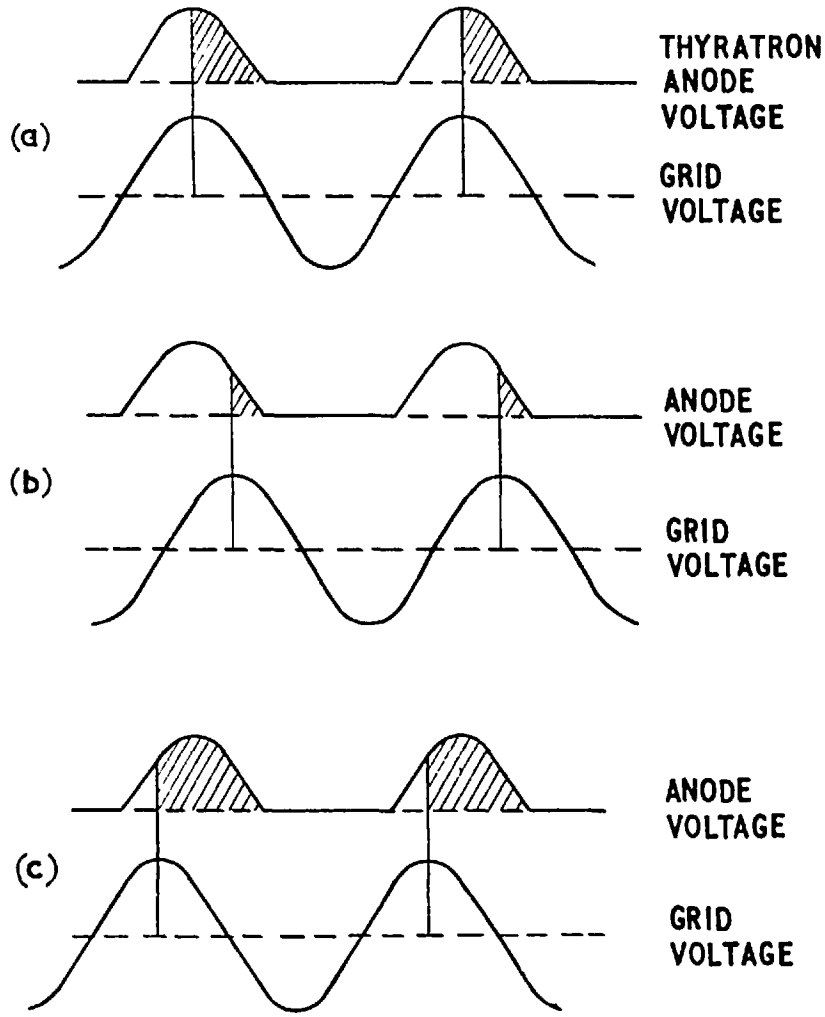

SHADED AREA REPRESENTS THYRATRON INPUT TO PREHEAT 'A'

FIG. 2.8. THYRATRON OPERATION (SCHEMATIC)

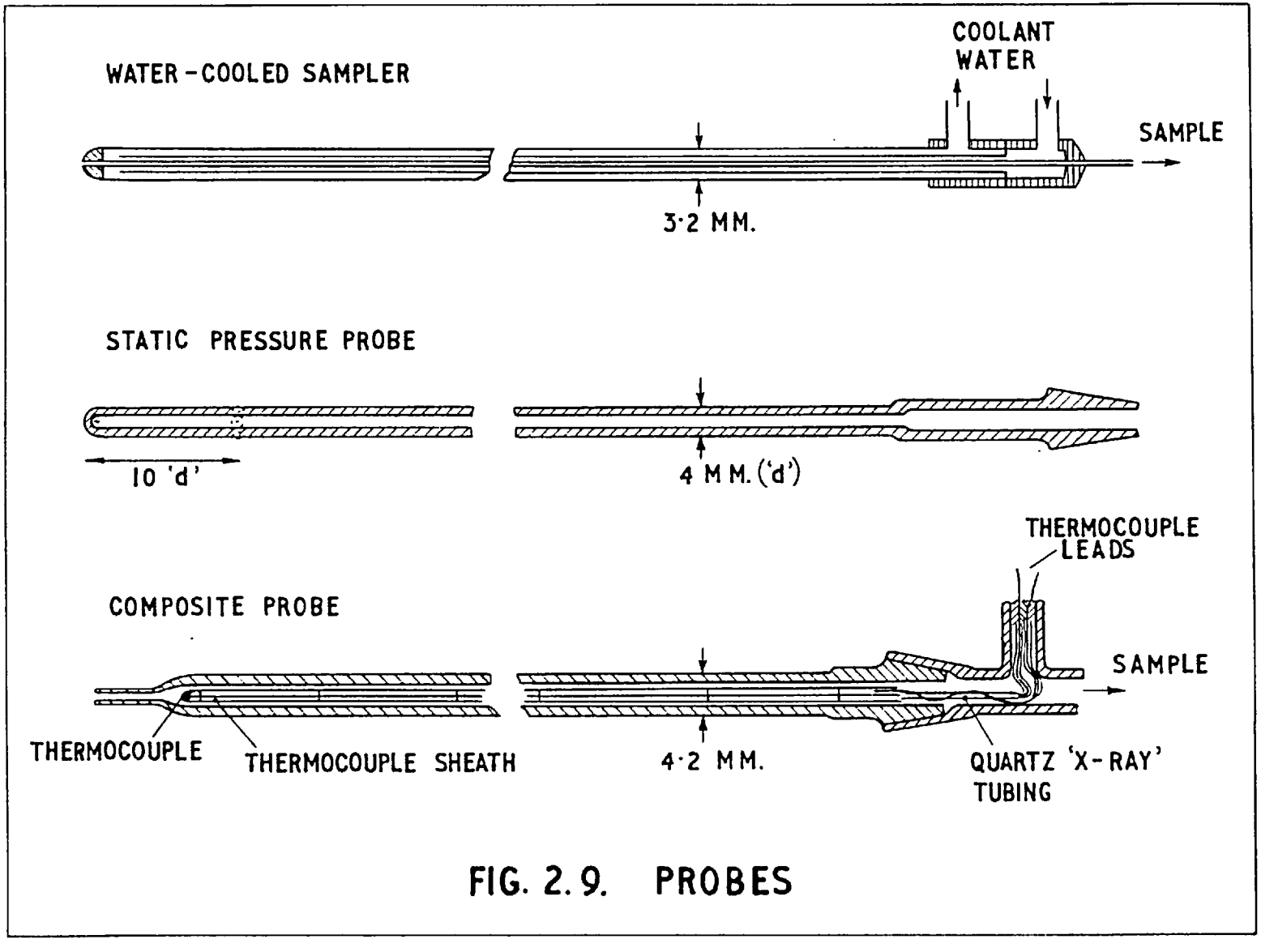

FIG. 2.9. PROBES

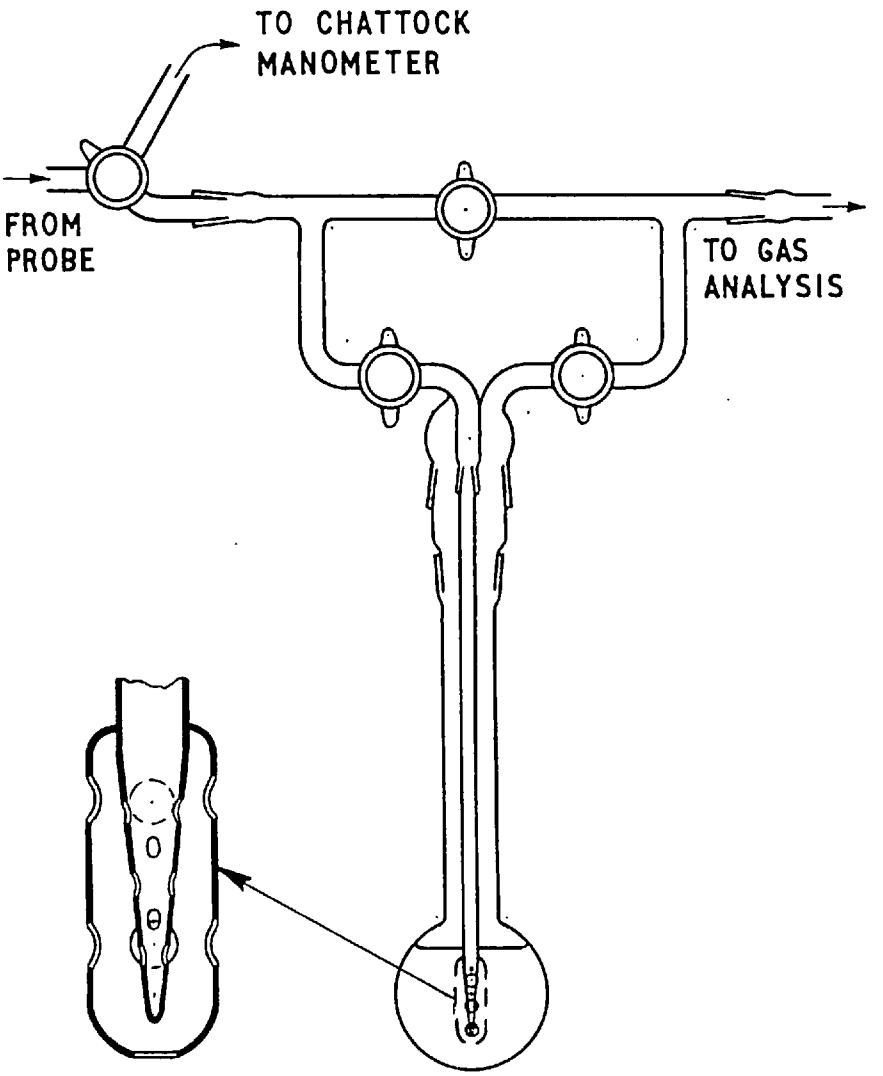

FIG. 2.10. EXTRACTION SYSTEM
(FORMALDEHYDE AND HYDROGEN PEROXIDE)

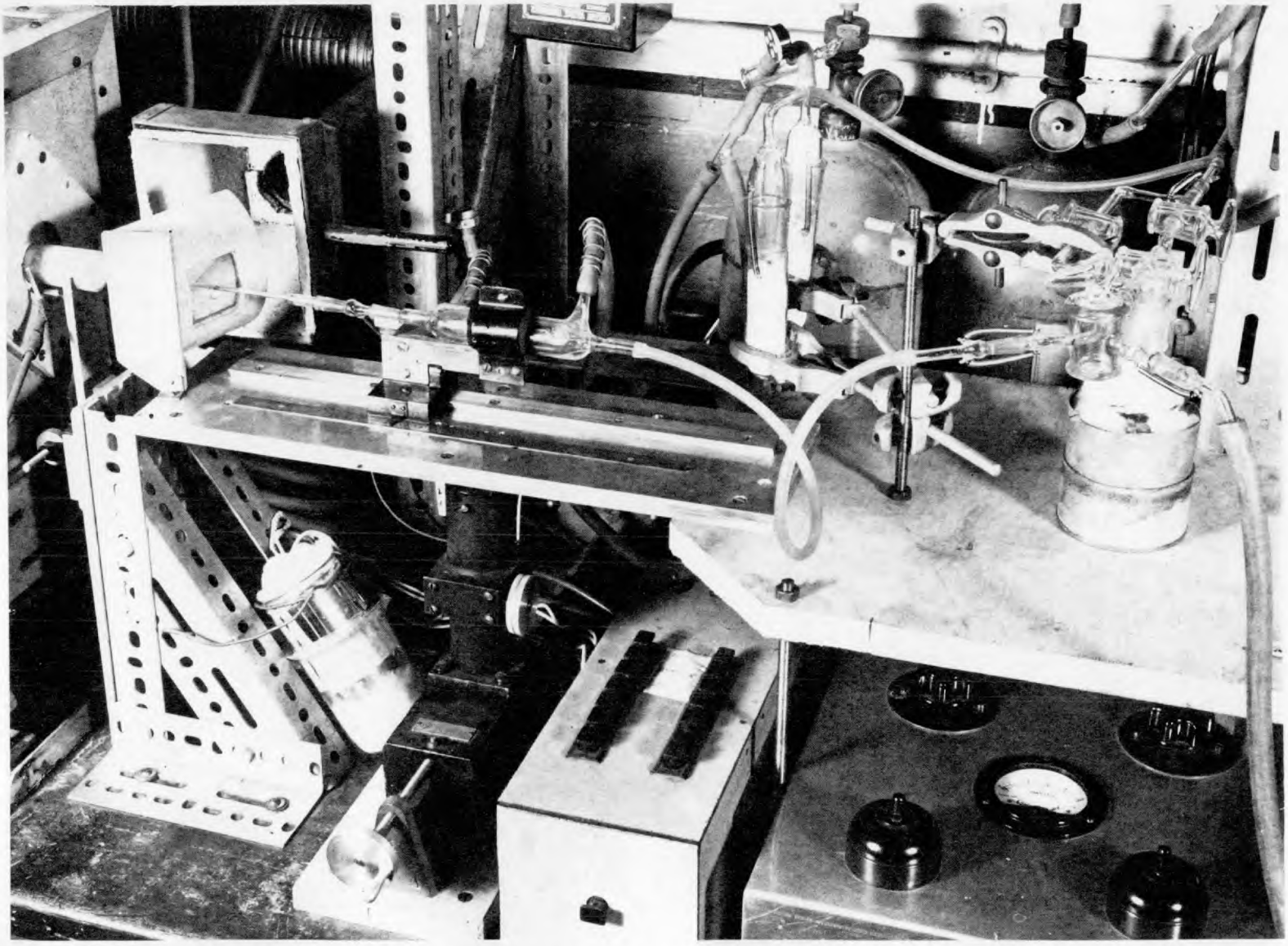

FIG. 2.11. PROBE MOUNTING AND PART OF ANALYSIS SYSTEM

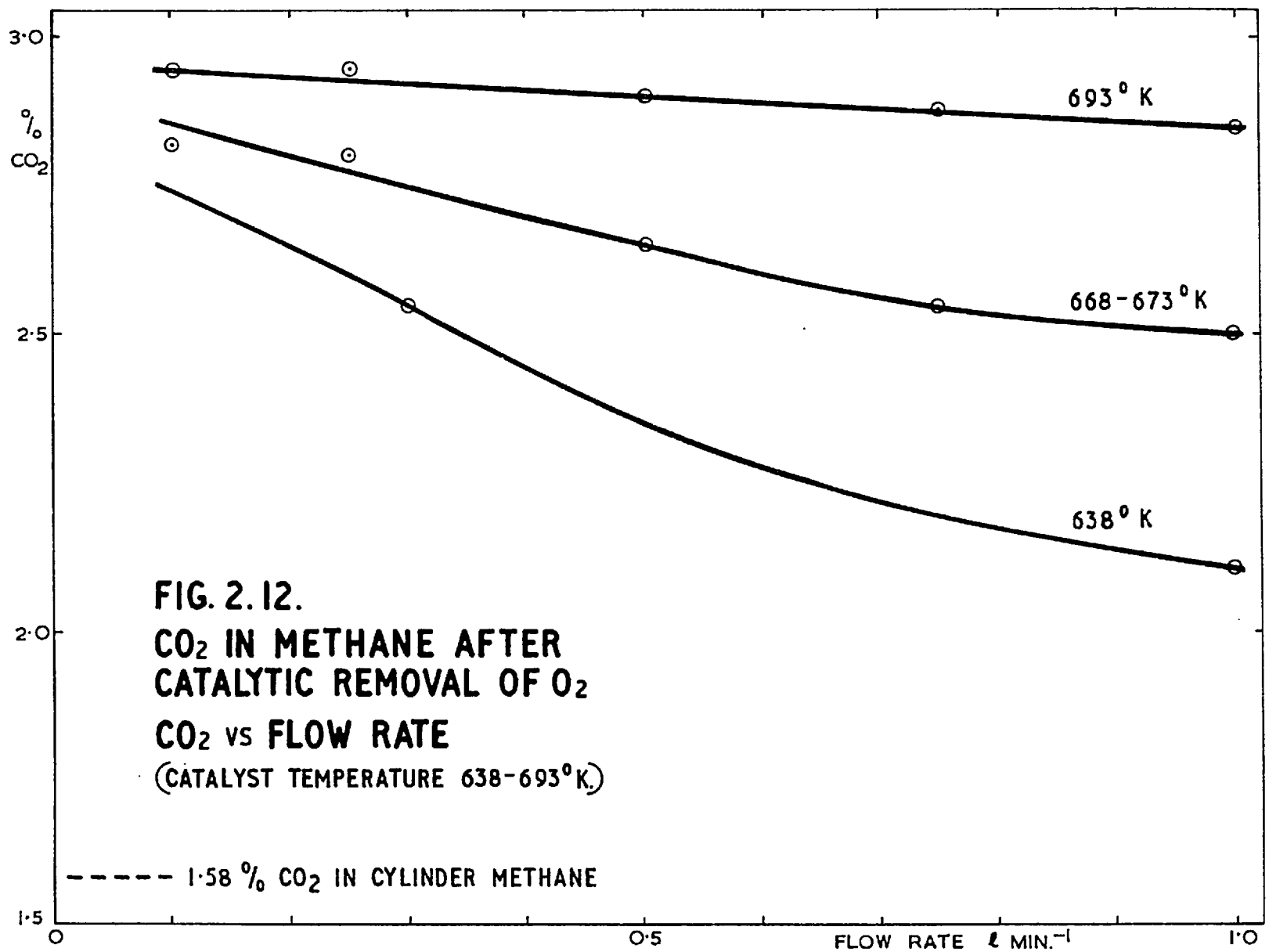
3·0
%
CO2
2·5
2·0
1·5
693° K
668-673° K
638° K
0
0·5
1·0
FLOW RATE ℓ MIN.⁻¹
FIG. 2.12.
CO2 IN METHANE AFTER CATALYTIC REMOVAL OF O2
CO2 vs FLOW RATE
(CATALYST TEMPERATURE 638-693°K.)
1·58 % CO2 IN CYLINDER METHANE

CHAPTER 3

The Apparatus (2)

Mixing and sampling

3.1 Introduction

As already indicated in Chapter 1 the success of the present method of studying high temperature reactions is largely dependent on a sufficiently detailed knowledge of (i) the mixing process and (ii) the effect of probing the reaction zone.

It was evident from the work of Egerton and Ray[35] that these two aspects needed thorough investigation. In the present experiments this became the more urgent for the mixing process as it was necessary, in order that more detailed sampling might be accomplished, to use a reaction tube of greater diameter than any used by Meads, Hirsch or Ray.

Part I - Mixing

3.2 Some theoretical considerations

Separate preheating is necessary to avoid pre-reaction and it can readily be appreciated that instantaneous mixing at the required high temperature is very desirable. However instantaneous mixing is not possible in practice. Further, for detailed kinetic studies laminar flow is much to be preferred. Rapid mixing can be achieved using a swirler at the end of the methane inlet, as was done by Ray[35], or by inducing turbulence, but this inevitably imparts a non-axial or random component to the gas flow - which is undesirable. The two

requirements, very rapid mixing and laminar flow, are thus seen to be mutually exclusive. Before proceeding further it seems appropriate, therefore, to examine the question: Is rapid mixing necessary?

Apart from complicating the analysis of any kinetic measurements, large concentration gradients at these temperatures at appreciable distances from the inlet (distances comparable to, or greater than, the 'induction period' - remembering that time is measured as a distance in these experiments) have been shown experimentally (see Chapter 4) to cause flashback and subsequent combustion as a series of diffusion flames on the inlet ports. The earliest possible uniform concentration profile is therefore required, preferably attained before the end of the induction period. For the subsequent analysis of the gas stream it is preferable that this mixing should occur in laminar flow. In practice, as will be discussed in Section 3.3 with some examples of such profiles in Chapter 4, it is not so easy to achieve the required uniform velocity profile across the inlet section using an inlet configuration favouring laminar flow. In fact, inlet designs likely to give laminar flow invariably resulted in more or less asymmetrical concentration and velocity distributions across the reaction zone. Hence compromise designs of the inlet were unavoidable, and these resulted in considerable induced turbulence. The intensity of this turbulence was not appreciated until the results had been fairly extensively analysed (see Chapters 5 and 6). The results of some calculations on the mixing problem are given below, based on an assumed

laminar flow. They are justified by the fact that they illustrate the type of calculations necessary before an inlet can be designed and because they result in a mixing length which will be an upper limit value.

From Fick's first law[81]

$$F = -D \frac{\partial c}{\partial x} \qquad \ldots 3.1$$

where F is the rate of transfer of diffusing substance through unit area.

D is the molecular diffusion coefficient

and $\frac{\partial c}{\partial x}$ is the concentration gradient.

Supposing that D may be considered constant - approximately true for small concentration and temperature gradients - the differential equation for diffusion in a cylinder may be written as

$$\frac{\partial c}{\partial t} = \left\{ \frac{1}{r} \frac{\partial}{\partial r} \left(r D \frac{\partial c}{\partial r} \right) + \frac{\partial}{\partial \theta} \left(\frac{D}{r} \frac{\partial c}{\partial \theta} \right) + \frac{\partial}{\partial z} \left(r D \frac{\partial c}{\partial z} \right) \right\} \qquad \ldots. 3.2$$

For the case where concentration is a function of radius and time only, i.e., neglecting the axial component, Equation 3.2 reduces to

$$\frac{\partial c}{\partial t} = \frac{1}{r} \frac{\partial}{\partial r} \left(r D \frac{\partial c}{\partial r} \right) \qquad \ldots. 3.3$$

We may consider the problem of an inlet as that of an instantaneous cylindrical source, with the diffusing substance distributed initially uniformly throughout a cylindrical element of length ∂z, of radius a, with concentration c_o, such that the general solution of Equation 3.3 is given by[82]

$$c = \frac{c_o}{2Dt} \exp^{\frac{-r^2}{4Dt}} \int_o^a \exp^{\frac{-r'^2}{4Dt}} I_o \left(\frac{rr'}{2Dt}\right) r' \, dr' \qquad \ldots. 3.4$$

where the integral must be evaluated numerically, I_o being the Bessel function of second kind of order zero. On the axis, the solution of Equation 3.3 becomes

$$c = c_o \left(1 - \exp^{\frac{-a^2}{4Dt}}\right) \qquad \ldots. 3.5$$

a solution which may also be considered approximately true for points sufficiently close to the axis, the region in which we are interested. But we are concerned with the case where diffusion takes place between two coaxial cylinders flowing in the z-direction with velocity v. Now if v_z is constant and equals v (say), which can be justified for equality of linear velocities of fuel and air streams and small temperature gradients, we may write

$$t = \frac{z}{v} \qquad \ldots. 3.6$$

and substituting from Equation 3.6 into Equation 3.5 we arrive at the solution

$$c = c_o \left(1 - e^{\frac{-a^2 v}{4Dz}}\right) \qquad \ldots. 3.7$$

from which

$$z = - \frac{a^2 v}{4D \, \ln\left(1 - \frac{c_z}{c_o}\right)} \qquad \ldots. 3.8$$

Since $\frac{c_z}{c_o}$ is a small fraction in the present case ($\sim\frac{1}{100}$th) the first

term of the logarithmic expansion is adequate and Equation 3.8 reduces to

$$z = \frac{c_o a^2 v}{4 D c_z} \qquad \ldots\ldots 3.9$$

The values of D, the binary diffusion coefficient, which must be substituted in Equation 3.9 may be obtained from the relation

$$D_{1,2} = \frac{\text{const} \sqrt{M_A + M_B / 2 M_A M_B}}{p \sigma_{12}^2 \Omega_{12}^{(1,1)*}(T^*)}$$

using the values for the const., σ_{12}, and $\Omega_{12}^{(1,1)*}(T^*)$ given in Reference 83, M_A is taken to be the molecular weight of air and M_B that of methane. But it can be shown (Appendix 3A) that it is unnecessary to use calculated values of D in the present case. It is probably more satisfactory to utilise the recently measured diffusion coefficients for the methane/oxygen system in the temperature range 300 to 1000°K[84] extrapolated to the temperature range of interest (~ 1200°K).

Using these data, relation 3.9 will be used in two ways:-

(i) To calculate the length z to achieve c_z = 1 per cent for various values of 'a' for a single inlet port.

(ii) From the results of (i) to select the most convenient (z,a) combination and calculate the number of inlet ports, nA, required, assuming a simple additive law. Assuming, that is, that a multiple inlet can be treated as the sum of a number of single inlet 'stream tubes', as done by e.g., Longwell and Weiss[85].

Thus, from the initial requirement that

$$\left(\frac{\pi a^2 v}{\pi r^2 v} = c_z \right)_{\lim_{z \to \infty}}$$

where πr^2 is the cross-sectional area of a single 'stream tube'; and the fact that

$$n = \frac{1}{\pi r^2} \qquad \text{inlets per cm}^2 \text{ of reaction tube cross-section,}$$

we have nA as the total number of inlets required to give 1 per cent mixture $\left(\frac{c_z}{c_o} = \frac{1}{100}\right)$ at a distance of z cm dowmstream from the mixing point (A is the reaction tube area).

Some typical values of z, a, n are given in Table 3.1, where v is given the value 1000 cm/s for the purposes of calculation. In making the selection of the most suitable z, a, n the following factors were taken into consideration.

(1) For the mixing length to be as small as possible a large number of inlets are required.

(2) For ease of construction the number of inlets needs to be as small as possible.

(3) Symmetry requirements give n certain preferred values, and

(4) 'a' must be such that the linear velocities of fuel and oxidant at the mixing point are approximately equal.

In the light of these considerations 5 inlets per cm^2 of cross-section was chosen as most suitable, requiring a total of 20 inlets.

Symmetry requirements modified this number slightly - to 19 in the case of the final model of the inlet.

3.3 Practical inlets constructed

Four different models of the inlet were constructed and for each one the mixing characteristics, rigidity, and stability over a period of time, were determined experimentally. Of the four, three proved unsatisfactory and will be mentioned briefly to demonstrate the evolution of the final model and the practical difficulties which had to be overcome. Some typical mixing profiles for the various models are shown in Figure 3.1.

Model A was constructed from 24 silica tubes of suitable diameter, of which 23 carried methane, arranged in three concentric rings of 1, 8, 15 with the heating coil wound on the central tube, then around the inner ring and finally forming the outer cover to the bundle. For satisfactory preheating the majority of the heating wire was at the 'cold' end of the bundle. The bundle was mounted in the reaction tube and the various connections made through an adaptor. Initially this model worked tolerably well, giving mixing profiles better than those obtained by Ray[35], but subsequently the flow pattern became progressively worse. This was shown to be caused by (i) the bundle 'settling down' within the reaction tube and (ii) the heating wires (Kanthal A) becoming brittle at the hot end, causing a variation in the day-to-day flow pattern attributable to small movements of the bundle over and above the 'settling down' tendency. For these reasons it was decided to avoid using the heating wires as a means of supporting the bundle.

Model B was constructed, by suitable re-choice of silica tubing, so that the bundle was a good fit in the reaction tube without any support apart from the confining influence of the reaction tube itself. In this model the heating elements were carried in twin bore silica tubes which ended some distance short of the mixing point. Additional spacing tubes were also included. This model, at its best, never gave much better mixing profiles than model A, but on the other hand was more stable over a period of time. It did suffer from a number of disadvantages, none-the-less, which included (i) an uneven velocity profile, due partly to the vacant space at the ends of the shorter heating elements and partly to a slight and unavoidable asymmetry in the arrangement of the bundle occasioned by imperfections in the straightness and small variations in the diameters of the silica tubes. (Precision tubing was not available in silica at the time.) (ii) Daily heating and cooling produced small changes in the relative positions of the tubes with consequent uncertainty in the downstream conditions. Model B was reluctantly discarded in favour of a more elaborate design.

Model C, the prototype of the model finally adopted, was constructed so as to overcome the two basic faults of model B. A silica sheath was chosen to give the best possible fit in the inlet end of the reaction tube. Into this sheath was constructed, with the help of a variety of jigs and specialised tools, a bundle of 19 inlet tubes and 91 short spacing tubes, the latter being attached in 'bundles' of 3 to 5 to the inlet tubes, at the mixing point end, by fine platinum wires and

silica 'hooks' on the inlet tubes. No support was provided in the sheath except at either end (a perforated ebonite disc was employed at the cold end). Not surprisingly the central sections of the inlet tubes, together with the twin bore heating tubes, were found to sag when heated in the furnace. In consequence poor mixing and velocity profiles were obtained downstream in the reaction zone. It was thought, however, from the nature of the velocity distribution obtained, that the flow was nearly laminar.

The next modification incorporated three platinum discs to act as supports in the central portion of the inlet sheath. A thermocouple was also added in this design, the junction situated just upstream of the 91 short spacer tubes. Considerable difficulty was encountered in the reconstruction of the inlet incorporating these additions. In particular it was found that the spacing tubes, which had given a close fit in the sheath when new had become brittle and enlarged due to some devitrification, and were no longer easily manipulated into position.

Although a number of other means of retaining the inlet bundle in the sheath were considered - these varied from sintering the ends together after a sufficient number of spacing elements had been placed in position, to fusing a mesh of fine silica strands across the end of the sheath - it was evident that this model had drawbacks of a constructional character. It would evidently be very difficult to repair or replace the various parts. However, the basic idea was considered to

be sound and hence the next, and final, model incorporated these ideas.

Model D had a fourth platinum disc in place of the 91 spacing tubes. This gave rise to a number of additional refinements compared with previous models and allowed more precise control of the air flow near the mixing point than had been achieved hitherto. The introduction of this platinum disc was a compromise. It would inevitably impart some turbulence to the flow, although the full extent of this contribution was only appreciated in retrospect.

To ensure a uniform velocity profile downstream of the inlet it was necessary to calculate the size, number and disposition of the perforations in the end platinum disc for the airflow. Some approximate calculations sufficed in this respect.

From orifice theory it can be shown that

$$m \approx A\sqrt{2\rho\Delta p_o} \qquad \ldots\ 3.11$$

where m is the mass flow rate, Δp_o the pressure drop across the orifice and A the orifice area. This relation holds where $\Delta p_o \ll p_o$ the total pressure, and A << area of the surrounding tube assuming a discharge coefficient of unity. The pitot pressure is given by the Bernouilli relation for an inviscid, incompressible fluid

$$p = \tfrac{1}{2}\rho v^2$$

For a typical set of experimental conditions (linear air velocity 1000 cms^{-1} at 1173°K) p ~1.3 mmH_2O gauge. If it is considered that

a value for Δp_o equal to 100 p is sufficient to smooth any non-uniformity in the velocity profile as the flow passes through the disc, then the total area occupied by the perforations in the disc must be given by Equation 3.11 knowing m, Δp_o(= 100 p) and ρ..

This gives a value of 0.4 cm^2 for the area occupied by perforation, and a linear air velocity through the perforations of 10^4 cm/s. This value is acceptable as it falls below sonic velocity at 1173°K. It might be argued that uniformity would be best achieved by making all the orifices sonic, but this would involve an unduly high pressure strain on the end disc and was therefore avoided. Selecting 1 mm as the perforation diameter, and taking account of symmetry requirements and disposition of the methane inlets, the most suitable number of perforations is 40. A sketch of this platinum disc is shown in Figure 3.2.

The effectiveness of the platinum disc in producing a uniform airflow was tested experimentally at room temperature. All holes apart from those intended to act as air passages were plugged with plasticine. With the disc fixed in its normal position at the end of the inlet sheath, and with an air mass flow rate identical with that occurring under furnace conditions, the flow rate through a number of the holes at different radial positions was determined. This was done by accurately positioning a 1 mm diameter hypodermic pitot tube 2 to 5 mm downstream from each hole under test. Maximum variation in pitot pressure recorded was less than 1 per cent. This was considered satisfactory confirmation of the effectiveness of the platinum disc as a matrix to the airflow.

Figure 2.5 shows the other essential features in the construction of this model of the inlet, while Figure 3.3 illustrates the set-up at the upstream end. The whole unit could be easily withdrawn for inspection - an essential feature - and all parts were either repairable or replaceable without totally dismantling the unit. Each methane carrying tube was held in the perforated ebonite disc at the upstream end with a high temperature rubber composition (Multi-lock BC 14/1 from National Adhesives Ltd.) which was readily soluble in methyl ethyl ketone. Although one of the original reasons for fusing short lengths of very fine silica tubing (from a single uniform length) to the downstream end of each inlet had been to serve as flow equalisers, it was found that there was always a small degree of constriction at the join between each 'inlet port' and delivery tube, causing an uneven methane distribution downstream. For this reason it was necessary to control the flow to the methane delivery tubes individually. This was achieved by placing a plastic burette tap in the upstream section of each methane flow line, outside the furnace, as illustrated in Figure 3.3. It was shown experimentally that equality of flow through the individual inlets could be maintained for all required flows and temperature conditions in the furnace when the pressure drop across the control taps was large compared with that across any constriction downstream. Retaining the final platinum disc in position presented something of a problem. A number of solutions were attempted, the one finally adopted consisted of a retaining ring fused to the central methane delivery tube which held the disc

against a seating - valve fashion - at the end of the inlet sheath, while at the opposite end the central delivery tube was held under slight tension by a spring. A small expansion gap was left around the edge of the disc and this was lightly filled with Alundum cement to prevent air leakage. Too heavy an application of this cement resulted in a fractured sheath on heating in the furnace.

This form of the inlet gave extremely good velocity and mixing profiles (Figure 3.1 and all profiles from Chapter 5 onwards). Its stability with time and day-to-day reproducibility were also of a high order, the limiting factor being the occasional need to check and adjust the burette taps in the methane lines. After considerable usage - circa 50 6-hour runs at 1173°K - the downstream end became rather brittle and difficult to repair, thus limiting the useful life of the inlet.

Part II - Sampling

A brief description of the probes and their use has been given in the previous chapter. Before proceeding to a more detailed account an assessment of probe techniques must be attempted; in particular their application to the present investigation and questions of interpretation and validity will be considered.

3.4 Guiding principles

Some consideration was given to the methods by which the parameters might be measured. The speed of the reaction to be studied,

coupled with the high temperatures in the reaction space and unavoidably long distances (to minimise flow disturbances) at relatively high temperature over which any measurement must be accomplished, severely limited the choice. It was evident at the outset that no single physical (or chemical) characteristic would adequately describe the state of the reacting gases without some à priori assumptions concerning the velocity distribution, heat transfer, and mechanism of the oxidation. No method on this basis was attempted.

Any valid assessment of the detailed kinetics and heat release rates in the reaction zone requires precise measurement of a number of parameters. In studies of the present type, employing a flow system under non-isothermal conditions, where not only temperature, but also concentration and velocity gradients occur, it is obviously necessary to know the point to point variation of species, velocity and temperature. An important consideration is the desirability of an instantaneous record of all the required parameters at sufficient points to characterise the reaction for any given set of experimental conditions. In the present case the ideal cannot be realised, for reasons which will become apparent later, but should nevertheless act as a guide in the choice and development of measuring techniques.

Although some detailed sampling studies have recently been made of flames at atmospheric and sub-atmospheric pressures[2-4,86,87], no attempt has been made to study high temperature flow reactions (as distinct from flames) in this detailed manner. Hitherto such detailed

studies have either been unnecessary[22,30,31], where isothermal conditions were maintained in small bore tubes, or impracticable[35]. Various sampling studies in industrial scale furnaces (as at the International Flame Research Centre, Ijmuiden), rocket nozzles[88], gas turbines and ramjets[89] have generally been either less detailed or unrelated to the present problem. Similar remarks apply to the various specialised sampling techniques employed in ion-extraction from flames[90,91] and other mass spectrometric studies[59].

In the present work attempts have been made to determine (i) the point values of gas stream velocity, temperature and composition (for the stable species methane, carbon monoxide and carbon dioxide) and (ii) a more detailed composition analysis (including hydrogen, formaldehyde and hydrogen peroxide) without such detailed knowledge of gas stream velocity and temperature. We may conclude that simultaneous measurement of the three parameters (velocity, temperature, composition) at all points in a furnace reaction space is impracticable. A plot of these parameters at a sufficient number of points is intrinsically possible and will not differ from the instantaneous record provided the furnace conditions can be held steady enough for long enough. The practical compromise involved the simultaneous measurement of the three parameters at any given point, with a sequence of such determinations forming a run.

Temperature was measured with a shielded thermocouple, gas stream velocity was determined from the total-head and static pressures, and composition was determined from a withdrawn sample.

3.5 The effects of probing

It is abundantly evident that any interfering method, such as probing, of analysing a reacting system must perturb that system. The question of the interpretation of such measurements therefore arises. The following is an attempt to answer this question in the present case. Relevance to either cooled or uncooled probes, or both, will be evident from the context.

In the somewhat different circumstances encountered in flame structure studies this problem has received critical attention in the recent literature[92,93] and is reviewed, with extensive references, by Fristrom in 104; but nothing* has appeared directly related to the present problem, although with a difference of emphasis similar considerations will be found to apply.

3.5.1 The effect of the probe on the reaction

(i) Aerodynamic effects

There are two basic effects to be considered here, one due to the probe geometry, the other related to the rate of sample withdrawal.

The geometric effects may be further classified as internal and external. The internal geometry determines the efficiency with which the sample is quenched (quenching refers to the process of stopping the reaction - in the sample - by lowering the pressure and temperature by expansion). This will be discussed later. The external geometry

*An attempt to survey the whole field of gas sampling (including the present situation) has recently been published [94].

determines the perturbation of the flow passing the probe. It will be appreciated that the two geometric requirements are opposed, and compromise designs must be employed. For minimum disturbance to the flow in the reaction zone the probe must be introduced along the streamlines. Because of the magnitude of the linear velocities to be employed wake effects preclude probe insertion from the upstream direction (quite apart from constructional considerations). The external dimensions of the probe are such as to occupy the cross-sectional area of the stream-tube vacated by the sample, (giving so-called iso-kinetic sampling) which again serves to minimise the disturbing effects. The upstream distortion of the flow caused by the sample withdrawal can be approximately estimated. Assuming a point sink model[93], and spherically symmetrical perturbation of the surrounding flow, the locus of 10 per cent distortion of the flow can be shown to occur at ~1.1 mm from the probe tip in the present case for typical sampling conditions. This is comparable with the positional accuracy in the axial direction (~1 mm) and it will be a constant error. The 'effective' sampling point will obviously be much nearer the probe tip than the 10 per cent perturbation locus. More elaborate models have been proposed[93,95] with particular reference to flames, but are unnecessary for the present purpose.

(ii) Thermal and diffusional effects

The probe may alter the heat flux in the sample region. It may also affect the diffusion of reactive species. With gas and furnace wall temperatures at any cross-section never differing by more than

100°K, it is unlikely that the probe tip temperature will differ significantly from the gas temperature and consequently the effect on the heat flux will be negligible. The low thermal conductivity of silica means very small errors due to conduction.

The question of diffusional transfer will only arise in a concentration gradient. It has been discussed at length for the gradients occurring in flames[93], where it has been shown that the probe samples a 'true' composition of the mixture at the sampling point (to a very close approximation) and does not measure the total flux (due to diffusion and convection) of each species through a cross section. In the present work, where concentration gradients are very much smaller, the problem becomes trivial.

(iii) Catalytic effects

Clean silica is noted for its lack of catalytic activity in flames. We can expect what effect there is to be reduced under the present conditions. For the water-cooled sampler (considered in more detail later) which will be at a considerably lower temperature than the gas, the effect will be one of quenching (or negative catalysis). The effect can only be transmitted into the upstream sampling region by species diffusion and heat transfer through the gas. Because of the high gas stream velocities the effect will be small for laminar flow and only noticeable for very short distances upstream. In the presence of considerable turbulence the picture is not so clear, but providing the sampling is iso-kinetic, cannot be appreciable.

3.5.2 The interpretation of the sample taken

Many of the factors involved here are implicit in the previous discussion. Three additional factors must be considered.

(i) Quenching

This depends on the history of the sample after entering the probe. The present problem, mainly from the necessity of bringing the sample through a considerable length of hot probe, differs considerably in this respect from those considered in the literature. The best method of quenching is to rely on a rapid adiabatic expansion inducing a steep downward temperature and pressure gradient. Surface chilling will help. Neither of these possibilities is completely realisable in the present investigation. However the half-life of the reaction (~20 to 30 milliseconds) is large compared with that encountered in most flames and rapid withdrawal aided by shallow pressure and temperature gradients has been adequate. (Under some extreme conditions in the present work, where annular flow is used in the sampling probe, some reaction does occur in the sample - see Chapters4 and 5.) Maximum use of the pressure gradient is made by careful shaping of the probe tip. The statement "rapid withdrawal ..... has been adequate", above, was deliberate, since neither internal kinetic heating nor conduction through the probe wall are necessarily negligible in a long narrow tube passing through a considerable length of hot gas.

(ii) Wall reaction

There will obviously be some reaction in the slow moving boundary layer in the probe. There does not seem to be any very suitable way of overcoming this (except by using a cooled sampler, which has other drawbacks). The error introduced will probably be small however. (e.g., Reference 92, where the error introduced into the analysis when the exterior of the probe was heated to the flame temperature was shown to be less than 3 per cent).

(iii) Radicals

If radical concentrations are assumed to have their equilibrium values, their contribution, via continuing chains in the sample, will be negligible[13]. [Even if their concentrations are greater than equilibrium predictions, their contributions are probably still negligible[13].]

3.5.3 Interpretation of the temperature measured

The majority of the gas-stream temperature measurements were made using a covered thermocouple in the probe, functioning as a suction pyrometer.

Two factors must be considered:-

(i) Radiation correction

This will be negligible in the present work where wall temperature, gas-stream temperature and probe-tip temperature never differ by more than 100°K at any particular cross-section.

(ii) Correction for axial displacement of the thermocouple junction

This is peculiar to the probe design employed. Since the thermocouple junction is situated about 2 cm downstream from the probe tip,

the relationship between the temperature recorded at this position and the temperature of the incoming gas at the probe tip had to be investigated. For a particular experimental condition the temperature was recorded. Withdrawal of the sample was then discontinued and a temperature versus time plot obtained. After initially rising a degree or two (due, most probably, to residual reaction in the probe) the temperature as recorded by the probe thermocouple fell about 5°K and then remained constant. Repositioning the probe to align the probe tip with the position previously held by the thermocouple junction, and re-applying the withdrawal suction, the temperature registered was the constant value previously achieved without withdrawal ($\pm\frac{1}{2}$°K). It was concluded that the gas sample temperature was being satisfactorily measured, with an accuracy of ±1°K.

3.5.4 Interpretation of the gas stream pitot and static pressures[79]

The basic assumptions affecting the use of pitot-static probes in the present context are:-

(i) that the pitot pressure is a measure of the time-mean velocity component in the direction of the probe axis. For the special case of laminar flow, with no swirl or radial component, the pitot pressure is a measure of the total gas velocity in the stream-tube. From subsequent analysis (Chapter 5) it is evident that both small radial and turbulent components are present. However the integrated mass flow rates, as measured at the beginning and end of the reaction space agreed

with the flow rate as measured on the flowmeters to within the experimental error of the method (see Chapter 5).

(ii) that the pitot pressure measured in a velocity gradient is the arithmetic mean of the total-head pressure in the area occupied by the pitot tube, less the static pressure at that cross-section. This may be considered correct to a good approximation for the gradients occurring in the present work.

(iii) that the pitot-static system employed is satisfactory without calibration. This is true to better than present experimental accuracy (1 to 2 per cent).

(iv) that slight malalignment of the probe(s) with respect to the gas stream (up to 5^{o}) will not alter the pitot-static reading.

(v) that the reacting gases may be treated as inviscid and incompressible and hence the first term of the Bernouilli equation is adequate to describe the system,

i.e., $$p = \tfrac{1}{2}\rho v^2$$

where p is the total-head/static difference, ρ and v are the density and gas stream velocity respectively, at a particular station.

Finally, to obtain the best radial velocity profiles, it is necessary to determine the total-head pressure at 0.026d from the wall, where d is the reaction tube diameter. This was impracticable; in any case the error introduced by neglecting this requirement is small compared with other errors.

The accuracy of the pitot measurements is difficult to assess. Results indicate an accuracy of 1 to 2 per cent at the reaction tube centre for time-mean gas velocities of 1000 cm s^{-1} at 1173°K. Proportionately less accuracy is achieved in slower flows and close to the wall.

3.6 Practical development

Brief descriptions and discussions of a number of different probes are given; the composite probe used to obtain the heat release rate data described in Chapters 5 to 7 is treated in more detail. Dimensions are as given in Table 2.1 or on the figures, while a flow diagram of the analysis line is given in Figure 2.4.

3.6.1 The water-cooled sampler (Figure 2.9)

This was made of Nimonic with a silver steel tip and manufactured by Joseph Lucas and Co. Ltd. Water was pumped between the outer annuli at a rate sufficient to keep the temperature difference between the inlet and outlet water less than 10°K (~300 cc min^{-1}). The coolant water was supplied at a line pressure of 300 p.s.i.a. by an Autometric Gear Pump GP$\frac{1}{4}$, having carbon bearing-cups, powered by a Griffon $\frac{1}{3}$ h.p. a.c. motor. The relatively small bore of the central tube limited the rate of sample withdrawal attainable to 200 to 250 cc min^{-1}. All sampling was achieved using diaphragm pumps to avoid contamination of the gas sample by oil vapour and/or selective absorption of the gases by the oil. Two types were employed, a Dymax Mark 1 made by Charles Austen Pumps Ltd., and an Autometric Diaphragm Pump made by

Autometric Pumps Ltd., the latter being considerably the more satisfactory.

3.6.2 Silica sampler

This was simply a small bore silica tube joined to a Quickfit B7 cone (silica) at one end and suitably shaped to extract a sample at the other. Various tip geometries were used, one with a V-shaped entry proving very satisfactory. Kay[35] had found that a sufficiently rapid extraction rate was maintained with a pressure gradient of $\sim\frac{1}{3}$ cm Hg/cm of probe length. Using similar dimensions of probe the pressure gradient was increased in the present work to ~1 cm Hg/cm of probe length without materially altering the composition (of stable species) of the sample withdrawn. This was taken as an indication that quenching was sufficient for the analysis of stable species. Samples withdrawn with silica probes were not used for unstable intermediate analyses.

3.6.3. Pitot and static probes (Figures 2.9 and 3.4)

Separate pitot and static probes were constructed. The technical difficulties involved in making a combined pitot-static probe of the required dimensions from silica tubing were greater than the situation warranted. It was shown that consecutive measurement of the total-head and static pressure was sufficiently accurate.

The static probe was of silica tubing with a hemispherical tip. On a circumference at ten diameters from the tip three equally spaced, 10 thou holes were drilled through the wall.

The first model of the pitot tube was made to allow measurement at 0.026d from the wall, but this gave an unduly long response time (due to the smallness of the tip) and was modified to give a pitot head of o.d. 2 mm, i.d. 1 mm. These tip dimensions were retained in the final model of the composite probe. The response time was reduced to approximately 1 minute.

Pressure measurements were made on a 13 in. Chattock manometer, having a relative sensitivity of 0.0002 in. water (equivalent to a linear air velocity of 17 cm/s at 1173°K). A full description of the construction and use of the Chattock manometer is given in Reference 79.

3.6.4 Temperature probes (Figure 3.4)

All five models consisted of some form of covered Pt/Pt 13 per cent Rh thermocouple. The first (1) was a suction pyrometer with the thermocouple junction held against a constriction in the probe tip. One lead passed through the bore of the tube, the other being wound around the outside in a long spiral of two or three turns. The junction and the first 6 to 8 cm of the leads had been sputtered with silica using a vacuum technique. The silica coating was found to be easily damaged mechanically and the recorded temperatures unreliable in consequence.

The second model (2) was completely enclosed. It had the thermocouple junction housed in a short length of fine silica tubing (<1 mm o.d., 0.5 mm bore) abutted to a stouter silica tube. In the fine tubing electrical insulation between the leads was provided by

thin strips of mica, in the stouter tube by enclosing one lead in a fine tube. This arrangement proved quite effective, with no noticeable delay in response on rapidly changing the temperature conditions. The remaining three models were incorporated in the three composite (= multipurpose) probes.

3.6.5 Composite probes (Figures 2.9 and 3.4)

(1) The first attempt involved ultrasonic drilling for 2 to 3 mm along the axis of a twin bore silica tube, abutting a short length of single bore tubing to this, drawing the end down and breaking at the appropriate diameter, leaving the probe tip to serve for both pitot tube and composition sampling. The thermocouple junction was situated in the wider cavity at the end of the twin bores down which the thermocouple leads were passed. These were coated with silica in a flame[96]. The coating was applied by holding the thermocouple leads in a flame to which a small percentage of a vaporised organo-silicon compound has been added via the fuel supply. In the present case silane was used. Unfortunately the thermocouple could not be satisfactorily mounted in the probe without mechanically damaging the coating, as shown up in subsequent trials. [Some American workers have had access to ceramic coated thermocouples (coated with N.B.S. Ceramic A-418)[3], but no such materials were known to be available at the time in this country[97].]

(2) The next composite probe reverted to a single bore sampling-plus-pitot tube, to which was 'strapped' a looped length of fine silica tubing containing the thermocouple junction at the extre-

mity of the loop. The 'strapping' consisted of three loops of silica by which the fine tubing was held alongside the stouter single bore tube. Although this model was intended as a temporary expedient it was relatively satisfactory in use, despite its cumbersome nature.

(3) Final form of composite probe (Figure 2.9)

The final form of the composite probe was a compromise. It can be shown (Appendix 3B) that in annular flow an optimum occurs in the relation between mean gas stream velocity and annulus area for a given pressure gradient because of the upper limit imposed on the sample withdrawal rate (see next chapter). The mean gas stream velocity is also a function of the ratio $\frac{r_1}{r_2 - r_1}$, where r_1 is the radius of the inner cylinder, and r_2 that of the outer cylinder. The maximum occurs when $r_1 = 0$ (i.e., for a pipe). From these considerations it was seen that adequate sampling velocities could be maintained in annular flow with appropriate selection of the variables. Thus with the thermocouple completely enclosed in a central tube of minimum diameter, the radius of the other wall of the annulus was calculated for optimum sampling conditions and the composite probe constructed accordingly. Into the central tube the thermocouple and leads were inserted, one lead being insulated by 3 in. lengths of quartz 'X-ray' tubing (0.19 to 0.32 mm o.d., 0.15 to 0.25 mm bore). The closure at the tip of the central tube was kept as thin as possible, and the thermocouple junction rested against it. The central tube was carefully mounted in the bore of the probe and suitable connections made to the thermocouple

through a side-arm. This probe proved to have certain limitations (see succeeding chapters) and a preliminary theoretical investigation of an alternative means of temperature measurement was carried out (Appendix 3C). It is designed to measure density variation as indicated by flow through a sonic orifice. A similar method has been reported in the literature under the name 'pneumatic probe'[98]. The time available did not allow the development of a 'sonic probe' for the present work. Such a device, with suitable calibration, should be capable of measuring temperature, velocity and composition consecutively.

APPENDIX 3A

Thermal conductivities and diffusion coefficients

1 Thermal conductivity

The error introduced by using thermal conductivity data for pure nitrogen throughout this work is approximately $\frac{1}{2}$ per cent (calculated for the case 1 per cent methane/nitrogen → 1 per cent CO_2 + 2 per cent H_2O/nitrogen at 1200°K. [In view of this an experimental value for nitrogen at 1200°K has been used. It is $\lambda_{N_2} = 1700 \times 10^{-7}$ from Reference 120].

The appropriate values for the conductivities are

$$\lambda_{CH_4} = 1360 \times 10^{-7} \ (1200^{\circ}K) \text{ cal cm}^{-1}\text{s}^{-1}\text{deg}^{-1}$$

$$\lambda_{CO_2} = 733 \times 10^{-7}$$

$$\lambda_{N_2} = 1214 \times 10^{-7}$$

$$\lambda_{N_2\ H_2O\ (2\ \text{per cent})} = 1230 \times 10^{-7}$$

These values have been calculated using the approximate expression[83]:-

$$\lambda \times 10^{7} = 1989.1 \frac{\sqrt{T/M}}{\sigma^2 \Omega^{(2,2)^*}(T^*)}$$

where M is the molecular weight, σ the collision diameter, and $\Omega^{(2,2)^*}(T^*)$ the collision integral at reduced temperature T^*, where $T^* = T/\varepsilon/\kappa$. Values of σ, ε/κ and Ω were taken from Reference 83. Water was treated empirically.

Consider the extreme cases (i) 1 per cent methane and 99 per cent nitrogen and (ii) 1 per cent carbon dioxide, 2 per cent water and 97 per cent nitrogen, compared with (iii) nitrogen

$$\lambda(i) \sim 1216 \times 10^{-7} \text{ cal cm}^{-1} \text{ s}^{-1} \text{deg}^{-1}$$

$$\lambda(ii) \sim 1224 \times 10^{-7}$$

$$\lambda(iii) \sim 1214 \times 10^{-7}$$

These are obtained using the approximation[99]

$$\lambda_m \approx \left(\sum_{i=1}^{n} p_i \sqrt{\lambda_i} \right)^2$$

where p_i is the partial pressure of the i^{th} component. From the values so obtained it can be seen that the maximum difference from the case of nitrogen is 10^{-6} cal cm^{-1} s^{-1} deg^{-1} ($\sim\frac{1}{2}$ per cent).

2 Diffusion coefficients

Neglecting material transport due to thermal gradients (thermal diffusion), it will be shown that use of the experimental transport coefficients for the methane- and carbon dioxide-oxygen gas pairs[84] for the methane- and carbon dioxide-air systems at the temperatures of interest introduces negligible error.

The following calculations show the ratio $D_{i,O_2}/D_{i,air}$ at 1100°K based on viscosity data[83]. The method of argument involves the assumptions (i) that the gases involved are unlikely to show any anomalous behaviour in their transport coefficients at high temperatures, which seems reasonable[100]; (ii) that whereas the absolute values of $D_{1,2}$ as

calculated from viscosity data may be in error the ratios will lie in the right sense and will be a good indication of the error involved by accepting the measured values in oxygen rather than in air.

We have

$$D_{1,2} = 0.002628 \frac{\sqrt{T^3 (M_1 + M_2)/2M_1 M_2}}{p \sigma_{1,2}^2 \Omega_{1,2}^{(1,1)*} (T_{1,2}^*)}$$

for the diffusion of a trace of species 1 into species 2, where M is the molecular weight, T the absolute temperature, p the pressure, $\sigma_{1,2}$ the collision diameter and $\Omega_{1,2}^{(1,1)*}$ the collision integral for the reduced temperature $T_{1,2}^*$, where $T_{1,2}^* = T/\varepsilon_{1,2}/\kappa$. Values of the collision integral $\Omega_{1,2}^{(1,1)*}$ and the parameter $\varepsilon_{1,2}/\kappa$ are taken from Reference 83. Taking $\sigma_{1,2} = \frac{1}{2}(\sigma_1 + \sigma_2)$ the expression is used in the form

$$\frac{D_{i,O_2}}{D_{i,air}} \frac{\sqrt{M_i + M_{O_2}/2M_i M_{O_2}}}{\sqrt{M_i + M_{air}/2M_i M_{air}}} \cdot \frac{\sigma_{i,air}^2 \Omega_{i,air}^{(1,1)*} (T_{i,air}^*)}{\sigma_{i,O_2}^2 \Omega_{i,O_2}^{(1,1)*} (T_{i,O_2}^*)}$$

where $T_{1,2}^* = \frac{T}{\left(\varepsilon_1/\kappa \times \varepsilon_2/\kappa\right)^{\frac{1}{2}}}$ and tabulations based on the 12,6 potential function for the collision integral are used.

For T = 1100°K, calculation showed

(a) $\frac{D_{CH_4,O_2}}{D_{CH_4,air}} = 1.005$ i.e., $+\frac{1}{2}$ per cent

(b) $\frac{D_{CO_2,O_2}}{D_{CO_2,air}} = 0.979$ i.e., -2 per cent

from which it is evidently justifiable to use available experimental data for methane- and carbon dioxide-oxygen mixtures rather than the calculated date for air. Further, it can be seen to be preferable since[84]

$$\frac{(D_{CH_4,O_2})_{exptl}}{(D_{CH_4,O_2})_{theor}} = 1.027 \qquad \text{i.e., } \sim 3 \text{ per cent}$$

It may be noted that the ratio involving carbon monoxide will fall between cases (a) and (b) while the other intermediates have been found in such small concentrations as not to affect the overall picture.

APPENDIX 3B

Annular flow in the sampling probe

It has been shown[101] that for streamline flow the following relationships hold:-

(1) For flow between parallel plates

$$\bar{v}_{p.p.} = -\varphi \frac{d^2}{12\eta}$$

(2) For flow through an annulus

$$\bar{v}_a = -\varphi \frac{1}{8\eta} \left\{ r_2^2 + r_1^2 - \frac{r_2^2 - r_1^2}{\ell n\, r_2/r_1} \right\}$$

(3) For flow through a pipe

$$\bar{v}_p = -\varphi \frac{a^2}{8\eta}$$

where φ = pressure gradient, $\bar{v}$ = mean velocity, η = viscosity, d = separation of plates, r_1 = inner radius of annulus, r_2 = outer radius of annulus, and a = the pipe radius.

It may be noted that on writing $r_2 = r_1 + f$ and expanding, expression (2) reduces to the form of (1) when $(f/r)^2$ is small (say when $f/r < 0.2$). Thus when f is small compared with r the actual value of r is unimportant and the simpler expression (1) is adequate. Secondly, at the limit $r_1 \to 0$ expression (2) reduces to (3), as is to be expected.

At constant temperature the optimum value of the annulus area for a particular value of r_i is demonstrated in Figure 3.5(a), where $\bar{v}_a$ (calculated as $\bar{v}_{p.p.}$) is plotted versus (i) annulus area, with φ constant, (ii)annulus area, with volumetric flow rate constant (flow rate = annulus area $\times$ $\bar{v}_a$). The point of intersection of these curves gives the optimum annulus area for the chosen value of r_i.

If r_i is allowed to vary, the numerical value of the maximum $\bar{v}_a$ achieved, as demonstrated in Figure 3.5(a), will also vary, having a maximum for the case where $r_i = 0$, i.e., for pipe flow. Figure 3.5(b) shows this variation with annulus area and φ kept constant. This is a qualitative curve, numerical values may be calculated using expression (2). The two points calculated have been enumerated using expression (1) for r_i large and (3) for $r_i = 0$.

These curves demonstrate the importance of the various parameters in the design of a composite probe in which an annulus is used to convey the sample through the probe.

Curve 3.5(a)(i) is calculated from $\bar{v}_a = Kf^2$ where $K = 7.62 \times 10^5$ $cm^{-1} s^{-1}$. K was determined using experimental values of $\bar{v}_a$ and volumetric flow rate for a particular annulus area. Annulus area was calculated as

$$\text{Ann. area} = \pi(f^2 + 2r_i f)$$

where $r_i = 0.130$ cm.

APPENDIX 3C

A 'sonic' probe

It will be shown that, in principle, an orifice-tipped probe is capable of determining the three parameters gas stream velocity, temperature and composition provided the orifice is sonic. A sonic orifice may be defined as one having a pressure ratio $p_2/p_1 < 0.525$[79].

The velocity of sound in a gas is given by

$$v_s = \sqrt{\frac{\gamma p}{\rho}}$$

where the symbols have their usual meaning.

Evidently $v_s \propto \sqrt{\frac{1}{\rho}}$, but $T \propto \frac{1}{\rho}$, $\therefore v_s \propto T$.

For a sonic orifice, m the mass flow rate is given by

$$m = A\rho v_s$$

where A is the orifice area.

Hence $$m = A\rho\sqrt{\frac{\gamma p}{\rho}}$$

$$= A\sqrt{\gamma p \rho}$$

Differentiating

$$\frac{dm}{m} = \frac{dA}{A} + \frac{1}{2}\left(\frac{d\gamma}{\gamma} + \frac{dp}{p} + \frac{d\rho}{\rho}\right)$$

we want to be able to measure δm due to $\delta\rho(\propto -\delta T)$ in the presence of interfering effects from δA, $\delta\gamma$, δp (and also $\delta\rho$ from causes other

than temperature variation). Table 3C shows the results of considering the worst likely experimental conditions in the present apparatus. For practical purposes one may neglect 'temperature' changes due to items (1) to (3). Corrections for ambient pressure variation and composition may be calculated. Hence the method is feasible if m can be determined with an accuracy of (say) 2 parts in 10^4, since composition and total-head pressure may be determined by this probe in the normal manner.

Two methods of measuring m suggest themselves; (i) to time a pressure change downstream of the orifice due to the orifice 'leak', which would involve thermostatting a volume V (>>V' the volume of the probe and its connections) with an accuracy of 10^{-3}°K in order to achieve the necessary accuracy in the measurement of m, or (ii) the use of a second orifice downstream at a carefully controlled (and known) temperature, to measure the flow through the sonic orifice.

An experiment was performed on the basis of the second method with the following result. m changed ~18 per cent for 180°K variation at a mean temperature of 673°K. This gives ~0.1 per cent change in m per degree at 673°C, which is equivalent to ~0.04 per cent per degree at 1173°K. Provided the measurement of m can be achieved with sufficient accuracy, the most likely source of error would be ablation of the sonic orifice at the high temperatures used.

TABLE 3C

Item	Quantity considered	Cause of variation at 1173°K	% change in m	Apparent T change
1	A	100°K T change	$\sim 9 \times 10^{-3}$	$\frac{1}{5}$°K
2	γ	100°K T change	$\sim 5 \times 10^{-2}$	1°K
3	p	Total head press. (relative to ambient) 0 to 1500 cm/s	$\sim 2 \times 10^{-2}$	$\frac{1}{2}$°K
4	p	Ambient press.	-	~10°K/cm Hg
5	ρ	1 per cent comp. change	$\sim 1 \times 10^{-1}$	2°K
6	ρ	1°K rise at 1173°K	4.6×10^{-2}	1°K

TABLE 3.1

Typical values of a, n, z, A × n

(Using the values

$D_{methane/air} = 2.65\ cm^2 s^{-1}$ at 1200^oK

$v_z = 1000\ cm\ s^{-1}$

$A = 4.15\ cm^2$)

a Diameter of inlet ports (mm)	n No. ports per cm^2	z Mixing length (cm)	A × n Total No. inlets required
0.1	31.8	0.95	132
0.2	8.0	3.8	33.2
0.25	5.1	5.9	21.2
0.4	2.0	15.1	8.3
0.6	0.94	34.0	3.9
0.8	0.50	60.5	2.1
1.0	0.318	94.5	1.3

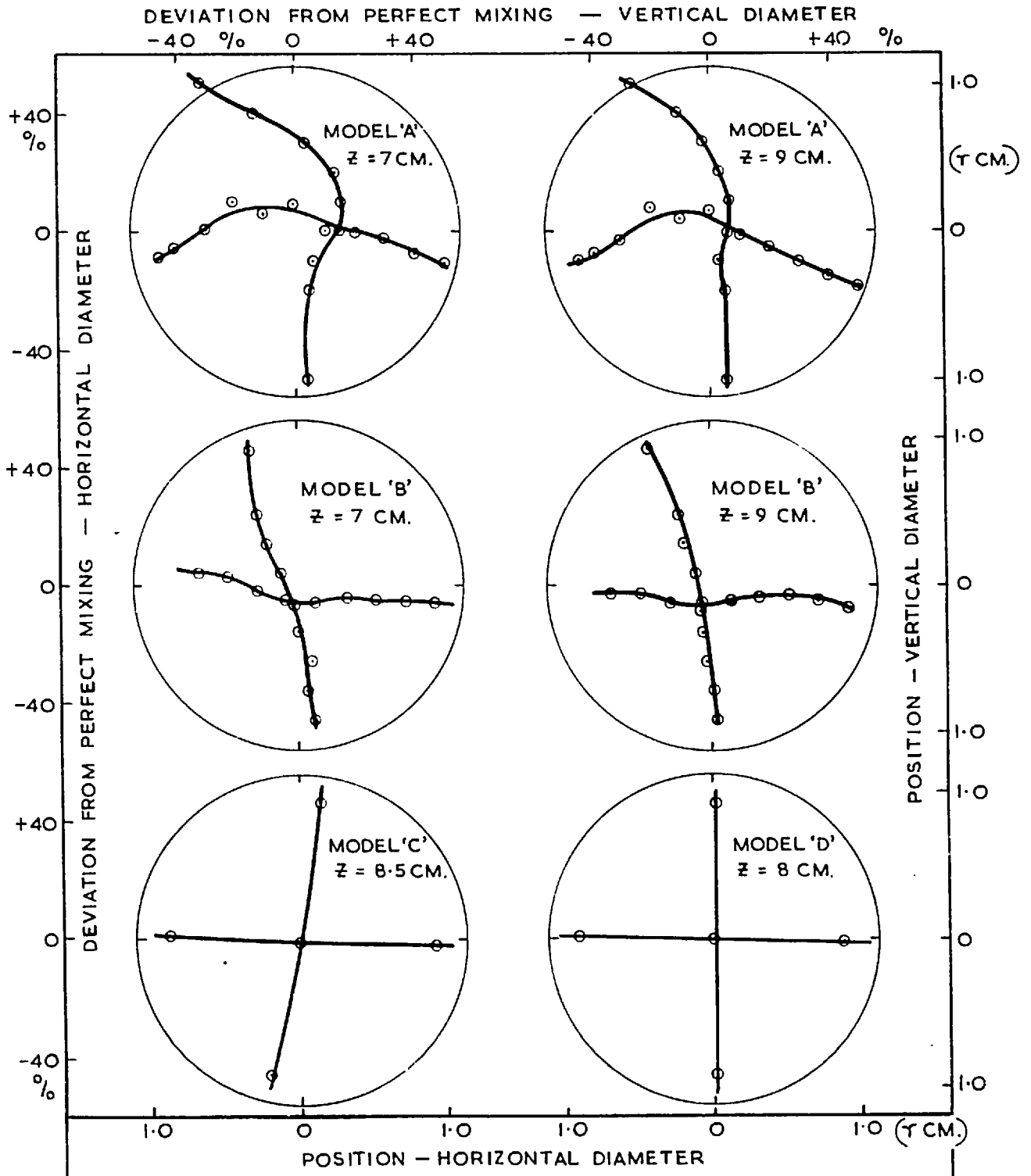

FIG. 3.1. MIXING EFFICIENCY OF INLETS

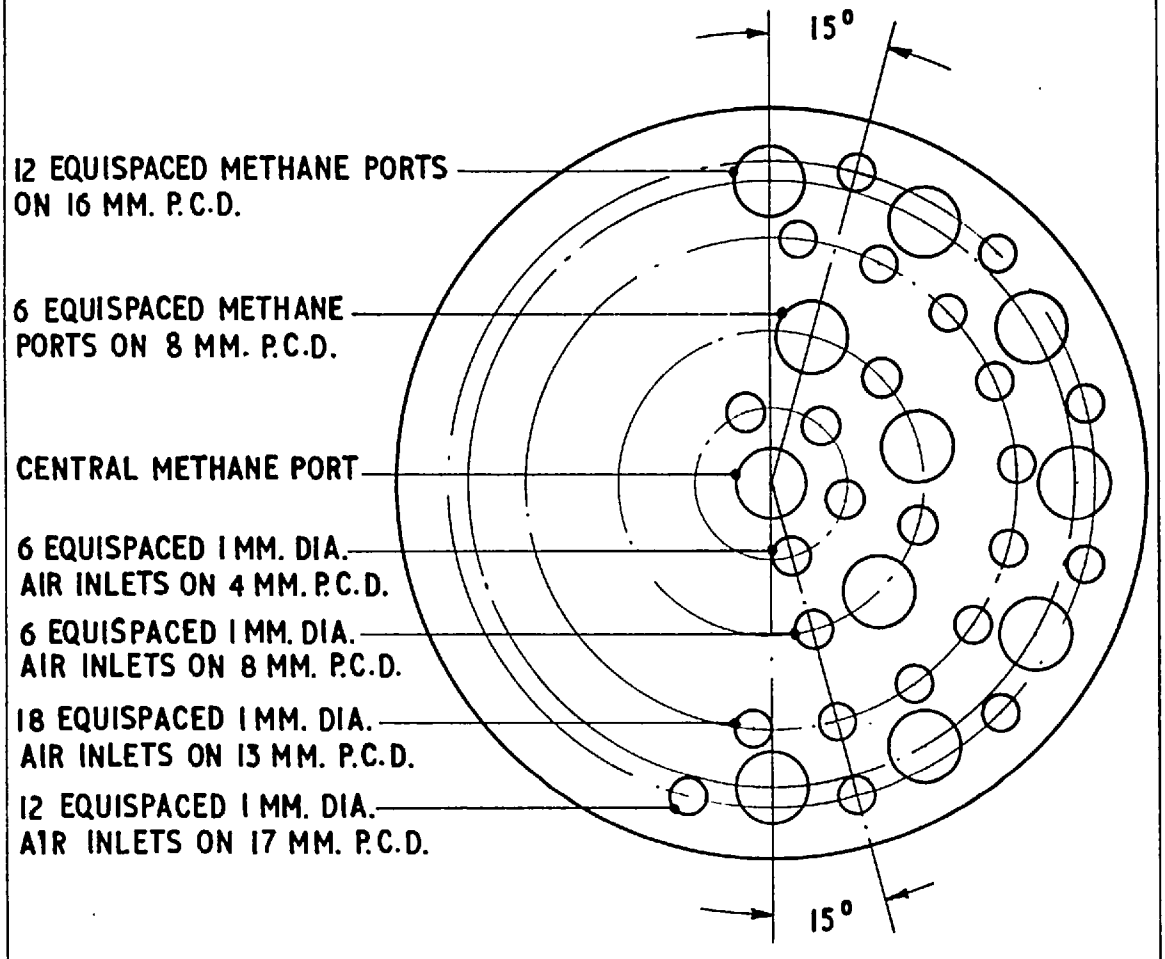

MATERIAL : PLATINUM

DIAMETER : 19·9 MM. THICKNESS : 0·75 MM.

FIG. 3.2. INLET END-PLATE DESIGN

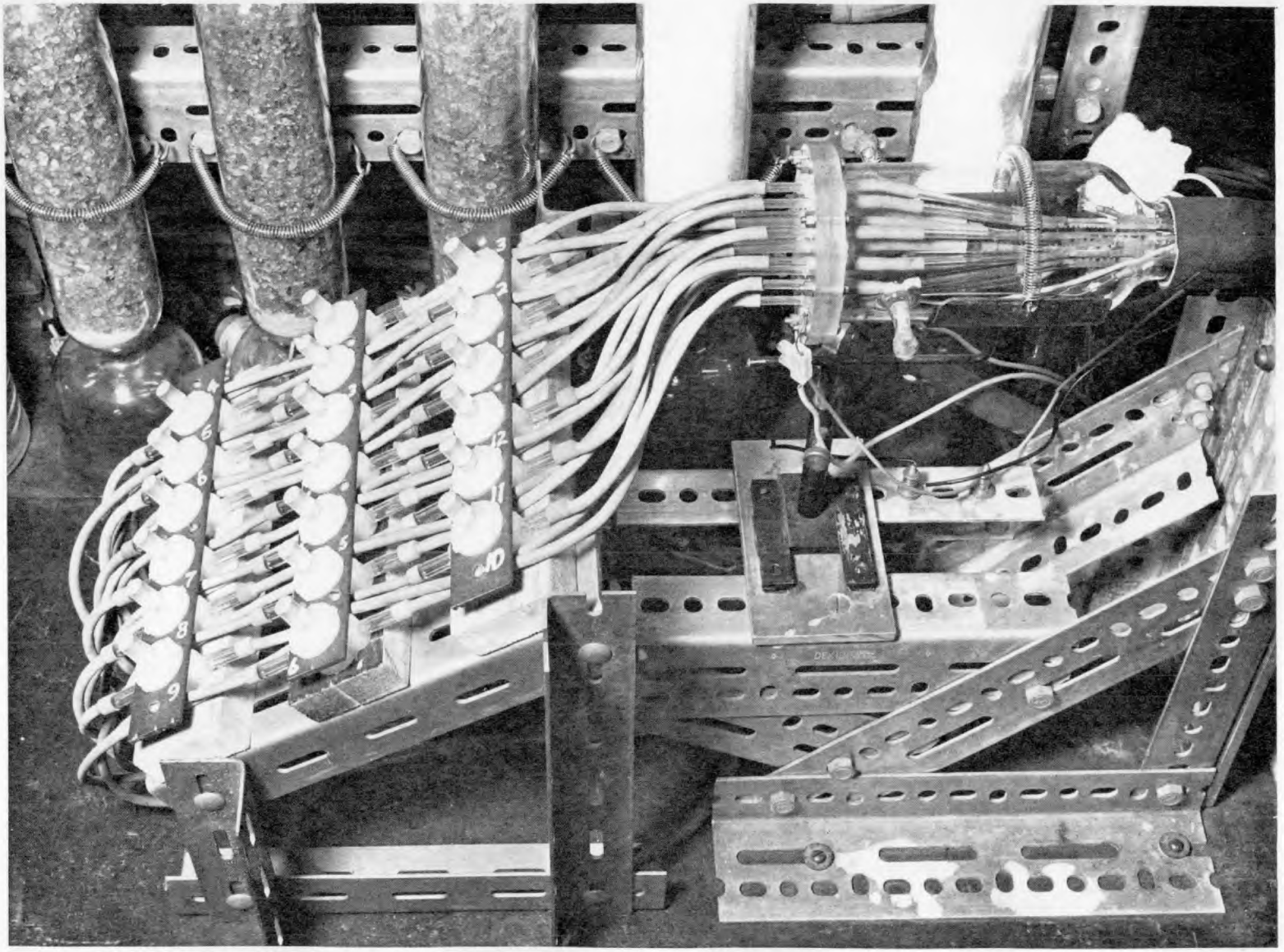

FIG. 3.3. METHANE SUPPLY AND CONTROL VALVES

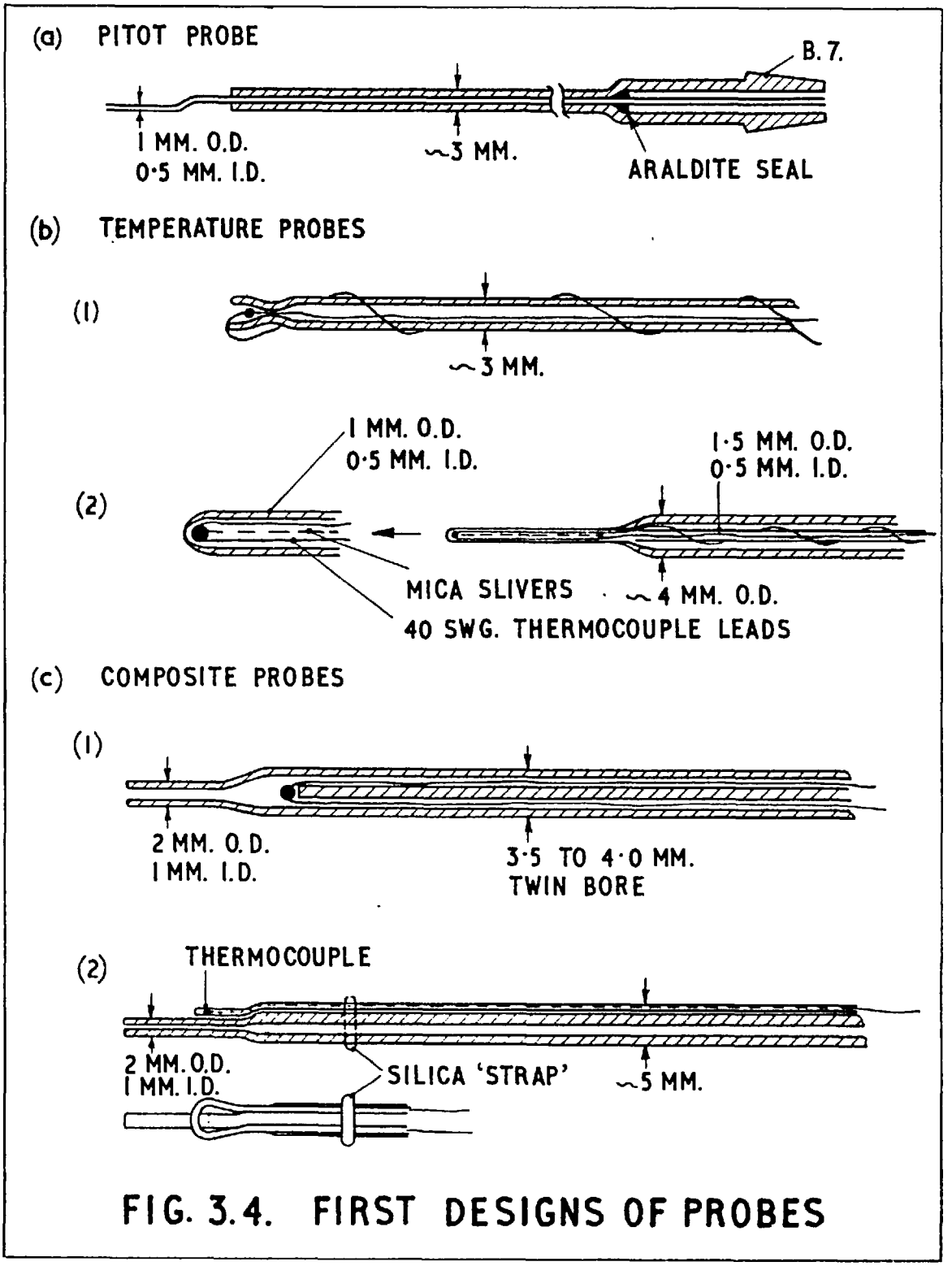

FIG. 3.4. FIRST DESIGNS OF PROBES

FIG. 3.5. SOME CHARACTERISTICS OF ANNULAR FLOW

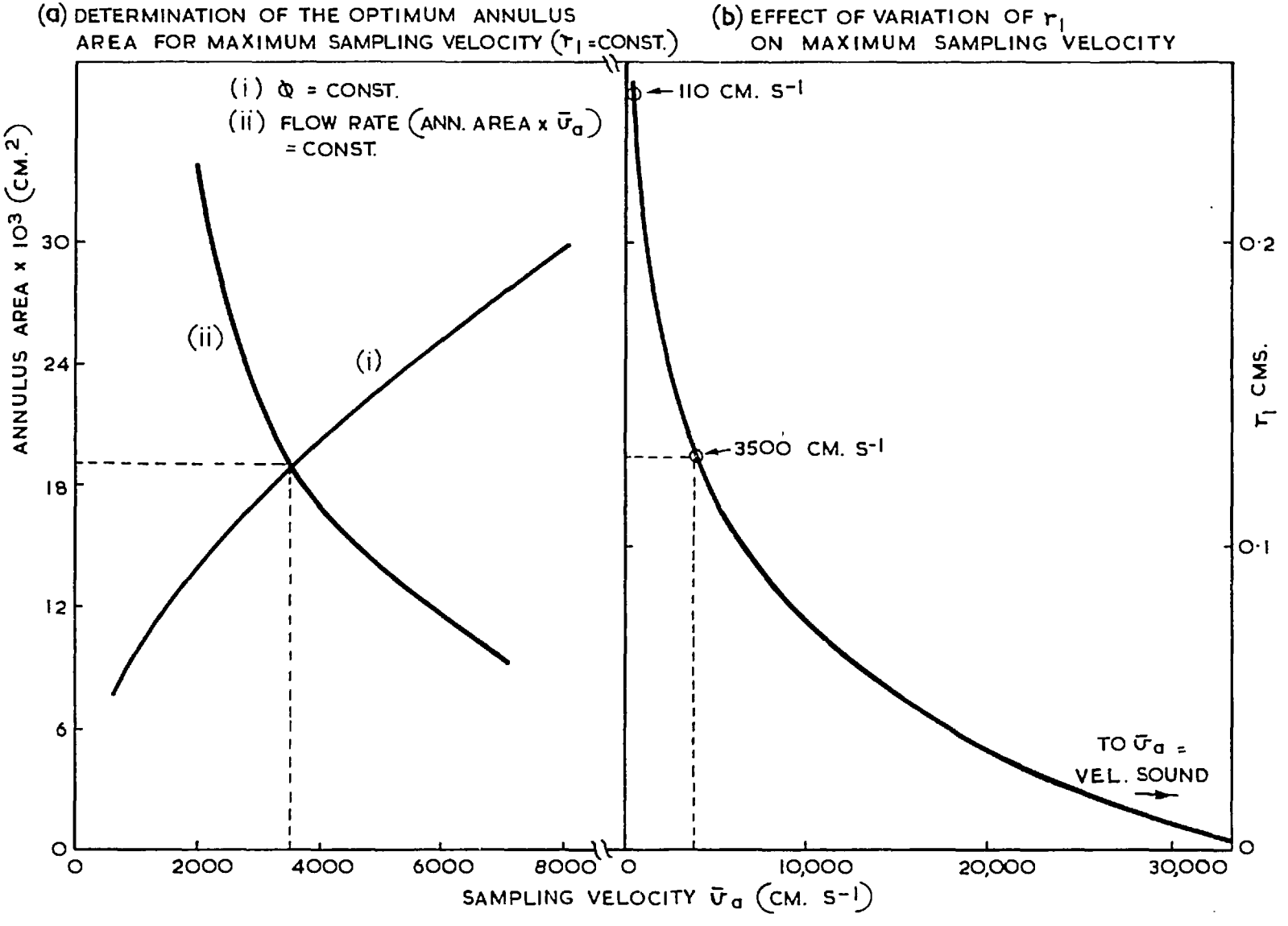

CHAPTER 4

Preliminary observations and conclusions

4.1 Exploratory experiments

4.1.1 The intention of the exploratory experiments

Concurrent with the development of the experimental techniques a number of exploratory experiments were undertaken. They were not intended, at this stage, to explore the effect of varying kinetic parameters, since the preliminary work of Ray[35] and the earlier work of Hirsch[22] had already laid the foundations in this direction.

4.1.2 Typical profiles

'Profile' refers to the continuous line drawn through a set of experimental measurements of a particular parameter, obtained by traversing the probe across a (usually horizontal) diameter in the reaction zone, at a specified axial distance from the mixing point. Typical profiles for a particular set of experimental conditions are shown in Figures 4.2 to 4.4. These were obtained using a model B inlet and model (2) temperature probe, with separate probing to determine the velocity and composition profiles (silica probes). Figure 4.1 shows the variation in temperature conditions in the reaction zone between different runs, for which the control conditions remained unchanged. This gives a measure of the daily reproducibility using an earlier form of the inlet construction, temperature being the most easily obtained and, for present purposes, the most informative measurement. The corresponding velocity and composition profiles are shown in Figures 4.3 and 4.4.

With a more uniform initial velocity profile, and a lower furnace temperature, Figure 4.5 shows the temperature and velocity profiles at three axial positions. These may be compared with the previous set, and show the effects of extensive reaction compared to very little reaction in the latter case, and the importance of uniformity of initial profiles.

Figure 4.6 shows the manner in which the velocity profile develops from an initially asymmetric air flow.

4.1.3 Attempts to vary and stabilise heat release rates

A range of heat release rates may be obtained by changing the overall temperature and the gas stream velocity. With the present apparatus it was found experimentally that mixing point temperatures in excess of 1183°K, with mean gas stream velocities at the inlet greater than 1000 cm s^{-1}, could not be maintained. At the other end of the scale velocities less than 500 cm s^{-1} induced fluctuation in the reaction zone, and consequently a lower limit to the temperature at the inlet (~1100°K) was imposed, since below this temperature level reaction rates were too low. A range of heat release rates may also be obtained by varying the fuel concentration. In this case it was found difficult to maintain stable conditions in the reaction zone if methane concentrations exceeded 1.2 per cent with combustion completed in the reaction zone. The reaction would either 'flash back' or 'blow-off' (see next section).

4.2 Phenomenological account of incidental observations

4.2.1 'Ignition'

With slowly rising furnace temperature and a fuel-lean mixture the following sequence of events took place. An increasingly powerful odour of formaldehyde could be detected in the exhaust gases (not the withdrawn sample) which was followed by the appearance of a long cone of blue flame apex downstream, which slowly encroached upstream into the reaction space. The smell of formaldehyde ceased abruptly as the base of the cone disappeared into the reaction tube. The progress of the reaction in the reaction space was then followed by sample withdrawal from a fixed position, typically 20 cm from the mixing point. Soon after the disappearance of the blue cone into the reaction zone, sampled gas composition showed a carbon monoxide peak, followed by a rapid decline in carbon monoxide and build up in carbon dioxide. Subsequently the nature of the combustion would change abruptly to a series of bright yellow diffusion flames on the inlet ports, usually audible. This change sometimes occurred before the carbon monoxide peak was reached, depending on the methane concentration, inlet conditions and profile non-uniformities of the particular experiment. The products of the diffusion flames were carbon dioxide and water with occasionally a very small percentage (<0.020 per cent) of carbon monoxide. With richer initial fuel concentration (>1.0 per cent methane) the diffusion flames were characteristically noisy. Apart from turning the fuel supply off, only drastic adjustment to the heating input of the furnace and preheat would dislodge these

flames. Temperature profiles indicated a peak in the temperature history of the gas, which occurred soon after the carbon monoxide peak, and that subsequent gas temperature with flames on the inlet ports was considerably lower than the peak value.

4.2.2 'Blow-off' and 'flashback'

For conditions where the majority of the reaction was completed in the reaction zone - under steady furnace temperature conditions - it was sometimes found that the reaction would 'die away' if either mains voltage dropped slightly (before the introduction of voltage stabilisation) or the air or fuel flow increased slightly. Conversely, variation of heating or flow in the opposite sense sometimes resulted in flashback, the general character of which was very similar to the process described in the previous paragraph. The likelihood of either of these features occurring was greatly reduced with the temperature control to preheat 'A' functioning normally.

4.2.3 Effects of asymmetric profiles

It was found, in all recorded instances, that excessive asymmetry of conditions in the reaction zone, whether of velocity or concentration profiles, or both, inevitably had two consequences. Firstly, flashback would occur at much smaller overall heat release rates compared to the case where the reaction proceeded symmetrically about the reaction tube axis. This feature was nearly always indicated by failure to achieve the required advanced stage of the reaction for study. Secondly, and

especially where asymmetrical airflow at the mixing point was subsequently detected, the flashback resulted in combustion as a series of diffusion flames on only a proportion of the inlet ports. A consequence of this was an abnormally shaped premixed combustion zone downstream of the remaining inlets. This zone also occasionally 'flashed back', resulting in a two-stage 'flash back'.

4.3 Effectiveness and comparison of water-cooled and silica samplers

It was originally intended that direct comparison should be made between the water-cooled and silica samplers in order to ascertain the efficiency of the silica sampler in withdrawing a representative and quenched sample from the reaction zone. Such a comparison of cooled and uncooled probes has been made under flame conditions[3]. In the latter case it was shown that the uncooled probe was effective in quenching the sample. In the present case circumstances are such that no direct experimental comparison is possible because of the perturbing influence of the water-cooled sampler on the temperature distribution in the reaction zone. Since the mode of quenching in the silica sampler used here is also different, being dependent to a large extent on the speed of withdrawal (see previous chapter) it is not possible to use the results of the flame comparison in this case.

However it is possible to assess the efficiency for the stable species. By plotting methane concentration in the sample versus sample flow rate, under steady furnace conditions, it can be seen (Figure 4.7)

that the composition of the sample varies only slightly in the range of sampling rates used for measurements. This applies to a cylindrical bore sampler used to obtain preliminary profiles. For the composite probe, where annular flow is necessary, the margin between satisfactory sampling and measurable reaction in the sampler is evidently very much less (Figure 4.8). A correction applied under the hottest furnace conditions will be described in the next chapter.

As was anticipated, variation in the sampling flow rate through the water-cooled sampler produced no measurable variation in the sample composition. (At extremely low sampling rates one might expect some variation due to prolonged residence at the probe tip, but this conjecture was not checked experimentally.)

4.4 Stability of reaction zone conditions

Maintenance of steady-state conditions in the reaction zone is of fundamental importance. The method of experimentation requires that the steady-state relation

$$\left(\frac{\partial c}{\partial t}\right)_{Z,r,T,v} = \left(\frac{\partial T}{\partial t}\right)_{Z,r,c,v} = \left(\frac{\partial v}{\partial t}\right)_{Z,r,T,c} = 0$$

be as nearly true as possible. Unless this condition is fulfilled little weight can be attached to the quantitative measurements. Several factors affect the stability.

4.4.1 Effect of heat input and flow fluctuation

Even with voltage stabilisation of the mains supply slight variations of voltage were still perceptible as small changes in the heat input from the main 'M' and preheat 'B' circuits. In the case of an increased input the reaction zone became slightly hotter, increasing the reaction rate, and thus moving the various profiles towards the mixing point and at the same time tending to contract the whole reaction zone in the axial direction. This meant higher heat release rates near the platinum resistance thermometer, which, sensing an increase in temperature, reduced the heat input to preheat 'A'. Conditions would eventually restabilise, providing no flash-back occurred, with the various profiles slightly shifted from their previous positions, often in an upstream direction. The implications of such disturbances of any magnitude occurring during a run are obvious; fortunately they were rarely more than 'just noticeable' and small adjustments to the main input 'M' were sufficient to re-establish the desired conditions. Heat input fluctuations requiring such attention were infrequent.

The main flow-variation encountered was a very slow change of air flow. This had consequences on the stability of the reaction similar to those induced by heat input fluctuation. A slight fall in flow had an effect equivalent to a slightly increased heat input. Occasional minor adjustment of the air flow controls was sufficient to virtually eliminate this cause of instability.

4.4.2 Effect of sample withdrawal on the reacting gas

Besides the direct effects of sampling discussed in Chapter 3, there are two indirect effects which have particular bearing on the stability. For the first - the effect of removing reacting gas from the reaction zone - both silica and water-cooled samplers may be considered together. The effect is best illustrated by consideration of an extreme case. Suppose a large proportion of the reacting gas were withdrawn by sampling near the mixing point before much reaction had occurred. Then for furnace and flow conditions appropriate to a majority of the heat release occurring in the reaction zone, the heat actually released would be considerably diminished. This is still true if one supposes the accompanying velocity reduction of the remaining gas to result in a total heat release in a smaller volume. If furnace and flow conditions were appropriate to a minority of the heat release occurring in the reaction zone, the opposite conclusion may be true - velocity reduction may result in overall increase in heat release in the reaction zone. In either case preheat 'A' will tend to correct, with a new steady-state differing from the unsampled one.

Experimentally it was found that these effects were not serious, although no quantitative measure was possible, provided less than 2 per cent of the reacting gases was sampled. The argument that any constant withdrawal rate will ensure steady-state conditions unfortunately only applies if the sampling point remains fixed relative to the reaction zone.

This leads to the second perturbing effect of the sampling technique, namely that of relative movement of the probe in the reaction zone. Here the silica and water-cooled samplers must be considered separately.

For the silica probe axial position variation will, in line with the previous discussion, only have noticeable effect if the volume sampled exceeds 2 per cent of the total. Radial movement will obviously perturb the downstream velocity profiles; however, no instability could be attributed to this cause.

The water-cooled sampler poses quite a different problem. Heat transfer from the reaction tube wall to the sampler varies with both the radial and axial position of the sampler. Some compensation was possible by adjusting the main input 'M', which proved moderately effective for changes in axial position. When the sampler was close to the wall, compensation was not so effective. In practice, therefore, such positions were never held for long. Typical values of 'M' for various positions of the sampler are given in Table 4.1, together with the appropriate inlet and furnace temperatures, which serve as a good indication of the stability of the reaction zone conditions.

4.4.3 Stability achieved in practice

Stability in the steady-state sense implied in this section is difficult to assess quantitatively. Table 4.2 (set 'A') sets out the experimental record of conditions for a half-hour interval of running which were considered stable, and for which continuous sampling was maintained from a fixed position throughout the period. No interim

adjustments were applied to the controls. The data of Table 4.2 (set 'B') apply to the position 20 cm from the mixing point before and after a typical run. The silica probe had been moved to some 30 different positions in the reaction zone in the 2 hour interim. In this case intermittent minor adjustments had been made to the furnace and flow controls throughout the course of the run.

4.5 Qualitative effects of certain additives

4.5.1 Acetone in the methane supply

An obvious gap in the study of the mechanism of the high temperature oxidation of methane is of the effect of methyl radical addition. Although this might prove quite difficult to do quantitatively, it appeared worth attempting qualitatively. A number of compounds might act as sources of methyl radicals[61]. These include azomethane, diacetyl, acetone, ethylene oxide and ketene. Acetone was chosen and was injected into the methane stream by bubbling the methane through an acetone trap immediately prior to the furnace. At room temperature this gave an acetone concentration in methane of ~25 per cent[102] (assuming saturation).

Acetone in the absence of oxygen may be expected to give methyl radicals according to the following scheme[61]:-

$$(CH_3)_2CO \rightarrow CH_3CO^{\bullet} + CH_3^{\bullet} \quad \ldots.(1)$$

$$CH_3CO^{\bullet} \rightarrow CH_3^{\bullet} + CO \quad \ldots.(2)$$

$$CH_3^{\bullet} + CH_3CO^{\bullet} \rightarrow CH_2CO + CH_4 \quad \ldots.(3)$$

If reaction (3), a radical-radical reaction, occurs only to a minor extent, the addition of acetone will be effectively an addition of carbon monoxide and methyl radicals. The effect of carbon monoxide is known to be small[22,35], and its own combustion will be inhibited by the methane. It was found that such an injection into 0.9 per cent methane/air at a furnace temperature of 1153°K, where comparatively little reaction was occurring in the reaction zone, caused a rapid acceleration of the rate, followed by some flashback and ignition on the inlet ports. This experiment was repeated several times with similar results. It is evident that acetone, and hence probably methyl radicals, markedly accelerate the high temperature reaction. It did not prove possible to follow up this observation.

4.5.2. Oxygen in the methane supply

Using methane with approximately 3 per cent oxygen (chromatographic analysis), it was found that the overall furnace temperature conditions had to be reduced about 40°K (from 1133°K to 1093°K in the particular case investigated) to achieve similar percentage conversion in the reaction zone compared with a de-oxygenated methane supply. In the first instance this was not a deliberate experiment, but the evident usefulness of such a scheme for the addition of small amounts of formaldehyde immediately suggests itself. For given experimental conditions it would be a simple matter to analyse the methane obtained direct from an inlet port and hence know the percentage formaldehyde, and any other intermediates, present.

4.5.3 Methane in the air supply

Whenever a methane inlet tube fractured, a small percentage (it could not exceed 1/19th of the total methane percentage for each fractured inlet tube) of methane leaked into the air supply in the preheat furnace. As might be expected it resulted in a rapid acceleration of the main reaction downstream, presumably due to the earlier formation of formaldehyde and reduction of the induction period[35].

4.6 Qualitative tests for intermediates

A number of attempts were made to isolate intermediates occurring in the early and middle stages of the reaction which were condensible at liquid-nitrogen temperature. The primary objective was to establish the presence or absence of peroxidic intermediates, since previous vessel work[80] had shown considerable amounts of hydrogen peroxide to be present at lower temperatures (713 to 793°K). The method of sampling was basically that described in Chapter 2, using the water-cooled sampler and a liquid-nitrogen trap in place of the bubble-trap. The condensibles from a 3-litre gas sample were dissolved in distilled water (3 ml) to which was added ferrous thiocyanate solution (1 ml) prepared in the manner described by Everett[103]. This was compared visually with a blank solution, the slightly deeper reddish colouring indicating peroxide. The titanous sulphate test[80] was then applied to another sample. The formaldehyde content of this sample was estimated on a separate portion by the method described by Bricker and Johnson[104] as modified by Salooja[80]. Two additional solutions were then made up, one containing the equivalent

amount of formaldehyde to the sample, the other a blank. The optical densities of the three solutions were then determined at 4100 A^{o} in a Unicam quartz spectrophotometer model SP 500. The optical densities of the blank and formaldehyde solutions were indentical to the accuracy of the instrument, while the sample solution showed a considerably greater optical density. Since the titanous sulphate test is specific for hydrogen peroxide it was concluded that hydrogen peroxide was present in the sample. No quantitative measurements were attempted at this stage.

To determine whether or not organic peroxides were also present the condensate from a much larger sample (10 litres) was collected and one drop of the liquid formed on warming this to room temperature was developed chromatographically with ether on a Whatman No. 1 filter paper[80]. A second drop was developed similarly with isopropyl alcohol. The developed chromatograms were tested for peroxide with a few drops of ferrous thiocyanate solution, but only one pinkish ring could be detected on either. The method had previously been tested by developing artificial dilute mixtures of hydrogen and organic (t-butyl) peroxide which invariably gave clearly separated rings on development and testing. It was concluded that hydrogen peroxide was the only peroxide which could be extracted in measurable quantities from the reaction studied. The condensate from a further sample was analysed by gas chromatography, but, as had been expected, the chromatogram was swamped by the formaldehyde. Without removing formaldehyde chemically -

a procedure which would most likely remove any other intermediates of interest - there seemed to be no easy way of detecting other possible low concentration intermediates. In any case related flame work[4] using mass spectrometric analysis gives no indication of the presence of other intermediates in significant concentration.

After an extensive sampling period and dissolution of the condensibles obtained, a white solid deposit remained on the walls of the cold trap. On analysis this proved to be polymerised formaldehyde $(CH_2O)_n$. This discovery resulted in the modification (described in Chapter 2) of the sampling technique for the quantitative work to be described in Chapters 5 and 8. No solid deposit remained when the sampled gas was passed through an 80 per cent sulphuric acid solution.

4.7 Preliminary conclusions

4.7.1 Experimental improvements required

The exploratory experiments indicated three ways in which it was advisable to improve the existing experimental arrangements, (i) the variation in the pattern of the reaction from one run to the next as recorded by the temperature profiles (Figure 4.1), pointed to one of the major difficulties of the experimentation and to the desirability of measuring the required parameters simultaneously. . It was as a direct result of these experiments that the composite probes were developed. (ii) Figure 4.5 showed that although a symmetrical flow pattern could be achieved near the mixing point, Figures 4.3 and 4.6 showed that this was not always achieved with the inlet design in use at the time

(model B). The asymmetry would make quantitative analysis unnecessarily difficult. In consequence the inlet was redesigned and model D eventually resulted. (iii) The need for a standard sampling procedure, as distinct from the experimental procedure described in Chapter 2, was emphasised by the experiments on stability in the reaction zone (Section 4.4). The experimental data presented subsequently in this thesis were obtained using the following standardised sampling procedure.

A run was commenced at the furthest necessary position on the axis from the mixing point and progressed point by point towards the inlet. Radial traverses were obtained, as required, by working from the axis towards the wall (usually on a horizontal diameter at geometrically similar positions for comparable runs). Furnace conditions, flows and general stability were checked between readings, but particularly after each radial traverse.

4.7.2 Limitations of the apparatus

The preliminary survey indicated three limitations of the apparatus.

(i) It was shown that a maximum throughput of ~50 l. min^{-1} could be satisfactorily heated to 1183^{o}K, or slower flows to correspondingly higher temperatures. The basically silica construction precluded much higher inlet temperatures. It was subsequently established that a lower limit to the throughput was also imposed (ca 20 to 25 l. min^{-1}). This was due to fairly regular sinusoidal fluctuations in the reaction at the sampling point, which the probe temperature record indicated had an

amplitude of $5^{o}K$ or $6^{o}K$ and a periodicity of about $\frac{1}{2}$ min. This effect was not investigated further.

(ii) A maximum permissible rate of sample withdrawal (2 per cent of total flow) was indicated. In practice sampling rates have been kept well below this figure. This was particularly necessary if values of the total-head pressure were to be obtained between samples, since minimal withdrawal rates caused the least possible change in conditions in the switchover.

(iii) The perturbing effect of the water-cooled sampler on the reaction has indicated that quantitative comparison between samples withdrawn by this means and those withdrawn by the silica sampler cannot be made. Further, the water-cooled sampler will be of only limited usefulness in the present system for quantitative work owing to the uncertainty of the temperature-time history of the reaction immediately prior to extraction and quenching.

Table 4.3 summarises the range of T, v, c for which the apparatus and techniques were considered suitable.

4.7.3 Additional remarks

If the locus of apparent maximum heat release is drawn from Figure 4.2 ('apparent' since no corrections for heat transfer are made) the resulting curve (Figure 4.9) is conical with its apex downstream. This shape is typical of 'normal' flames with cylindrical symmetry, (e.g., a bunsen burner flame). Taking this feature in conjunction with the 'flash back' (or ignition) and 'blow-off' characteristics of the

reaction, it is evident that the mode of reaction is intermediate between the outwardly controlled isothermal fast reactions of classical kinetics and the 'free' flame. Thus it appears that the experimental arrangement presents the opportunity for a study of heat release rates in a situation analogous in many respects to that occurring in 'normal' flames. At the same time the system is susceptible to greater external control, and particularly amenable to the study of what are effectively extremely lean flames, with appropriately slow heat release rates. It would evidently be useful to compare quantitative measurements of the heat release rates derived from suitably corrected profiles, of the gas temperature on the one hand and the specie profiles on the other. This comparison is attempted in Chapters 5 to 7. An incidental consequence of the comparisons will be an additional assessment of the techniques.

Any detailed knowledge of the reaction mechanism will depend on sufficient knowledge of the reaction intermediates, especially the very reactive radical species. The present methods will not allow direct measurement of radical concentrations but useful information can be obtained from rapidly quenched samples such as are obtained by the water-cooled sampler. In this respect the kinetic role of the minor constituents is analysed in Chapter 8. It is evident that particular note should be taken of the kinetics in relation to concentration, heat release rates, and wall effects. Information on the induction period might also be forthcoming.

TABLE 4.1

Main heat input for various* positions of water-cooled sampler

z (Axial position of probe tip from inlet) (cm)	Heat input 'M' arb. units	Furnace Temp ^{o}K	Inlet Temp ^{o}K
22	152	1131	1131
20	152	1132	1132
18	152.5	1132	1132
16	154	1131.5	1132.5
14	157	1131.5	1132.5
12	160	1130.5	1132.5

*Other heat inputs constant

TABLE 4.2

Set 'A'*

Continuous fixed-location sampling (20 cm) from reaction zone with no interim correction to heat input and flows

	$\not X_{CO} \times 10^2$	$X_{CO_2} \times 10^2$	i amps	Furnace T ^oK	Air flow l. min^{-1}
Initial conditions	0.32	0.54	2.93	1166	41.1
Conditions $\frac{1}{2}$ hr later	0.29	0.56	2.93	1166	41.0

*Here variation in CO, CO_2 may be attributed to a slight fall in air flow

$\not X_i$ is mole fraction of species i.

Set 'B'

Variation in conditions during a typical run, as indicated at 20 cm sampling position, interim corrections applied

	$X_{CH_4} \times 10^2$	$X_{CO} \times 10^2$	$X_{CO_2} \times 10^2$	i amps	'M' arb. units	Temperature ^oK		
						Furnace	Inlet	Probe
Initial conditions	0.295	0.325	0.020	2.89	141.5	1155	1156	1187
Conditions ~2 hr later	0.305	0.320	0.015	2.90	142.0	1155	1156	1185

TABLE 4.3

Range of conditions for which the apparatus was applicable

	Minimum	Maximum
Mixing Point temperature	1123°K	1183°K
Flow - litres cold	~25 l min^{-1}	50 l min^{-1}
Mean gas velocity (hot)	~650 cm s^{-1}	~1400 cm s^{-1}
Concentration $X_{CH_4} \times 10^2$	0.15	1.2

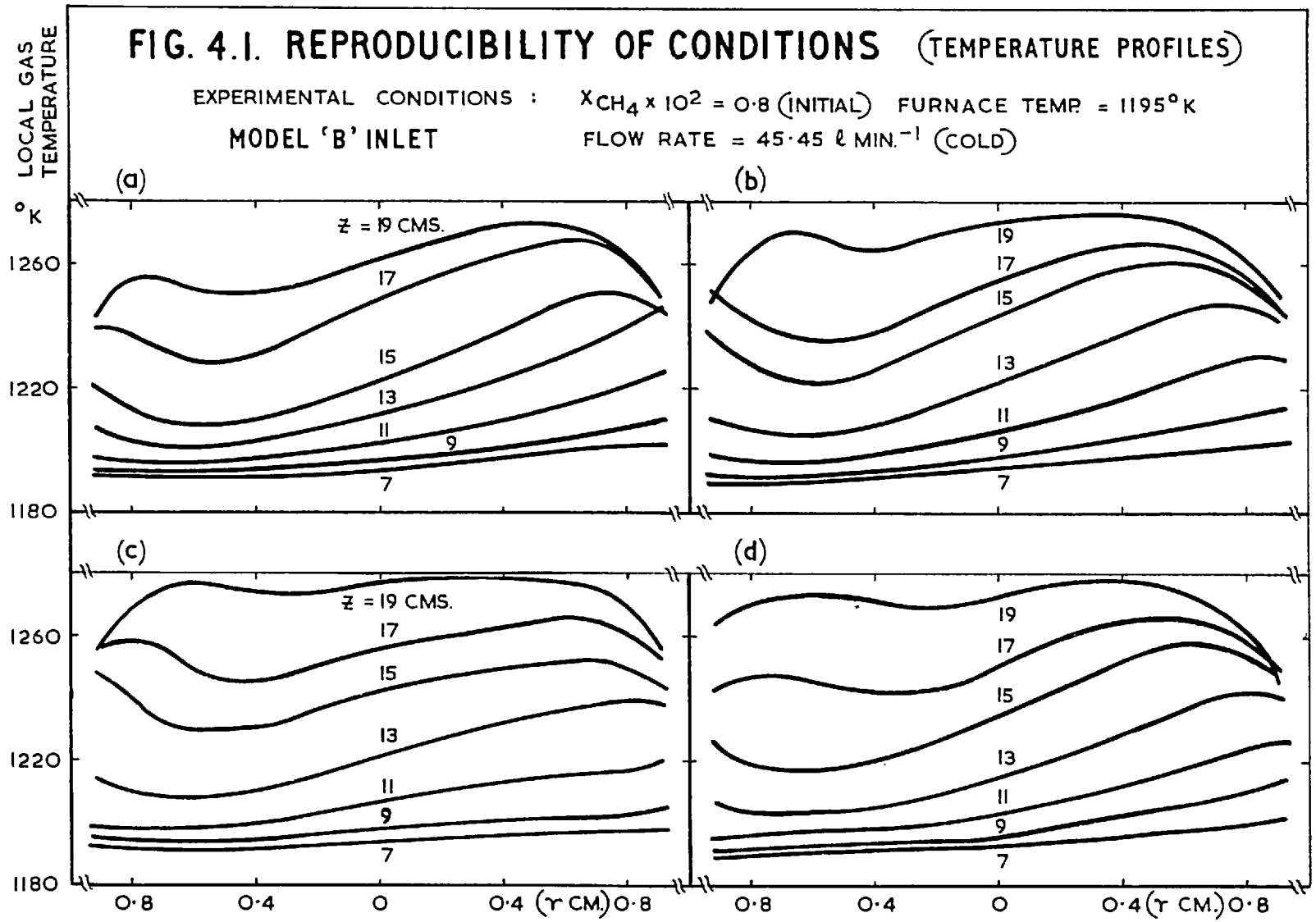
FIG. 4.1. REPRODUCIBILITY OF CONDITIONS (TEMPERATURE PROFILES)
EXPERIMENTAL CONDITIONS : $X_{CH_4} \times 10^2 = 0.8$ (INITIAL) FURNACE TEMP. = 1195°K
MODEL 'B' INLET FLOW RATE = 45·45 ℓ MIN.$^{-1}$ (COLD)
LOCAL GAS TEMPERATURE °K
(a)
(b)
(c)
(d)
z = 19 CMS.
19
17
15
13
11
9
7
1260
1220
1180
0·8
0·4
0
0·4 (r CM.) 0·8

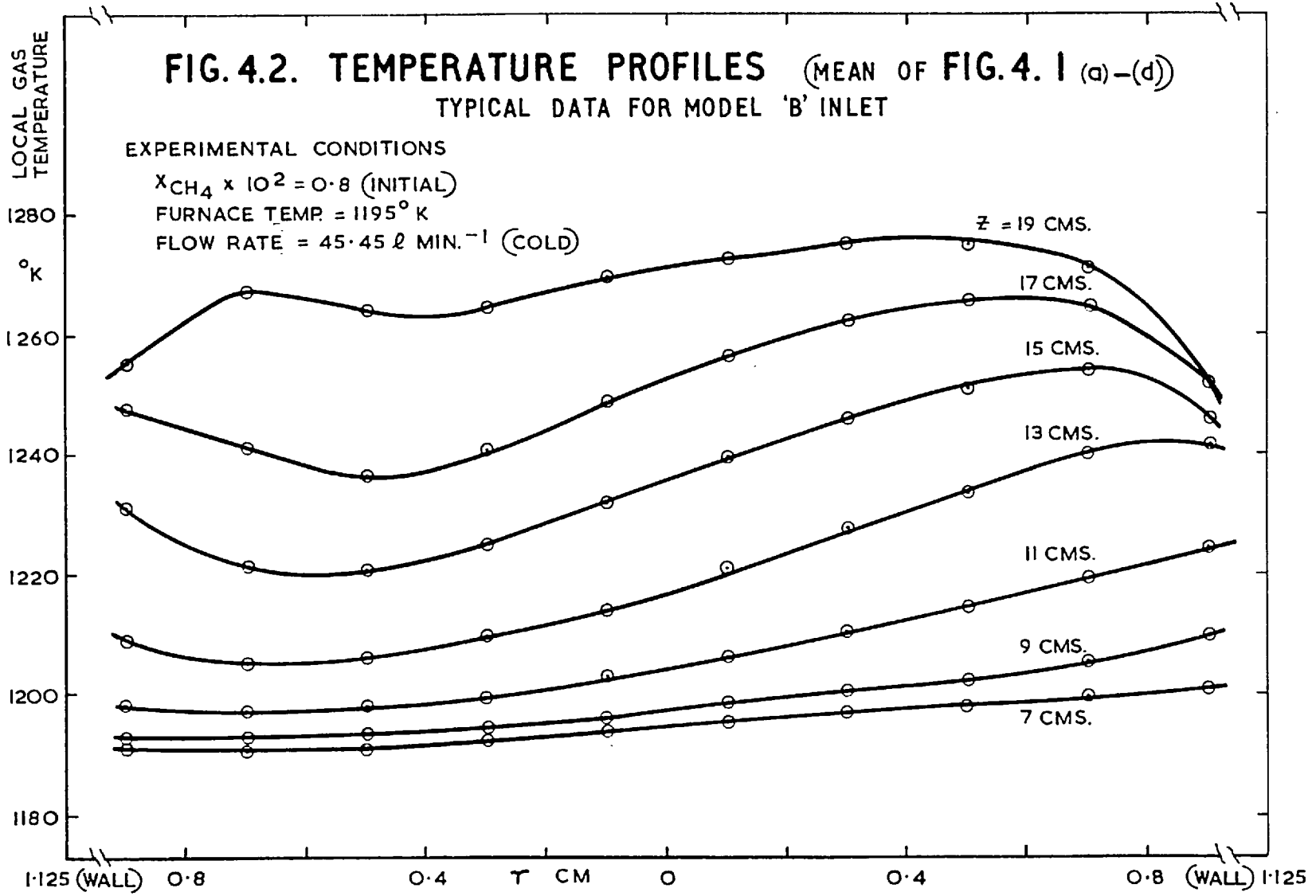
FIG. 4.2. TEMPERATURE PROFILES (MEAN OF FIG. 4. 1 (a)–(d))
TYPICAL DATA FOR MODEL 'B' INLET
EXPERIMENTAL CONDITIONS
$X_{CH_4} \times 10^2 = 0{\cdot}8$ (INITIAL)
FURNACE TEMP. = 1195° K
FLOW RATE = 45·45 ℓ MIN.$^{-1}$ (COLD)
LOCAL GAS TEMPERATURE
°K
1280
1260
1240
1220
1200
1180
z = 19 CMS.
17 CMS.
15 CMS.
13 CMS.
11 CMS.
9 CMS.
7 CMS.
1·125 (WALL)
0·8
0·4
r CM
0
0·4
0·8
(WALL) 1·125

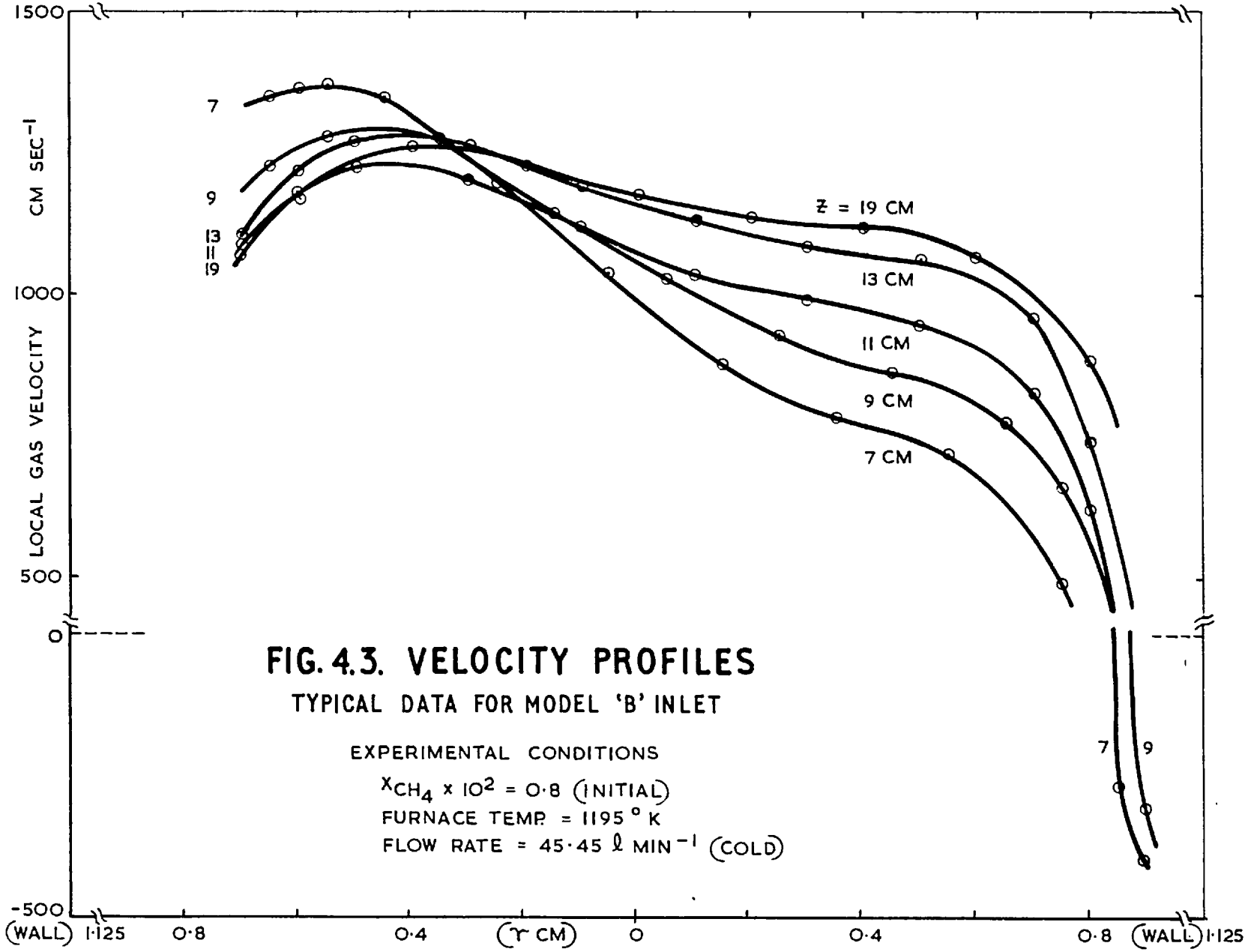

FIG. 4.3. VELOCITY PROFILES

TYPICAL DATA FOR MODEL 'B' INLET

EXPERIMENTAL CONDITIONS

$X_{CH_4} \times 10^2 = 0{\cdot}8$ (INITIAL)

FURNACE TEMP. = 1195 °K

FLOW RATE = 45·45 ℓ MIN^{-1} (COLD)

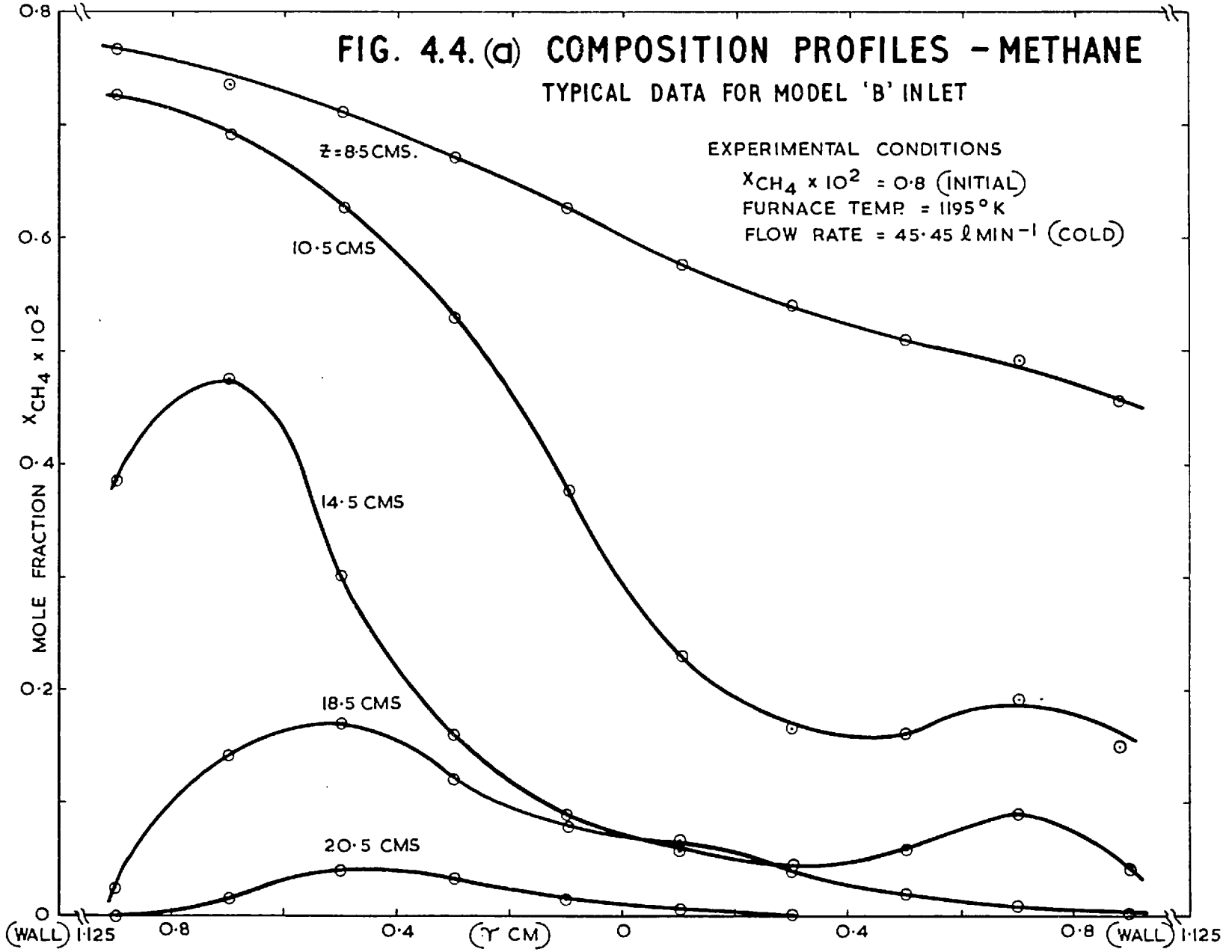
FIG. 4.4.(a) COMPOSITION PROFILES - METHANE
TYPICAL DATA FOR MODEL 'B' INLET
EXPERIMENTAL CONDITIONS
$X_{CH_4} \times 10^2$ = 0·8 (INITIAL)
FURNACE TEMP. = 1195°K
FLOW RATE = 45·45 ℓ MIN^{-1} (COLD)
z = 8·5 CMS.
10·5 CMS
14·5 CMS
18·5 CMS
20·5 CMS
MOLE FRACTION $X_{CH_4} \times 10^2$
0·8
0·6
0·4
0·2
0
(WALL) 1·125
0·8
0·4
(r CM)
0
0·4
0·8
(WALL) 1·125

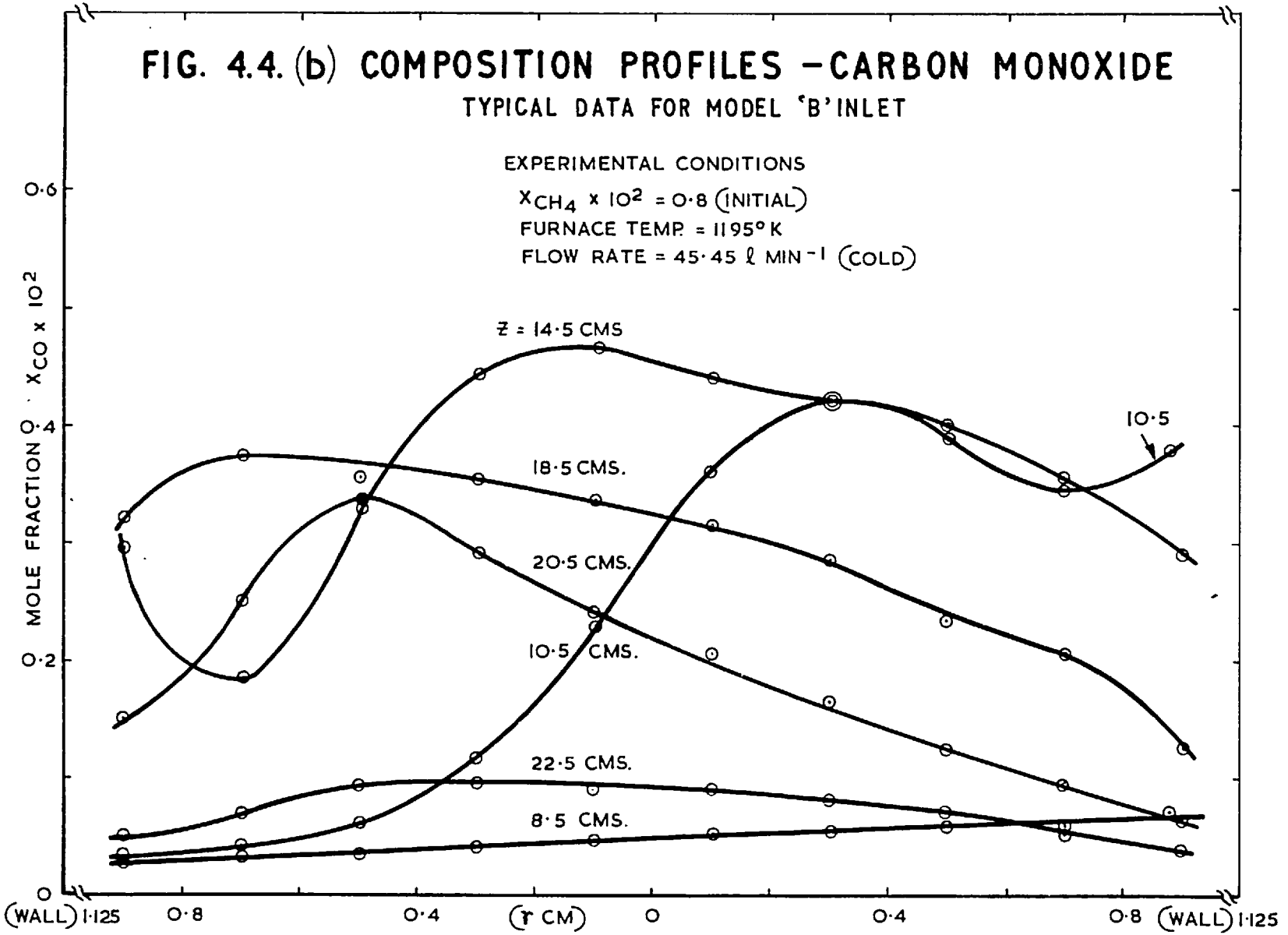
FIG. 4.4. (b) COMPOSITION PROFILES – CARBON MONOXIDE
TYPICAL DATA FOR MODEL 'B' INLET
EXPERIMENTAL CONDITIONS
$X_{CH_4} \times 10^2 = 0.8$ (INITIAL)
FURNACE TEMP. = 1195° K
FLOW RATE = 45·45 ℓ MIN⁻¹ (COLD)
MOLE FRACTION $X_{CO} \times 10^2$
0·6
0·4
0·2
0
z = 14·5 CMS
18·5 CMS.
20·5 CMS.
10·5 CMS.
22·5 CMS.
8·5 CMS.
10·5
(WALL) 1·125
0·8
0·4
(r CM)
0
0·4
0·8
(WALL) 1·125

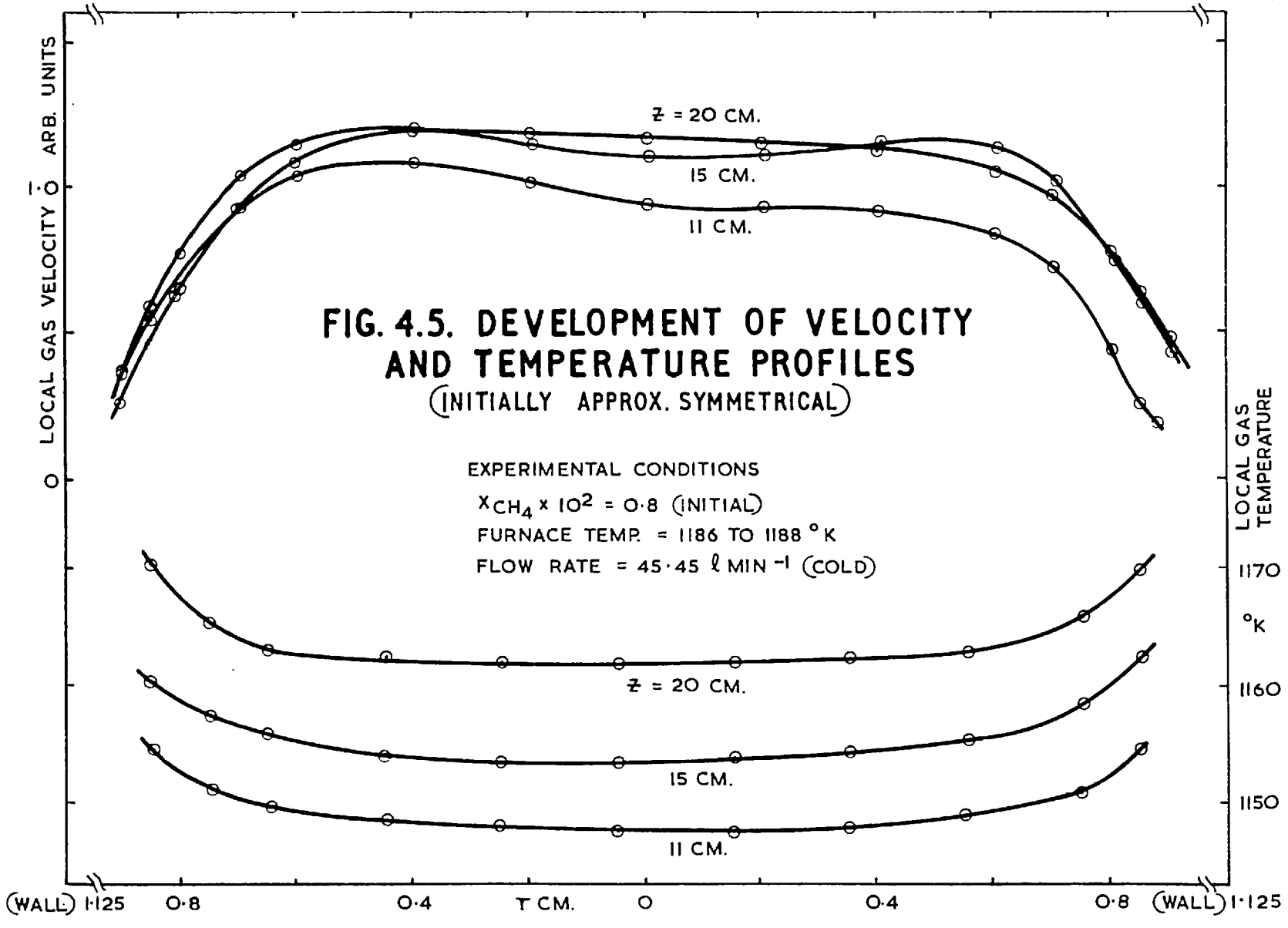

FIG. 4.5. DEVELOPMENT OF VELOCITY AND TEMPERATURE PROFILES
(INITIALLY APPROX. SYMMETRICAL)

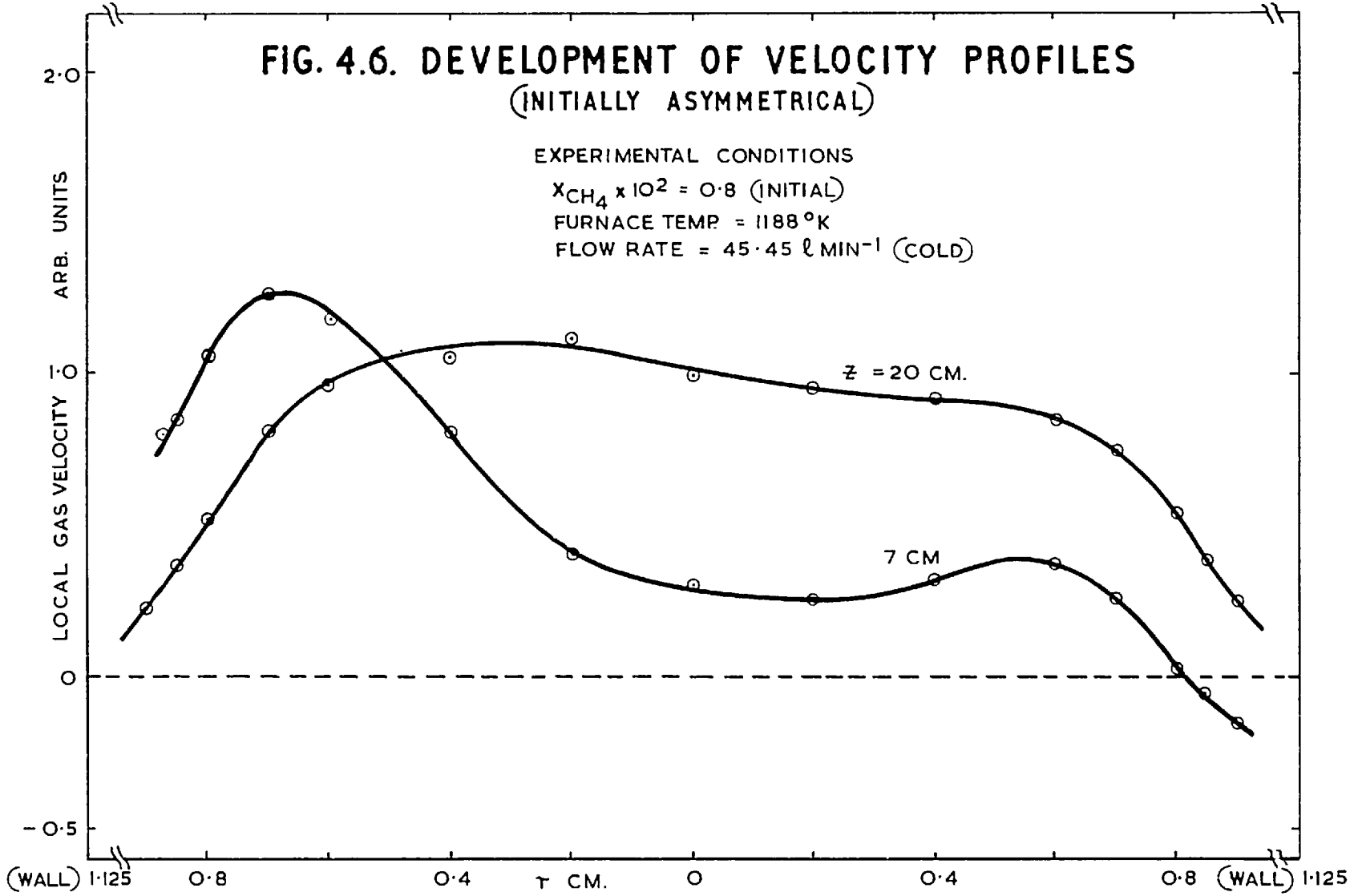
FIG. 4.6. DEVELOPMENT OF VELOCITY PROFILES
(INITIALLY ASYMMETRICAL)
EXPERIMENTAL CONDITIONS
$X_{CH_4} \times 10^2 = 0.8$ (INITIAL)
FURNACE TEMP. = 1188 °K
FLOW RATE = 45·45 ℓ MIN^{-1} (COLD)
LOCAL GAS VELOCITY ARB. UNITS
2·0
1·0
0
−0·5
z = 20 CM.
7 CM
(WALL) 1·125
0·8
0·4
r CM.
0
0·4
0·8
(WALL) 1·125

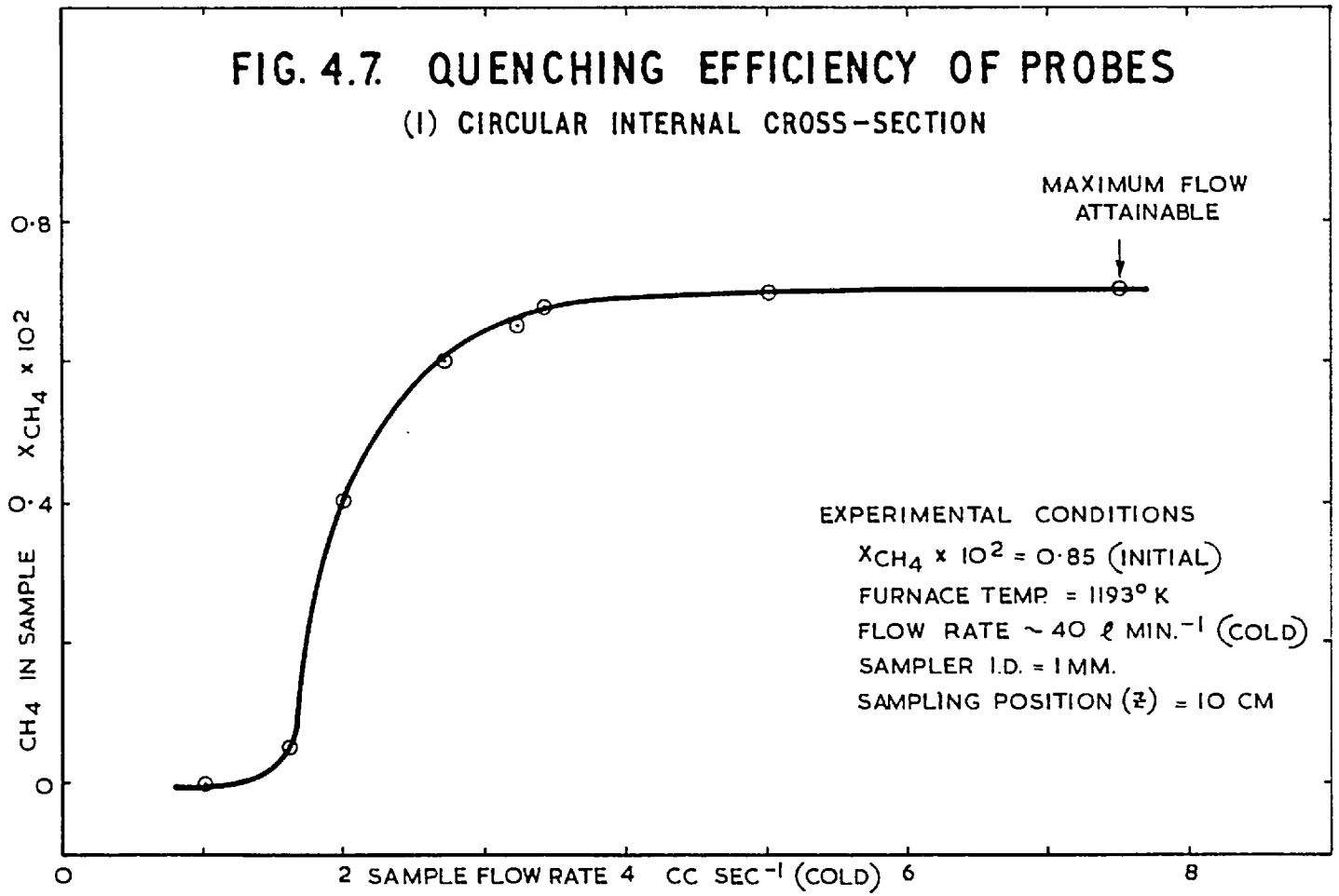
FIG. 4.7. QUENCHING EFFICIENCY OF PROBES
(I) CIRCULAR INTERNAL CROSS-SECTION
MAXIMUM FLOW ATTAINABLE
EXPERIMENTAL CONDITIONS
$X_{CH_4} \times 10^2 = 0.85$ (INITIAL)
FURNACE TEMP. = 1193° K
FLOW RATE ~ 40 ℓ MIN.$^{-1}$ (COLD)
SAMPLER I.D. = 1 MM.
SAMPLING POSITION (ℨ) = 10 CM
CH_4 IN SAMPLE $X_{CH_4} \times 10^2$
0·8
0·4
0
0
2
4
6
8
SAMPLE FLOW RATE CC SEC^{-1} (COLD)

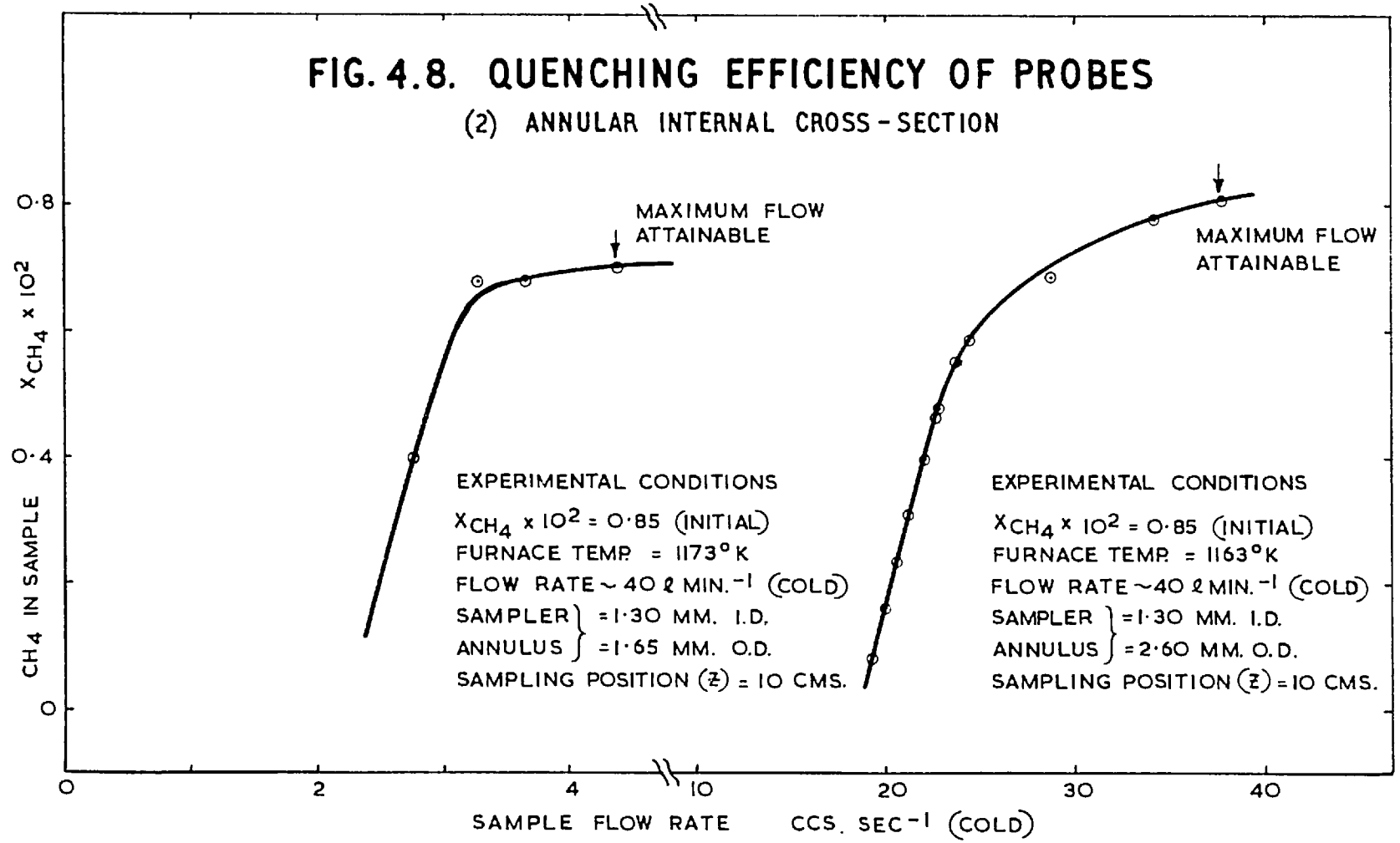
FIG. 4.8. QUENCHING EFFICIENCY OF PROBES
(2) ANNULAR INTERNAL CROSS-SECTION
MAXIMUM FLOW ATTAINABLE
MAXIMUM FLOW ATTAINABLE
EXPERIMENTAL CONDITIONS
$X_{CH_4} \times 10^2 = 0.85$ (INITIAL)
FURNACE TEMP. = 1173°K
FLOW RATE ~ 40 ℓ MIN.$^{-1}$ (COLD)
SAMPLER = 1·30 MM. I.D.
ANNULUS = 1·65 MM. O.D.
SAMPLING POSITION (z) = 10 CMS.
EXPERIMENTAL CONDITIONS
$X_{CH_4} \times 10^2 = 0.85$ (INITIAL)
FURNACE TEMP. = 1163°K
FLOW RATE ~ 40 ℓ MIN.$^{-1}$ (COLD)
SAMPLER = 1·30 MM. I.D.
ANNULUS = 2·60 MM. O.D.
SAMPLING POSITION (z) = 10 CMS.
CH_4 IN SAMPLE $X_{CH_4} \times 10^2$
0
0·4
0·8
0
2
4
10
20
30
40
SAMPLE FLOW RATE CCS. SEC^{-1} (COLD)

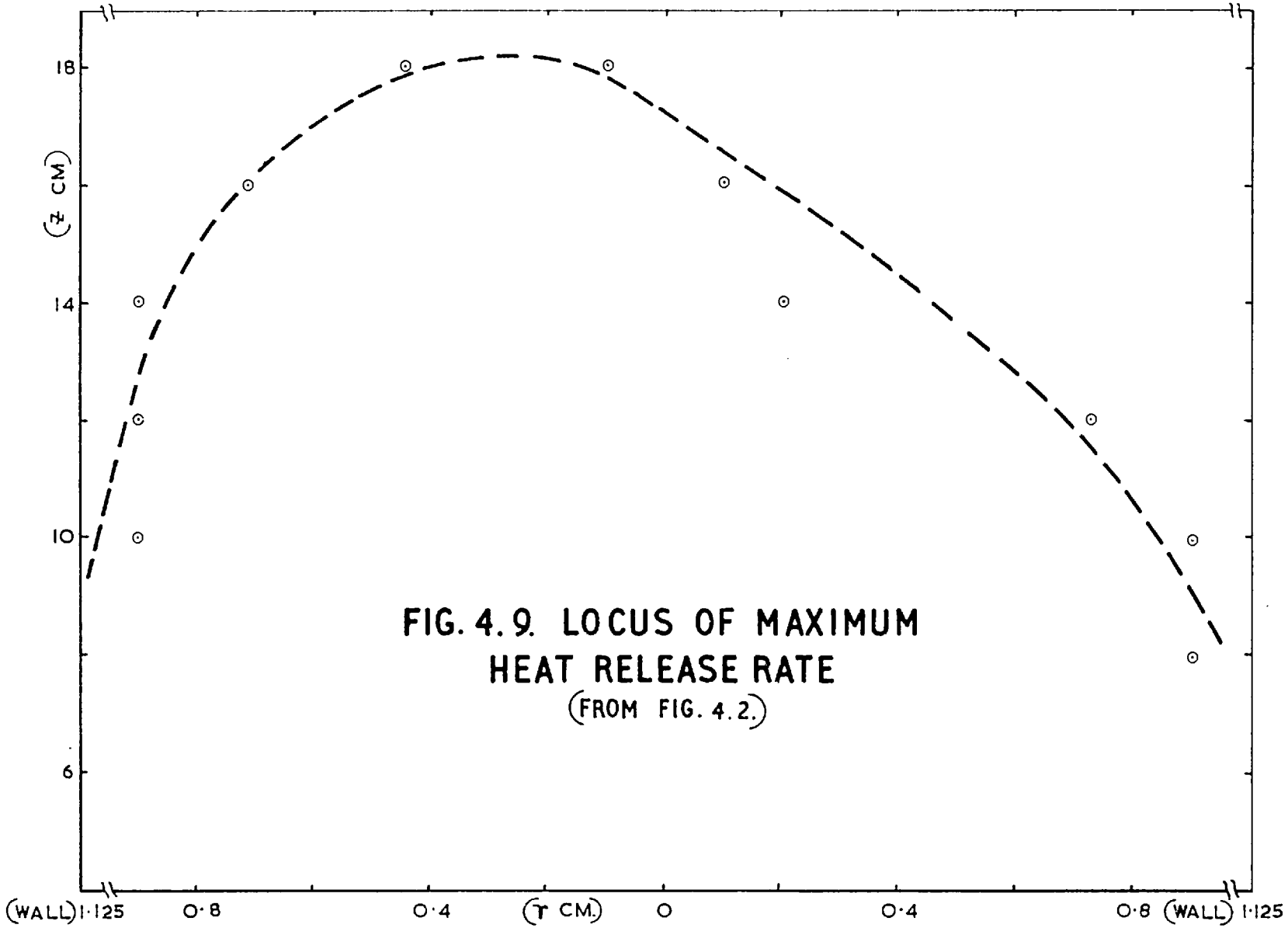

FIG. 4.9. LOCUS OF MAXIMUM HEAT RELEASE RATE
(FROM FIG. 4.2.)

CHAPTER 5

Experimental results and data reduction

5.1 Introduction

So far this thesis has considered a number of exploratory experiments which were intended to assess the techniques, to study the behaviour of the apparatus as a whole, and to indicate the most worthwhile areas for more detailed investigation. This chapter is concerned with the results of these more detailed investigations. As already indicated, this closer look was aimed at two aspects of the methane oxidation reaction at high temperatures, namely (i) the heat release rates, and (ii) the intermediates. From (i) it was hoped to learn more of the physical factors affecting branched chain combustion reactions and from (ii) it was hoped to deduce some useful new information on the mechanism and kinetics of this particular reaction.

Before detailing the results, a few words on the plan of the experimental programme will be appropriate. Much has been written on the subject of the proper design of an experiment (e.g., Reference 105) and it would be inappropriate here to do more than make a brief qualitative statement of the principles adopted in the present experiments.

Quite generally two approaches are possible in the design of an experiment. These are commonly denoted as (a) classical, and (b) factorial. The classical is the simpler approach and requires each variable to be examined separately, whilst holding the remainder constant. Unfortunately this ideal is not realisable in the present

experiments, as is evident from the preliminary work. The alternative - the factorial approach (b) - attempts to handle the situation where the dependent variable is affected by experimental variables which are not independent. In the present case the reaction rate or heat release is probably affected by at least the three experimental variables temperature, concentration and gas stream velocity (mass flow). Each of these experimental variables cannot be varied individually and separately over a very wide range of values without also affecting one or more of the remainder, in addition to producing the desired change in the dependent variable under study. Indeed, although the 'independent' variables are far less strongly coupled than in, say, a flame, the coupling is still significant.

If each variable is examined at only a small number of levels, say 2 or 3, then the following combinations would be required. The situation is illustrated for the case where 2 levels of each of 3 variables are examined, and is made specific to the present situation by designating the variables as velocity (v), concentration (c), and temperature (T):-

(1)	v_1, c_1, T_1,	(5)	v_2, c_2, T_2,
(2)	v_1, c_1, T_2,	(6)	v_2, c_1, T_2,
(3)	v_1, c_2, T_1,	(7)	v_2, c_2, T_1,
(4)	v_1, c_2, T_2,	(8)	v_2, c_2, T_2.

Thus 8 combinations arise. Each combination is equivalent to a run and hence 8 runs are required to investigate and correlate the influence on the dependent variable of 3 experimental variables at 2 levels.

It will be seen from Tables 5.1 and 5.18, which give a résumé of the conditions of each run in terms which correspond to the v, c, T above, that the idealised scheme has been modified to throw more weight on to 2 of the variables (T, c). This was deliberate, since (i) the full programme would have consumed too much time and (ii) the dependence of heat release rate on v was of less interest than the dependence on T and c.

5.2 Experimental results

5.2.1 Range of experimental conditions

Summaries of all the quantitive runs are given in Tables 5.1 and 5.18. Table 5.1 is concerned with investigations of the heat release rates, Table 5.18 with runs investigating the intermediates.

The data covered the following range of conditions in the reaction zone:-

Temperature (T) - 1133°K to 1289°K

Time average mid-stream gas velocity (v_z) - 500 to 1200 cm s^{-1}

Composition (c_i, X_i, m_i) - 0 to 0.0114 mole fraction methane (X_{CH_4})

5.2.2 Composition data

The composition data are presented in the tables as mass fractions m_i, defined by

$$m_j = \frac{\text{mass of } j^{th} \text{ specie per unit volume}}{\text{total mass per unit volume}} = \frac{m_j}{\sum_{i=1}^{n} m_i}$$

The experimental data were in partial volume units. It is worth stating the relation between the experimental and derived units.

Experimental data $= X_i \times 10^2$

$$\left[c_i\right] = \frac{X_i \rho_T}{M_m} = \frac{m_i \rho_T}{M_i} \quad \text{i.e., } m_i = \frac{\text{exptl data}}{100} \cdot \frac{M_i}{M_m}$$

where M_i, M_m are the molecular weights of the i^{th} species and local mean composition respectively, ρ_T is the local gas density and c_i a concentration in moles cm^{-3}.

Two corrections were applied to the experimental composition data.

(a) Individual specie concentrations were corrected for drift of the infra-red gas analysers, the correction being determined at the end of each run. This procedure was found more convenient than the alternative whereby the analysers are re-zeroed intermittently during a run.

(b) An additional adjustment - that mentioned previously in Chapter 4 - was found necessary in some instances. Under the more severe furnace conditions the sample withdrawal rate was just inadequate to prevent detectable reaction in the probe. An estimated correction, never greater than 10 per cent of the experimental value, was applied in these instances. It is thought that the estimation has been accomplished with reasonable accuracy by comparing the temperature and composition radial profiles in the instance under correction with analogous profiles under conditions where the correction was unnecessary. This admittedly arbitrary procedure appears justified by the results -

subsequent analysis with the correction applied gave sensible results, whereas analysis without an initial correction resulted in distinct discrepancies which could reasonable be attributed to inadequate quenching.

5.2.3 Gas velocity data

Local time-mean gas stream velocities have been computed from the total-head pressure profiles and the static pressure. It was shown experimentally that one of the distinct advantages of very lean fuel/air mixtures was the essential independence of the mass flow rate profiles (ρv_z)s of the reaction zone conditions. Neither composition nor temperature affected these profiles. In the case of the composition this was due to the adequacy of using the density of air for that of the mixture (an error of less than 0.2 per cent is introduced by so doing). In the case of the furnace temperature, the independence was attributed to the insignificant effect of total temperature variation on the shapes of the (ρv_z) profiles for a single total mass flow. A single measurement of the total-head pressure profiles for each total mass flow used was therefore adequate.

In order to compute the (ρv_z) profiles from the pressure profiles the temperature at each station was also needed. Fortunately pressure - plus - temperature was the most easily obtained of the coupled measurements with the composite probe. Hence, since

$$p_{to} - p_s = p = \tfrac{1}{2}\rho v_z^2$$

and ρ can be determined from T (using tabulated values for air[106]) (ρv_z) and v_z profiles were computed. Since (ρv_z) profiles were constant for a given total mass flow, velocity profiles for other runs at the same total mass flow were computed from the temperature profiles of the particular run and the common (ρv_z) profiles.

In the few cases where the total mass flow rate differed from that for which (ρv_z) profiles were available, a linear interpolation was employed to obtain the required velocity profiles. Spot checks indicated adequate agreement. Linear extrapolations were limited to the runs where temperature and composition readings were made at stations further downstream than usual (more than 20 cm from the inlet), and the 25 litre/min flow rate (Run 20). Figure 5.1 shows some typical profiles of p, using the model 'D' inlet.

5.2.4 Temperature data

Four temperatures, T_f, T_i, T_e and T_c are recorded in the tables. In Tables 5.1 and 5.18 T_f and T_i refer respectively to the mean furnace temperature recorded by the thermocouple situated in the annulus between the reaction tube and the furnace core and the mean inlet temperature recorded by the thermocouple in the inlet bundle; in both cases the value quoted is the time-mean for the run, the variation about the mean being normally $1^{\circ}K$ or $2^{\circ}K$ and in no case more than $4^{\circ}K$. In Tables 5.2 to 5.17, T_e (column 3) is the gas temperature recorded by the probe thermocouple, T_c is a calculated temperature, (see Section 5.3.3(b) and subsequently) - in the case of T_e the values are quoted to the nearest 0.5°, otherwise values are to the nearest degree.

5.2.5 Tables

Tables 5.1 to 5.17 present the results of 16 out of 25 runs completed in a study of the factors affecting the heat release rates. Of the 25, 10 were sufficiently detailed for a full analysis, 6 were partially analysed and 3 were concerned with gas stream velocity alone. The remainder were considered inadequate for quantitative analysis, for a variety of reasons, and were discarded.

The sampling stations in the reaction zone are given in terms of the axially symmetric cylindrical co-ordinates z and r. Thus the first column in the tables (z) indicates the axial position of the probe tip downstream of the inlet mixing point and the second column (r) indicates the radial position relative to the reaction tube axis (where $r = 0$) on a horizontal diameter in the reaction zone. T_e has already been considered (previous sub-section). Gas stream time-mean velocity v_z is computed from T_c and ρv_z (columns 3 and 5). Columns 6 to 8 give the mass fractions of the three stable species analysed. The last three columns present derived data which will be considered in Chapter 7. T_c is a calculated temperature, $\frac{\partial T}{\partial z}$ a temperature gradient and q''' a volumetric heat release rate.

Tables 5.18 to 5.37 are concerned with the data from 19 out of 21 runs investigating the intermediates and mechanism of the reaction under study. Tables 5.19 to 5.23 present the most detailed data, in terms of analyses, for approximately constant flow rate and composition, and slightly variable temperature. From these five runs and the following three, which deal in a similar manner with the effect of

radial position, a picture of the inter-relationships between formaldehyde, hydrogen and hydrogen peroxide is constructed. The remaining runs in this series attempt to analyse the effects of variation of the parameters on the formaldehyde concentration.

These two aspects of the work on the intermediates are dealt with more fully with the kinetics and mechanism of the reaction in Chapter 8.

5.3 Analysis of the results

5.3.1 Nature of the analysis

The instantaneous conditions at any station in the reaction zone may be described by a set of conservation equations. The first stage in the analysis of the results is therefore to write down the required relations in an appropriate form. Both energy and matter must be conserved at all points in the reaction zone. In order to set the scene for the statement of the conservation equations, the quantities which must appear in any energy and material balance are listed.

(i) Energy

The main source term will be the energy released by combustion of the fuel. Thus in any elemental volume in the reaction zone the energy balance will be determined by

(a) heat released by combustion,

(b) energy transported to or from the volume element by the processes of conduction, convection and radiation,

(c) latent energy terms, which will account for internal forms of energy such as dissociation, electronic and vibrational excitation and the occurrence of radical

species; all in excess of (or less than) the values required for thermodynamic equilibrium.

(ii) Matter

Here the main source (or sink) term will be the creation (or consumption) of species by chemical reaction. Thus by analogy with the energy balance, a material balance in any elemental volume will be determined by

(a) species created or destroyed by reaction,

(b) material transport by diffusion and convection.

A very informative and simple test for the overall conservation of matter and energy is the comparison of the measured temperature with a temperature calculated from the fuel disappearance rate. The remainder of the present chapter (after the statement of the conservation equations) and the whole of the following chapter are therefore taken up with an examination of the consequences of this comparison.

5.3.2 Steady-state conservation equations

For steady-state conditions the continuity relations for conservation of matter and energy are required to specify the system. If momentum effects and radiation losses are neglected, the equations may be written in terms of cylindrical co-ordinates as

$$\frac{1}{r}\,\frac{\partial}{\partial r}\,r\,F_r + \frac{\partial F_z}{\partial z} - R = 0 \quad \ldots \quad \ldots \quad \ldots \quad 5.1$$

for an axisymmetric system, where F is a flux such that F_r is the flow rate per unit area of some property of the gas (heat etc.,) in the radial direction and F_z is the flow rate per unit area of the same

property in the axial direction. R is the rate of generation (or diminution) of the property per unit volume.

In the absence of chemical reaction, heat sources or sinks, R will be zero and

$$\frac{1}{r}\frac{\partial}{\partial r} r F_r + \frac{\partial F_z}{\partial z} = 0 \qquad \ldots \quad \ldots \quad \ldots \quad 5.2$$

Consideration is now given to the particular forms of Equation 5.1 for the various properties of the system which must be conserved.

(a) Conservation of mass

Since matter can be neither created nor destroyed (R = 0), substitution of the mass flow rate in the r and z directions in Equation 5.2 yields directly

$$\frac{1}{r}\frac{\partial}{\partial r} r\rho v_r + \frac{\partial \rho v_z}{\partial z} = 0 \qquad \ldots \quad \ldots \quad \ldots \quad 5.3$$

(b) Conservation of heat

Here R may be non-zero and the fluxes may be written

$$F_r = \rho v_r H - \lambda \frac{\partial T}{\partial r} \qquad \ldots \quad \ldots \quad 5.4$$

$$F_z = \rho v_z H - \lambda \frac{\partial T}{\partial z} \qquad \ldots \quad \ldots \quad 5.5$$

where H is the enthalpy of the local mixture and λ is the thermal conductivity (of nitrogen). λ must be replaced by an eddy conductivity term in turbulent flow. R takes the form

$$R = \sum_i K_j \Delta H_{c,j} = q''' \qquad \ldots \quad \ldots \quad \ldots \quad 5.6$$

where K_j is the net reaction rate of the j^{th} species per unit volume and $\Delta H_{c,j}$ the heat of combustion of the j^{th} species. Thus $\sum_i K_j \Delta H_{c,j}$ is a volumetric heat release rate and may be designated q'''. Substitution of Equations 5.4 to 5.6 in 5.1 results in the continuity relation for the conservation of heat.

$$\rho v_r \frac{\partial H}{\partial r} - \frac{1}{r}\frac{\partial}{\partial r}\left(\lambda r \frac{\partial T}{\partial r}\right) + \rho v_z \frac{\partial H}{\partial z} - \frac{\partial}{\partial z}\left(\lambda \frac{\partial T}{\partial z}\right) - q''' = 0 \quad \ldots \ldots \ldots 5.7$$

where the effect of viscosity on the velocity gradients has been neglected as has radiation, while effects such as latent energy are included in the $\Delta H_{c,j}$ and therefore appear in q'''.

(c) Conservation of species

By analogy with the conservation of heat, consideration of the j^{th} specie results in

$$\rho v_r \frac{\partial m_j}{\partial r} - \frac{1}{r}\frac{\partial}{\partial r}\left(D_j \rho r \frac{\partial m_j}{\partial r}\right) + \rho v_z \frac{\partial m_j}{\partial z} - \frac{\partial}{\partial z}\left(D_j \rho \frac{\partial m_j}{\partial z}\right) - K_j \nu_j = 0 \quad \ldots \ldots \ldots 5.8$$

where D_j is the molecular binary-diffusion coefficient (which must be replaced by an eddy diffusivity in turbulent flow.) D_j is in terms of $\frac{\partial c_j}{\partial r}$ so that $D_j\rho$ is the form required for gradients written in terms of $\frac{\partial m_j}{\partial r}$ for a trace of j in air. (The secondary dependence of the diffusion coefficient on temperature has been ignored.) ν_j is a conversion factor required to convert the net volumetric rate K_j into a net mass reaction rate. $K_j\nu_j$ is concerned only with those reactions in

which the j^{th} species participates. Thus a separate partial differential equation of the form of Equation 5.8 will be required to describe the distribution of each species in the reaction zone.

(d) The equation of motion

The equation of motion can now be added to complete the set of equations. It is

$$\rho v_z \frac{\partial v_z}{\partial z} + \rho v_r \frac{\partial v_z}{\partial r} - \frac{1}{r} \frac{\partial}{\partial r} \left(\mu r \frac{\partial v_z}{\partial r} \right) = 0 \quad \ldots \quad \ldots \quad 5.9$$

where μ is the local value of the viscosity.

It is not proposed to attempt the simultaneous solution of these equations, but rather to use them to guide the analysis of the experimental data.

5.3.3 Initial data reduction

(a) Conservation of mass

Integrating F_z as a function of r for the case where $F_z = \rho v_z$ we obtain the total mass flow rate across any section, M

$$M = 2\pi \int_o^{r_o} \rho v_z \, r \, dr \quad \ldots \quad \ldots \quad \ldots \quad 5.10$$

This integration was performed graphically for the data of run 12 (Table 5.16) at z = 9 and z = 19 cm, plotting ρv_z r versus r. This resulted in

$$M_9 = 0.941 \text{ gm s}^{-1}$$

$$M_{19} = 0.964 \text{ gm s}^{-1}$$

which may be compared with the mass flow rate deduced from the measured volumetric flow rate (cold),

$$M_v = 0.966 \text{ gm s}^{-1}$$

The variation is 2.5 per cent, suggesting there can be no major quarrel with the pitot-static method. Similar results may be obtained from other runs.

Having established that the data were adequate for the analysis, a comparison of ρv_z at different values of z was made. Equation 5.3 shows that if $\frac{\partial \rho v_z}{\partial z} = 0$, then $\rho v_r = 0$, and conversely if $\frac{\partial \rho v_z}{\partial z} \neq 0$, then $\rho v_r \neq 0$. Comparison of ρv_z at r = 0 for z = 9 and z = 19 shows an increase of 6 per cent in ρv_z at z = 19. Inspection of intermediate values of z shows this to be in accord with the general trend of the ρv_z values. Evidently $\rho v_r \neq 0$, a result common to all the runs, and one which is to be expected where transition to laminar flow is occurring (see Chapter 6).

(b) Conservation of species and energy

A test of the combined effects of matter and energy transport may be accomplished by comparing the measured temperature profile along the axis through the reaction zone, with a temperature calculated from the reactant disappearance rate.

Inspection of Equations 5.7 to 5.9 indicates that all transport properties are gradient dependent. Thus in regions where no gradients occur, or where the gradient controlled term is negligible by comparison with the convective term, the source term, R, should exactly balance the convective terms. The experimental values of the specie and temperature profiles in the radial direction for the central core of the flow ($0.6 > r > -0.6$ cm) in the majority of the runs recorded in

Tables 5.2 to 5.17, coupled with the shallowness of the gradients in the axial direction, suggested that to a good approximation the balance between convective and source terms should obtain in the present case. Hence a direct comparison of the measured temperature profile with a profile calculated from the composition data, neglecting gradient transport processes, should be informative. The only additional proviso, which in fact is implicit in the neglect of gradient dependent properties, is that an atom balance be maintained. It is only possible to test this for the carbon atom in the experiments described here, for which it is adequate. The test is insufficiently sensitive for the inclusion of low concentration intermediates, such as formaldehyde, to be legitimate.

Run 12 (Table 5.16) was selected and a calculated temperature profile obtained in the following manner. Consider any interval Δz along the axis. Let the difference in the values of the specie mass fractions at either end of the interval be Δm_{CH_4}, Δm_{CO}, Δm_{CO_2} and assume the reaction to be energetically equivalent to

$$CH_4 + 1\tfrac{1}{2}O_2 \rightarrow CO + 2H_2O \quad \Delta H_c' = 7739 \text{ cal gm}^{-1}$$

and

$$CO + \tfrac{1}{2}O_2 \rightarrow CO_2 \quad \Delta H_c'' = 2415 \text{ cal gm}^{-1}$$

then the temperature rise for the interval Δz may be obtained from the relation

$$\Delta T_c = -\frac{\Delta m_{CH_4} \times \Delta H_c'}{Cp(air)} + \frac{\Delta m_{CO_2} \times \Delta H_c''}{Cp(air)} \cdot \frac{M_{CO}}{M_{CO_2}}$$

where it is permissible to use the mean specific heat of air over the temperature range of the experiments, in place of the specific heat of

the combustion gases, because of the extreme dilution. The required thermochemical data were obtained from Reference 107. M_{CO} and M_{CO_2} are the molecular weights of carbon monoxide and carbon dioxide respectively. Starting at the position nearest the inlet for which data were available, the axial profile of T_c was computed by forward integration using Δz intervals of 1 cm or 2 cm. The result for run 12 is shown in Figure 5.2. A considerable divergence is apparent. Because of this a similar procedure was carried through for all the runs listed in Tables 5.2 to 5.17. The results showed a similar and consistent trend.

It is therefore evident that either or both energy and species are not conserved - within the limitations of the assumptions made - or the flow model assumed (transport properties gradient dependent) is inadequate to describe the core of the flow. The latter is obviously the more likely alternative and attempts to find an improved model of the fluid mechanics in the reaction zone are presented in Chapter 6. Before proceeding with this, however, it is necessary to demonstrate (a) that the assumptions in the preceding calculations are adequate and (b) that the divergence cannot be reasonably attributed to poor experimentation.

5.4 Adequacy of the calculation and experimentation

5.4.1 Adequacy of the calculation of T_c

There are three respects in which the calculation of T_c may be inadequate.

(a) It may be inadequate because of the neglect of the radial convective term ρv_r and neglect of the axial gradient terms $\lambda \frac{\partial m_i}{\partial z}$ and $\rho D_j \frac{\partial m_i}{\partial z}$. In both cases the consequences will be to produce a divergence between T_e and T_c of the form found. However, in run 12 ρv_r has been shown to produce an increase in ρv_z at the axis of 6 per cent in proceeding from z = 9 to z = 19 cm. On a laminar model of the flow with no radial gradients in the core a negligible effect would result from this convective term. A similar statement is true for the small axial gradients by comparison with the bulk convective term in the z direction. In a turbulent flow the situation is less easily assessed. Qualitatively it is evident that what effects there are will be magnified. Even so, fairly appreciable gradients would be required in the radial direction to account for the observed divergence. This aspect is treated in more detail in the next chapter. It is sufficiently unlikely that an explanation on the basis of gradient dependent transport processes will succeed that alternative explanations should be investigated.

(b) Calculation of T_c may be incorrect because the thermochemical representation of the reaction as the two steps $CH_4 \rightarrow CO + H_2O$ followed by $CO \rightarrow CO_2$ is unrealistic. Since no water analyses were carried out no atom balance for H was possible, nor for O.

(c) No allowance has been made for a storage or latent energy term. Thus excess internal energy, excited species and radicals may be present, and would result in T_e being lower than T_c, since T_c is computed on the assumption of thermodynamic equilibrium.

Both (b) and (c) may be disposed of as serious sources of error on the basis of a single argument. It is that if (b) and (c) are valid explanations of the divergence observed, then eventually T_c and T_e will converge in the later stages of the reaction. There is no sign of this happening in any of the runs examined.

5.4.2 Adequacy of the sampling techniques

The appraisal will be made by stating and assessing the possible weaknesses or faults one by one. No apology is made for re-iterating previous statements.

(i) It was appreciated at the outset that the design of the composite probe was a compromise (see discussion in Chapters 3 and 4). This may give rise to two distinct inaccuracies. In some circumstances the quenching of the sampled gas may be inadequate. This will result in incorrect composition data being recorded. However, there are at least two arguments against this possibility being of more than minor importance in the present case. The first has already been given in the context of the previous section; it is that for inadequate sampling to be a major cause of the divergence between T_c and T_e, the two profiles should converge at large z, to give a hysteresis-shaped figure. That this is not true is apparent from Figure 5.2 and it is equally demonstrable from plots of all the runs in this series. The second argument is indicated by Figure 5.3, where the profiles for the leanest mixture studied are plotted. The experimental temperature profile here has a zero or negative slope throughout, which is of the same order of magnitude as the positive slope of the calculated

profile. In this case therefore the composition 'inaccuracy' cannot possibly account for more than half the discrepancy.

This state of affairs immediately leads to a consideration of the second possible inaccuracy due to the compromise in the probe design. The quenching action of the probe is in part accomplished by the pressure drop along its length, which will be accompanied (adiabatic assumption) by a fall in temperature. Hence there is a distinct possibility of the thermocouple reading too low, particularly in view of its geometric disposition. This possibility has already been investigated in Chapter 3, Section 3.5.3, where it was shown that the error in the temperature measurement from this cause was negligible. (It is plausible that this is due to local stagnation temperature recovery immediately ahead of the thermocouple junction.) Thus the negative slope of the experimental temparature profile in Figure 5.3 must be real.

(ii) Explanations of the divergence on the basis of instrumental inaccuracies are soon dealt with. Taking the composition analyses first it is clear that an explanation in terms of inaccurate analysis by the infra-red gas analysers is possible only if the carbon dioxide and carbon monoxide analysers are reading too high (or conversely the methane analyser is reading too low) with the result that a detailed atom balance will show an increase in carbon with increasing reactedness. In fact carbon balances are constant to within the experimental accuracy, thus disposing of this possibility. The accuracy of the temperature measurement would not be expected to vary

significantly with change of station in the reaction zone, especially as neither aspiration rate (sampling rate) nor temperature differential between probe and wall vary appreciably. A typical case has already been investigated (see Chapter 3) and been shown to be sufficiently accurate. In any case a constant error will not show up in the method used and therefore cannot be invoked as a cause of the divergence.

(iii) There are a number of minor faults which would (and sometimes did) occur in the instrumentation and sampling which it is not worth listing individually here. Suffice it to say that the predictable, and in some cases experimentally known, effects of these faults are not in accord with the two major pieces of experimental evidence already introduced in support of the general correctness of the results obtained.

(iv) The accuracy and validity of the velocity measurement need not be considered in this context because the gas stream velocity does not appear in the calculations.

The deductions of the present section may be summarised as indicating the general validity of both the method of calculation and of the experimental methods. It follows that the observed divergence between T_c and T_e is realistic and explanations for this must now be found.

TABLE 5.1(a)

Summary of heat release runs

Table number	Run number	Flow rate 293°K litre min^{-1}	Methane Mole Fraction $\times 10^2$	Furnace Temperature °K	Inlet Temperature °K
5.2	20	24.93	0.685	1134	1134
5.3	13	32.32	0.460	1145	1146
5.4	10	32.32	0.630	1152	1152
5.5	18	32.32	0.885	1146	1145
5.6	14	32.32	0.900	1152	1153
5.7	25	41.08	0.146	1168	1168
5.8	23	41.08	0.240	1177	1177
5.9	24	41.08	0.250	1161	1162
5.10	8	41.08	0.475	1167	1169
5.11	21	41.08	0.655	1155	1156
5.12	22	41.08	0.660	1151	1150
5.13	6	41.08	0.700	1172	1173
5.14	3	41.08	0.795	1166	1169
5.15	7	41.08	0.920	1175	1172
5.16	12	49.75	0.460	1177	1178
5.17	11	49.90	0.650	1189	1189

TABLE 5.1(b)

Notation of Tables 5.2 to 5.37

Symbol	Meaning	Units
z, r	Position co-ordinates	cm
T_e	Experimental Gas Temperature	^oK
v_z	Axial component of gas velocity	cm s^{-1}
ρV_Z $(= m'')$	Mass flow rate	g cm^{-2} s^{-1}
$m_{CH_4}, m_{CO}, m_{CO_2}$ $m_{HCHO}, m_{H_2O_2}, m_{H_2}$	Specie mass fraction	$g.g^{-1}$
T_c	Calculated Gas Temperature	^oK
$\left(\frac{\partial T}{\partial z}\right)_{r=o}$	Mean temperature * gradient, Z component	^oK cm^{-1}
q'''	Volumetric heat release rate	cal cm^{-3} s^{-1}

* Calculated from $T = \left(\frac{T_e + T_c}{2}\right)$ or $T = T_{i,o} + \Delta T \times 1.3$ (see Section 7.2)

TABLE 5.2

(Run 20)

Z	r	T_e	V_Z	ρV_Z	$m_{CH_4} \times 10^3$	$m_{CO} \times 10^3$	$m_{CO_2} \times 10^3$	T_c	$\left(\frac{\partial T}{\partial Z}\right)_{r=0}$	q'''
20	0	1228	729	0.210	0.06	1.11	8.66	1293	4.95	0.294
19	0	1223	718	0.207	0.11	2.03	6.99	1284	8.2	0.481
19	0.2	1223	718	0.207	0.11	2.08	6.99			
19	0.4	1222	717	0.207	0.08	1.88	7.14			
19	0.6	1217	680	0.197	0.06	1.55	7.67			
19	0.8	1199	501	0.148	0.06	0.97	8.81			
19	0.9	1187	331	0.098	0.03	0.73	9.26			
18	0	1216	698	0.203	0.19	2.85	5.77	1274	12.2	0.705
17	0	1206	686	0.201	0.47	3.77	3.34	1254	15.6	0.888
17	0.2	1206	692	0.202	0.47	3.87	3.19			
17	0.4	1204	695	0.204	0.53	4.06	2.73			
17	0.6	1206	661	0.194	0.47	3.92	3.19			
17	0.8	1201	495	0.145	0.25	3.19	4.86			
17	0.9	1196	325	0.096	0.17	2.51	6.23			
15	0	1180	660	0.197	1.38	3.53	1.14	1207	14.5	0.822
13	0	1162	639	0.194	2.41	2.03	0.30	1174	10.3	0.566
13	0.2	1162	658	0.200	2.52	1.88	0.30			
13	0.4	1162	667	0.202	2.55	1.84	0.30			
13	0.6	1165	634	0.192	2.46	1.98	0.30			
13	0.8	1168	469	0.142	2.05	2.71	0.38			
13	0.9	1165	309	0.094	1.69	3.34	0.53			
13	-0.2	1163	-	-	2.30	2.13	0.38			
13	-0.4	1166	-	-	2.16	2.37	0.46			
11	0	1150	623	0.191	3.10	1.01	0.08	1154	6.0	0.324
9	0	1143	608	0.188	3.49	0.48	0	1145	3.0	0.160
9	0.2	1143	634	0.196	3.49	0.48	0			
9	0.4	1143	647	0.200	3.52	0.53	0			
9	0.6	1143	611	0.189	3.52	0.48	0			
9	0.8	1143	451	0.139	3.49	0.53	0			
9	0.9	1143	292	0.090	3.49	0.53	0			

TABLE 5.3

(Run 13)

Z	r	T_e	V_Z	ρV_Z	$m_{CH_4} \times 10^3$	$m_{CO} \times 10^3$	$m_{CO_2} \times 10^3$	T_c	$\left(\frac{\partial T}{\partial Z}\right)_{r=o}$	q'''
20	0	1207	811	0.237	0.03	0.63	6.00	1236	2.64	0.177
19	0	1206	799	0.235	0.03	1.01	5.32	1231	3.18	0.212
19	0.2	1206	799	0.235	0.03	1.01	5.24			
19	0.4	1206	799	0.235	0.03	0.97	5.32			
19	0.6	1203	756	0.223	0	0.82	5.39			
19	0.8	1189	561	0.166	0	0.68	5.77			
19	0.9	1179	373	0.111	0	0.53	6.08			
18	0	1203	784	0.230	0.06	1.50	4.48	1226	4.21	0.274
17	0	1199	776	0.228	0.11	2.37	3.04	1218	5.00	0.323
17	0.2	1197	784	0.230	0.14	2.61	2.74			
17	0.4	1197	788	0.231	0.11	2.42	2.96			
17	0.6	1196	744	0.219	0.08	2.32	3.19			
17	0.8	1191	553	0.164	0.06	2.03	3.95			
17	0.9	1185	371	0.109	0.03	1.50	4.63			
15	0	1191.5	757	0.224	0.25	3.00	1.97	1207	5.37	0.342
13	0	1182.5	737	0.220	0.66	2.95	0.76	1190	6.85	0.427
13	0.2	1182	759	0.226	0.66	2.95	0.76			
13	0.4	1182	769	0.229	0.66	2.95	0.76			
13	0.6	1183	729	0.218	0.66	2.95	0.76			
13	0.8	1179	541	0.161	0.66	2.95	0.76			
13	0.9	1175	356	0.106	0.64	3.00	0.76			
13	-0.9	1172	-	-	0.44	3.10	1.14			
11	0	1169	717	0.216	1.12	1.93	0.46	1175	5.74	0.351
9	0	1160	698	0.212	1.63	1.21	0.15	1160	5.03	0.303
9	0.2	1160	728	0.221	1.66	1.16	0.15			
9	0.4	1159	742	0.226	1.66	1.16	0.15			
9	0.6	1159.5	701	0.213	1.66	1.16	0.15			
9	0.8	1160	517	0.157	1.66	1.16	0.15			
9	0.9	1158.5	335	0.102	1.63	1.21	0.15			
9	-0.9	1158.5	-	-	1.58	1.30	0.15			

TABLE 5.4

(Run 10)

Z	r	T_c	V_Z	ρV_Z	$m_{CH_4} \times 10^3$	$m_{CO} \times 10^3$	$m_{CO_2} \times 10^3$	T_c	$\left(\frac{\partial T}{\partial Z}\right)_{r=0}$	q'''
20	0	1244	836	0.237	0	1.40	7.75	1288	7.94	0.533
19	0	1237	823	0.235	0.06	2.32	6.23	1278	10.63	0.710
19	0.2	1237	823	0.235	0.06	2.32	6.23			
19	0.4	1237	823	0.235	0.06	2.27	6.23			
19	0.6	1236	780	0.223	0.06	2.22	6.30			
19	0.8	1225.5	577	0.166	0.03	1.69	7.06			
19	0.9	1215	381	0.111	0	1.26	8.05			
18	0	1225	798	0.230	0.17	3.38	4.25	1265	13.0	0.846
17	0	1213	783	0.228	0.36	4.16	2.58	1245	14.7	0.950
17	0.2	1211	790	0.230	0.44	4.40	1.82			
17	0.4	1212	794	0.231	0.44	4.35	1.90			
17	0.6	1215	755	0.219	0.47	4.16	2.05			
17	0.8	1218	567	0.164	0.36	3.72	2.96			
17	0.9	1213	373	0.109	0.22	3.34	4.02			
15	0	1191	755	0.224	1.25	3.43	0.76	1216	12.8	0.814
13	0	1174	731	0.220	2.30	1.84	0.08	1184	10.0	0.622
13	0.2	1174	753	0.226	2.30	1.84	0.08			
13	0.4	1174	764	0.229	2.30	1.84	0.08			
13	0.6	1176	725	0.218	2.30	1.84	0.08			
13	0.8	1180	537	0.161	2.19	1.98	0.15			
13	0.9	1181	354	0.106	1.97	2.37	0.23			
11	0	1165	714	0.216	2.80	1.01	0	1170	5.62	0.344
9	0	1158	697	0.212	3.24	0.39	0	1158	3.16	0.189
9	0.2	1158	727	0.221	3.24	0.39	0			
9	0.4	1158	741	0.226	3.24	0.39	0			
9	0.6	1158	701	0.213	3.24	0.39	0			
9	0.8	1158.5	517	0.157	3.18	0.48	0			
9	0.9	1158.5	335	0.102	3.16	0.53	0			

TABLE 5.5

(Run 18)

Z	r	T_e	V_Z	ρV_Z	$m_{CH_4} \times 10^3$	$m_{CO} \times 10^3$	$m_{CO_2} \times 10^3$	T_c	$\left(\frac{\partial T}{\partial Z}\right)_{r=0}$	q'''
20	0	1194	803	0.237	2.08	4.45	0.61	1229	17.5	1.178
19	0	1185	785	0.234	2.77	3.38	0.38	1209	13.2	0.877
19	0.2	1185	785	0.234	2.71	3.38	0.46			
19	0.4	1194	795	0.235	2.41	3.72	0.68			
19	0.6	1210	762	0.222	1.88	4.30	1.44			
19	0.8	1218	572	0.166	0.69	4.11	5.32			
19	0.9	1215	386	0.112	0.39	3.53	7.22			
18	0	1176	767	0.230	3.27	2.61	0.15	1194	10.40	0.677
17	0	1171	756	0.228	3.76	1.84	0.08	1180	7.70	0.498
17	0.2	1171	766	0.231	3.80	1.78	0.08			
17	0.4	1174	773	0.232	3.74	1.84	0.15			
17	0.6	1183	736	0.220	3.46	2.27	0.15			
17	0.8	1194	559	0.165	2.38	3.82	0.68			
17	0.9	1196	376	0.111	1.55	4.98	1.59			
15	0	1163	738	0.224	4.35	1.06	0	1164	4.55	0.292
13	0	1156	721	0.220	4.54	0.68	0	1158	2.94	0.183
13	0.2	1156	742	0.226	4.54	0.68	0			
13	0.4	1156	753	0.230	4.54	0.68	0			
13	0.6	1158	710	0.216	4.52	0.68	0			
13	0.8	1162	533	0.162	4.46	0.82	0			
13	0.9	1164	356	0.108	4.27	1.01	0			
11	0	1152.5	707	0.217	4.71	0.48	0	1153	1.93	0.118
9	0	1149	691	0.212	4.88	0.29	0	1149	1.30	0.078
9	0.2	1149	721	0.221	4.88	0.29	0			
9	0.4	1149	735	0.226	4.88	0.29	0			
9	0.6	1149.5	695	0.213	4.88	0.29	0			
9	0.8	1150	512	0.157	4.90	0.29	0			
9	0.9	1150	332	0.102	4.90	0.29	0			

TABLE 5.6

(Run 14)

Z	r	T_e	V_Z	ρV_Z	$m_{CH_4} \times 10^3$	$m_{CO} \times 10^3$	$m_{CO_2} \times 10^3$	T_c	$\left(\frac{\partial T}{\partial Z}\right)_{r=o}$	q'''
20	0	1265	850	0.237	0.08	2.32	10.18	~1335	-	-
19	0	1255	832	0.234					17.25	1.13
18	0	1234	804	0.230					38.5	2.56
17	0	1208	780	0.228					37.2	2.41
15	0	1176	747	0.224					11.35	0.721
13	0	1166	727	0.220					5.83	0.364
11	0	1159	713	0.217					2.86	0.175
9	0	1153	693	0.212					2.73	0.164
5	0	1147	-	-						

TABLE 5.7

(Run 25)

Z	r	T_e	V_Z	ρV_Z	$m_{CH_4} \times 10^3$	$m_{CO} \times 10^3$	$m_{CO_2} \times 10^3$	T_c	$\left(\frac{\partial T}{\partial Z}\right)_{r=o}$	q'''
26	0.2	1167	1011	0.305	0.11	1.06	0.27	1181	-0.16	-0.014
26	0.4	1166.5	-	-	0.08	1.11	0.30			
26	0.6	1165	-	-	0.08	1.07	0.33			
26	0.8	1158	-	-	0.06	1.10	0.39			
26	0.9	1153	-	-	0.03	1.12	0.47			
23	0.2	1170	982	0.296	0.17	1.01	0.21	1179	0	0
23	0.4	1170	-	-	0.17	1.00	0.24			
23	0.6	1168.5	-	-	0.14	1.00	0.29			
23	0.8	1164	-	-	0.11	1.03	0.35			
23	0.9	1161	-	-	0.08	1.04	0.41			
20	0.2	1172.5	959	0.288	0.22	0.92	0.18	1177.5	0	0
20	0.4	1172.5	965	0.290	0.22	0.91	0.20			
20	0.6	1171.5	933	0.281	0.22	0.94	0.21			
20	0.8	1168	776	0.234	0.19	0.95	0.26			
20	0.9	1165	590	0.179	0.17	0.99	0.29			
18	0.2	1172.5	940	0.283	0.25	0.82	0.20	1177	0.11	0.009
16	0.2	1173	930	0.280	0.30	0.78	0.17	1175	0.24	0.019
16	0.4	1173	941	0.283	0.30	0.78	0.17			
16	0.6	1173	927	0.279	0.28	0.79	0.18			
16	0.8	1172.5	753	0.226	0.28	0.82	0.18			
16	0.9	1171	583	0.176	0.25	0.89	0.18			
14	0.2	1173	923	0.278	0.36	0.71	0.06	1173	0.286	0.023

TABLE 5.8

(Run 23)

Z	r	T_e	V_Z	ρV_Z	$m_{CH_4} \times 10^3$	$m_{CO} \times 10^3$	$m_{CO_2} \times 10^3$	T_c	$\left(\frac{\partial T}{\partial Z}\right)_{r=0}$	q'''
20	0	1198	975	0.287	0	1.16	1.75	1223	0	0
19	0	1198	965	0.284						
18	0	1198	958	0.282						
17	0	1197.5	950	0.280					0.13	0.010
15	0	1196.5	939	0.277						
13	0	1195.5	928	0.274					0.86	0.067
11	0	1194	917	0.271					1.22	0.094
9	0	1191.5	902	0.267					1.43	0.108
7	0	1189	-	-						
5	0	1186	-	-						
2.3	0	1181	-	-						

TABLE 5.9

(Run 24)

Z	r	T_e	V_Z	ρV_Z	$m_{CH_4} \times 10^3$	$m_{CO} \times 10^3$	$m_{CO_2} \times 10^3$	T_c	$\left(\frac{\partial T}{\partial Z}\right)_{r=0}$	q'''
22	0	1179.5	982	0.294	0.06	2.00	0.74	1189.5	0.39	0.033
22	0.4	1179.5	981	0.293	0.06	1.93	0.79			
22	0.6	1177	950	0.285	0.03	1.81	0.97			
22	0.8	1169	-796	0.240	0	1.49	1.52			
22	0.9	1166	-604	0.183	0	1.38	1.66			
20	0	1179.5	960	0.287	0.11	1.94	0.76	1188	0.51	0.041
18	0	1179.5	942	0.282	0.22	1.69	0.71	1186	0.64	0.051
18	0.2	1180	945	0.282	0.22	1.73	0.70			
18	0.4	1180	958	0.286	0.19	1.76	0.73			
18	0.6	1179.5	933	0.279	0.19	1.71	0.79			
18	0.8	1176	769	0.231	0.17	1.74	0.87			
18	0.9	1172	587	0.177	0.14	1.65	0.94			
16	0	1178	928	0.278	0.28	1.52	0.64	1183	0.83	0.065
16	0.4	1178	946	0.283	0.25	1.54	0.61			
16	0.6	1177	931	0.279	0.28	1.54	0.58			
16	0.8	1175	759	0.228	0.28	1.60	0.49			
16	0.9	1171	578	0.174	0.25	1.66	0.46			
14	0	1175	919	0.276	0.36	1.39	0.46		1.26	0.100
12	0	1174	907	0.273	0.44	1.29	0.30	1176	1.62	0.126
12	0.4	1174	929	0.279	0.44	1.30	0.27			
12	0.6	1175	928	0.279	0.44	1.31	0.26			
12	0.8	1174	756	0.227	0.41	1.32	0.26			
12	0.9	1172	587	0.177	0.41	1.34	0.23			
10	0	1171.5	895	0.269	0.58	1.15	0.18	1172.5	1.95	0.151
10	0.4	1171.5	920	0.277	0.58	1.13	0.18			
10	0.6	1171.5	924	0.278	0.61	1.09	0.18			
10	0.8	1171	739	0.223	0.61	1.06	0.18			
10	0.9	1170.5	575	0.173	0.58	1.09	0.18			
8	0	1168	881	0.266	0.72	0.88	0.11	1168	2.06	0.158
5	0	1163	-	-	-	-	-			

TABLE 5.10

(Run 8)

Z	r	T_e	V_Z	ρV_Z	$m_{CH_4} \times 10^3$	$m_{CO} \times 10^3$	$m_{CO_2} \times 10^3$	T_c	$\frac{\partial T}{\partial Z}_{r=o}$	q'''
20	0	1229	1000	0.287	0	1.55	4.71	1257	3.60	0.293
19	0	1225	985	0.284	0.03	1.98	4.10	1253	4.50	0.364
19	0.2	1225	988	0.285	0.03	1.93	4.18			
19	0.4	1225	999	0.288	0.06	1.98	4.02			
19	0.6	1225	971	0.280	0.03	1.69	4.33			
19	0.8	1219	801	0.232	0.03	1.40	4.63			
19	0.9	1212	605	0.176	0.03	1.21	5.16			
18	0	1222	976	0.282	0.08	2.51	3.34			
17	0	1219	966	0.280	0.14	2.95	2.58	1242	5.5	0.44
17	0.2	1219	970	0.281	0.14	2.95	2.58			
17	0.4	1219	984	0.285	0.14	3.00	2.58			
17	0.6	1219	966	0.280	0.14	3.00	2.58			
17	0.8	1215.5	790	0.229	0.08	2.66	3.04			
17	0.9	1208.5	597	0.174	0.11	2.66	3.04			
15	0	1206	945	0.277	0.47	3.10	1.44	1227	6.41	0.51
13	0	1196	929	0.274	0.83	2.71	0.76	1213	7.15	0.563
13	0.2	1195.5	938	0.277	0.83	2.76	0.76			
13	0.4	1195.5	952	0.281	0.83	2.71	0.76			
13	0.6	1195.5	945	0.279	0.83	2.71	0.76			
13	0.8	1196	760	0.224	0.80	2.71	0.76			
13	0.9	1196	588	0.174	0.77	2.76	0.76			
11	0	1186	910	0.271	1.44	1.64	0.30	1194	7.04	0.549
9	0	1177	891	0.267	2.02	1.06	0.08	1177	6.33	0.487
9	0.2	1177	901	0.270	2.02	1.06	0.08			
9	0.4	1177.5	918	0.275	2.02	1.06	0.08			
9	0.6	1178.5	925	0.277	2.02	0.97	0.08			
9	0.8	1179	738	0.221	1.99	0.92	0.08			
9	0.9	1179.5	576	0.172	1.99	0.92	0.15			

TABLE 5.11

(Run 21)

Z	r	T_e	V_Z	ρV_Z	$m_{CH_4} \times 10^3$	$m_{CO} \times 10^3$	$m_{CO_2} \times 10^3$	T_c	$\left(\frac{\partial T}{\partial Z}\right)_{r=o}$	q'''
25	0	1229	1061	0.305	0.19	3.87	3.57	1266	9.1	0.788
24	0	1222	1038	0.300	0.36	4.64	2.13	1254	10.65	0.910
24	0.2	1224	1040	0.300	0.30	4.45	2.43			
24	0.4	1227	1036	0.298	0.25	4.01	3.04			
24	0.6	1231	1006	0.288	0.17	3.29	4.33			
24	0.8	1219	846	0.245	0.03	1.98	6.60			
24	0.9	1209	635	0.185	0	1.50	7.51			
23	0	1210.5	1018	0.297	0.66	4.74	1.06	1241	12.2	1.035
22	0	1200	998	0.294	1.02	4.20	0.68			
21	0	1190	980	0.291	1.38	3.67	0.53	1218	9.18	0.767
21	0.2	1193	988	0.292	1.25	3.87	0.61			
21	0.4	1199	993	0.292	1.11	4.01	0.68			
21	0.6	1208	970	0.283	0.83	4.06	1.29			
21	0.8	1210	816	0.238	0.39	3.58	3.49			
21	0.9	1207	619	0.181	0.28	3.34	4.18			
20	0	1186	965	0.287	1.75	3.14	0.30			
19	0	1182	954	0.285	2.08	2.47	0.23	1197	7.05	0.582
19	0.2	1183	958	0.286	2.08	2.47	0.23			
19	0.4	1185	961	0.288	1.97	2.66	0.30			
19	0.6	1191	944	0.280	1.72	3.00	0.38			
19	0.8	1198	787	0.232	1.05	3.92	0.99			
19	0.9	1196	597	0.176	0.80	4.16	1.37			
18	0	1178	941	0.282	2.44	1.84	0.15			
17	0	1173	931	0.280	2.69	1.45	0.08	1179	5.58	0.443
17	0.2	1173	933	0.281	2.69	1.45	0.08			
17	0.4	1174.5	949	0.285	2.63	1.50	0.15			
17	0.6	1176	930	0.279	2.60	1.59	0.15			
17	0.8	1184	770	0.229	2.22	2.27	0.23			
17	0.9	1185.5	586	0.174	1.77	3.10	0.38			
15	0	1167	918	0.277	3.07	0.87	0	1168.5	3.33	0.262
13	0	1162	903	0.274	3.30	0.58	0	1162	2.06	0.160
13	0.4	1162	926	0.281	3.32	0.58	0			
13	0.8	1163.5	737	0.223	3.32	0.63	0			
13	0.9	1164.5	573	0.174	3.27	0.72	0			
5	0	1152	–	–	–	–	–	1153	1.0	0.070

TABLE 5.12

(Run 22)

Z	r	T_e	V_Z	ρV_Z	$m_{CH_4} \times 10^3$	$m_{CO} \times 10^3$	$m_{CO_2} \times 10^3$	T_c	$\left(\frac{\partial T}{\partial Z}\right)_{r=0}$	q'''
27	0	1211	1072	0.312	0.47	4.64	1.75	1248	12.8	1.135
26.5	0	1205	1059	0.310	0.75	4.54	1.23			
26	0	1200	1048	0.308	0.89	4.50	0.99	1233	11.5	1.005
25.5	0	1195	1038	0.306	1.12	4.03	0.76			
25	0	1191	1028	0.305	1.26	3.78	0.61			
24	0	1184	1011	0.301	1.63	3.12	0.38	1209	8.47	0.726
24	0.2	1184	1011	0.301	1.63	3.12	0.38			
24	0.4	1189	1015	0.301	1.50	3.26	0.53			
24	0.6	1199	980	0.288	1.08	3.78	1.06			
24	0.7	1207	943	0.276	0.66	3.78	2.05			
24	0.8	1205	836	0.245	0.33	3.35	3.95			
24	0.9	1196	629	0.186	0.17	2.80	5.17			
23	0.9	1194	622	0.184	0.06	3.54	3.65			
22	0.9	1191	615	0.182	0.61	3.86	2.28	1190	5.54	0.463
21	0	1171	965	0.291	2.57	1.32	0.15			
21	0.2	1171	965	0.291	2.52	1.42	0.15			
21	0.4	1176	974	0.292	2.35	1.60	0.23			
21	0.6	1184	948	0.284	2.02	2.32	0.46			
21	0.8	1190	803	0.238	1.12	3.59	1.37			
21	0.9	1189	609	0.180	0.91	3.82	1.60			
20	0	1169	951	0.287	2.77	1.21	0.05	1177	3.76	0.307
20	0.9	1184	601	0.179	1.24	3.59	0.91			
19	0.9	1179	593	0.179	1.61	3.01	0.61			
18	0	1164	932	0.282	3.05	0.77	0	1168	2.78	0.223
18	0.9	1174	588	0.177	2.16	2.10	0.23			
17	0	1162	925	0.280	3.16	0.58	0			
17	0.2	1162	925	0.281	3.16	0.58	0			
17	0.4	1162.5	940	0.285	3.13	0.63	0			
17	0.6	1164	921	0.279	3.10	0.68	0			
17	0.8	1169	761	0.230	2.88	1.03	0.08			
17	0.9	1170	583	0.176	2.63	1.39	0.15			
16	0	1166	912	0.276	3.32	0.43	0	1162	2.23	0.178
16	0.9	1160	573	0.174	2.82	1.10	0.08			
14	0	1158	897	0.273	3.43	0.24	0	1159	1.64	0.130
12	0	1155	890	0.272	3.54	0.10	0	1155	1.11	0.088

TABLE 5.13

(Run 6)

Z	r	T_e	V_Z	ρV_Z	$m_{CH_4} \times 10^3$	$m_{CO} \times 10^3$	$m_{CO_2} \times 10^3$	T_c	$\frac{\partial T}{\partial Z}_{r=o}$	q'''
20	0	1265	1029	0.287	0	2.27	7.37	~1306	5.00	0.407
19	0	1258	1012	0.284					8.63	0.698
19	0.2	1259	1017	0.285						
19	0.4	1260	1029	0.288						
19	0.6	1260	1000	0.280						
19	0.8	1257.5	827	0.232						
18	0	1250	998	0.282						
17	0	1237	981	0.280					18.9	1.50
17	0.2	1237	985	0.281						
17	0.4	1235.5	997	0.285						
17	0.6	1236.5	981	0.280						
17	0.8	1241	805	0.229						
15	0	1206	946	0.277					13.9	1.095
13	0	1190	924	0.274					8.4	0.655
13	0.2	1190.5	934	0.277						
13	0.4	1190.5	948	0.281						
13	0.6	1193	943	0.279						
13	0.8	1196.5	760	0.224						
11	0	1180	907	0.271					5.62	0.435
9	-0.2	1172	-	-						
9	0	1172	868	0.267					4.03	0.308
9	0.2	1172	897	0.270						
9	0.4	1174	915	0.275						
9	0.6	1174	922	0.277						
9	0.7	1175	-	-						
9	0.8	1176	737	0.221						
5	0	1162	-	-					2.55	0.195
2.5	0	1160	-	-						

TABLE 5.14

(Run 3)

Z	r	T_e	V_Z	ρV_Z	$m_{CH_4} \times 10^3$	$m_{CO} \times 10^3$	$m_{CO_2} \times 10^3$	T_c	$\left(\frac{\partial T}{\partial Z}\right)_{r=o}$	q'''
20	0	1260	1025	0.287	0.03	1.60	9.57	~1336	8.95	0.727
18	0	1238	990	0.282					17.9	1.43
16	0	1210	953	0.278					16.63	1.31
14	0	1192	933	0.276					7.94	0.622
12	0	1182	915	0.273					5.53	0.430
10	0	1175	896	0.269					3.67	0.282
8	0	1170	883	0.266					2.44	0.185
6	0	1167	868	0.262					1.41	0.107

TABLE 5.15

(Run 7)

Z	r	T_e	V_Z	ρV_Z	$m_{CH_4} \times 10^3$	$m_{CO} \times 10^3$	$m_{CO_2} \times 10^3$	T_c	$\left(\frac{\partial T}{\partial Z}\right)_{r=o}$	q'''
20	0	1276	1038	0.287	0.05	2.37	10.33	1355	15.6	1.27
19	0	1260	1014	0.284					23.8	1.92
19	0.2	1257	1016	0.285						
19	0.4	1266	1013	0.288						
19	0.6	1274	1011	0.280						
19	0.8	1281	842	0.232						
19	0.9	1276	636	0.176						
19	1.0	1272	-	-						
19	-0.2	1261.5	-	-						
19	-0.4	1273	-	-						
19	-0.6	1285	-	-						
19	-0.7	1287	-	-						
19	-0.8	1280	-	-						
18	0	1237	989	0.282					26.30	2.10
17	0	1225	971	0.280					18.50	1.46
17	0.2	1228	977	0.281						
17	0.4	1233	996	0.285						
17	0.6	1242	986	0.280						
17	0.8	1256	815	0.229						
15	0	1201	942	0.277					9.80	0.765
13	0	1191.5	925	0.274					6.40	0.494
13	0.2	1191.5	935	0.277						
13	0.4	1192	946	0.281						
13	0.6	1192	942	0.279						
13	0.8	1195.5	759	0.224						
13	0.98	1203	-	-						
13	-0.7	1202	-	-						
13	-0.83	1205	-	-						
11	0	1181	907	0.271					4.57	0.350
9	0	1175.5	890	0.267					3.73	0.281
9	0.2	1175.5	900	0.270						
9	0.4	1176	917	0.275						
9	0.6	1176	923	0.277						
9	0.8	1178	738	0.221					-	-
5	0	1166	-	-					2.66	0.199

TABLE 5.16

(Run 12)

Z	r	T_e	V_Z	ρV_Z	$m_{CH_4} \times 10^3$	$m_{CO} \times 10^3$	$m_{CO_2} \times 10^3$	T_c	$\left(\frac{\partial T}{\partial Z}\right)_{r=o}$	q'''
20	0	1243	1186	0.337	0.03	1.06	5.31	1270	2.57	0.246
19	0	1240	1169	0.334	0.03	1.35	4.71	1267	4.22	0.400
19	0.2	1240	1169	0.334	0.03	1.35	4.71			
19	0.4	1240	1169	0.334	0.03	1.35	4.78			
19	0.6	1239	1152	0.324	0.03	1.35	4.86			
19	0.8	1229	998	0.288	0	1.06	5.24			
19	0.9	1221	742	0.220	0	0.97	5.47			
18	0	1234	1153	0.330	0.06	1.89	4.02			
17	0	1228	1137	0.329	0.08	2.51	3.04	1256	7.57	0.709
17	0.2	1228	1137	0.329	0.08	2.56	2.96			
17	0.4	1228	1140	0.328	0.08	2.56	2.88			
17	0.6	1227	1122	0.323	0.08	2.66	2.81			
17	0.8	1223	972	0.281	0.08	2.56	2.96			
17	0.9	1217	755	0.219	0.06	2.18	3.49			
15	0	1212	1110	0.326	0.50	3.24	0.83	1233	9.43	0.876
13	0	1197	1086	0.324	1.11	2.47	0.15	1213	7.94	0.733
13	0.2	1197	1086	0.320	1.11	2.47	0.15			
13	0.4	1197	1093	0.322	1.11	2.47	0.15			
13	0.6	1198	1086	0.320	1.11	2.42	0.15			
13	0.8	1199	928	0.273	1.05	2.37	0.38			
13	0.9	1198	743	0.219	0.94	2.51	0.46			
11	0	1188.5	1072	0.321	1.72	1.21	0.08	1195	5.55	0.505
9	0	1182	1058	0.316	2.13	0.53	0	1182	3.91	0.351
9	0.2	1182	1058	0.315	2.13	0.53	0			
9	0.4	1182.5	1062	0.317	2.13	0.53	0			
9	0.6	1182.5	1062	0.317	2.13	0.53	0			
9	0.8	1183	913	0.272	2.13	0.53	0			
9	0.9	1183	757	0.226	2.13	0.53	0			
9	-0.9	1182.5	696	0.208	2.10	0.58	0			
5	0	1172	-	-	2.55	0.10	0	1170	2.17	0.192

TABLE 5.17

(Run 11)

Z	r	T_e	V_Z	ρV_Z	$m_{CH_4} \times 10^3$	$m_{CO} \times 10^3$	$m_{CO_2} \times 10^3$	T_c	$\left(\frac{\partial T}{\partial Z}\right)_{r=o}$	q'''
20	0	1315	1256	0.337	0	0.39	9.65	1336		
19	0	1314	1244	0.334					~2.78	0.263
18	0	1312	1227	0.330					5.2	0.486
17	0	1303	1215	0.329					9.62	0.898
15	0	1266	1170	0.326					28.6	2.64
13	0	1232	1131	0.324					17.55	1.61

TABLE 5.18

Summary of Runs concerned with Intermediates

Table Number	Run Number	Flow rate $293^{\circ}K$ Litre Min^{-1}	Methane Mole Fraction $\times 10^{3}$	Furnace Temperature $^{\circ}K$	Inlet Temperature $^{\circ}K$	Intermediates analysed (Number of analyses in brackets) HCHO	H_2O_2	H_2	Purpose
5.19	C	41.17	0.755	1165	1170	(8)	(8)	(8)	Investigation of relations between intermediates
5.20	D	41.08	0.740	1168	1157	(4)	(4)	(4)	
5.21	E3	41.00	0.675	1183	1161	(4)	(4)	-	
5.22	F	41.00	0.705	1171	1157	(4)	(3)	(4)	
5.23	H	41.00	0.680	1167	1154	(5)	(5)	(5)	
5.24	J	41.08	0.700	1168	1156	(5)	(5)	(5)	Investigation of radial conditions
5.25	I	41.00	0.690	1166	1158	(10)	-	-	
5.26	Q	41.08	0.710	1131	1131	(9)	-	-	
5.27	M	32.32	0.640	1131	1132	(10)	-	-	Investigation of the effects of flow, composition and temperature variation on formaldehyde concentration
5.28	T	32.32	0.660	1141	1141	(5)	-	-	
5.29	P	41.20	0.225	1143	1143	(10)	-	-	
5.30	R	41.08	0.435	1152	1150	(5)	-	-	
5.31	L	41.08	0.640	1141	1142	(11)	-	-	
5.32	K	41.08	0.630	1151	1154	(11)	-	-	
5.33	A	41.00	0.650	1170	1174	(8)	(1)	-	
5.34	S	41.08	0.930	1164	1162	(5)	-	-	
5.35	O	41.08	1.140	1160	1163	(11)	-	-	
5.36	N	49.90	0.660	1167	1168	(11)	-	-	
5.37	U	49.85	0.625	1174	1174	(5)	-	-	

N.B. Bracketed values of mass fraction in the following tables indicate the known possibility of error due to mishandling during sampling or analysis.

TABLE 5.19

(Run C)

Z	r	ρV_Z	$m_{CH_4} \times 10^3$	$m_{CO} \times 10^3$	$m_{CO_2} \times 10^3$	$m_{HCHO} \times 10^3$	$m_{H_2O_2} \times 10^6$	$m_{H_2} \times 10^6$
20	0	0.287	3.52	1.16	0	0.106	3.2	31.3
15	0	0.277	3.93	0.39	0	0.087	1.1	20.8
15	0.9	0.176	3.05	1.84	0	0.129	3.5	20.8
12	0.9	0.177	3.54	0.87	0	0.107	2.7	11.9
10	0	0.269	4.10	0.19	0	0.08^6	0.8^7	16.4
10	0.9	0.177	3.71	0.58	0	0.112	2.0	7.4
8	0.9	0.178	3.71	0.48	0	0.094	1.9	7.4
7.15	0	0.263	4.13	0.14	0	0.063	0.7^4	16.4

TABLE 5.20

(Run D)

Z	r	ρV_Z	$m_{CH_4} \times 10^3$	$m_{CO} \times 10^3$	$m_{CO_2} \times 10^3$	$m_{HCHO} \times 10^3$	$m_{H_2O_2} \times 10^6$	$m_{H_2} \times 10^6$
25	0	0.305	2.02	3.58	0.23	0.074	6.4^5	31.3
22.5	0	0.296	3.16	1.45	0.08	0.107	4.3	20.2
20	0	0.287	3.46	1.21	0	0.108	3.7	21.6
15	0	0.277	3.93	0.29	0	0.092	1.7	9.7

TABLE 5.21

(Run E)

z	r	ρV_z	$m_{CH_4} \times 10^3$	$m_{CO} \times 10^3$	$m_{CO_2} \times 10^3$	$m_{HCHO} \times 10^3$	$m_{H_2O_2} \times 10^6$
25	0	0.305	0	0.72	8.74	0.041	5.3
22.5	0	0.296	1.02	2.42	3.34	0.228	4.9
21	0	0.291	2.05	2.22	1.14	(0.520)	4.7
20	0	0.287	2.71	1.74	0.46	0.286	1.2

TABLE 5.22

(Run F)

z	r	ρV_z	$m_{CH_4} \times 10^3$	$m_{CO} \times 10^3$	$m_{CO_2} \times 10^3$	$m_{HCHO} \times 10^3$	$m_{H_2O_2} \times 10^6$	$m_{H_2} \times 10^6$
30	0	0.320	0	0.24	10.86	0.012	-	(29.1)
25	0	0.305	0.20	3.05	5.55	0.085	4.2	25.3
22.5	0	0.296	1.75	2.95	1.14	0.530	12.4	29.1
20	0	0.287	3.00	1.60	0.15	0.330	11.0	26.1

TABLE 5.23

(Run H)

Z	r	ρV_Z	$m_{CH_4} \times 10^3$	$m_{CO} \times 10^3$	$m_{CO_2} \times 10^3$	$m_{HCHO} \times 10^3$	$m_{H_2O_2} \times 10^6$	$m_{H_2} \times 10^6$
27.5	0	0.313	0.69	3.38	2.89	0.074	6.9	4.5
26	0	0.308	1.47	3.04	1.37	0.166	7.1^5	23.1
25	0	0 305	1.72	3.04	0.91	0.213	14.6	27.6
22.5	0	0.296	2.66	1.93	0.15	0.267	14.4	22.3
20	0	0.287	3.32	0.97	0.08	0.284	10.0	20.8

TABLE 5.24

(Run J)

Z	r	ρV_Z	$m_{CH_4} \times 10^3$	$m_{CO} \times 10^3$	$m_{CO_2} \times 10^3$	$m_{HCHO} \times 10^3$	$m_{H_2O_2} \times 10^6$	$m_{H_2} \times 10^6$
20	0	0.287	3.29	1.11	0	0.294	14.0	16.4
20	0.2	0.288	3.18	1.30	0	0.330	13.0	17.9
20	0.4	0.290	2.96	1.55	0.08	0.350	18.2	20.8
20	0.6	0.281	2.44	2.32	0.53	0.239	12.6	20.8
20	0.8	0 234	1.22	2.90	2.43	0.196	15.8	14.9

TABLE 5.25

(Run I)

Z	r	ρV_Z	$m_{CH_4} \times 10^3$	$m_{CO} \times 10^3$	$m_{CO_2} \times 10^3$	$m_{HCHO} \times 10^3$
20	0.9	0.179	0.91	3.43	2.43	0.130
20	0.7	0.261	2.10	2.56	0.68	0.243
20	0.5	0.287	2.85	1.64	0.15	0.287
20	0.3	0.289	3.16	1.26	0.03	0.319
20	0.1	0.287	3.27	1.11	0	0.296
20	-0.1	-	3.24	1.11	0.03	0.308
20	-0.3	-	3.16	1.26	0.08	0.293
20	-0.5	-	2.85	1.64	0.15	0.306
20	-0.7	-	2.10	2.61	0.53	0.248
20	-0.9	-	1.16	3.67	1.59	0.153

TABLE 5.26

(Run Q)

Z	r	ρV_Z	$m_{CH_4} \times 10^3$	$m_{CO} \times 10^3$	$m_{CO_2} \times 10^3$	$m_{HCHO} \times 10^3$
10	0.85	0.200	3.93	0.05^8	0	0.144
10	0.7	0.265	3.96	0.05^8	0	0.141
10	0.6	0.278	3.93	0.06^8	0	0.127
10	0.3	0.275	3.93	0.05^8	0	0.126
10	0	0.269	3.93	0.05^8	0	0.129
10	-0.3	-	3.93	0.06^8	0	0.139
10	-0.6	-	3.90	0.06^8	0	0.148
10	-0.7	-	3.88	0.06^8	0	0.149
10	-0.95	-	3.82	0.08^7	0	0.169

TABLE 5.27

(Run M)

Z	r	ρV_Z	$m_{CH_4} \times 10^3$	$m_{CO} \times 10^3$	$m_{CO_2} \times 10^3$	$m_{HCHO} \times 10^3$
22	0	0.245	2.71	1.35	0.15	0.279
20	0	0.237	3.02	0.87	0.08	0.251
18	0	0.230	3.24	0.58	0.03	0.253
18	0.3	0.231	3.13	0.68	0.03	(0.329)
18	0.6	0.221	3.04	0.77	0.08	0.279
18	0.75	0.185	2.91	0.92	0.15	0.259
18	0.9	0.110	2.74	1.16	0.23	0.262
16	0	0.226	3.35	0.44	0	0.233
14	0	0.222	3.40	0.34	0	0.236
12	0	0.218	3.46	0.24	0	0.214

TABLE 5.28

(Run T)

Z	r	ρV_Z	$m_{CH_4} \times 10^3$	$m_{CO} \times 10^3$	$m_{CO_2} \times 10^3$	$m_{HCHO} \times 10^3$
22	0	0.245	2.27	2.03	0.52	0.282
20	0	0.237	2.80	1.26	0.18	0.317
18	0	0.230	3.10	0.87	0.11	0.301
16	0	0.226	3.29	0.63	0.05	0.295
14	0	0.222	3.46	0.41	0.04	0.287

TABLE 5.29

(Run P)

Z	r	ρV_Z	$m_{CH_4} \times 10^3$	$m_{CO} \times 10^3$	$m_{CO_2} \times 10^3$	$m_{HCHO} \times 10^3$
22	0	0.294	0.58^4	1.12	0.18^2	0.110
20	0	0.287	0.69^2	0.90^9	0.12^2	0.113
18	0	0.282	0.77^5	0.80^8	0.07^0	0.135
16	0	0.278	0.58^8	0.65^7	0.06^4	0.132
14	0	0.276	0.91^3	0.51^2	0.04^6	0.140
12	0	0.273	1.02	0.36^7	0.03^9	0.133
12	0.3	0.276	0.99^7	0.37^7	0.04^6	0.134
12	0.6	0.279	0.99^7	0.37^7	0.04^6	0.137
12	0.7	0.257	0.99^7	0.37^7	0.04^6	0.138
12	0.8	0.227	0.96^9	0.43^5	0.06^4	0.155
12	0.9	0.177	0.94^1	0.46^4	0.06^4	-

TABLE 5.30

(Run R)

Z	r	ρV_Z	$m_{CH_4} \times 10^3$	$m_{CO} \times 10^3$	$m_{CO_2} \times 10^3$	$m_{HCHO} \times 10^3$
26	0	0.308	1.33	1.78	0.30	0.191
24	0	0.300	1.61	1.38	0.15	0.213
22	0	0.294	1.85	0.87	0.09	0.208
20	0	0.287	1.99	0.66	0.05	0.226
18	0	0.282	2.10	0.43	0.02	0.226

TABLE 5.31

(Run L)

Z	r	ρV_Z	$m_{CH_4} \times 10^3$	$m_{CO} \times 10^3$	$m_{CO_2} \times 10^3$	$m_{HCHO} \times 10^3$
22	0	0.294	3.04	0.68	0.08	(0.343)
20	0	0.287	3.13	0.53	0.08	0.200
18	0	0.282	3.29	0.34	0	0.205
16	0	0.278	3.40	0.14	0	0.183
14	0	0.276	3.49	0.10	0	0.205
12	0	0.273	3.49	0.10	0	0.149
12	0.3	0.276	3.49	0.14	0	0.155
12	0.6	0 279	3.49	0.14	0	0.171
12	0.7	0 257	3.46	0.19	0	0.177
12	0.8	0.227	3.46	0.24	0	0.183
12	0.9	0.177	3.43	0.24	0.03	0.196

TABLE 5.32

(Run K)

Z	r	ρV_Z	$m_{CH_4} \times 10^3$	$m_{CO} \times 10^3$	$m_{CO_2} \times 10^3$	$m_{HCHO} \times 10^3$
25	0	0.305	0.19	3.29	3.95	0.040
23	0	0.297	0.83	3.72	1.75	0.136
21	0	0.291	1.55	3.09	0.68	0.194
19	0	0.285	2.41	1.74	0.15	0.244
17	0	0.280	2.85	1.06	0.08	0.258
15	0	0.277	3.10	0.68	0	0.249
13	0	0.274	3.21	0.48	0	0.241
13	0.3	0.279	3.24	0.48	0	0.238
13	0.6	0.279	3.24	0.48	0	0.234
13	0.8	0.223	3.21	0.53	0	0.250
13	1.0	0 223	3.18	0.53	0	0 241

TABLE 5.33

(Run A)

Z	r	ρV_Z	$m_{CH_4} \times 10^3$	$m_{CO} \times 10^3$	$m_{CO_2} \times 10^3$	$m_{HCHO} \times 10^3$
25	0	0.305	1.11	4.06	0	0.071
20	0	0.287	3.13	0.82	0	0.075
15	0	0.277	3.60	0.19	0	0.104
15	0.9	0.175	2.82	1.30	0	0.098
12	0.9	0.177	3.32	0.44	0	0.106
10	0	0.269	3.74	0.05	0	0.097
10	0.9	0.173	3.43	0.14	0	0.095
8	0.9	0.173	3.49	0.14	0	0.078

TABLE 5.34

(Run S)

Z	r	ρV_Z	$m_{CH_4} \times 10^3$	$m_{CO} \times 10^3$	$m_{CO_2} \times 10^3$	$m_{HCHO} \times 10^3$
24	0	0.300	3.60	2.10	0.64	0.408
22	0	0.294	4.35	1.32	0.18	0.399
20	0	0.287	4.65	0.79	0.08	0.314+
18	0	0.282	4.98	0.44	0.02	0.312
16	0	0.278	5.10	0.32	0	0.333

TABLE 5.35

(Run O)

Z	r	ρV_Z	m_{CH_4} $\times 10^3$	m_{CO} $\times 10^3$	m_{CO_2} $\times 10^3$	m_{HCHO} $\times 10^3$
22	0	0.294	3.68	2.80	2.35	0.352
20	0	0.287	4.87	1.69	0.53	0.360
18	0	0.282	5.51	0.92	0.15	0.367
16	0	0 278	5.90	0.58	0	0.360
14	0	0 276	6.15	0.34	0	0.344
12	0	0.273	6.31	0.19	0	0.297
12	0.3	0.276	6.31	0.19	0	0.292
12	0.6	0.279	6.29	0.29	0	0.289
12	0.7	0.257	6.26	0.34	0	0.289
12	0.8	0 227	6.26	0.34	0	0.316
12	0.9	0.177	6.20	0.48	0	0.329

TABLE 5.36

(Run N)

Z	r	ρV_Z	m_{CH_4} $\times 10^3$	m_{CO} $\times 10^3$	m_{CO_2} $\times 10^3$	m_{HCHO} $\times 10^3$
22	0	0.345	2.52	1.64	0.23	(0.290)
20	0	0.337	2.82	1.40	0.08	0.282
18	0	0.330	3.02	0.92	0.03	0 271
16	0	0.327	3.32	0.63	0	(0.282)
14	0	0.325	3.43	0.39	0	0.251
12	0	0.322	3.54	0.34	0	(0.213)
12	0.3	0.320	3.49	0.39	0	0.237
12	0.6	0.319	3.52	0.39	0	(0.265)
12	0.7	0.303	3.54	0.29	0	0.240
12	0.8	0.273	3.52	0.34	0	0.246
12	0.9	0.221	3.46	0.44	0	0.244

TABLE 5.37

(Run U)

Z	r	ρV_Z	$m_{CH_4} \times 10^3$	$m_{CO} \times 10^3$	$m_{CO_2} \times 10^3$	$m_{HCHO} \times 10^3$
22	0	0.345	2.13	1.93	0.52	0.315
20	0	0.337	2.49	1.40	0.23	0.324
18	0	0.330	2.94	0.97	0.11	0.324
16	0	0.327	3.16	0.68	0.05	0.320
14	0	0.325	3.32	0.43	0.04	0.296

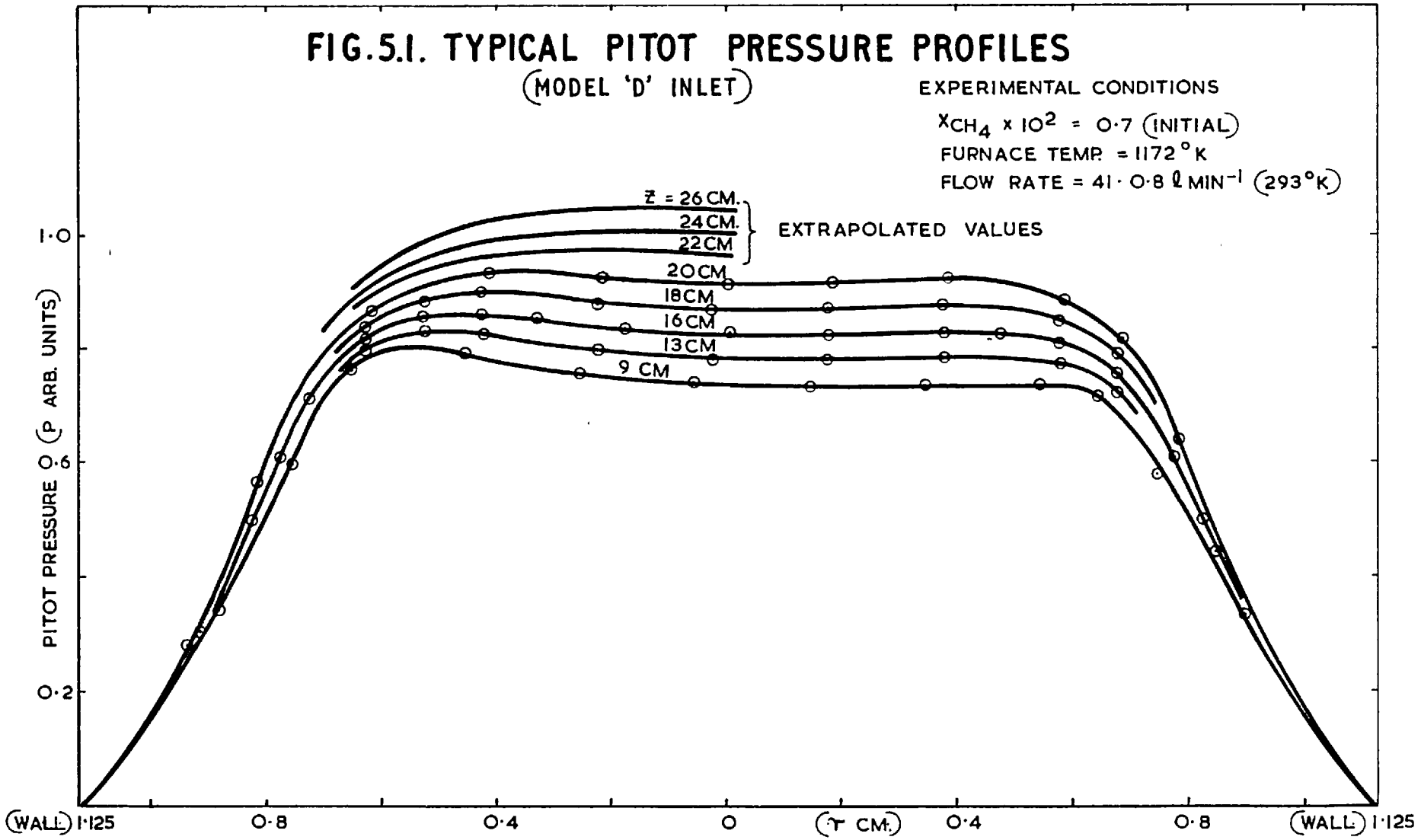
FIG.5.1. TYPICAL PITOT PRESSURE PROFILES
(MODEL 'D' INLET)
EXPERIMENTAL CONDITIONS
$X_{CH_4} \times 10^2 = 0.7$ (INITIAL)
FURNACE TEMP. = 1172°K
FLOW RATE = 41 · 0.8 ℓ MIN^{-1} (293°K)
z = 26 CM.
24 CM.
22 CM
EXTRAPOLATED VALUES
20 CM
18 CM
16 CM
13 CM
9 CM
PITOT PRESSURE (P ARB. UNITS)
1.0
0.6
0.2
(WALL) 1.125
0.8
0.4
0
(r CM.)
0.4
0.8
(WALL) 1.125

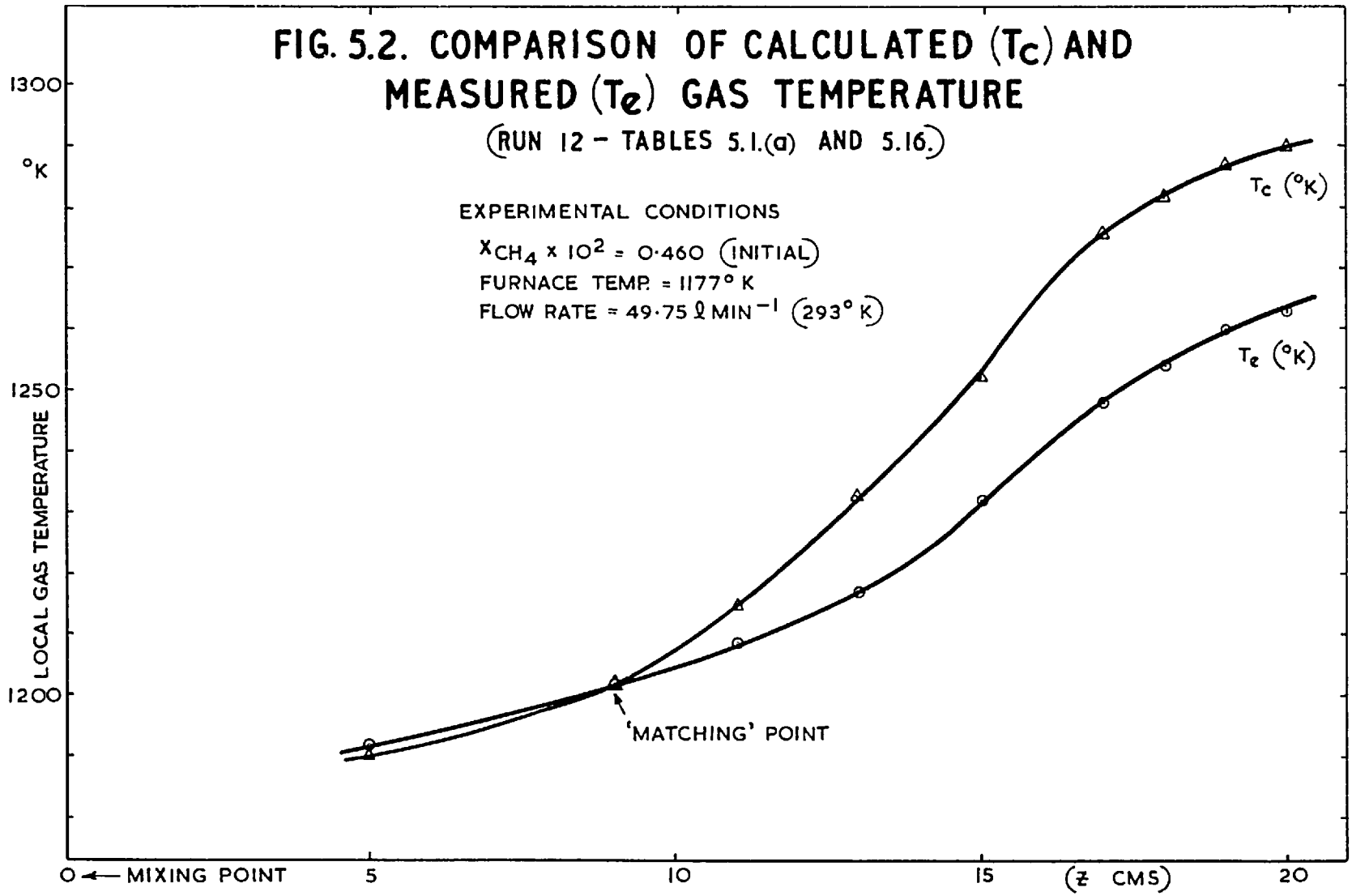
FIG. 5.2. COMPARISON OF CALCULATED (T_c) AND MEASURED (T_e) GAS TEMPERATURE
(RUN 12 – TABLES 5.1.(a) AND 5.16.)
EXPERIMENTAL CONDITIONS
$X_{CH_4} \times 10^2 = 0.460$ (INITIAL)
FURNACE TEMP. = 1177° K
FLOW RATE = 49.75 ℓ MIN^{-1} (293° K)
T_c (°K)
T_e (°K)
'MATCHING' POINT
LOCAL GAS TEMPERATURE °K
1300
1250
1200
0 ← MIXING POINT
5
10
15
20
(z CMS)

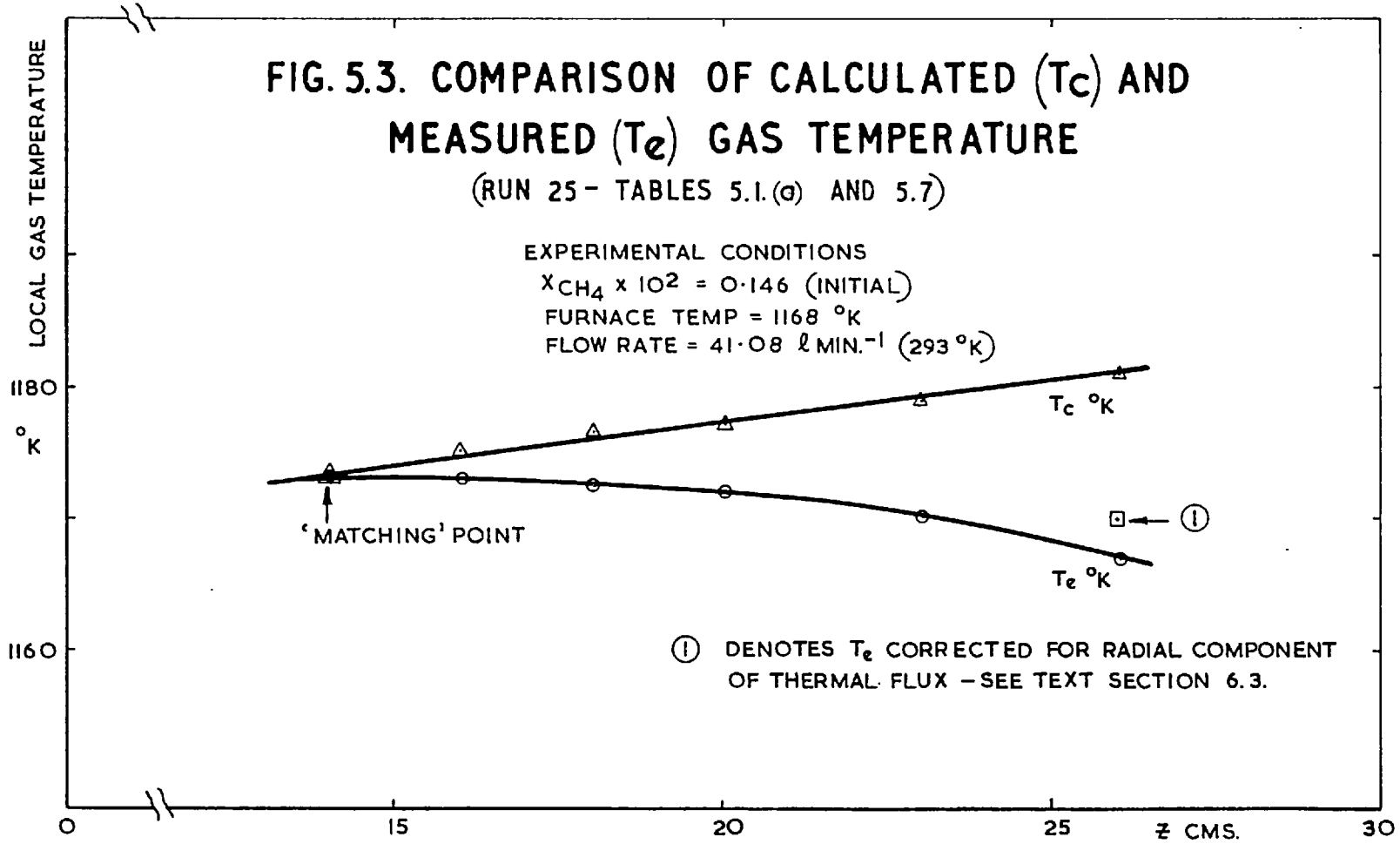
FIG. 5.3. COMPARISON OF CALCULATED (Tc) AND MEASURED (Te) GAS TEMPERATURE
(RUN 25 - TABLES 5.1.(a) AND 5.7)
EXPERIMENTAL CONDITIONS
$X_{CH_4} \times 10^2 = 0.146$ (INITIAL)
FURNACE TEMP = 1168 °K
FLOW RATE = 41.08 ℓ MIN.$^{-1}$ (293 °K)
LOCAL GAS TEMPERATURE °K
1180
1160
Tc °K
Te °K
'MATCHING' POINT
① DENOTES Te CORRECTED FOR RADIAL COMPONENT OF THERMAL FLUX - SEE TEXT SECTION 6.3.
0
15
20
25
30
z CMS.

CHAPTER 6

The fluid mechanics of the reaction zone

6.1 Attempts to correlate ($T_c - T_e$) with reaction zone conditions

Figure 6.1 illustrates the divergence observed between the calculated and measured temperatures along the axis through the reaction zone. Some insight into the cause of the divergence may be obtained from Figure 6.2, where log percentage discrepancy is plotted against the log of the magnitude of the variables in the reaction zone, namely velocity, methane concentration, temperature and the magnitude of $T_c - T_e$. From Figure 6.2 it appears that the percentage discrepancy varies approximately as the first power of the methane concentration and inversely as the first power of the mean gas stream velocity. No correlation could be shown between percentage discrepancy and mean gas temperature (it is a relatively insensitive test over the range of temperature available) nor with the magnitude of $T_c - T_e$.

There are a number of reasons why the correlations may not be very exact. (i) The interdependence of the variables makes a clear-cut answer unlikely from so simple a test. (ii) Some variability in the axial disposition of the region of maximum reaction from one run to another was unavoidable, hence the integrated radial transport rates would be expected to vary because of this for otherwise similar control conditions. (iii) The furnace heating rate, particularly 'M', was varied from one run to another to compensate for variation in the heat generated by the reaction. This fact in itself is strong evidence

for a significant energy exchange between reaction tube wall and reacting gases. The inference therefore is that the correlations demonstrated are suggestive rather than conclusive, but at least the suggestions support the contention that the discrepancy is due to transport properties in the flow.

A more informative picture of what is happening may be obtained by plotting the incremental divergence as a function of axial position (i.e., as a function of reactedness). This is shown in Figure 6.3, the position of maximum reaction rate being marked by an arrow. It will be seen that it corresponds closely with the point at which the maximum discrepancy is occurring. It is significant that at this point the maximum gradients in both species and temperature occur.

6.2 Qualitative fluid mechanical description of the flow in the reaction zone

Some familiarity on the part of the reader with the concepts and terms used in aerodynamics is assumed in this section. The discussion given here draws heavily on References 51, 108 and 109 and on work cited therein. Recently a contribution concerned specifically with transition from turbulent to laminar pipe flow has appeared[110]. It covers the range of Reynolds numbers used in the present work.

The Reynolds number of the flow in the present experiments, based on the reaction tube diameter, is always less than 2000, so that the fully developed flow will be laminar and have a Poiseuille distribution of velocities. Inspection of the velocity profiles obtained (Figure 5.1) shows that it has not developed very far even at z = 25 cm,

although the fact that the mass flow on the axis has increased by 6 per cent between z = 9 and z = 19 cm for a typical run indicates that transition is taking place.

6.2.1 Flow effects attributable to the inlet geometry

In aerodynamic terms the inlet consists of a grid (the platinum end-plate) through which project an array of round jets. Transport rates in the ensuing flow will therefore be closely linked with the flow in the wake of a grid, and flow downstream of a round jet. In addition the influence of the rim of the inlet sheath on the developing boundary layer must be considered.

Although wake flow (e.g., Reference 111) and the flow downstream of a round jet (e.g., Reference 112) have been studied, the writer is unaware of any work where the combined effects of a wake and a jet have been considered. The present case carries the additional complication of the interaction of multiple parallel round jets. Nevertheless some general deductions on the influence of the inlet geometry may be made.

(a) Although the end of the inlet sheath has been shaped so that it acts as a diffuser, the relatively sharp trailing edge, despite the attempt to profile it, may be expected to shed vortices which may not be small compared with the size of the inlet. In consequence turbulence may be induced at a relatively low Reynolds number.

(b) The spacing of the perforations in the end-plate, together with the spacial arrangement of the inlet ports, will considerably influence the scale of the turbulence downstream.

(c) The intensity of the turbulence will also be determined by the inlet geometry and dimensions, since both scale and intensity are partially determined by the general properties of the flow, rather than by the local conditions.

(d) The grid effect of the inlet design dictates that the initial time-mean velocity profiles will be flat. The extent of the flat region will slowly diminish, while that of the boundary layer, in which the velocity gradients occur, will increase. Because of the continuity relation (ρvA = const) the central region of the flow will accelerate giving rise to steeper static pressure gradients than would be the case where the only cause of a pressure gradient is friction. Fairly steep static pressure gradients along the axis have been observed in the present experiments.

6.2.2 The nature of the boundary layer flow

At the wall, besides the effect of the inlet sheath, a region of shear flow is developed which may be an additional inducement towards turbulence, due to the retarding effect of the wall and the mixing of streams of different velocity.

Schubauer and Tchen[113] have given a convenient description of turbulent boundary layers based on the boundary layer thickness δ. Three fairly distinct regions are recognised. The first is a laminar sublayer close to the wall, typically 0.01 to 0.001 of δ, the next 0.1 to 0.2 of δ is a turbulent region which comprises the inner part of a layer where the mean flow is virtually unaffected by the pressure gradient. Finally there is the outer 0.8 to 0.9 of δ where eddies are

limited in lateral extent only by the confines of the layer, and mixing is relatively free. In the lamina sublayer molecular diffusion predominates, being exclusively this at the wall. Turbulent diffusion progressively increases from the wall, until it predominates over molecular diffusion.

Remembering that the Reynolds number in the present experiments is always below the critical value, it was thought worthwhile to test whether the whole of the boundary layer was laminar. This is done in Section 6.3, where it will be shown that the boundary layer most probably contains some turbulence, at least in the outer region of δ. This is not unexpected in view of the work of Corrsin[114] and others who have shown that a phenomenon termed intermittency is characteristic of the outer edge of a boundary layer in turbulent flow. This term refers to the process whereby the free stream makes periodic incursions into the boundary region and hence enhances the mixing rate.

6.2.3 The nature of the core flow

Transport processes in free turbulent flow are the concern of this section. The following effects must be included in any description of the flow in the core; effects due to the inlet geometry, wake effects, jet effects and the interactions of all three.

There will be the nozzle effect of the individual inlets giving rise to a potential core of relatively smooth flow bounded by a layer in which free mixing begins. Kuethe[115] found the potential core of an axially symmetric round jet is consumed between 4 and 5 nozzle diameters

downstream of the plane of the nozzle, and fully developed jet flow established at 8 nozzle diameters. These regions will evidently be extended in the present experiments where the surrounding flow is also in motion. The outer regions of the individual jet flows will show intermittency[114], and it is in these regions that the mixing effect is greatest. The mixing is dependent on the relative velocity of the jet and the surrounding flow.

Besides the jet effects of the individual inlets there are the wake effects of the multiple perforated grid[51] and of the inlet tubes. Some distance downstream of a multiple perforated grid a field of isotropic turbulence is developed. This develops after the non-isotropic effects due to the symmetry of the perforations have decayed. The distance required to establish isotropy is about 80 times the characteristic dimension of the plate (the distance between perforations). Since this characteristic dimension is about 1 to 2 mm in the present case, isotropy might be expected about 5 to 10 cm downstream of the mixing point. Unfortunately the wake effects due to the individual inlet tubes will interfere and may cause a considerable extension of the non-isotropic region if Townsend's results[111] on the wake of a cylinder may be taken as a guide.

One further feature of the flow downstream of the inlet requires consideration. The intermittency of the outer regions of adjacent jets may interact far downstream, as also may their wake effects. It is difficult to predict the consequences of these interactions even

qualitatively. It appears likely, in view of the greater extent of mixing already present in the outer regions of the individual jets, that the interactions will tend to enhance both the mixing rate and the non-isotropy of the flow.

The lack of isotropy in the core flow leads to a consideration of the laws of mean spreading and decay[113], and of transport processes in free turbulent flow[116]. Townsend[117] postulates a double structure of large eddies with relatively little energy by which the fluid is convected in bulk, and smaller eddies with relatively large energy content. On this description heat and matter will spread faster than momentum. The possibility of transport by processes other than those which are gradient dependent now becomes apparent. There is some experimental evidence for this in the case of jets and wakes[115], which is best explained as a bulk transfer mechanism on the basis of Townsend's double structure postulate.

The importance of this for the present experiments is that it may not be possible to explain the transport rates in terms of local gradients. If the eddies are large by comparison with the distances over which the gradients act, and this possibility may be increased in a non-isotropic field, then the transport rates will be more a property of the inlet geometry than of the local flow.

6.2.4 Conclusions concerning transport rates

As a result of the foregoing qualitative theoretical considerations it is possible to explain a number of further features of the

experimental results and thereby draw support for the postulates put forward.

The model of the flow proposed predicts transition from a flow and transport processes dominated by turbulence to one in which the laminar properties predominate as distance from the mixing point increases. Some support for this is forthcoming from an inspection of the experimental results. Where reactedness has reached a given stage at different axial positions in the reaction zone in two comparable runs, the one where the reaction occurs further downstream shows larger gradients in the radial profiles, and these gradients penetrate further into the core of the flow. This increase in gradient dependence is more than would be expected from the rate of ingress of the boundary layer. Figures 7.1 and 7.2 show a typical comparison.

Another feature, which is suggested by the description given of the boundary layer, concerns the relation between the axial profiles of T_e and T_c at or near the wall. Figure 6.4 shows the comparison between T_e and T_c for two runs at r = 0.9 cm. Here the divergence is much greater than in the centre of the core flow and may be attributed partly to the slower flow in the annular boundary layer, and partly to the increased effective area available for radial transport near the wall (the area available is $\propto$ r).

Although no measurement of the axial variation of the wall temperature was made, it is evident from the majority of the runs, in particular Run 25, from the calculations of the next section, and also from the decrease in temperature downstream of flame combustion on the

inlet (Section 4.2.1), that the heat transfer rates can be considerable. It is also apparent that in regions where specie concentrations are relatively high and radially non-uniform, usually at positions near the mixing point, material transport will be important. Thus an overall qualitative picture emerges of the transport phenomena occurring in the reaction tube. Near the mixing point there will be no net radial transfer of material or heat because, although it is postulated that the flow has its maximum turbulence in this region, there are no gradients at the walls. Next comes a region where considerable radial specie gradients develop near the wall, and where, because specie concentrations are relatively high, material transport has its greatest effect. Lastly, in the latter part of the combustion zone, where wall temperatures are beginning to fall, heat transfer becomes the dominant transport mechanism, although in this region the process is more nearly gradient dependent.

6.3 Analysis of the boundary layer transport rates

Since the stable fully developed flow in the present experiments was laminar, the quantitative treatment of the transport rates in the boundary layer was based on assumed laminar flow in this region. This assumption allows the conservation equations for species and heat to be used in the form in which they are stated in Chapter 5. It will be further assumed that transport in the radial direction predominates, and that molecular diffusion and thermal conductivity are the only mechanisms of transport between annular stream-tubes. These are assumed parallel to each other and to the reaction tube wall (i.e., $v_r = 0$).

With these assumptions incorporated in Equations 5.7 and 5.8 we have, for the conservation of heat,

$$\rho v_z \frac{\partial H}{\partial z} - \frac{1}{r} \frac{\partial}{\partial r} (\lambda r \frac{\partial T}{\partial r}) - q''' = 0 \qquad \ldots 6.1$$

and for the conservation of species j,

$$\rho v_z \frac{\partial m_j}{\partial z} - \frac{1}{r} \frac{\partial}{\partial r} (D_j \rho r \frac{\partial m_j}{\partial r}) - K_j \nu_j = 0 \qquad \ldots 6.2$$

In order to keep a clear physical picture of the steps involved the data have been handled in a more laborious manner than is mathematically necessary. It is proposed to seek corrections to the T_e and T_c axial profiles of Run 21 (Table 5.11). The uncorrected and corrected profiles are compared in Figure 6.5.

T_c (uncorrected) is obtained from Equation 6.1 and 6.2 as follows: the radial transport terms are ignored and the K_i are obtained for the species methane and carbon monoxide from the mass fraction profiles along the axis and Equation 6.2. The K_i are then summed to give q''' ($q''' = \sum_i K_j \Delta H_{c,j}$) using the assumptions of Section 5.3.3(b), and δH is then obtained from Equation 6.1 (again ignoring the radial transport term) for small intervals of z. For any given z interval δz, the temperature rise δT_c is given by $\delta T_c = \frac{\delta H}{C_p}$. In the run chosen methane alone was considered, carbon monoxide undergoing virtually no reaction in the axial region considered.

T_0 (uncorrected) is the experimental temperature profile along the axis.

If it is assumed that each volume element $\pi r^2 \delta z$ contributes uniformly to the radial flux across the surface $2\pi r \delta z$ then evaluation of the radial transport term in Equation 6.2 will allow a correction to be applied to the T_c profile. Similarly the radial transport term in Equation 6.1 allows a correction to be applied to the experimental T_e profile. For the purpose of calculation the actual form of the radial transport terms have been slightly modified. They have then been applied to the conditions of Run 21 at r = 0.8 cm. The transport flux across a cylinder of this radius, between z = 13 and z = 24 cm is then evaluated graphically. Figure 6.6 shows the radial diffusive mass flux for methane and Figure 6.7 the radial flux for heat conduction. Diffusion coefficients for the methane-oxygen system were used (see Reference 84 and Appendix 3A of this work); thermal conductivity data for nitrogen at 1200°K were taken from Reference 120. The term plotted against z in Figure 6.6 is $\frac{2}{r} D_{CH_4} \frac{\partial m_{CH_4}}{\partial r} \cdot \frac{1}{(v_z)_r}$ (mass fraction change per cm length due to radial diffusion) and in Figure 6.7 is $\frac{2}{r} \lambda \frac{\partial T_e}{\partial r} \cdot \frac{1}{(v_z)_r}$ (heat change per cm length due to radial conductivity - cal cm^{-3}). The required corrections to the axial temperature profiles at z = 24 cm are then given by

$$\frac{\Delta H_{c,CH_4}}{C_p} \cdot \frac{2}{r} \int_{z=13}^{z=24} D_{CH_4} \frac{\partial m_{CH_4}}{\partial r} \cdot \frac{1}{(v_z)_r} \, \partial z$$

and $$\frac{1}{\rho . C_p} \cdot \frac{2}{r} \int_{z=13}^{z=24} \lambda \frac{\partial T_e}{\partial r} \cdot \frac{1}{(v_z)_r} \partial z$$

respectively. The results indicate that on the basis of the assumptions made some 65 per cent of the difference between the uncorrected T_e and T_c can be accounted for, leaving approximately 12°K unaccounted for in this particular case.

In view of the very small correction to T_e obtained for Run 21, a similar calculation was performed on the data of Run 25. In this case a more significant correction is forthcoming (20 per cent of $T_c - T_e$, indicated on Figure 5.3 by the arrowed point, using the value $\lambda_{N_2} = 1700 \times 10^{-7}$ at 1200°K [120]) but it still suggests that the heat transport correction is inadequate, since the corrected T_e at z = 26 cm is lower than T_e at z = 16 cm where the integration of the radial heat flux was commenced.

6.4 Significance of radial transport fluxes computed in the boundary layer

Quite apart from experimental errors the actual value of the radial transport flux at the axis and its division between species and heat is rather less certain than suggested by the calculations just performed. This is because (a) specie diffusion and thermal conduction across the cylindrical surface considered in the boundary layer are the sum of contributions over all other cylindrical surfaces within the radius considered, modified by the distribution of reaction rates in the

various annuli. It follows that the assumption of uniform depletion over the whole cross-sectional area within the cylinder considered would be difficult to justify quantitatively. (b) The heat flux due to thermal conductivity can be shown to underestimate the correction required at the axis (e.g., Run 25), in conditions where alternative modes of heat loss from the axis are likely to be negligible. There are two fairly likely reasons for this, one peculiar to the method of temperature measurement, the other affecting specie diffusion as well. The first is attributable to the probe dimensions and rather remote location of the thermocouple junction from the point requiring measurement. Error in the measured radial temperature profiles - a smoothing effect - is possible for this reason. This could cause an underestimate of the heat conduction in the boundary layer. (This would not conflict with, nor detract from, the experimental evidence - Section 3.4 - that a satisfactory temperature measurement is obtained in midstream.) (c) The second reason why thermal conductivity estimates may be too low is the neglect to consider any contribution from turbulent transport in the boundary layer. This would also affect the specie diffusion rates.

Despite the qualifications just made the results of the calculations of the previous section (which may be regarded as typical) suggest that laminar processes are predominating in the boundary layer. If this is true then the intensity of turbulence and the magnitude of the eddy transport processes, including non-gradient processes, in the core flow need not be very high in order to account for the observed lack of

radial gradients in species and temperature in the core. It then follows that neglect of the axial components of the transport fluxes - excluding convection - is justifiable to a first approximation.

To allow energy and material balances to be undertaken in the core of the flow, the conservation equations for heat and species require modification. Since the experimental information available would be inadequate for their use it is not proposed to do more than indicate the simplest form they might take. Terms accounting for turbulent gradient-dependent transport and non-gradient transport must be added to Equations 5.7 and 5.8. Denoting an eddy diffusivity by ε and writing the symbol G for the non-gradient term, Equation 5.8 becomes

$$\rho v_z \frac{\partial m_j}{\partial r} - \frac{1}{r} \frac{\partial}{\partial r} \left\{ (\varepsilon + D_j)\ \rho r \frac{\partial m_j}{\partial r} \right\} + \rho v_z \frac{\partial m_j}{\partial z} - \frac{\partial}{\partial z} \left\{ (\varepsilon + D_j) \rho \frac{\partial m_j}{\partial z} \right\}$$

$$+ G - K_j \nu_j = 0$$

where the values of ε and G must be derived from the local aerodynamic properties of the flow.

Since neither ε nor G can be evaluated in the present case, and in view of the uncertainties present in the calculations based on the boundary layer flow, it was regretfully decided to employ an empirical treatment of the data for the purpose of further analysis in this Thesis. Since different treatments have been employed for the heat release rates (Chapter 7) and for the kinetics (Chapter 8) they will be detailed in the appropriate chapters.

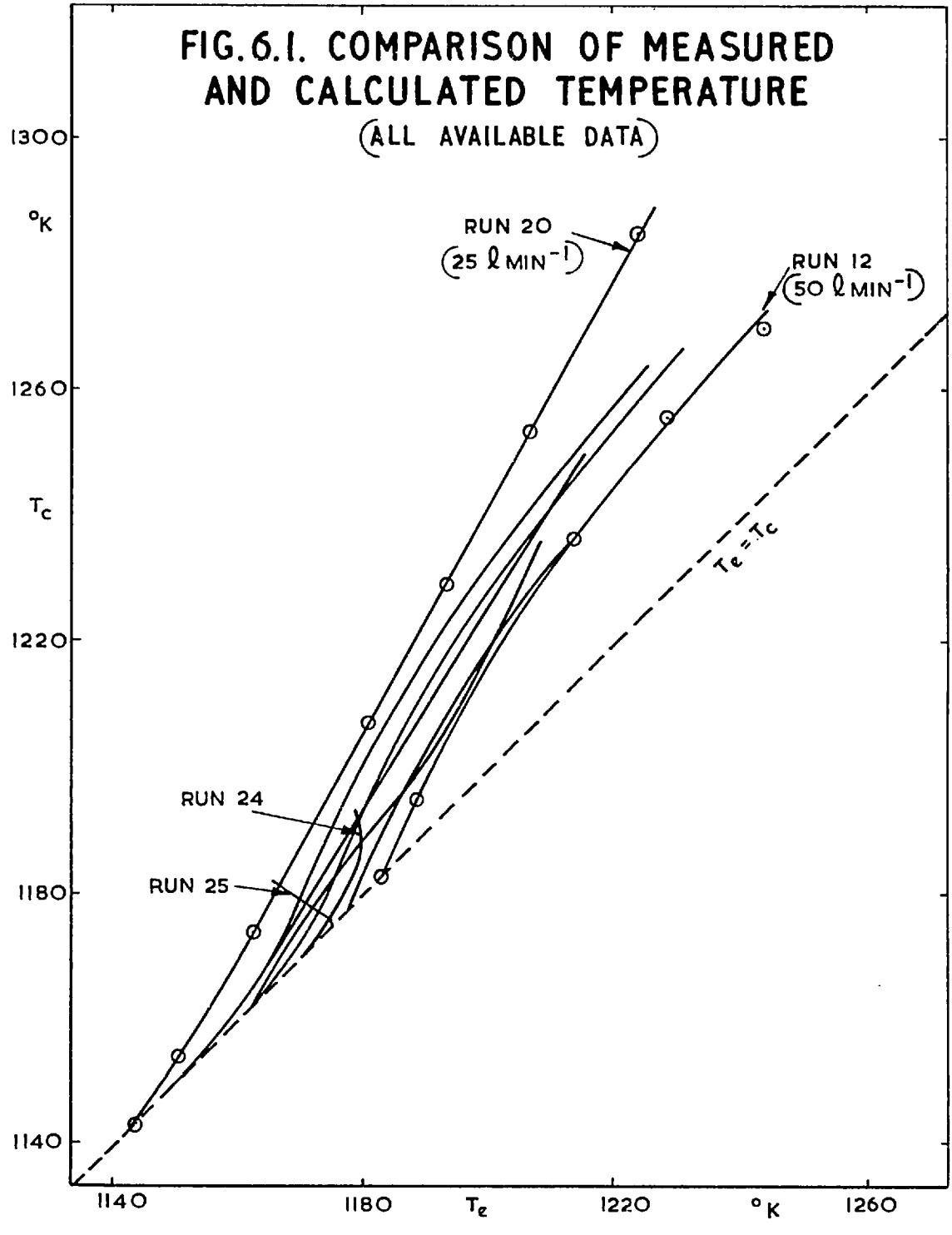
FIG. 6.1. COMPARISON OF MEASURED AND CALCULATED TEMPERATURE
(ALL AVAILABLE DATA)
1300
°K
1260
Tc
1220
1180
1140
RUN 20
(25 ℓ MIN⁻¹)
RUN 12
(50 ℓ MIN⁻¹)
RUN 24
RUN 25
Te=Tc
1140
1180
Te
1220
°K
1260

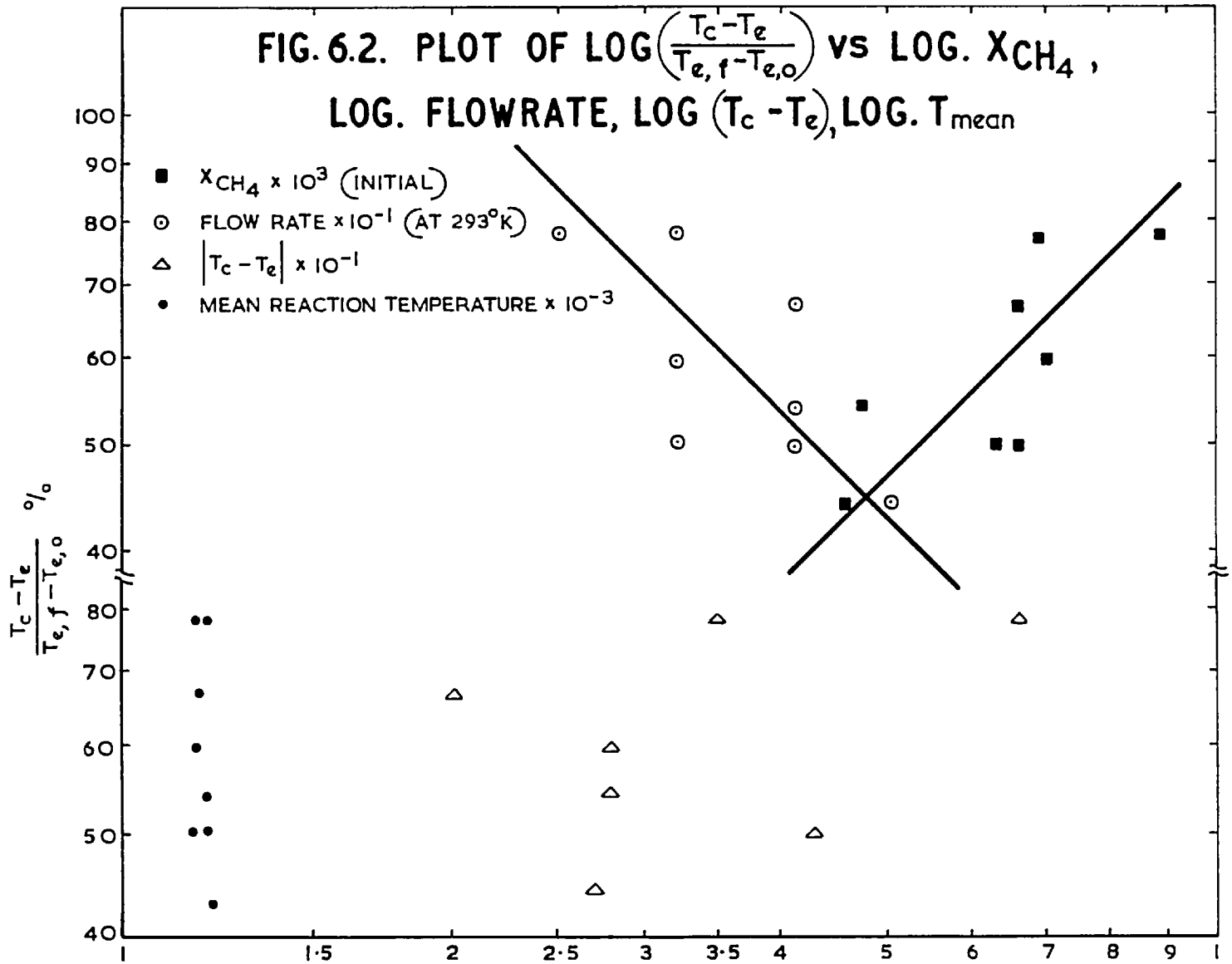
FIG. 6.2. PLOT OF LOG $\left(\frac{T_c - T_e}{T_{e,f} - T_{e,o}}\right)$ vs LOG. X_{CH_4}, LOG. FLOWRATE, LOG $(T_c - T_e)$, LOG. T_{mean}
$X_{CH_4} \times 10^3$ (INITIAL)
FLOW RATE $\times 10^{-1}$ (AT 293°K)
$|T_c - T_e| \times 10^{-1}$
MEAN REACTION TEMPERATURE $\times 10^{-3}$
$\frac{T_c - T_e}{T_{e,f} - T_{e,o}}$ %
100
90
80
70
60
50
40
80
70
60
50
40
1
1·5
2
2·5
3
3·5
4
5
6
7
8
9

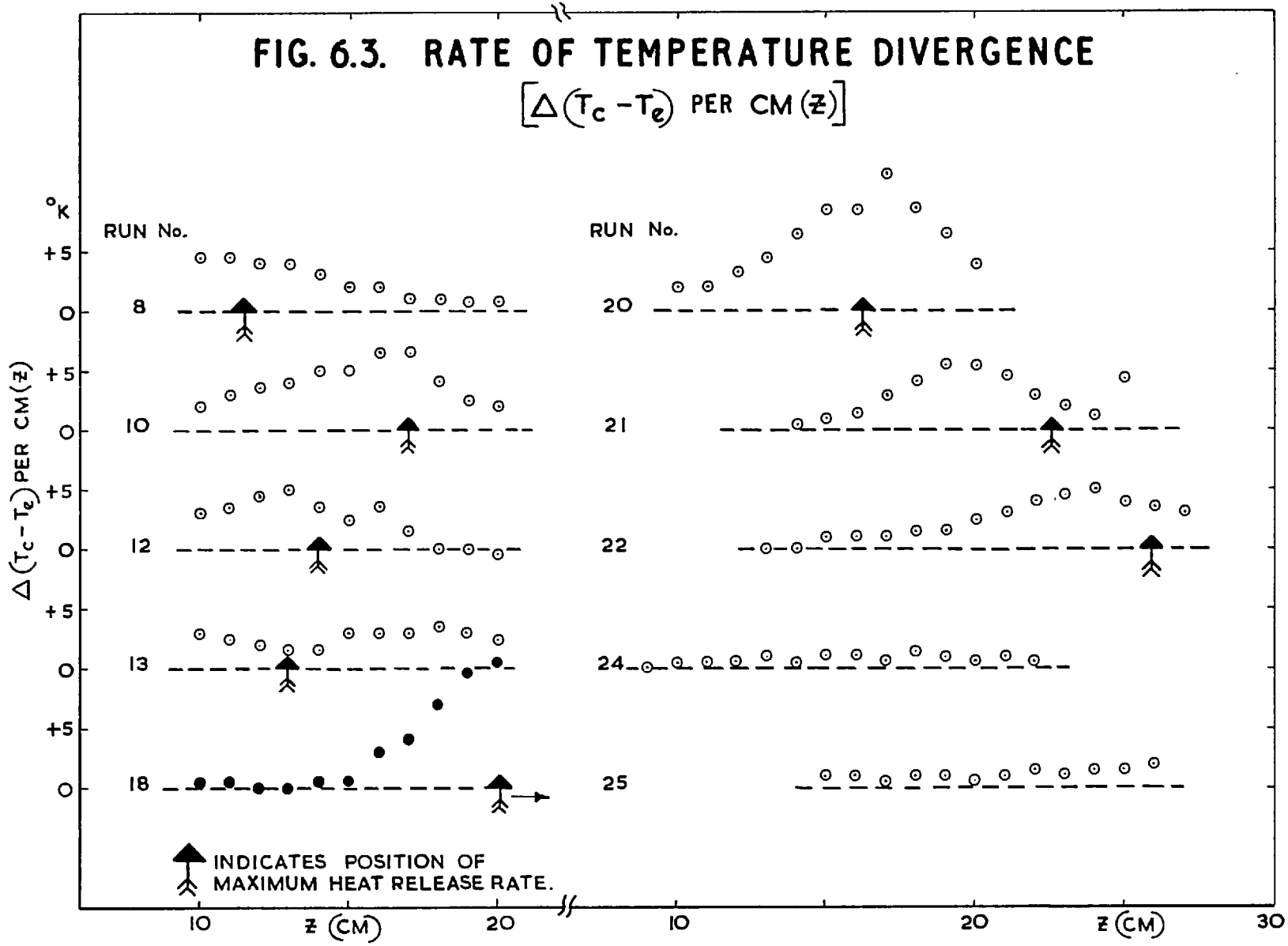
FIG. 6.3. RATE OF TEMPERATURE DIVERGENCE
[Δ(Tc - Te) PER CM (z)]
°K
Δ(Tc - Te) PER CM (z)
RUN No.
8
10
12
13
18
RUN No.
20
21
22
24
25
+5
0
INDICATES POSITION OF MAXIMUM HEAT RELEASE RATE.
10
20
z (CM)
30

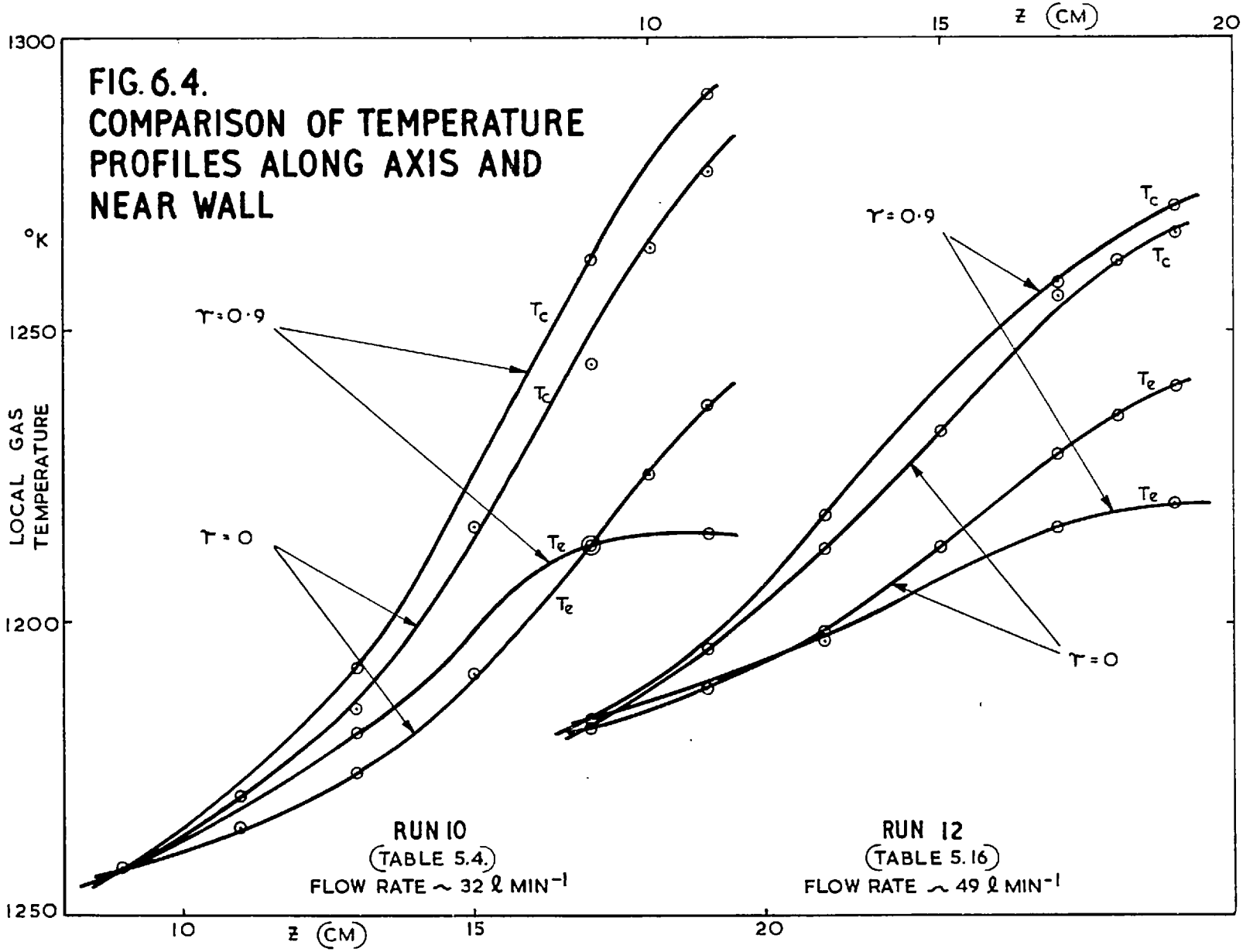
FIG. 6.4.
COMPARISON OF TEMPERATURE PROFILES ALONG AXIS AND NEAR WALL
LOCAL GAS TEMPERATURE °K
1300
1250
1200
1250
10
15
20
z (CM)
r = 0·9
r = 0
T_c
T_e
RUN 10
(TABLE 5.4.)
FLOW RATE ~ 32 ℓ MIN^{-1}
RUN 12
(TABLE 5.16)
FLOW RATE ~ 49 ℓ MIN^{-1}

FIG. 6.5. EFFECT OF CORRECTING TEMPERATURE PROFILES FOR RADIAL TRANSPORT

RUN 21 (SEE TABLE 5.11, FIGS. 6.6, 6.7, 7.2 AND SECTION 6.3.)

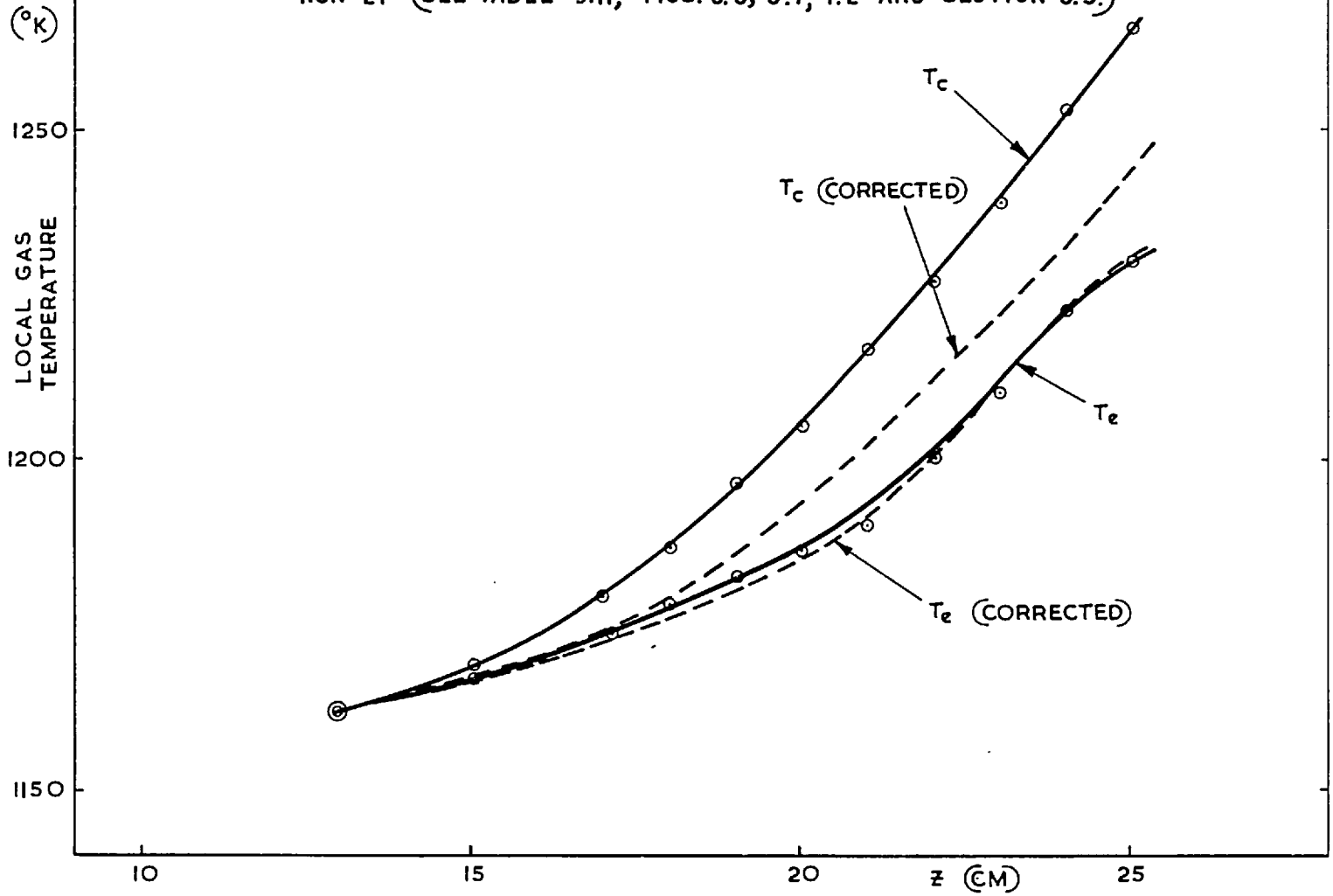

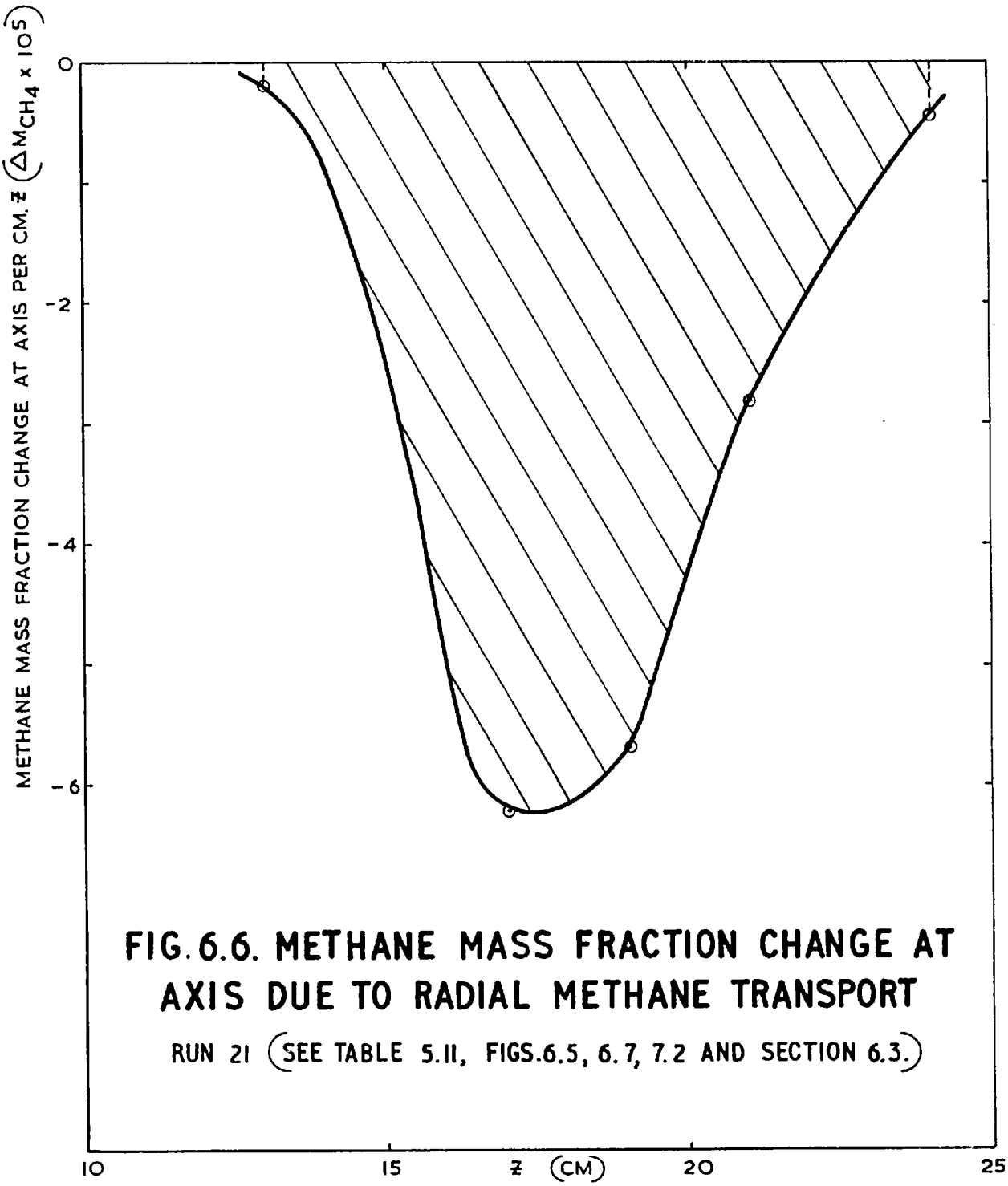

FIG. 6.6. METHANE MASS FRACTION CHANGE AT AXIS DUE TO RADIAL METHANE TRANSPORT

RUN 21 (SEE TABLE 5.11, FIGS. 6.5, 6.7, 7.2 AND SECTION 6.3.)

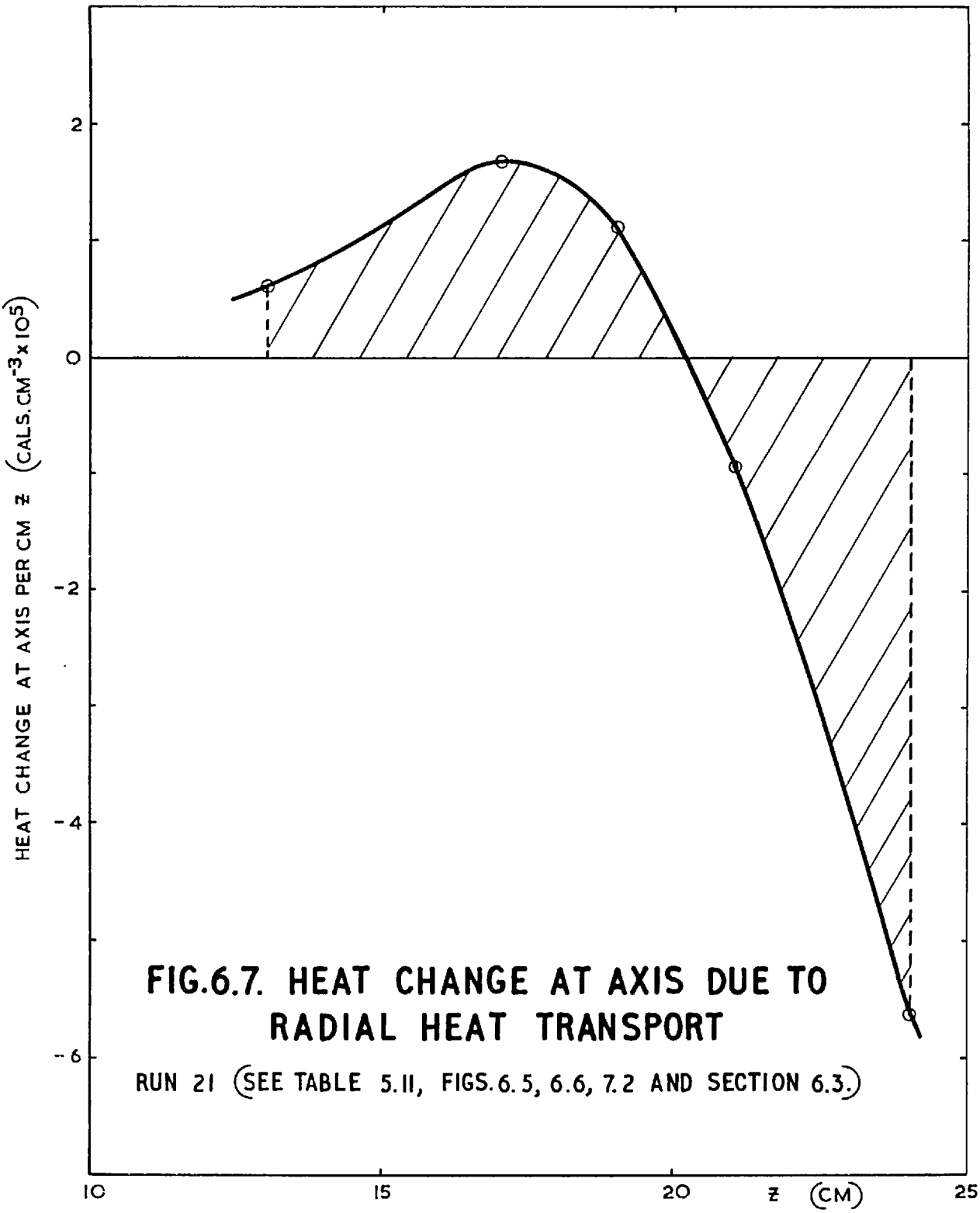

FIG.6.7. HEAT CHANGE AT AXIS DUE TO RADIAL HEAT TRANSPORT

RUN 21 (SEE TABLE 5.11, FIGS. 6.5, 6.6, 7.2 AND SECTION 6.3.)

CHAPTER 7

Factors affecting the rate of heat release

7.1 Typical data

In order to obtain a better appreciation of the data from which the heat release rates have been calculated, some typical sets of the tabulated data (Tables 5.2 to 5.17) have been plotted as Figures 7.1 to 7.5. They have been selected to illustrate four features of the results.

(i) Comparison of radial gradients for given reactedness at different axial positions; Runs 10 and 21 as Figures 7.1 and 7.2: this topic has already received mention in the previous chapter, Section 6.2.4.

(ii) Data from one of the higher and the lowest fuel concentration, Runs 10 and 25, are shown as Figures 7.1 and 7.3. This illustrates the trend from practically isothermal conditions at very low fuel concentrations to more nearly adiabatic conditions with a short reaction zone as the fuel concentration is increased. The self-inhibiting effect of methane on its own oxidation is also apparent from this comparison.

(iii) The effect of the total flow rate on the data is illustrated by Runs 12 and 20, shown as Figures 7.4 and 7.5. Reducing the flow rate causes the reaction zone to contract, although not in quite the same way as increasing the fuel concentration, and permits larger total radial transport for comparable axial distances.

(iv) The two cases (a) zero and negative radial temperature gradients and (b) both negative and positive radial temperature gradients are illustrated in Figures 7.2 and 7.4.

7.2 Calculation of the heat release rate q'''

The volumetric heat release rate q''', as a function of position along the axis through the reaction zone, should in principle be calculated from the heat conservation Equation 5.7 or from the specie conservation Equation 5.8. Assuming, as before, that the radial transport term is the only correction term which need be considered, it follows that the observed temperature profile T_e must be corrected for the radial heat flux according to Equation 5.7. However, it was shown in Chapter 6 that this term could not be obtained in the core flow, due to uncertainty concerning the aerodynamics of the flow in this region, and could be obtained only qualitatively in the boundary layer region, where it appeared that the correction term based on a laminar flow model produced an under-estimate of the radial heat flux. A similar uncertainty affects the calculation of a correction to the volumetric heat release rate obtained from the measured specie distribution and Equation 5.8. In this case, because water concentration was not determined experimentally, an additional assumption would be required relating the reactedness and the water concentration.

Some empiricism in the treatment of the experimental data was therefore necessitated. As a consequence the derived volumetric heat release rates were subject to some uncertainty in their absolute magnitude, but remained informative in a comparative sense.

The heat release rate q''' was computed from the relation

$$q''' = v_z C_p \left(\frac{\partial T}{\partial z}\right)_{r=o} \text{ cal cm}^{-3}\text{s}^{-1} \quad \ldots \quad \ldots \quad 7.1$$

where ρv_z was obtained from the pressure and temperature profiles. The specific heat, C_p, was shown to be effectively constant over the temperature range of the experiments, and to differ negligibly from the value for air. A value of 0.283 cal $gm^{-1}\,^oK$ was used and applied over the temperature range $1143^oK < T < 1293^oK$. q''' at r = o is tabulated in the final column of Tables 5.2 to 5.17.

The $\frac{\partial T}{\partial z}$ term of Equation 7.1 was obtained by numerical or graphical differentiation of a mean temperature profile. The mean profile was obtained (a) as the mean of the T_e and T_c profiles where the data allowed the calculation of T_c. In this case $T_m = \frac{T_e + T_c}{2}$. (b) where it was not possible to calculate T_c (for runs where the composition data were suspect and have been discarded), the mean temperature profile was obtained from the relation $T_m = T_{e,o} + \Delta T_e \times 1.3$, where $T_{e,o}$ was the temperature at which the measured and calculated profiles were matched. The subscript 'm' will now be dropped.

The following argument may serve to justify the course taken to determine T by method (a) above. For the experimental conditions employed the true integrated heat release must lie between (i) an integrated heat release calculated from the uncorrected composition data, which will give an upper limit and (ii) an integration based on the experimental temperature profile T_e, which will result in a lower limit.

These limits are imposed by the condition that the integrated (in the z direction) radial correction terms invariably tend to correct the T_e profiles in a positive sense and the T_c profiles in a negative sense.

A qualification must be made. It does not follow that the maximum slope of the true heat release curve will be intermediate between the maximum slopes of the T_c -derived and T_e-derived curves (although, of course, the maximum slope of the mean curve must be). However a sufficient condition for the true maximum to lie between the two derived maxima is that the differentials of the radial correction terms remain constant in sign. This condition is always fulfilled in the case of the composition correction term, but not invariably in the case of the radial heat flux. Figure 6.5 illustrates a case where the radial correction term changes sign. Closer inspection of these exceptions shows that the effect in the case of the heat release rate determined from the T_e-corrected profiles is in a sense to enhance the maximum. We have already shown that it cannot exceed the maximum slope of the upper limit curve; therefore the true maximum heat release rate must lie between the maxima obtained from uncorrected composition data and the uncorrected temperature profile T_e. Without detailed knowledge of the aerodynamics in the reaction zone it is not profitable to pursue this argument. Consequently the use of a mean temperature profile is justified as the one most likely to minimise error.

The 1.3 factor used to obtain a 'mean' temperature profile in those runs where the composition data were considered unreliable - method (b) above - was based on an average correction found in the

treatment of the runs where both T_c and T_e profiles were available. Some estimate of the reliability of this procedure was possible by comparing the T_c calculated for these runs at z_{max}. At this point the composition data have maximum reliability. The comparison showed that the arbitrary procedure was qualitatively successful; the difference between $T = T_{e,o} + \Delta T_e \times 1.3$ and $T = \frac{T_e + T_c}{2}$ at z_{max} was never greater than $10^{o}K$.

7.3 The volumetric heat release rate profiles

7.3.1 Typical heat release rate profiles

The volumetric heat release rates have been plotted as a function of z at r = o. Typical plots are presented as Figure 7.6. It is interesting to note the way in which the heat release rate profiles develop as the fuel concentration is increased from the nearly isothermal case reminiscent of classical kinetics to something approaching the adiabatic curves familiar in flame structure studies.

They also illustrate the self-inhibiting effect of methane on its own oxidation; the heat release rates at the higher methane concentrations being initially lower than the corresponding rates for leaner mixtures and then crossing over to give a higher maximum.

7.3.2 The effect of flow rate on the maximum heat release rate

The maximum heat release rate has been selected as the most informative single dependent variable for the context of the remainder of the present chapter.

For constant initial methane concentration and constant initial temperature Figure 7.7 indicates that the maximum heat release rate is

independent of the flow rate. This is to be expected if the empirical correction for heat and specie transfer is adequate and the wall surface plays no dominant role in the kinetics. The rather larger maximum at the highest flow rate may be attributed to a slightly higher initial temperature in this case.

As a consequence of this demonstration that the maximum heat release rate is essentially independent of the flow rate, the flow rate as such may be ignored and the results for all the flow rates used may be considered together in the remaining sections of the chapter.

7.3.3 The effect of methane concentration on the maximum heat release rate

Since the maximum heat release rate nearly always occurs before the further oxidation of carbon monoxide to carbon dioxide becomes significant, it is valid to consider the effect of the methane concentration on the heat release rate. There are a number of ways in which this might be done.

(i) to compare q'''_{max} with $m_{CH_4,i}$ at constant T_i

(ii) to compare q'''_{max} with $m_{CH_4,i}$ at constant $T_{q'''_{max}}$

(iii) to compare q'''_{max} with $m_{CH_4,q'''_{max}}$ at constant T_i

(iv) to compare q'''_{max} with $m_{CH_4,q'''_{max}}$ at constant $T_{q'''_{max}}$

or to compare the heat release rate at a fixed reactedness for different methane concentrations.

Remembering that methane shows both self-inhibiting and autocatalytic characteristics in its oxidation it is evident that care must be exercised in the interpretation of any of these comparisons. If it is assumed that the most important step at the point of maximum heat

release is the main propagating step in the methane oxidation to carbon monoxide

$$CH_4 + \left(OH,\ O,\ HO_2,\ H\right) \rightarrow \text{products}$$

then the comparisons (i) to (iv) above will tend to be of an 'overall' nature, since they will incorporate any effects due to variation in radical concentration.

Figure 7.8 shows a typical plot of q'''_{max} versus $X_{CH_4,i}$ at constant T_i. Above a certain minimum methane concentration it indicates a second power dependence, which will incorporate effects due to the q'''_{max} occurring at higher temperatures for higher initial methane concentration. Thus the order with respect to methane will be less than second order.

7.4 An activation energy derived from the maximum heat release rate

By grouping all the results, and normalising the maximum heat release rates to some arbitrary methane concentration (1 per cent was chosen and a direct proportionality was assumed) an activation energy is obtainable on the assumption that

$$q'''_{max} \propto \exp^{-E/RT}$$

Evidently $\ell n \left(\frac{q'''}{c_{CH_4}\ c_{O_2}} \right) = -\frac{E}{RT} + \text{const.}$ is true if the heat release rate may be expressed as a function of the reactant concentration. Since c_{CH_4}, c_{O_2} may be transferred to the const. if they are themselves constant, we immediately obtain

$$\ell n\ q'''_{max} = -E/RT + \text{const.}$$

if the constant value of c_{CH_4} is that occurring at the point of maximum heat release rate (oxygen is always effectively constant).

This procedure is a modified form of an analysis carried out by Levy and Weinberg[1] to obtain effective activation energies from an ethylene-air flame.

Figure 7.9 shows the result of plotting log q'''_{max} versus $\frac{1}{T_{q'''_{max}}}$. Considering the assumptions and approximations implicit in this approach the result is reasonable. From the slope of the best straight line an activation energy of ~ 58 kcal is obtained. This value may be compared with values of an 'overall' activation energy of 60 kcal obtained by Kozlov[30], of 64 kcal obtained by Hirsch[22], and of 87 kcal obtained by Ray[35], all from flow reactors under comparable conditions.

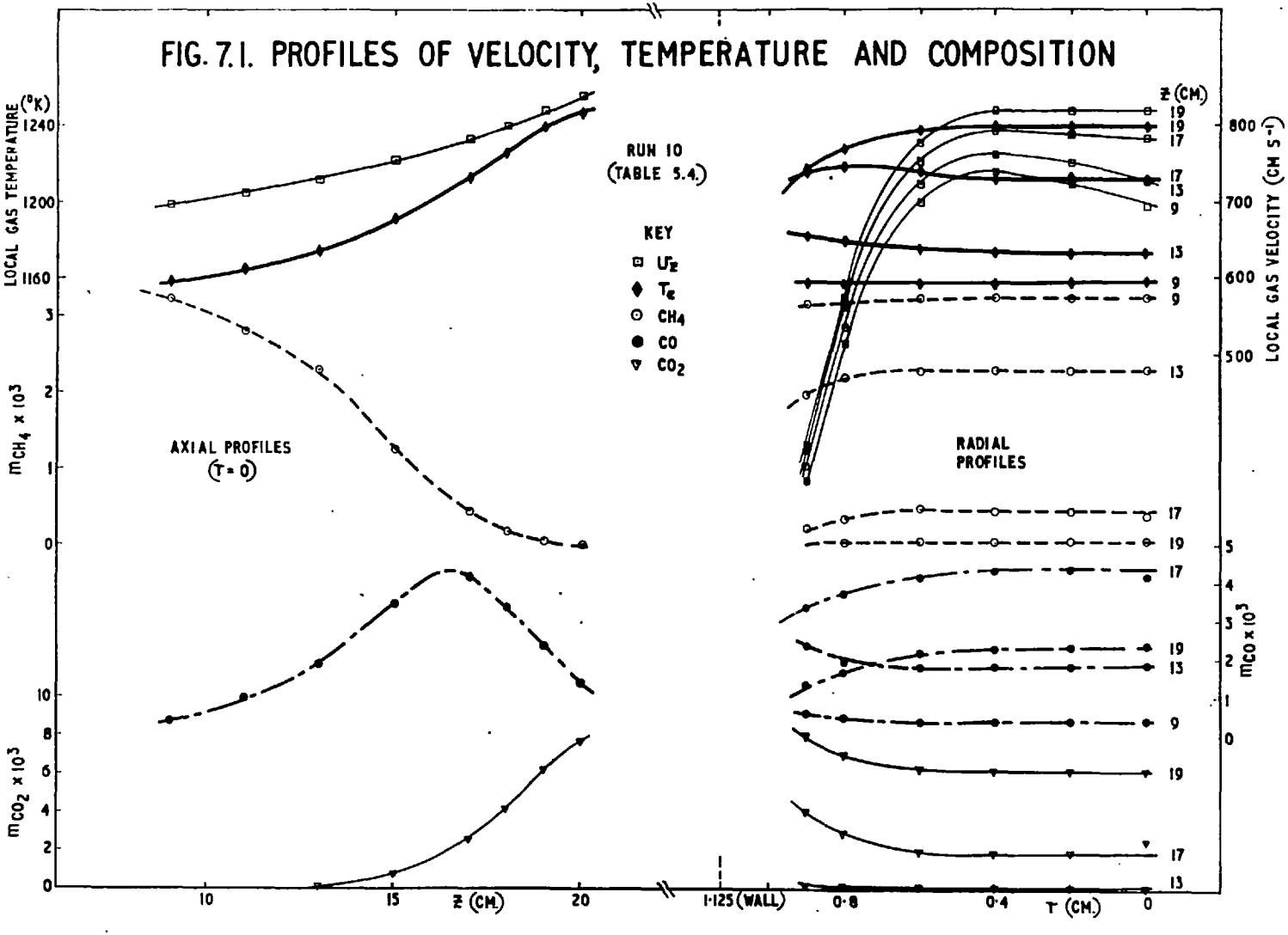
FIG. 7.1. PROFILES OF VELOCITY, TEMPERATURE AND COMPOSITION
LOCAL GAS TEMPERATURE (°K)
1240
1200
1160
RUN 10
(TABLE 5.4.)
KEY
U_z
T_e
CH_4
CO
CO_2
AXIAL PROFILES
(r = 0)
$m_{CH_4} \times 10^3$
$m_{CO_2} \times 10^3$
z (CM.)
RADIAL
PROFILES
LOCAL GAS VELOCITY (CM S^{-1})
$m_{CO} \times 10^3$
r (CM.)
1·125 (WALL)

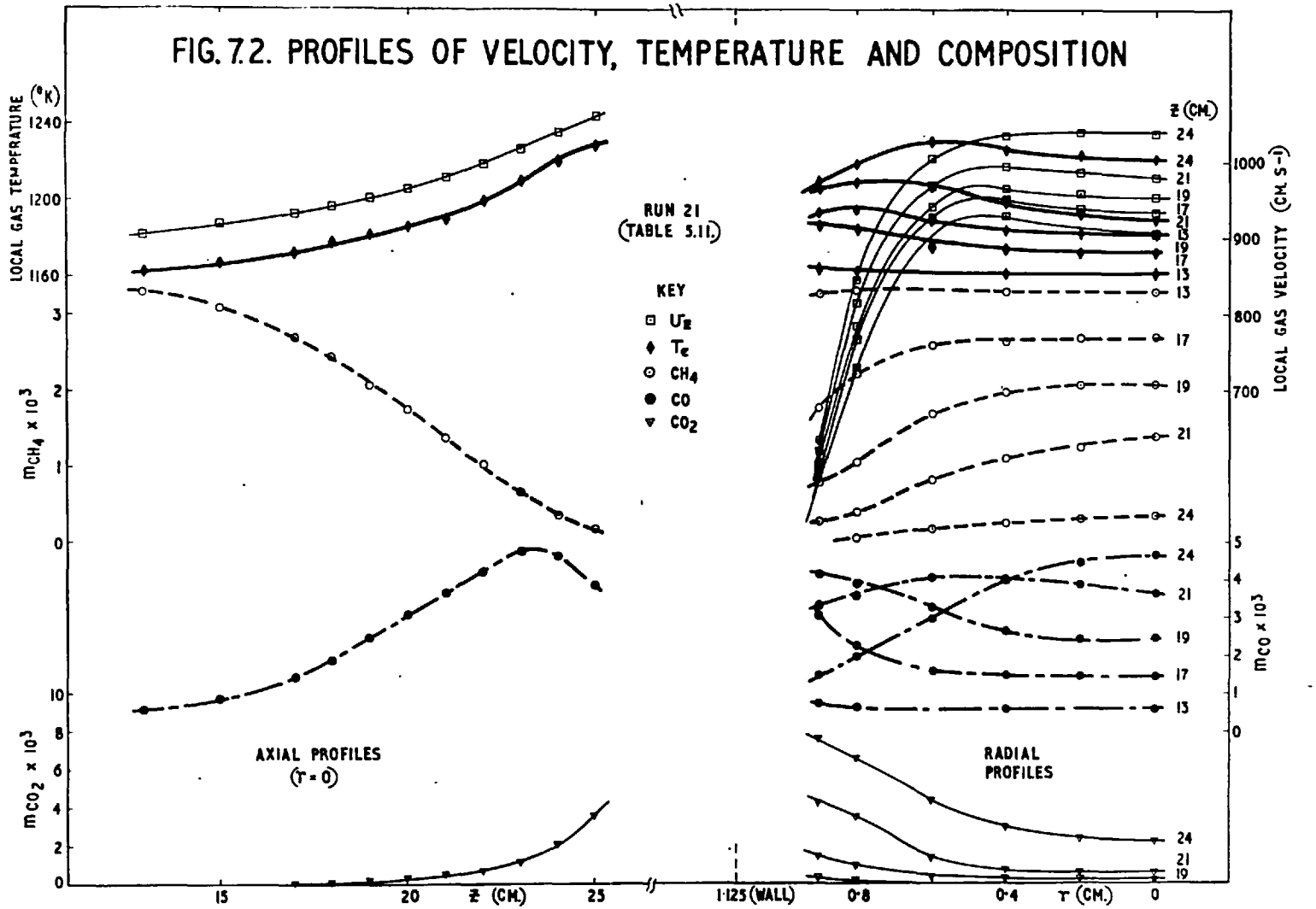
FIG. 7.2. PROFILES OF VELOCITY, TEMPERATURE AND COMPOSITION
LOCAL GAS TEMPERATURE (°K)
1240
1200
1160
$m_{CH_4} \times 10^3$
3
2
1
0
$m_{CO_2} \times 10^3$
10
8
6
4
2
0
RUN 21
(TABLE 5.11.)
KEY
U_z
T_e
CH_4
CO
CO_2
AXIAL PROFILES
(r = 0)
15
20
z (CM.)
25
z (CM.)
24
24
21
19
17
15
19
17
13
13
17
19
21
24
24
21
19
17
13
24
21
19
1·125 (WALL)
0·8
0·4
r (CM.)
0
RADIAL
PROFILES
LOCAL GAS VELOCITY (CM. S-1)
1000
900
800
700
$m_{CO} \times 10^3$
5
4
3
2
1
0

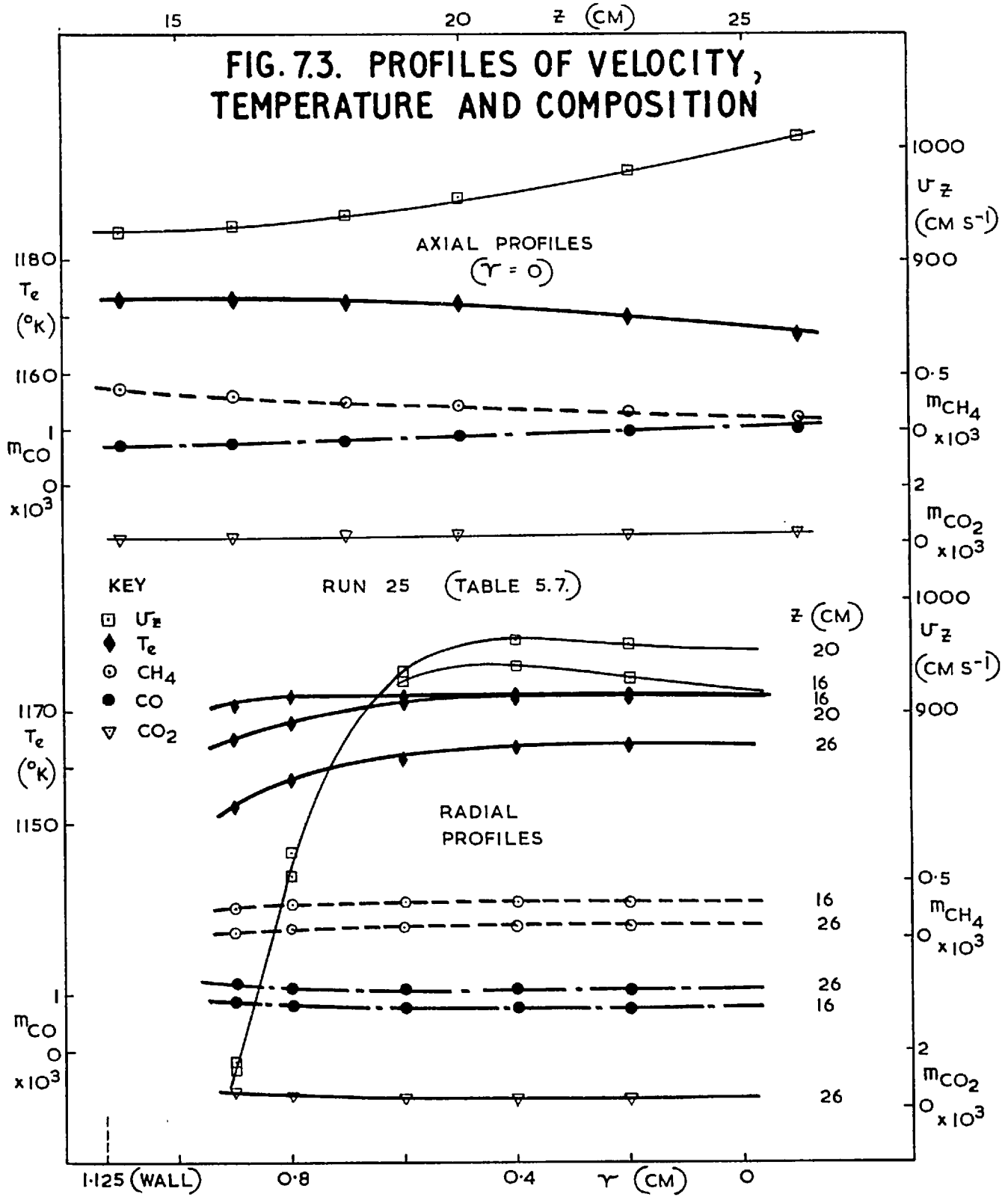
15
20
z (CM)
25
FIG. 7.3. PROFILES OF VELOCITY, TEMPERATURE AND COMPOSITION
AXIAL PROFILES
(r = 0)
1000
u_z (CM S^{-1})
900
1180
T_e (°K)
1160
0·5
m_{CH_4} x10³
0
1
m_{CO} x10³
0
2
m_{CO_2} x10³
0
KEY
u_z
T_e
CH_4
CO
CO_2
RUN 25 (TABLE 5.7.)
z (CM)
20
16
16
20
26
1000
u_z (CM S^{-1})
900
1170
T_e (°K)
1150
RADIAL PROFILES
16
26
26
16
26
0·5
m_{CH_4} x10³
0
1
m_{CO} x10³
0
2
m_{CO_2} x10³
0
1·125 (WALL)
0·8
0·4
r (CM)
0

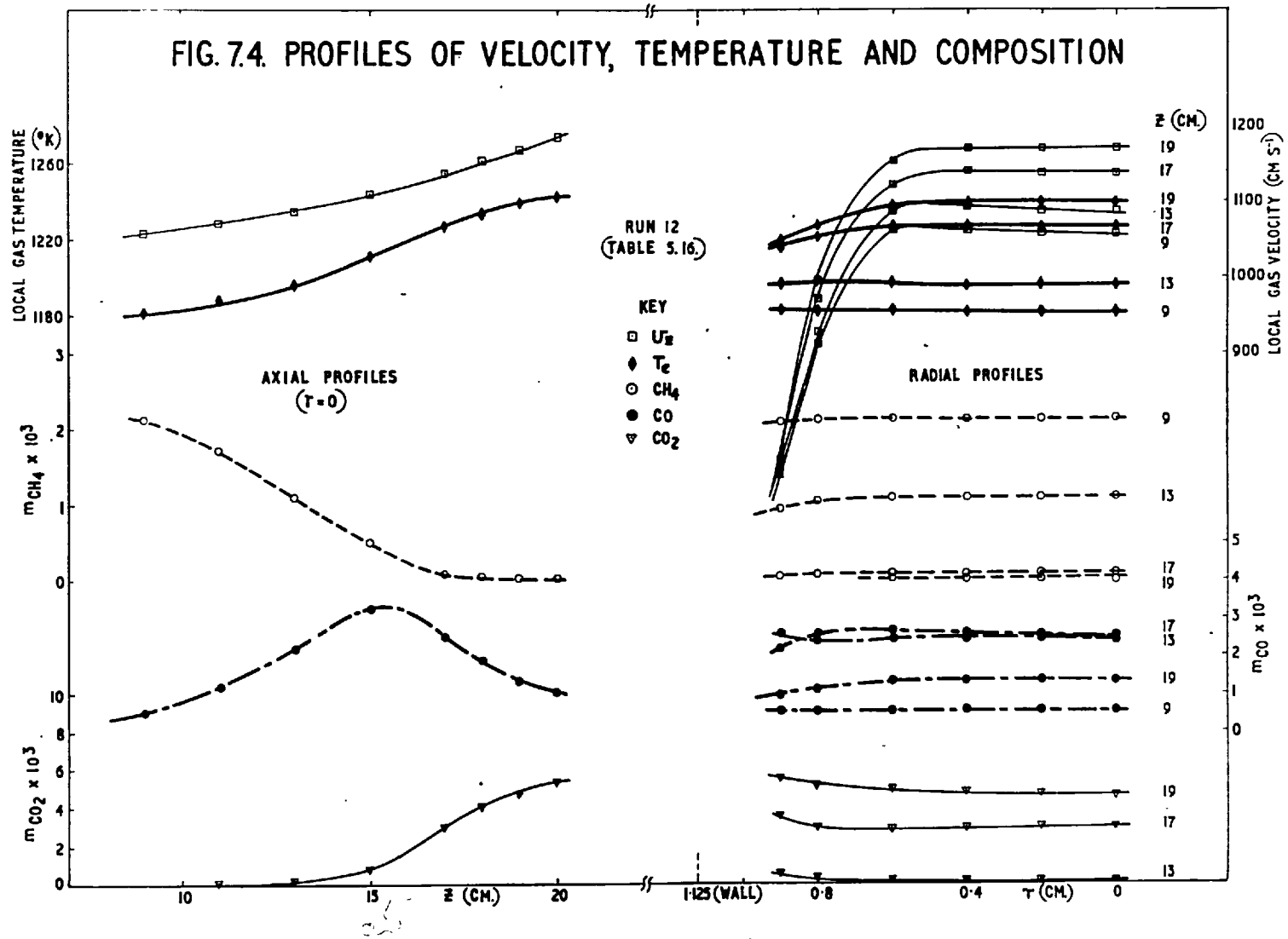
FIG. 7.4. PROFILES OF VELOCITY, TEMPERATURE AND COMPOSITION
LOCAL GAS TEMPERATURE (°K)
1260
1220
1180
AXIAL PROFILES
(r = 0)
$m_{CH_4} \times 10^3$
3
2
1
0
$m_{CO_2} \times 10^3$
10
8
6
4
2
0
10
15
z (CM.)
20
RUN 12
(TABLE 5.16.)
KEY
U_z
T_g
CH_4
CO
CO_2
RADIAL PROFILES
z (CM.)
19
17
19
13
17
9
13
9
9
13
17
19
17
13
19
9
19
17
13
1.125 (WALL)
0.8
0.4
r (CM.)
0
1200
1100
1000
900
LOCAL GAS VELOCITY (CM S⁻¹)
5
4
3
2
1
0
$m_{CO} \times 10^3$

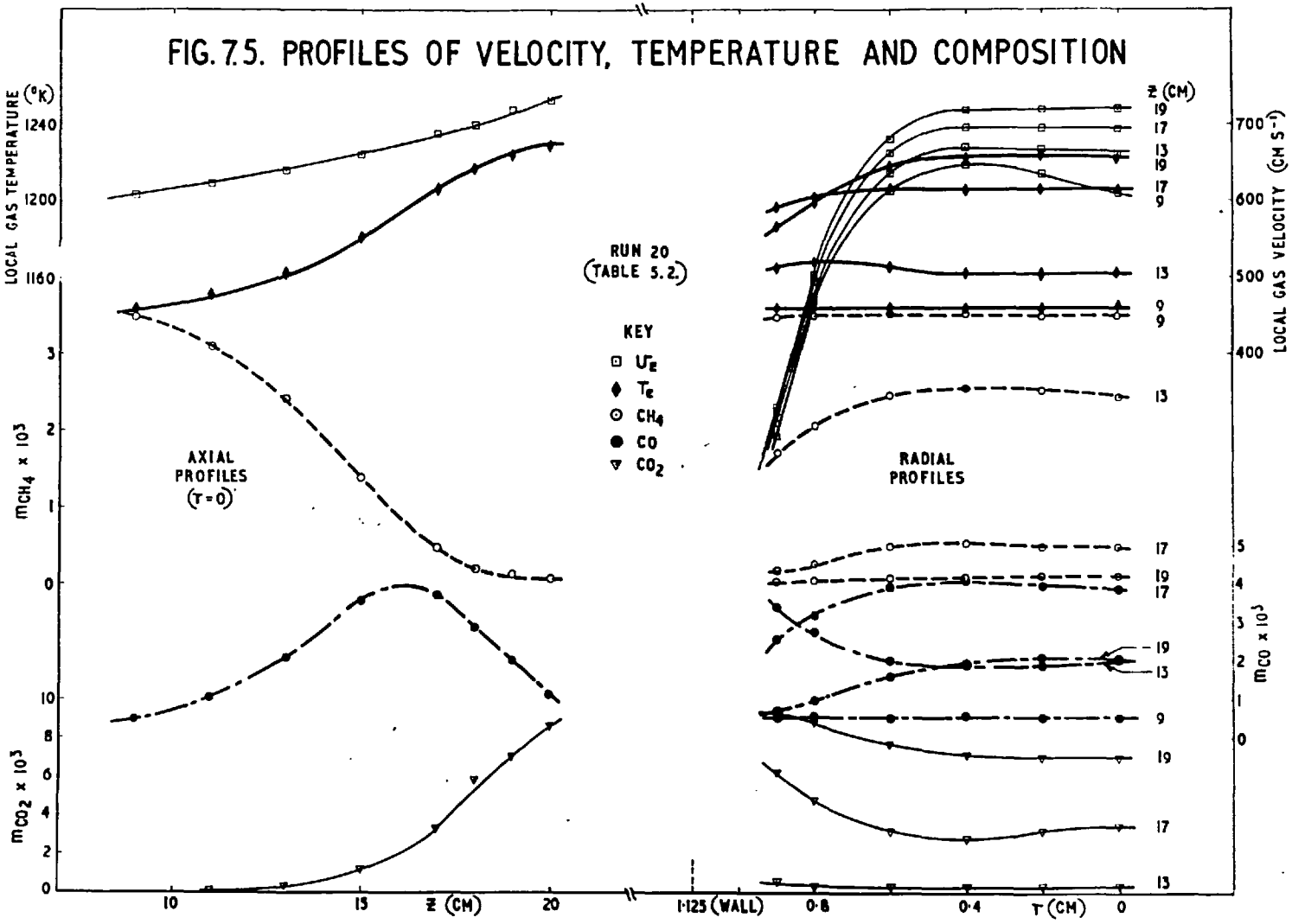
FIG. 7.5. PROFILES OF VELOCITY, TEMPERATURE AND COMPOSITION
LOCAL GAS TEMPERATURE (°K)
1240
1200
1160
$m_{CH_4} \times 10^3$
$m_{CO_2} \times 10^3$
AXIAL PROFILES (r = 0)
RUN 20 (TABLE 5.2.)
KEY
U_z
T_e
CH_4
CO
CO_2
RADIAL PROFILES
z (CM)
LOCAL GAS VELOCITY (CM S^{-1})
700
600
500
400
$m_{CO} \times 10^3$
10
15
z (CM)
20
1·125 (WALL)
0·8
0·4
r (CM)
0

FIG. 7.6. TYPICAL HEAT RELEASE RATE PROFILES

RUN No.	10	13	14	18
$X_{CH_4} \times 10^2$ (INITIAL)	0·630	0·460	0·900	0·885
FURNACE TEMP. °K	1152	1145	1152	1146
FLOW RATE ℓ MIN^{-1} (293°K)	32·32	32·32	32·32	32·32

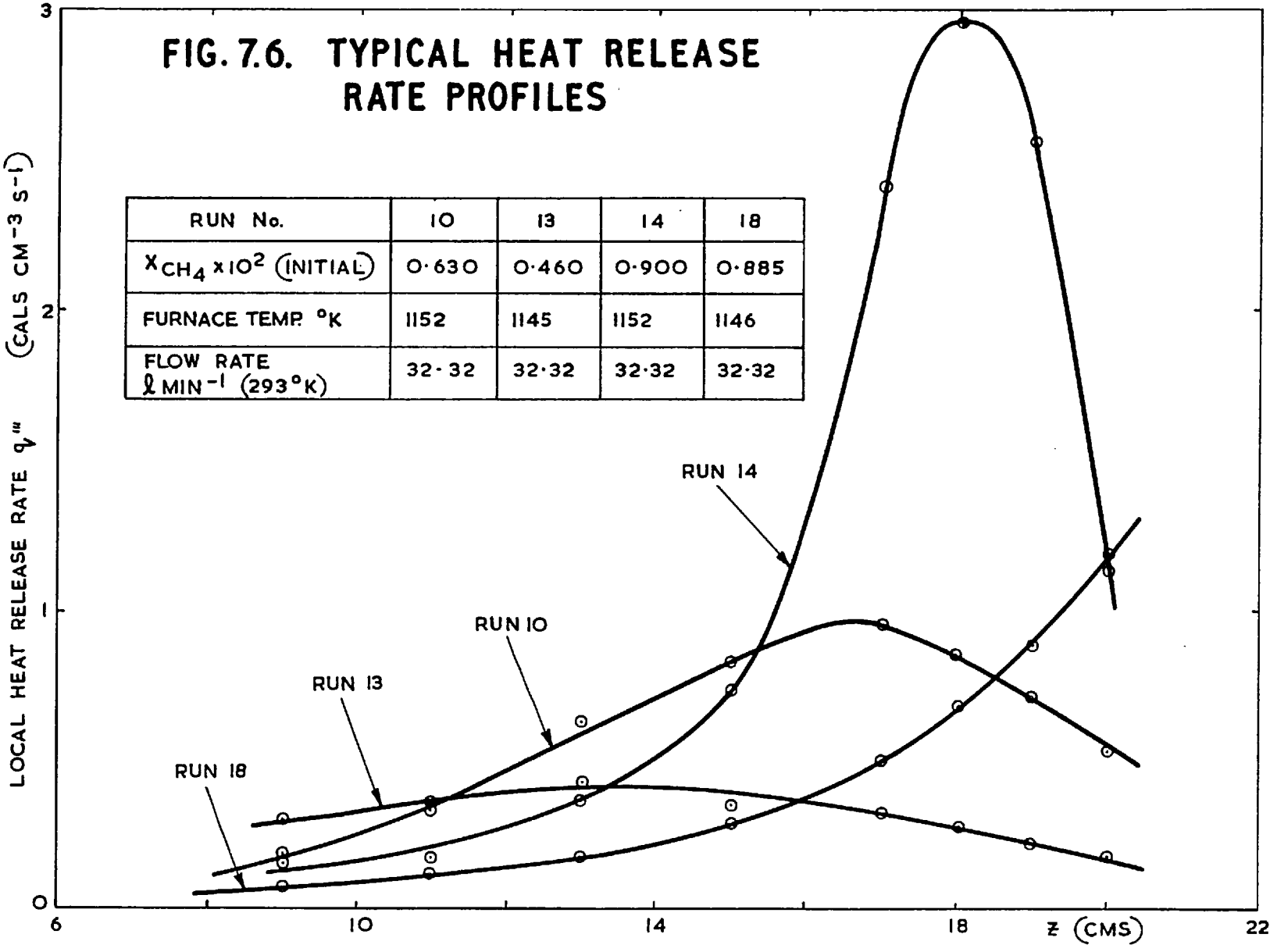

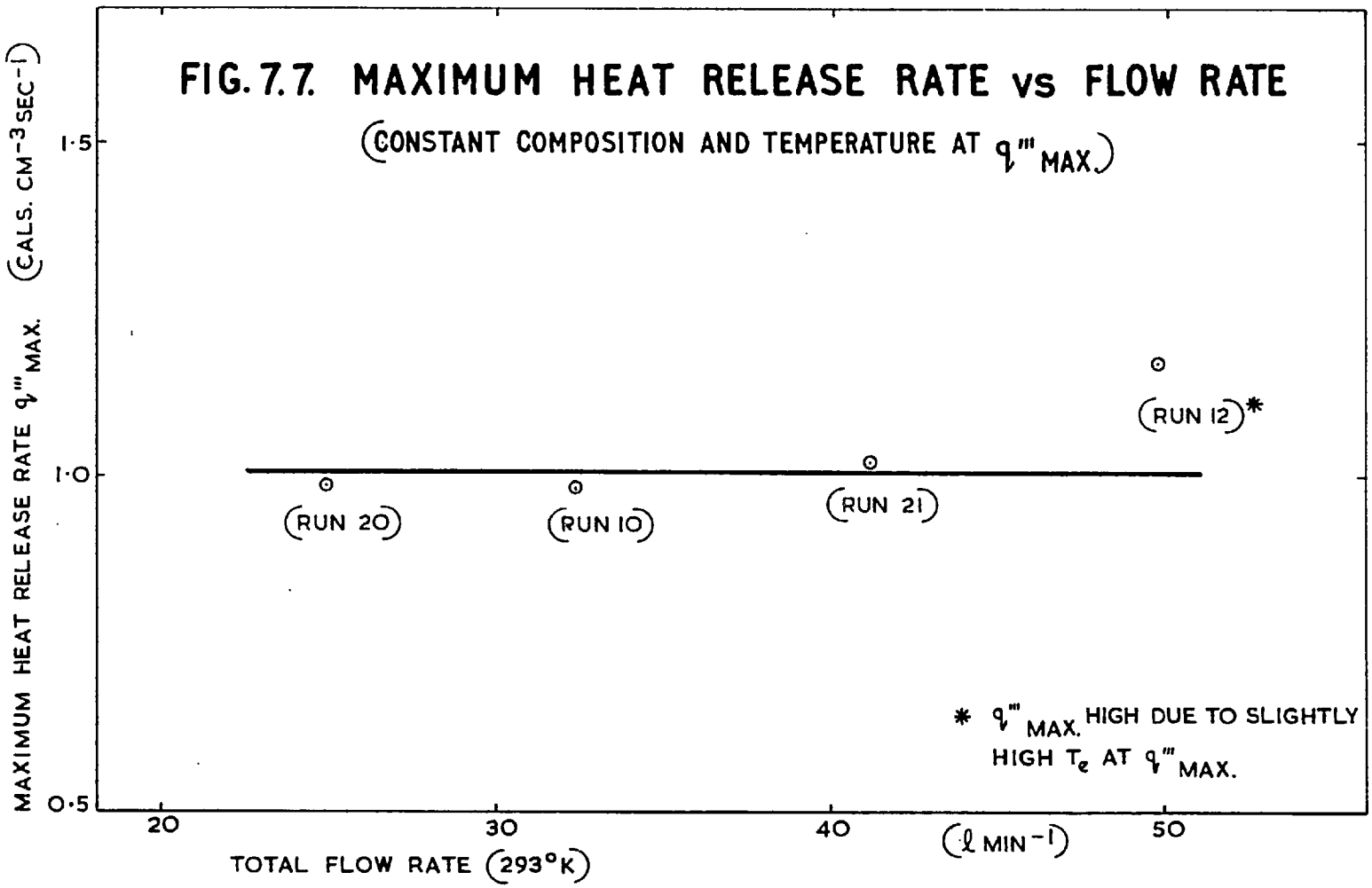
FIG. 7.7. MAXIMUM HEAT RELEASE RATE vs FLOW RATE
(CONSTANT COMPOSITION AND TEMPERATURE AT q‴ MAX.)
MAXIMUM HEAT RELEASE RATE q‴ MAX. (CALS. CM⁻³ SEC⁻¹)
1·5
1·0
0·5
(RUN 12)*
(RUN 20)
(RUN 10)
(RUN 21)
* q‴ MAX. HIGH DUE TO SLIGHTLY HIGH Tₑ AT q‴ MAX.
20
30
40
50
TOTAL FLOW RATE (293°K)
(ℓ MIN⁻¹)

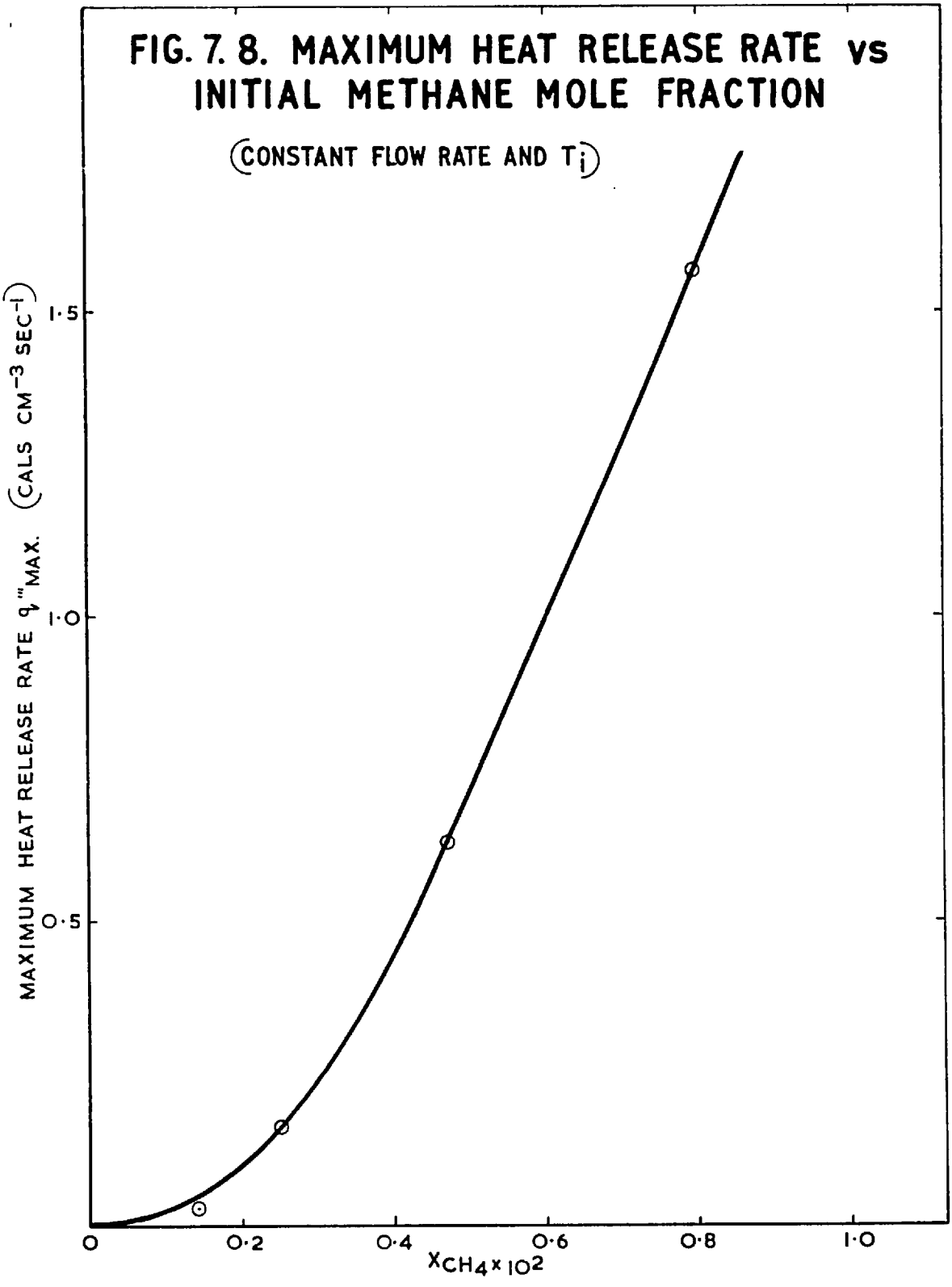
FIG. 7. 8. MAXIMUM HEAT RELEASE RATE vs INITIAL METHANE MOLE FRACTION
(CONSTANT FLOW RATE AND T_i)
MAXIMUM HEAT RELEASE RATE $q'''_{MAX.}$ (CALS CM^{-3} SEC^{-1})
1·5
1·0
0·5
0
0·2
0·4
0·6
0·8
1·0
$X_{CH_4} \times 10^2$

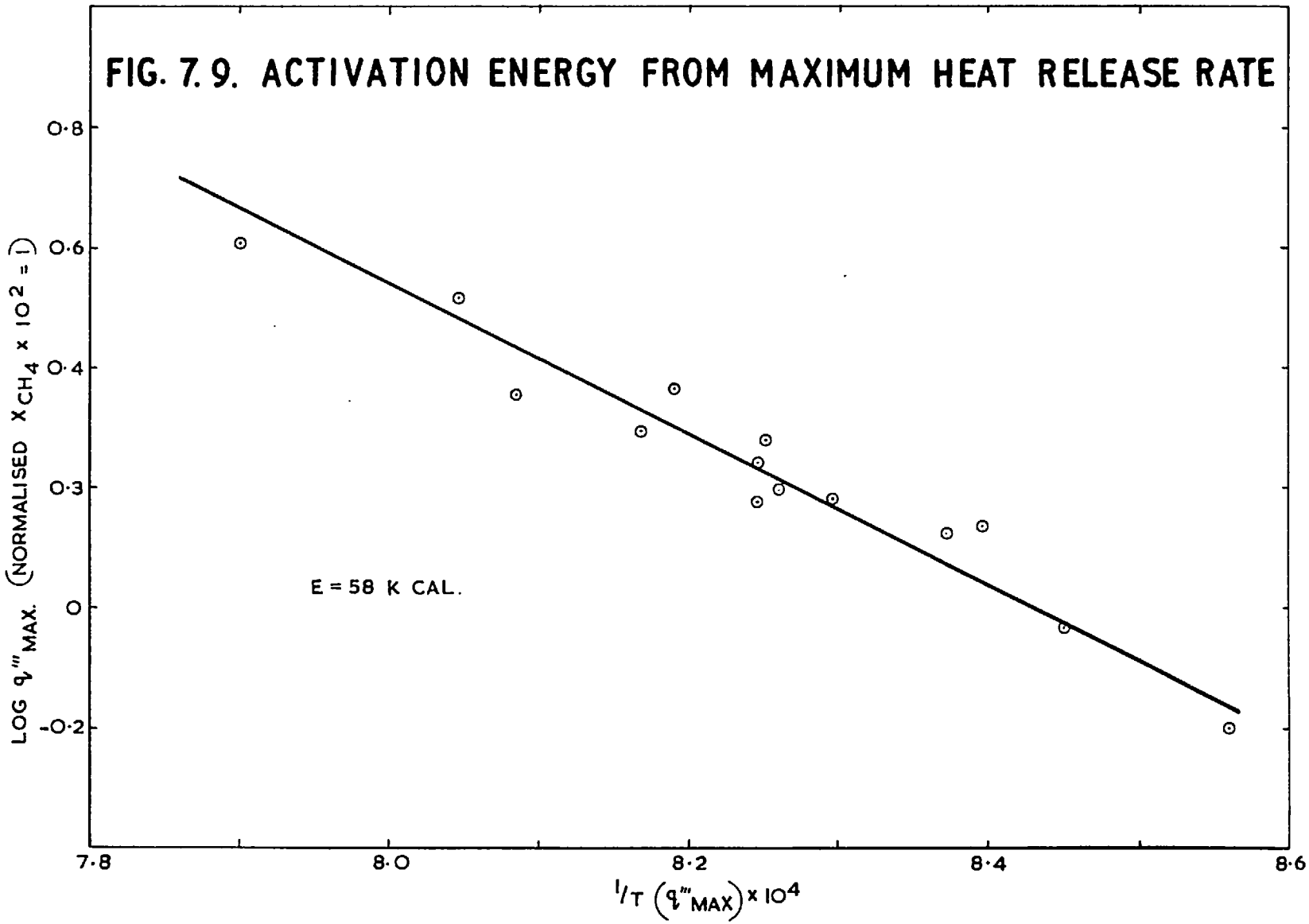
FIG. 7.9. ACTIVATION ENERGY FROM MAXIMUM HEAT RELEASE RATE
LOG q'''MAX. (NORMALISED XCH4 x 10^2 = 1)
0·8
0·6
0·4
0·3
0
-0·2
E = 58 K CAL.
7·8
8·0
8·2
8·4
8·6
1/T (q'''MAX) x 10^4

CHAPTER 8

Kinetics and mechanism

8.1 Treatment of the composition data

Chapters 5 and 6 have shown how the data should be corrected for diffusion. In Chapter 7 an empirical adjustment to account for transport processes was applied. In the present chapter the composition data for all the runs listed in Tables 5.2 to 5.17 and 5.19 to 5.37 have been used without any correction for radial diffusion. Two lines of reasoning led to this decision. In the first place the type of analysis proposed was concerned with relative effects. Since the omission of a correction term for diffusion caused all rates to be overestimated, some cancellation of the correction terms will result. Secondly, over and above the difficulties inherent in estimates of the diffusion terms mentioned previously, there were two additional features which increased the difficulty of finding an accurate expression for the correction for present purposes; (a) the individual specie data, including the low concentration intermediates, required separate correction, (b) the two sets of data, those obtained using the composite probe and those obtained using the water-cooled sampler, had to be considered in conjunction. It appeared that the latter comparison was best accomplished by taking the whole of the data at face value. The difficulty of estimating corrections to the data obtained by the water-cooled sampler was enhanced by the lack of gas temperature values in the reaction zone. It can be seen from the discussion of the previous

chapter, Section 7.2, that even where absolute rather than relative magnitudes are required the error incurred by ignoring the correction terms was unlikely to more than double (because of the differentiation) the uncertainty of about 40 to 50 per cent in the uncorrected data.

8.2 Reaction order

8.2.1 Effective order with respect to methane

Measuring rates by graphical differentiation of the data for a reaction path along the axis through the reaction zone, the results listed as Tables 5.2 to 5.17 were used to investigate the partial order with respect to methane at all stages of reactedness.

A plot of $\log\left(\frac{dX_{CH_4}}{dt}\right)$ against $\log X_{CH_4}$ at four temperature levels is shown in Figure 8.1. The local value of the concentration was used for this purpose. While other influences are undoubtedly present to a minor extent, the effective orders which are obtained may be accounted for as follows. The approximately first order dependence shown by the methane at concentrations below ~0.3 per cent are probably due to the oxidant having effectively constant concentration at these extreme dilutions. Since the oxidant must be a radical this suggests that the steady-state approximation, $\frac{d[\text{oxidant}]}{dt} = 0$, is valid under some conditions in the present experiments. This idea is supported by the fact that the two leanest mixtures studied, the two points at 1173°K, show this dependeance fairly early in the oxidation, at a reactedness where the other runs were still exhibiting self-inhibition.

The data at the lowest temperature (1160°K) refer to conditions at low relative reactedness and higher concentrations of methane. Here an effective order of ~-2 is obtained. Remembering that at low relative reactedness methane shows self-inhibition (at least above ~0.3 per cent) at high temperature, this may be interpreted as indicating a mechanism of inhibition which is effectively second-order with respect to methane. It does not follow that the partial mechanism is second-order with respect to methane. Three more likely alternatives may be suggested, deliberately not specifying the particular species involved. The inhibiting mechanism may be

(i) First-order with respect to methane and first-order with respect to a methane-derived radical.

(ii) First-order with respect to each of two different methane-derived radicals.

(iii) Second-order with respect to a single methane-derived radical.

It is interesting to note that a number of workers, e.g., Kozlov[30] and Hirsch[22], have obtained an overall order with respect to methane of ~-0.5 under comparable experimental conditions.

8.2.2 Effective order with respect to carbon monoxide and oxygen

A plot of $\log \left(\frac{dX_{CO_2}}{dt}\right)$ against $\log X_{CO}$ at two temperature levels revealed no convincing correlation. This is hardly surprising, however, when it is remembered that at constant temperature neither methane

nor, in general, radicals are likely to be at constant concentration. The effect of variation in the local methane concentration will result in a range of inhibitions in the carbon monoxide rate.

The extremely lean methane/air mixtures used in the present experiments rendered impracticable any attempt to determine the order with respect to oxygen.

8.3 Estimation of hydroxyl radical concentration

On the assumption that the only important mechanism for the oxidation of carbon monoxide at high temperature in the presence of water vapour is the forward part of the equilibrium

$$CO + OH \rightleftarrows CO_2 + H \qquad \ldots\ (1)$$

which has been shown to be extremely likely at slightly higher temperatures by recent flame work[8,9,10,11,41], it is possible to calculate a profile for the hydroxyl concentration using the rate constants for (1) available in the literature[71,8,10]. The assumption made means that the rates of $CO + O_2 \rightarrow$ products and $CO + HO_2 \rightarrow$ products may be neglected by comparison with the forward rate of (1). This was obviously adequate in the case of oxygen because no carbon monoxide was oxidised in the presence of excess oxygen in the early stages of the reaction. Some justification for ignoring the reaction with HO_2 came from the fact that the results were sensible without considering the latter.

The net forward rate of (1) may be written as

$$K_{CO_2} = k_1 \left[CO\right] \left[OH\right] - k_{-1} \left[CO_2\right] \left[H\right]$$

where both k_1 and k_{-1} are known with 2 to 3-fold accuracy. Since $k_1/k_{-1} \sim 8 \times 10^{-3} \exp^{23000/RT}$ the backward rate of (1) may be ignored where $\left[H\right]$ is likely to be less than $\left[OH\right]$, as in the present case. Hence we need only consider

$$K_{CO_2} = k_1 \left[CO\right] \left[OH\right] \quad \ldots\ 8.1$$

A mean value for k_1 was taken from the three values $3 \times 10^{12} \exp^{-7000/RT}$ (Reference 71), obtained by a flow technique at $\sim 700^{\circ}K$; $2 \times 10^{13} \exp^{-10000/RT}$ (Reference 10); $5 \times 10^{12} \exp^{-7000/RT}$ (Reference 8); the latter two values were obtained from flame studies.

Equation 8.1 may be rewritten in terms of mass fractions to give

$$\left[OH\right] = \frac{(dm_{CO_2}/dt)}{m_{CO}\, k_1} \cdot \frac{M_{CO}}{M_{CO_2}} \quad \ldots\ 8.2$$

from which a profile of $\left[OH\right]$ along the axis through the reaction zone may be obtained. A typical profile from Run 10 is shown in Figure 8.2. It is of interest to compare the value deduced from expression 8.2 with the equilibrium value of the hydroxyl concentration.

Assuming that the reactions

$$OH + OH \rightleftarrows H_2O + O \qquad \ldots\ldots (2)$$

$$O + O + M \rightleftarrows O_2 + M \qquad \ldots\ldots (3)$$

remain in equilibrium and that carbon monoxide and methane have no influence on these equilibria, the equilibrium value of the hydroxyl concentration is given by the relation[8]

$$\frac{[OH]_{eq} M_m}{\rho T} = X_{OH} = \frac{(X_{H_2O})^{\frac{1}{2}}(X_{O_2})^{\frac{1}{4}}}{K_2^{\frac{1}{2}} K_3^{\frac{1}{4}} P^{\frac{1}{2}}} \qquad \ldots\ldots 8.3$$

where $K_2 = \frac{p_{H_2O} \cdot p_O}{(p_{OH})^2}$, $K_3 = \frac{p_{O_2}}{(p_O)^2}$ and $P = 1$ atm

p_i is the partial pressure of the i^{th} constituent. Values for the equilibrium constants K_n (not to be confused with K_i, the net reaction rates) were obtained from the data of Reference 107. The only outstanding quantity required is the water concentration. This was estimated by stoichiometry from the methane consumed. A comparative $[OH]_{eq}$ profile for Run 10 is plotted in Figure 8.2. It may be regarded as typical.

It is interesting that the hydroxyl concentration, as calculated from Equation 8.2, should reach a maxium so late in the reaction. A qualitative explanation for this feature will be discussed in the following chapter.

8.4 The reaction between methane and hydroxyl radicals

Using the estimates of the hydroxyl radical concentration obtained above, it is possible to calculate the forward rate constant for the reaction

$$CH_4 + OH \rightleftarrows CH_3 + H_2O \qquad \ldots\ (4)$$

To do this it must be assumed that (i) all other reactions involving the disappearance of methane are negligible by comparison with Equation (4), and (ii) all reactions tending to form methane (i.e., all reverse reactions) are negligible compared with the forward rate of Equation (4).

These assumptions may be stated as

$$\left[CH_4\right]\left\{k'\left[O_2\right] + k''\left[O\right] + k'''\left[H\right] + \ldots.\right\} \rightarrow CH_3 + \ldots. \rightarrow \text{eventually CO}$$
$$\ll k_4\left[CH_4\right]\left[OH\right] \rightarrow CH_3 + \ldots\ldots \rightarrow \text{eventually CO}$$

and

$$\left\{\left[CH_3\right] + \left[\ldots.\right]\right\}\left\{k^*\left[H_2\right] + k^{**}\left[OH\right] + k^{***}\left[H_2O\right] + \ldots.\right\} \rightarrow CH_4 + \ldots\ldots$$
$$\ll -k_4\left[CH_4\right]\left[OH\right] \ldots\ldots$$

Some estimates of the various rate constants involved are available in the literature. For instance, k' must be small because of the large activation energy involved (see discussion in Chapter 1), k'' is probably no larger than 2×10^{12} $cm^3 mole^{-1}$ s^{-1} at $1600^{\circ}K$[12], and k''' is about 2×10^{11} $\exp^{-11500/RT}$ (Reference 12). In fuel-lean conditions the reverse reactions may be ignored[12]. The only possible exception appears to be $CH_3 + HO_2 \xrightarrow{k^{****}} CH_4 + O_2$. If it is supposed that $[HO_2]$ cannot greatly exceed $[OH]$, and the rate constant k^{****} is unlikely to be greater than k^{**}, then this reaction may also be ignored.

Provided these assumptions are sufficiently accurate the measured methane disappearance rate will be given by

$$K_{CH_4} = -k_4 [CH_4] [OH]$$

Substituting for $[OH]$ from Equation 8.2 and converting to mass fraction units, k_4 is given by

$$k_4 = -\left(k_1 \left[\frac{m_{CO}}{m_{CH_4}} \cdot \frac{M_{CO_2}}{M_{CO}} \cdot \frac{(dm_{CH_4}/dt)}{(dm_{CO_2}/dt)} \right] \right) \quad \ldots\ 8.4$$

Eleven estimates of k_4 are listed in Table 8.2. There is approximately six-fold variation between the extreme values, which cannot be obviously related to the difference in experimental conditions. However, since the composition data are being used uncorrected for diffusion, the graphically differentiated profiles will obviously be subject to

some error, even allowing for the self-cancelling effect previously mentioned. The relatively wide range of conditions for which the rate constant has been evaluated (ten-fold variation in $[OH]$, the full range of methane/air ratios and flow rates), coupled with the inherent difficulty of selecting a z at which all four of the required measurements have maximum reliability, prejudice close agreement between individual estimates of the rate constant. Despite the individual variation the mean value is in good agreement with the few experimental determinations available in the literature (see Table 8.3).

The sensible value of the rate constant obtained supports, though does not necessarily vindicate, the view that the assumptions made are legitimate. A slightly low value of the rate constant indicates that no other mechanism for the disappearance of methane can be very important in the present experiments.

The immediate significance of this result is that it is unnecessary to postulate any propagating mechanism apart from attack by the hydroxyl radical. This applies equally to reactions (1) and (4).

It is not possible to make any quantitative deductions concerning the mechanism and rate of the subsequent oxidation of the methyl radical.

8.5 The intermediates H_2 O_2, H_2 and HCHO

Figure 8.3 is a plot of the axial profiles of all the species measured and shows the relation of the intermediates to the reactants and products. The figure has been composed by careful matching from

the runs listed as Tables 5.19 to 5.23. This is legitimate since the figure is only intended to convey a qualitative picture of what is happening.

8.5.1 Hydrogen peroxide

There is some evidence in the present results that the hydrogen peroxide concentration reaches a maximum slightly later in the reaction than the formaldehyde (see Figure 8.3). The experimental evidence is rather too flimsy to make the statement any more definite at this stage; however should it be confirmed it would be of interest to make quantitative comparison with the lower temperature work, where Salooja[56] has shown that the hydrogen peroxide maximum occurs at about the same stage in the reaction as the formaldehyde maximum.

Since the experimental hydrogen peroxide concentration was so small ($\sim 10^{-5}$ mole fraction) a single estimate of an equilibrium concentration was made for a mixture of 1 per cent water in air at 1200°K. To do this an estimate of the equilibrium constant for reaction (5) is required.

$$H_2O + O \rightleftarrows H_2O_2 \qquad \ldots\ (5)$$

The O-atom concentration is available from reaction (3). K_5 was obtained from an estimate of the free energy change for reaction (5)

$$\Delta G_T = -RT \ln K_5$$

$$\Delta G_{1200} = \Delta H_{1200} - T \Delta S_{1200}$$

$$= \Delta H_{298} + \int_{298}^{1200} \Delta Cp \, dT - T \left(\Delta S_{298} + \int_{298}^{1200} \frac{\Delta Cp}{T} \, dT \right)$$

ΔCp for reaction (5) was evaluated at 298°K and was used unmodified ($Cp(H_2O_2) \approx 18$ cal deg^{-1} mole^{-1}, $Cp(H_2O) \approx 9$, $Cp(O) \approx 5$, therefore $\Delta Cp \approx 4$ cal deg^{-1} mole^{-1}). ΔS_{298} was obtained from S_{298} $(H_2O_2) \approx$ 51 cal mole^{-1} (Reference 118), S_{298} $(H_2O) \approx 45$, S_{298} $(O) \approx 38$, so that $\Delta S_{298} \approx -32$ cal mole^{-1}. Enthalpies were obtained from Reference 119. The resulting estimate of K_5 is $K_5 \sim 0.18$. Substitution in the equilibrium equation for reaction (5) gave $(H_2O_2)_{eq} \sim 10^{-11}$ mole fraction. This must be compared with the measured value of $\sim 10^{-5}$ mole fraction. The ratio will be modified if the O-atom concentration is not the equilibrium one. Obviously the peroxide is many times its equilibrium value even with an O-atom concentration considerably in excess of equilibrium.

Figure 8.4 illustrates the data of Tables 5.24 to 5.26 and indicates that there is nothing obviously anomalous in the radial distribution of H_2O_2. The few other measurements of H_2O_2 near the wall (see Table 5.19) support this view.

8.5.2 Hydrogen

The few measurements of hydrogen which were made agreed fairly well with those made by Hirsch[23].

8.6 The effect of variation of temperature, flow rate and methane concentration on the maximum formaldehyde concentration

It was considered that of the three low concentration intermediates studied the quantitative measurements of formaldehyde were the most accurate. For this reason a more detailed study was undertaken of the effect of varying temperature, flow rate and methane concentration on its maximum concentration.

8.6.1 The effect of surface and temperature on formaldehyde

The radial profile shown in Figure 8.4, together with the data of Tables 5.19, 5.27, 5.29, 5.31, 5.32, 5.35 and 5.36 indicate that the surface does not play any more significant role in the production or oxidation of formaldehyde than it does in the case of methane, carbon monoxide or carbon dioxide under the conditions of the present experiments.

This is supported by the fact that the flow rate appears to have no significant effect on the maximum formaldehyde concentration.

The results are such as not to adequately distinguish between the effects of temperature and flow variation beyond saying that neither has a marked effect on the value of the maximum formaldehyde concentration. This was concluded from inspection of Tables 5.27 to 5.37,

where rather less than two-fold variation in flow rate and ~40°K change in T_i occurred.

8.6.2 The effect of methane concentration on the formaldehyde maximum

Because of the small effect of the temperature and flow rate on the value of the maximum formaldehyde concentration, it was possible to group all the data from Tables 5.27 to 5.37 to investigate the effect of five-fold variation in the initial methane concentration on the formaldehyde maximum.

Figure 8.5 shows the relation between the formaldehyde maximum and the initial methane concentration. Run A (Table 5.33) is evidently anomalous and has been discarded. The best straight line through the remainder (it could be argued that a parabolic curve would give a better fit) results in a relation of the form

$$(HCHO)_{max} = 0.04(CH_4)_i + \text{constant}$$

for the extremely lean mixtures considered.

Apart from the obvious cause of variation due to considering data from runs which were not strictly comparable (i.e., different temperature and flow conditions), this analysis reveals to the full the limitations in the experimentation and data handling. Although the data for individual runs are consistent to a high accuracy (see Figure 8.4 for instance - ignoring H_2O_2), the comparison of data from a series of runs,

such as Figure 8.5, which were accomplished over a period of time, reflects both the difficulty and importance of achieving exactly repeatable control conditions. Other factors, such as the lack of any correction for diffusion, undoubtedly contribute.

TABLE 8.1

$[OH]$ computed from Equation 8.2
$[OH]_{eq}$ computed from Equation 8.3
} for Run 10 (Table 5.4)

z	$m_{CO_3} \times 10^3$	T_e	$k_1 \times 10^{-12}$	$[OH]$ mole $cm^{-3} \times 10^9$	$[OH]_{eq}$ mole cm^{-3} 10^{11}	$[OH]/[OH]_{eq}$
20	1.36	1244	0.279	1.64	1.10	150
19	2.32	1237	0.274	1.48	1.05	140
18	3.34	1225	0.265	1.02	0.97	105
17	4.14	1213	0.246	0.61	0.87	70
16	4.20	1202	0.249	0.44	0.78	56
15	3.42	1191	0.241	0.30	0.66	45
14	2.52	1181	0.235	0.24	0.54	44

TABLE 8.2

Rate constant k_4 for $CH_4 + OH \rightarrow$ products

Run	z	$m_{CH_4} \times 10^3$	$m_{CO} \times 10^3$	T_e	$k_4 \times 10^{-12}$
10	19	0.05	2.32	1237	0.51
10	17.5	0.30	3.80	1220	0.86
10	15	1.27	3.44	1191	1.05
10	14	1.80	2.52	1183	0.82
12	15	0.50	3.24	1212	1.05
13	17	0.12	2.36	1200	0.41
13	12	0.85	2.46	1175	1.41
13	9	1.62	1.20	1160	2.71
18	19	2.73	3.36	1184	0.44
20	15	1.38	3.54	1180	0.87
21	23	0.66	4.72	1210	1.26

Mean $k_4 = 1.0 \times 10^{12}$ cm^3 $mole^{-1}$ s^{-1} at ~1200°K

TABLE 8.3

Comparison of rate constants

$CH_3 + OH \rightarrow$ products

Author	Ref.	Method	Temperature of measurement ^oK	$10^{-12} \times k_4$ (1200^oK) $cm^3\ mole^{-1}\ s^{-1}$ (approximate)
This work		Flow technique	~1200	1.0
Avramenko and Lorentso	Quoted in 58	Flow technique	~ 700	1.7
Fristrom and Westenberg	8	Flame	1650 to 1840	6.1 *
Fenimore and Jones	12	Flame	1220 to 1800	7.8

*Using a value of ~9 kcal for E_4

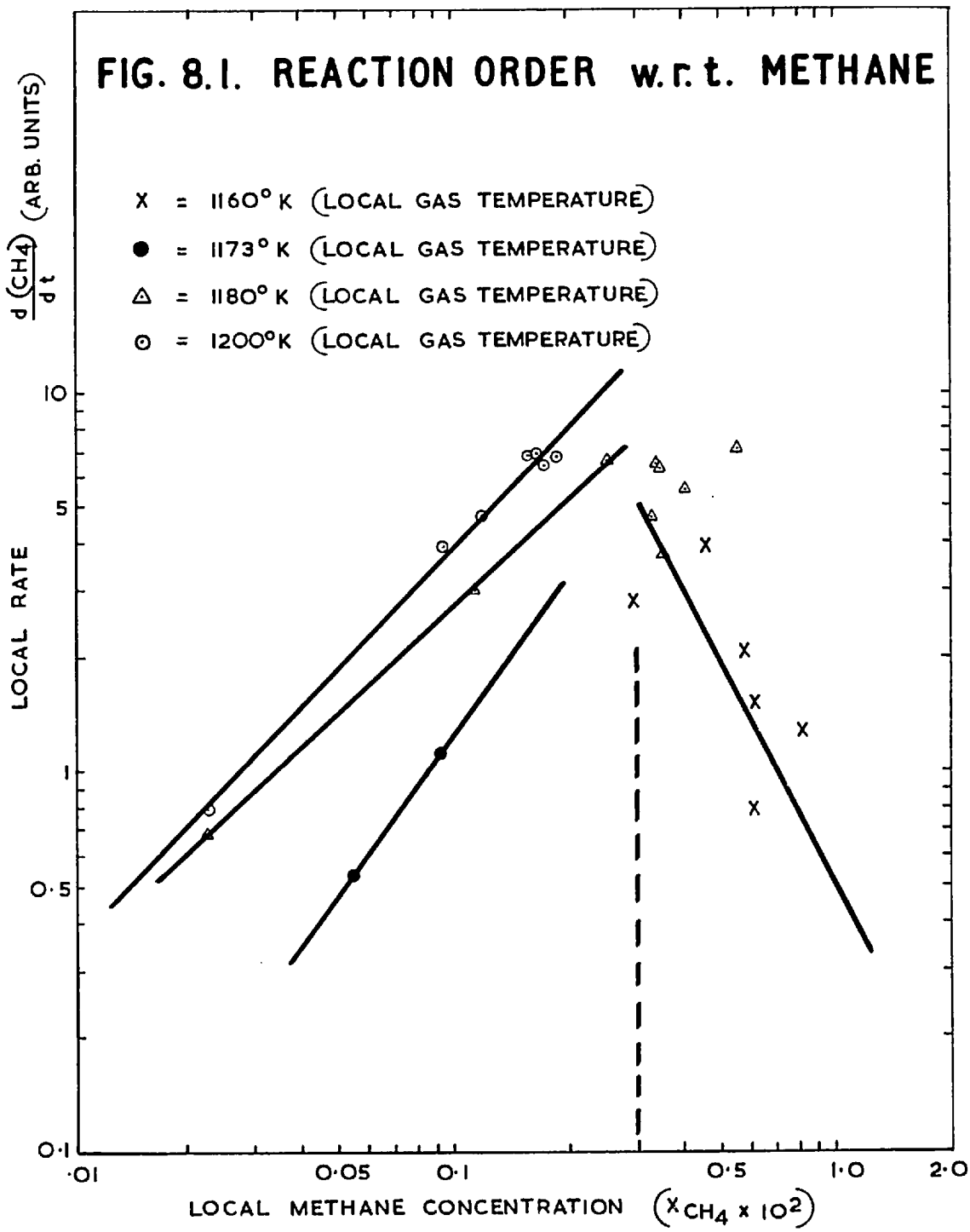
FIG. 8.1. REACTION ORDER w.r.t. METHANE
X = 1160° K (LOCAL GAS TEMPERATURE)
● = 1173° K (LOCAL GAS TEMPERATURE)
△ = 1180° K (LOCAL GAS TEMPERATURE)
⊙ = 1200° K (LOCAL GAS TEMPERATURE)
d(CH4)/dt (ARB. UNITS)
LOCAL RATE
10
5
1
0·5
0·1
·01
0·05
0·1
0·5
1·0
2·0
LOCAL METHANE CONCENTRATION (XCH4 x 10²)

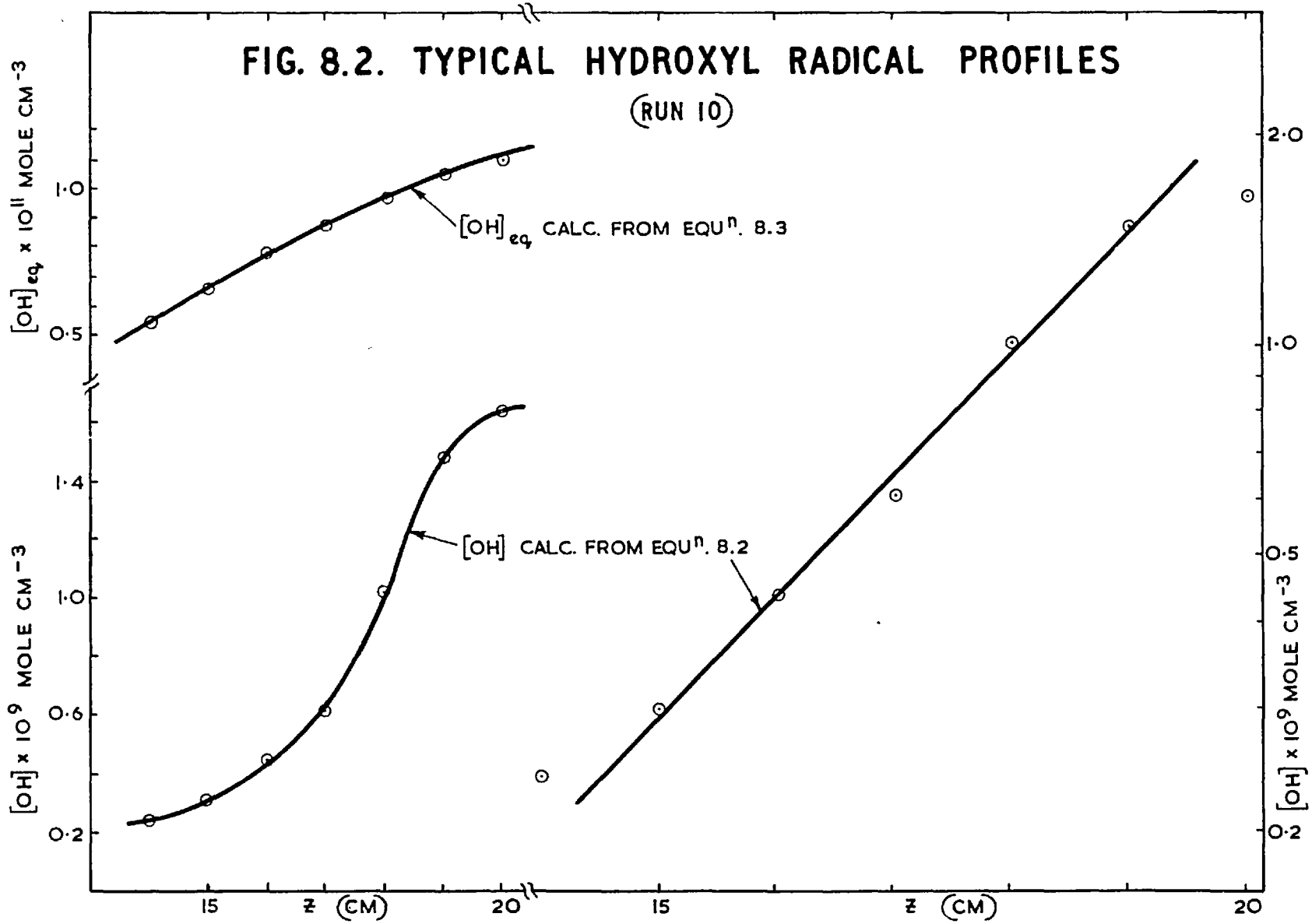
FIG. 8.2. TYPICAL HYDROXYL RADICAL PROFILES
(RUN 10)
[OH]eq x 10^11 MOLE CM^-3
[OH]eq CALC. FROM EQUn. 8.3
[OH] x 10^9 MOLE CM^-3
[OH] CALC. FROM EQUn. 8.2
z (CM)
z (CM)

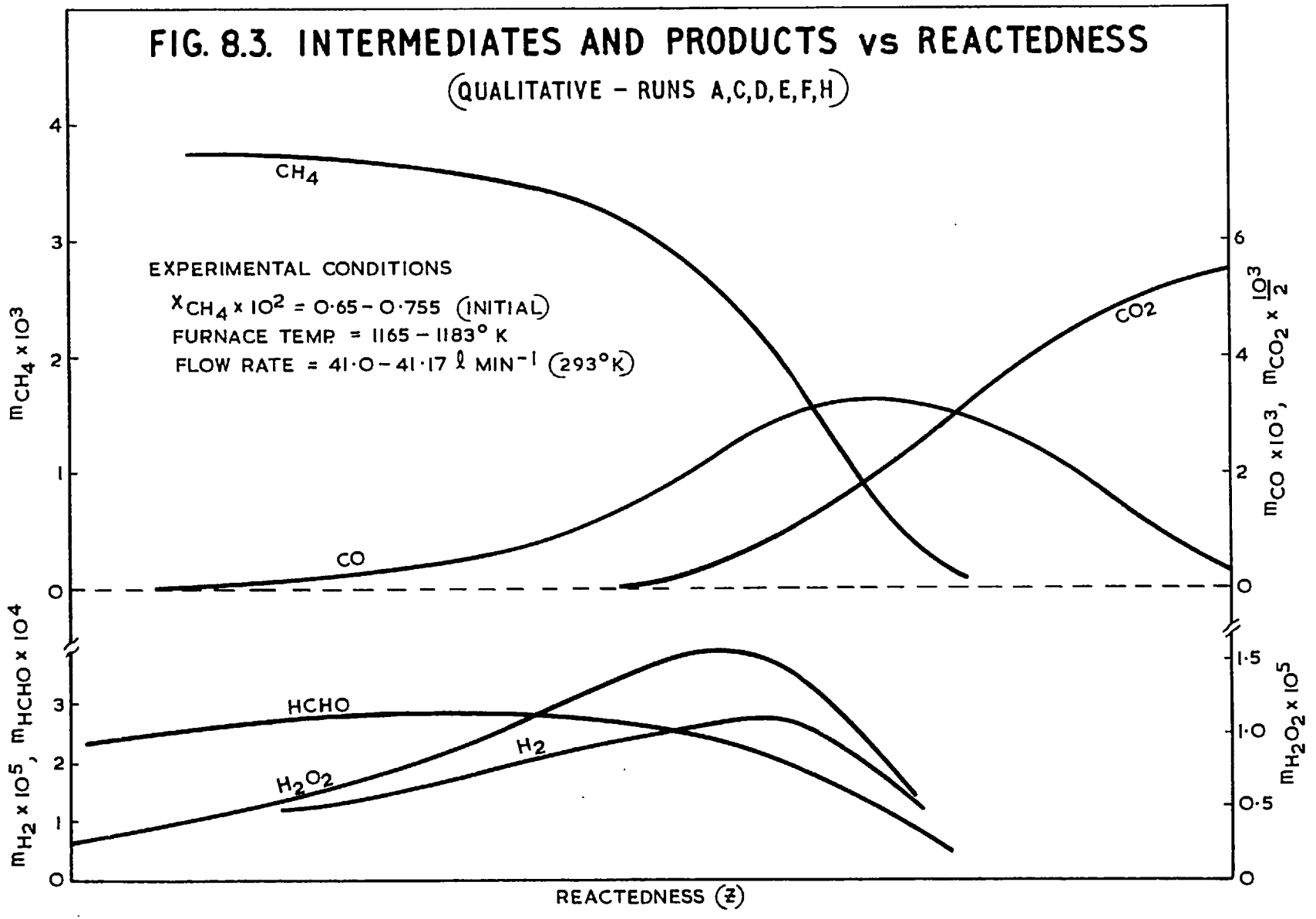
FIG. 8.3. INTERMEDIATES AND PRODUCTS vs REACTEDNESS
(QUALITATIVE - RUNS A,C,D,E,F,H)
EXPERIMENTAL CONDITIONS
$X_{CH_4} \times 10^2 = 0.65 - 0.755$ (INITIAL)
FURNACE TEMP. = 1165 - 1183° K
FLOW RATE = 41.0 - 41.17 ℓ MIN^{-1} (293°K)
CH_4
CO
CO_2
HCHO
H_2
H_2O_2
$m_{CH_4} \times 10^3$
$m_{CO} \times 10^3$, $m_{CO_2} \times \frac{10^3}{2}$
$m_{H_2} \times 10^5$, $m_{HCHO} \times 10^4$
$m_{H_2O_2} \times 10^5$
REACTEDNESS (z)

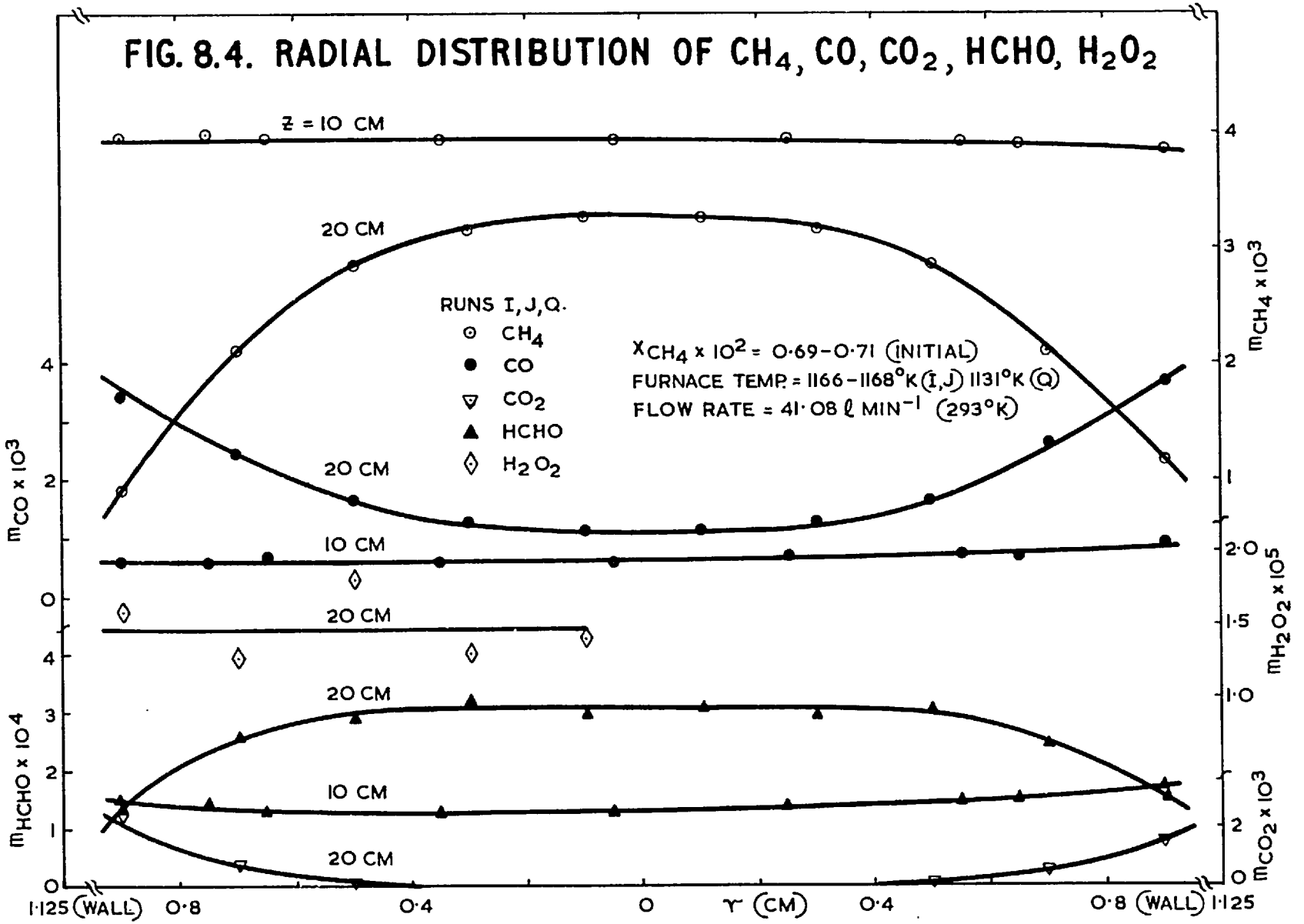
FIG. 8.4. RADIAL DISTRIBUTION OF CH_4, CO, CO_2, HCHO, H_2O_2
z = 10 CM
20 CM
20 CM
10 CM
20 CM
20 CM
10 CM
20 CM
RUNS I, J, Q.
CH_4
CO
CO_2
HCHO
H_2O_2
$X_{CH_4} \times 10^2$ = 0·69–0·71 (INITIAL)
FURNACE TEMP. = 1166–1168°K (I, J) 1131°K (Q)
FLOW RATE = 41·08 ℓ MIN^{-1} (293°K)
$m_{CO} \times 10^3$
$m_{CH_4} \times 10^3$
$m_{HCHO} \times 10^4$
$m_{H_2O_2} \times 10^5$
$m_{CO_2} \times 10^3$
1·125 (WALL)
0·8
0·4
0
r (CM)
0·4
0·8 (WALL)
1·125

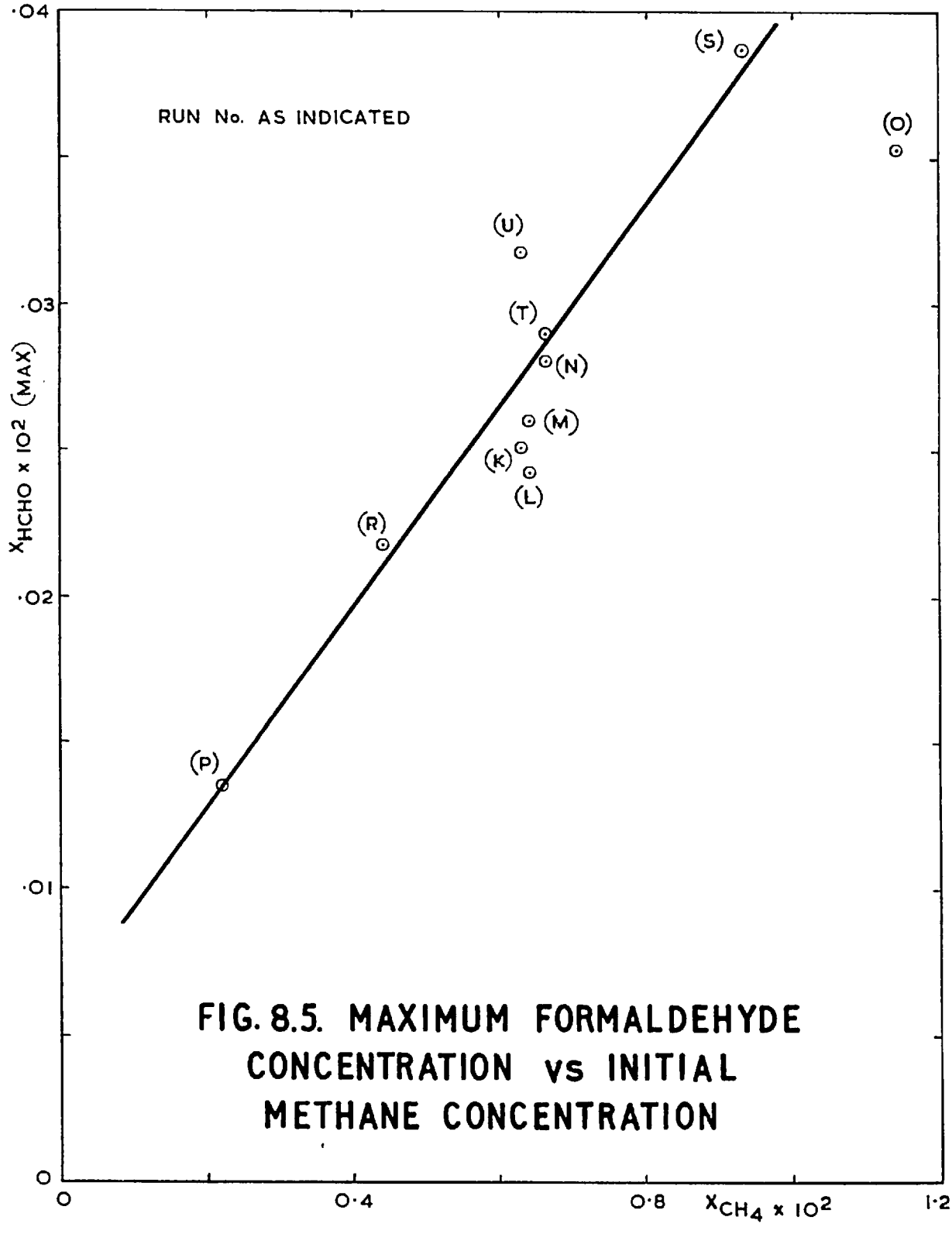

FIG. 8.5. MAXIMUM FORMALDEHYDE CONCENTRATION vs INITIAL METHANE CONCENTRATION

CHAPTER 9

Discussion and conclusions

9.1 Main features and comparisons

The methane oxidation reaction zone in the flow reactor may conveniently be discussed in terms of three regions. Such a three-fold classification is of general utility in hydrocarbon oxidation systems. Immediately downstream of the mixing point the induction period occurs. In the present work, where reactants were separately preheated, this region is complicated by the mixing process. In the comparable work of Kozlov[30] no such mixing was necessary. The induction period is followed by the main reaction region, where, in the case of methane oxidation, the bulk of the conversion of methane to carbon monoxide occurs. Finally the carbon monoxide is oxidised in the carbon monoxide oxidation region.

An analogous spatial separation has been proposed by Fristrom and Westenberg[4] for the methane/oxygen flame. They describe the three regions as (i) transport region, (ii) primary reaction region and (iii) secondary reaction region. The only, and significant, difference is in the first region.

A similar classification may be applied to the slow vessel reaction at lower temperatures (where the separation is defined temporally rather than spatially). In this case however the third phase in the reaction may not occur, depending on the experimental conditions. Thus the induction period is followed by the main reaction which may or

may not be followed by further oxidation of the carbon monoxide formed. Shock tube work may be grouped with either the flow reactor or the vessel studies for this purpose, depending on the temperature-time history of the shocked gases.

If it is accepted that the second and third regions are mechanistically similar in the various systems (some evidence for the truth of this will be presented) then the differences in mechanism in the first region must be largely responsible for the observed differences in behaviour between the systems. The three regions are further discussed in the following sections with comparison between the present work and that of other workers both in the flow reactor and in other systems.

Some of the more general features of the present work will now be briefly considered.

Transition processes

The present results indicate that there are two transition processes involved in any change from 'fast' reaction to 'flame' reaction. The two are not normally separable, although it is suggested that a two-stage flashback - see Chapter 4 - involves such a separation. The two transition processes are (i) fast reaction to pre-mixed flame, (ii) fast reaction to diffusion flame. (The term 'ignition' has been avoided deliberately.) Process (ii) may or may not involve (i). Process (i) appears to occur as the result of the build-up of a sufficiently steep local gradient of radicals to permit the back diffusion of radicals to

supersede the degenerate branching processes in the induction period. Consequently the nature of the combustion changes. The occurrence of such local gradients will be assisted by mixing, temperature, and velocity non-uniformities in the gas flow. Where such non-uniformities become excessive a situation may be envisaged analogous to the 'stirred reactor' of Longwell and Weiss[126]. Once a sufficiently steep gradient is achieved, the local flame front will propagate upstream to stabilise at some position dictated by both local and overall conditions. Transitions of type (ii) may be similarly initiated and become stabilised along the 'stoichiometric profile' around each methane inlet jet, to give a series of diffusion flames. Evidently a considerable extension of the present research will be required to make the above description quantitative.

Heat release rates

It is of interest to note that Fristrom and Westenberg[4] in their study of the fuel-lean methane/oxygen flame obtained poor correlation between the heat release rates derived from the measured temperature profiles and those derived from the specie profiles. The difference was a factor of two at the point of maximum heat release rate. In the present work what are effectively integrated forms of their analyses are available as the 'corrected' temperature profiles of Figure 6.5. There may be no significance in the fact that both analyses (this and Fristroms') show lack of correlation in the same sense - that is specie-derived rates exceeding temperature-derived rates. This is because of the uncertainty

concerning the aerodynamics in the present work; a better understanding of this might have resulted in a superposition of the two corrected profiles of Figure 6.5. By similar reasoning, of course, the poor correlation in Fristrom's work may be due to an inadequate allowance for aerodynamic effects.

The heat release rate profiles which have been obtained (Figure 7.6) are similar in outline, under the richer conditions, to those obtained from flame structure studies, in particular those of Fristrom and Westenberg[4] for the methane/oxygen system, Levy and Weinberg[1] for the ethylene/air system and Friedman and Burke[127] for the propane/air system. Quantitatively the first two give rates on order of magnitude greater than those obtained in this work. However Friedman and Burke working at 0.06 atm obtained maximum heat release rates (~ 1.2 cals cm^{-3} s^{-1}) closely similar to this work. It is therefore interesting to compare their reaction zone thickness, ca 2 cms, with the ca 10 cms of the present work.

Another interesting feature of this work is the ability which has been demonstrated to perform a smooth transition from the adiabatic situation characteristic of 'free' flames to the nearly isothermal conditions of the 'ideal' homogeneous reaction zone.

A bye-product of the heat release analysis is the suggestion that Ray's[35] supposed surface effects on the methane oxidation reaction are attributable to the presence of temperature gradients in the reaction zone. If the furnace temperature conditions of this work are compared

with those of Ray[35] and Hirsch[22] it will be noted that for similar reaction rates the furnace temperature conditions fall as the reaction tube diameter increases. This suggestion cannot be considered conclusive however, because both Hirsch amd Ray used mullite reaction tubes, whereas silica has been used for all the quantitative work reported here.

Luminescence

The brief description of a pale blue 'glow' given in Chapter 4 should be related to Vanpée and Wolfhard's[128] description of the anomalous behaviour of methane when subjected to a jet of hot nitrogen. It was found that outside the flammability limits methane/air mixtures exhibited a luminous glow when in contact with the jet, at temperatures below the 'ignition' temperature. The minimum temperature occurred for 1.5 per cent methane in air. Gaydon and Moore[129] have observed a similar phenomenon in engine work with methane addition to carbon monoxide, and attributed the radiation to the cool flame of formaldehyde. Because of these anomalies it is possible that Mullins[27] work on ignition lags in methane/vitiated air mixtures, where the 'lag' was timed to the point of visible radiation, will have a different significance depending on which side of the flammability limit the observations were made.

9.2 The induction period

Ideas concerning the processes occurring in the induction period of methane oxidation are among the least satisfactory aspects of current theories of the oxidation mechanism. Both low temperature vessel studies and higher temperature shock tube work are particularly concerned with

this aspect of the oxidation. Semenov et al[58,121,122] have put forward a theory applicable at the lower temperatures, but Kistiakowsky and Willard Richards[130] have recently shown that this cannot account for the high temperature (~2000°K) induction period. Skinner and Ruehrwein[17] working at intermediate temperatures using a shock tube note the production of C_2 hydrocarbons in the induction period. Vanpée[39] also postulates C_2 hydrocarbons to explain his vessel studies at relatively high temperatures. Hirsch[22] has indicated that the mechanism of the oxidation changes in the region of 840°K and Kozlov's[30] results suggest this change is complete at ~1200°K. The present work has little to contribute beyond indicating that there is an inhibiting mechanism at ~1200°K, which was previously well known, and that it appears to be second-order with respect to methane. The latter fact supports suggestions that C_2 hydrocarbons are formed in the induction period. No attempt was made to isolate these products in this work, but their concentrations could not have been large or they would have resulted in observable discrepancies in the carbon-atom balance. The methane infra-red gas analyser responds to C_2 hydrocarbons - approximately 50 per cent deflection for ethane compared with methane - therefore care is necessary in drawing firm conclusions from the carbon-atom balance in the present context.

The present work, besides confirming the self-inhibiting effect of methane on its own oxidation under the experimental conditions used, suggested that at very lean conditions (methane < 0.3 per cent) this

effect disappeared. This should be compared with the reported[50] accelerating effect of small additions of methane on the carbon monoxide flame, whereas the effect at higher concentrations is to produce both self-inhibition and inhibition of the carbon monoxide oxidation.

The second-order inhibiting mechanism would reasonably account for the length of the induction period, or ignition delay, in the case of methane (which is anomalous in this respect). If the calculations resulting in a profile of the hydroxyl radical are valid, then an extrapolation of this profile back into the induction period would suggest that the effect of the self-inhibition is to deplete the system of hydroxyl radicals.

No attempt has been made to analyse the induction period quantitatively because of the additional complication of the superposed mixing process and the need for a thorough understanding of the aerodynamics.

It is of interest that virtually no C_2 hydrocarbons have been found in the methane/oxygen flame, and this must be attributed to the swamping of the induction period by the transport region in the 'free' flame.

9.3 The main propagating sequence

In deriving some of the kinetic parameters in the previous chapter it was assumed that data obtained under flame conditions were directly comparable to the present situation. Two indirect assessments of this assumption are possible. The second will be considered in the next section.

Following Semenov et al[122] we may write down the elementary steps in the formation and destruction of formaldehyde as

$$CH_4 + OH \rightarrow .... \rightarrow HCHO \qquad .... 9.1$$

$$CH_4 + HO_2 \rightarrow .... \rightarrow HCHO \qquad .... 9.2$$

$$HCHO + OH \rightarrow .... \rightarrow CO \qquad .... 9.1'$$

$$HCHO + HO_2 \rightarrow .... \rightarrow CO \qquad .... 9.2'$$

Assuming that the elemontary rate constants k_1, k_1', k_2, k_2' represent the rate limiting steps, and that other mechanisms for the formation and destruction of formaldehyde are negligible by comparison, we may write down an expression for the rate of accummulation of formaldehyde as

$$K_{HCHO} = \left\{ 1 - \frac{\left([HCHO]\ [OH]\ k_1' \right)\left([HCHO]\ [HO_2]\ k_2' \right)}{\left([CH_4]\ [OH]\ k_1 \right)\left([CH_4]\ [HO_2]\ k_2 \right)} \right\} R \qquad .... 9.3$$

where R involves rate processes of minor importance for the present purpose. When the maximum formaldehyde concentration is reached, $K_{HCHO} = 0$, and the expression in curly brackets in Equation 9.3 may also be equated to zero. Then the maximum formaldehyde concentration is given by

$$[HCHO]_{max} = \left(\frac{k_1 k_2}{k_1' k_2'} \right)^{\frac{1}{2}} [CH_4] \qquad .... 9.4$$

By assuming that the pre-exponential factors of the rate constants in Equation 9.4 cancelled, Semenov et al showed that the maximum formaldehyde concentration had a temperature dependence of the form

$$\frac{[HCHO]_{max}}{[CH_4]} = \exp(-8500/RT) \quad \ldots\ldots 9.5$$

Table 9.1 compares the prediction of this theory with the experimental value of the maximum formaldehyde concentration obtained in the present work. A similar estimate has been made for the maximum formaldehyde concentration obtained in the methane/oxygen flame of Fristrom et al[4,123]. The fact that the experimental value of the formaldehyde maximum exceeds the theoretical prediction in each case may be significant. Leaving this point aside, the fact that the theoretical expression predicts the maximum with comparable accuracy in each case suggests that the mechanisms of formation and destruction of formaldehyde are the same under all three conditions of temperature, pressure and system. Poor correlation is to be expected if the mechanism changes because Equation 9.5 is effectively a measure of the activation energy difference between the formation and destruction of formaldehyde. Unfortunately this test is rather insensitive to the relative importance of the hydroxyl and hydroperoxy radicals in the mechanism.

In principle it should prove possible to perform a similar steady-state analysis on the maximum hydrogen peroxide concentration. Such an analysis is complicated, however, by the lack of quantitative experimental data and the increase in the number of possible reaction paths which must be considered. The latter feature is due mainly to the fact that hydrogen

peroxide can be formed at one or two stages removed from the primary reactants.

Thus we may gather together the likely mechanisms for the formation of hydrogen peroxide.

$$CH_4 + HO_2 \rightarrow CH_3 + H_2O_2 \quad \ldots\ldots 9.2$$

$$HCHO + HO_2 \rightarrow HCO + H_2O_2 \quad \ldots\ldots 9.2'$$

$$M + 2\,OH \rightleftarrows H_2O_2 + M \quad \ldots\ldots 9.6$$

$$2\,HO_2 \rightarrow H_2O_2 + O_2 \quad \ldots\ldots 9.7$$

$$HO_2 + H_2 \rightarrow H_2O_2 + H \quad \ldots\ldots 9.8$$

At $\sim 750^{\circ}K$ Semenov[58] suggests 9.2' is $\sim 10^3$ faster than 9.2. At higher temperatures, comparable to those used in the present work, but at pressures of ~ 10 mm Hg, Fabian and Bryce[59] have reported that approximately 50 per cent of the hydroperoxy radical formed in the methane oxidation reaction was converted to hydrogen peroxide. Reaction 9.6 may well require a third body and will consequently be ignored. 9.7 has been suggested by Baldwin and co-workers[132,133] as the chief source of hydrogen peroxide in the hydrogen/oxygen reaction, being more important than 9.8 at lower temperatures than of concern here. At much higher temperatures Bauer, Schott and Duff[134] have postulated hydrogen peroxide in the mechanism for the decomposition of water vapour.

Perhaps the most likely mechanism for the destruction of hydrogen peroxide is reaction 9.6., as is suggested by Baldwin and co-workers[133] at lower temperatures. Destruction to give water directly must also be considered.

The experimental data given in Chapter 8 held the suggestion, and no more, that the peroxide peak occurred slightly later in the reaction zone than the formaldehyde peak. A similar suggestion is apparent in Enikolopyan's[121] results, although inspection suggests that his data are not so consistent as the comparable work of Salooja[56,80], where no such distinction is apparent. Nevertheless the point requires watching and may provide a significant clue to the mechanism by which the hydrogen peroxide exists in the methane oxidation.

Very little experimental evidence for hydrogen peroxide is available from flame studies of this reaction. The suggestion is usually made[13,92] that it will not survive the sampling process. However Laffitte[135] has shown its existence in the methane/air flame.

9.4 The carbon monoxide oxidation phase

A comparison of the 'overall' reaction rate of carbon monoxide found in this work with that found in flame studies will now be made.

Westenberg and Fristrom[42] have deduced an overall rate expression for the carbon monoxide oxidation

$$K_{CO_2} = 3 \times 10^{13} \exp\left(-45{,}000/RT\right)\left[CO\right]\left[H_2O\right]^{\frac{1}{2}}\left[O_2\right]^{\frac{1}{4}} \quad \ldots\ldots 9.9$$

A very similar expression has been found empirically by Kozlov[30], which he claims correlates much of the Russian work. A comparison using Kozlov's expression might equally well have been made, but this would be of less significance, since one of the factors requiring examination

is the validity of using rate parameters derived from flame data in the present work.

Table 9.2. illustrates the comparison. Although the water concentration was not measured experimentally, an estimate based on the methane consumption should be adequate for the comparison. The comparison shows that the present results fall within the spectrum of values obtained in flame structure studies. The two-fold discrepancy between experimental and the calculated rates is also reasonable by comparison with the other data.

The present results are also in good agreement with the rates obtained by Hirsch[22] and by Ray[35]. No quantitative comparison is presented because it would add nothing to the discussion.

The fact that flow reactor studies are comparable with flame studies in this, albeit overall, way supports the use of kinetic data obtained in flame studies in more practical situations, particularly at higher temperatures, where conventional rate measurements become increasingly difficult.

Having established that the carbon monoxide disappearance rate has at least a reasonable value, it is necessary to account for the hydroxyl radical concentrations derived from the assumed rate constant of the elementary process (see Section 8.3)

$$CO + OH \rightarrow CO_2 + H$$

and the experimentally measured K_{CO_2} and $[CO]$. The results of these calculations showed a hydroxyl radical concentration reaching a maximum many times the local equilibrium value fairly late in the reaction (see Figure 8.2). In this respect the present results differ from flame results in that in flames the hydroxyl radical concentration peaks close to the region of maximum reaction rate[41,42,136]. What is considered a reasonable explanation of this difference will now be given.

Kaskan[41] has shown that at the lower temperatures in his work on the carbon monoxide flame, the radical concentrations tended to exceed the equilibrium values by a larger factor than at the higher temperatures. This he attributed not so much to any change in the actual hydroxyl concentration, but to the decrease in the equilibrium value as the temperature is lowered. Evidently in the present work where the temperature is low and the concentrations of radical-forming species are very low the equilibrium value for the hydroxyl concentration will be extremely suppressed. These facts suggest that a fairly large ratio of $[OH]/[OH]_{eq.}$ is to be expected.

We can now consider the mechanism of the processes tending to produce and destroy hydroxyl radicals. Taking destruction first, we may reasonably ignore surface reactions to a first approximation in the present context and consider only homogeneous processes.

Both Kaskan[41,137] and Sugden and co-workers[138] have shown that the total value of the function, F, which has zero time dependence, of the

concentrations of the species in excess of equilibrium cannot decrease except by recombination reactions.

$$F = [OH] + 2[CO] + 2[O] + 2[H_2] + 3[H] \quad \ldots\ldots 9.10$$

F has the form of 9.10 for a C, H, O system. (We may ignore nitrogen in this context.) The necessary recombination processes will be comparatively slow due to their requirement of a third body and to the extremely low concentrations of the atoms and radicals under the conditions of the present work.

For the necessary adjustment in the relative concentrations in Equation 9.10 to occur it must be assumed that as

$$CO + OH \rightarrow CO_2 + H \quad \ldots\ldots 9.11$$

the reactions

$$OH + H_2 \rightleftarrows H_2O + H \quad \ldots\ldots 9.12$$

$$O + H_2 \rightleftarrows OH + H \quad \ldots\ldots 9.13$$

$$H + O_2 \rightleftarrows OH + O \quad \ldots\ldots 9.14$$

remain in equilibrium.

There is nothing to prevent the total of radicals in F from increasing, however, and it is suggested that this is most probably happening via

$$CO + OH \rightarrow CO_2 + H$$

$$H + H_2O \rightarrow H_2 + OH$$

$$H + O_2 \rightarrow OH + O$$

$$H_2 + O \rightarrow OH + H$$

i.e., a net increase in the radicals on the right. Provided 9.12 to 9.14 are fast compared with 9.11 (but particularly 9.12) the carbon monoxide

will be oxidised, and since the recombination reaction rates are likely to be relatively slow, an increase in radicals is quite possible.

Inspection of the relevant rate constants available in the literature[11,42,14,139-141] indicates (a) that 9.11 will be slow compared to 9.12 provided $[H]/[OH]$ is an equilibrium ratio, and (b) the recombination processes

$$2OH + M \rightarrow H_2O + O + M$$

$$OH + H + M \rightarrow H_2O + M$$

$$H + H + M \rightarrow H_2 + M$$

will be relatively slow.

It thus appears not unlikely that an increase in radical concentration will be occurring even relatively late in the reaction zone, and that this is a reflection of a difference in the experimental conditions between the present flow reactor work and flames, and not due to a fundamental difference in mechanism.

9.5 Suggestions for further work

As a result of the experience gained during the course of this work a number of points may be made concerning the experimental approach which has been used. These will serve as a background to the specific proposals for further study.

A high temperature flow reactor has certain advantages over some other systems. In particular, since it will allow reaction rates in very weak mixtures to be studied, it is a particularly valuable tool in the study of extremely exothermic reactions. In addition the use of very

lean mixtures results in an extension of the reaction zone, which may be particularly useful in some situations. For instance, as has been demonstrated by the present work, it allows flame-type processes to be studied at atmospheric pressure with a spatial resolution which would otherwise only be achieved at low pressure.

There are two features of the experimental work which have been pushed close to the limit of their successful operation. These are the sampling and the analysis techniques. The former because of the high reaction rates which it is necessary to quench efficiently, the latter because of the low concentration of the various species of interest. Future work which overcomes or avoids these difficulties is therefore to be preferred.

Confining the discussion to proposals with immediate relevance to the present work, four aspects may be singled out as requiring further study.

(i) Aerodynamics

It is particularly important that a thorough understanding of the aerodynamics in the reaction zone be obtained, or that a much simpler system be devised. In this connection it is worth drawing attention to the qualitatively similar flow patterns obtained in turbulent flames with cylindrical symmetry[145], where factors affecting the flame stability have been investigated.

With an experimental arrangement similar to that described in this work, the use of a tracer gas (say from a single inlet on the axis) is

suggested as a first step in investigating the laws of spreading and decay. If helium is used, care must be exercised in the interpretation of the results because of its high diffusion coefficient.

(ii) Induction period processes

Once the aerodynamics are understood, it should prove possible to examine the induction period in more detail, particularly looking for C_2 hydrocarbons. Because of their likely low concentration, a sampler of the water-cooled type may well be necessary.

(iii) Radicals

Some attempt should be made to measure radical concentrations directly. The species of prime importance in this respect is probably the hydroxyl radical, and for this spectroscopic techniques are available and proven (see, for instance, Reference 131 for the results of a successful application). The relatively small radial concentration gradients which may be obtained by suitable adjustment of the conditions in the flow reactor should prove of value, as will the ability to vary the site of the reaction zone with respect to the z co-ordinate.

With such a technique, not only will it be possible to check the predictions of the present work concerning the exponential branching late in the reaction history, (Figure 8.2) but it should also prove possible to study the effect of various additives (such as formaldehyde) on the hydroxyl, or any other spectroscopically visible, radical concentration.

(iv) Transition processes

The factors influencing the transition from 'fast' reaction to 'flame' should reward further study. Qualitatively it is fairly obvious how this occurs. Quantitatively the detailed knowledge of local conditions, and how the various factors influence each other, is not available. This will probably require a non-steady state analysis. Quite apart from any non-steady state analysis, the steady state analysis used in this thesis is extremely simplified and requires development, perhaps along lines indicated in the recent literature[142-144]. It may then become clear if and what form of non-steady analysis is best suited to a study of the transition processes.

9.6 Summary and conclusions

This thesis has presented the results of a study of the factors influencing reactions in a high temperature flow reactor.

Fuel-lean methane/air mixtures have been used and the heat release rates obtained by two methods, from temperature measurements and from specie concentrations, have been compared. As a result it was concluded that a considerable inlet induced turbulence was present in the gas stream. Comparison of the heat release rate profiles with those obtained from other work showed them to be qualitatively similar to those obtained from flame structure studies. A kinetic analysis of the results has suggested that most of the experimental features can be reasonably accounted for on the basis of available theory. More important however, has been the demonstration that the situation in a flow reactor falls intermediately between

conditions in a flame and in a vessel. It is suggested that the greatest difference occurs in the nature of the induction period.

It has been shown that

(i) A rate constant deduced for the reaction CH_4 + OH is in fair agreement with those obtained in flames.

(ii) The main propagating sequence does not appear to change mechanistically over the temperature, pressure and composition ranges covered by the present work, vessel studies and flames.

(iii) The overall oxidation rate of carbon monoxide is similar to some values deduced in flames.

(iv) The build-up of hydroxyl radical concentration which has been calculated is reasonably to be expected and explained by current ideas of recombination processes in flame after-burning regions.

TABLE 9.1

Comparison of maximum formaldehyde concentration with theory

Author(s)	Ref.	Experimental system and conditions	$[CH_2O]_{max}/[CH_4]$		
			Expt.	Theory (Eq. 9.5)	Approx. Ratio Exp/Theor.
Semenov et al	58, 121, 122	Vessel, CH_4/O_2 235 mm Hg 760°K	4.4×10^{-3}	3.8×10^{-3}	1.2
This work		Flow reactor, CH_4/air 760 mm Hg, ~ 1200°K	$\sim 4.0 \times 10^{-2}$	2.9×10^{-2}	1.4
Calc. from data of Fristrom et al	4, 123	Flame CH_4/O_2 38-76 mm Hg, ~ 1400°K	$\sim 6.1 \times 10^{-2}$	4.8×10^{-2}	1.3

TABLE 9.2*

Comparison of 'overall' rates of carbon monoxide oxidation

Author	Ref.	Experimental conditions	$K_{CO_2}/[CO]$ Eq. 9.9 sec^{-1}	$K_{CO_2}/[CO]$ exptl. sec^{-1}
This work		Flow reactor, CH_4/air 1 atm 1228°K (Run 12, z = 17)	156	340
Westenberg and Fristrom	42	Flame, CH_4/O_2 0.1 atm 1950°K	2900	3000
Westenberg and Fristrom	42	Flame, CH_4/O_2 0.05 atm 1950°K	1400	1500
Friedman and Cyphers	3	Flame, C_3H_8/air 0.06 atm 1600°K	73	231
Friedman and Nugent	124	Flame, CO/O_2 0.04 atm 1780°K	210	185
Fenimore and Jones	125	Flame C_2H_2/air 1 atm 1885°K	2900	700

* With the exception of the data referred to this work, this Table has been copied, with some omission, from Reference 42.

Bibliography

1. A. Levy and F. J. Weinberg, Combustion and Flame, 3, 229 (1959)

2. G. H. Markstein, "Seventh Symposium on Combustion", Butterworths, London, 1959, p.289

3. R. Friedman and J. A. Cyphers, J. Chem. Phys., 23, 1875 (1955)

4. R. M. Fristrom and A. A. Westenberg, "Eighth Symposium on Combustion", Williams and Wilkins, Baltimore, 1962, p.438

5. R. M. Fristrom, C. Grunfelder and S. Favin, J. Phys. Chem., 64, 1386 (1960)

6. R. Prescott, S. Foner, R. Hudson and W. H. Avery, J. Chem. Phys., 22, 145 (1954)

7. S. R. Smith and A. S. Gordon, ibid., 22, 1150 (1954)

8. A. A. Westenberg and R. M. Fristrom, J. Phys. Chem., 64, 1393 (1960)

9. C. P. Fenimore and G. W. Jones, ibid., 62, 693 (1958)

10. - - , ibid., 62, 1578 (1958)

11. - - , ibid., 63, 1154 (1959); 63, 1834 (1959)

12. - - , ibid., 65, 1532 (1961); 65, 2200 (1961)

13. S. Foner and R. Hudson, J. Chem. Phys., 21, 1374 (1953)

14. W. E. Kaskan, Combustion and Flame, 2, 229 (1958)

15. E. M. Bulewicz, C. G. James and T. M. Sugden, Proc. Roy. Soc., A235, 89 (1956)

16. W. E. Kaskan, "Sixth Symposium on Combustion", Reinhold, New York, 1957, p.134

17. G. B. Skinner and R. A. Ruehrwein, J. Phys. Chem., 63, 1736 (1959)

18. F. J. Weinberg, Ph. D. Thesis, London, 1954

19. J. A. Powling, Fuel, 28, 25 (1949)

20. H. Roxbee-Cox, Hawksley Lecture, Inst. Mech. Eng., Nov. 16th, 1951

21. A. Meads, Ph. D. Thesis, London, 1951

22. H. Hirsch, Ph. D. Thesis, London, 1953

23. J. H. Burgoyne and H. Hirsch, Proc. Roy. Soc., A227, 73 (1954)

24. P. Lloyd, "Proc. Sixth International Congress for Applied Mech.", Paris, 1946

25. P. Lloyd, Proc. Inst. Mech. Engrs., 153, 462 (1945)

26. B. P. Mullins, Fuel, 32, 211 (1953)

27. B. P. Mullins, ibid, 32, 343 (1953)

28. H. Sachsse, Z. Phys. Chem., B33, 229 (1936)

29. Sakharov and Durynina, C. R. Acad. Sci. U.R.S.S., 60, 1539 (1948); C. A. 42, 8597

30. G. I. Kozlov, "Seventh Symposium on Combustion", Butterworths, London, 1959, p.142

31. G. K. Sobolev, ibid, p.386

32. L. N. Khitrin and L. S. Solovyeva, ibid., p.532

33. H. G. Wolfhard, Jet Propulsion, December, 1958

34. E. M. Magee, J.A.C.S., 81, 278 (1959)

35. K. K. Ray, Ph. D. Thesis, London, 1956

36. A. C. Egerton and K. K. Ray, Zeitschrift für Elektrochemie, 61, 584 (1957)

37. A. C. Egerton and K. K. Ray, Rev. Inst. Franc. Pétrole, XIII, 366 (1958)

38. A. C. Egerton, A.R.C. A.3. Report, 19277, (C.F. 399), 16th May, 1957

39. M. Vanpée, 7th. Int. Conf. of Directors of Safety in Mines Research, Paper 15, July, 1952

40. A. C. Egerton, unpublished work

41. W. E. Kaskan, Combustion and Flame, 3, 49 (1959)

42. A. A. Westenberg and R. M. Fristrom, J. Phys. Chem., 65, 591 (1961)

43. W. A. Bone and J. B. Gardner, Proc. Roy. Soc., A154, 297 (1936)

44. M. W. Evans, Chemical Rev., 51, 363 (1952)

45. D. B. Spalding, Phil. Trans., A249, 1 (1956)

46. T. von Karman and S. S. Penner, "Selected Combustion Problems", AGARD Colloquium, Butterworths, 1954, p.5.

47. J. O. Hirschfelder, C. F. Curtiss and D. E. Campbell, "Fourth Symposium on Combustion", Williams and Wilkins, Baltimore, 1953, p.153

48. M. Vanpée and F. Grard, "Fifth Symposium on Combustion", Reinhold, New York, 1955, p.484

49. D. E. Hoare and A. D. Walsh, ibid., p.467

50. P. L. Walker and C. C. Wright, Fuel, 31, 37, 45 (1952)

51. B. Lewis and G. von Elbe, "Combustion, Flames and Explosions in Gases", Academic Press, New York, 2nd Ed., 1961

52. R. G. W. Norrish, Far. Soc. Disc. No. 10, 1951, p.269

53. A. D. Walsh, Rev. Inst. Franc. Pétrole, IV, (1949)

54. M. J. Ridge, Rev. Pure and Appl. Chem. (Australia), 6, 121 (1956)

55. C. F. Tipper, Quart. Rev., 11, 313 (1957)

56. A. C. Egerton, G. J. Minkoff and K. C. Salooja, Proc. Roy. Soc., A235, 158 (1956)

57. A. C. Egerton, Bull. Soc. Chim. France, p.1733 (1959)

58. N. N. Semenov, "Some problems of chemical kinetics and reactivity", Pergamon, 1959, Vol. II

59. D. J. Fabian and W. A. Bryce, "Seventh Symposium on Combustion", Butterworths, London, 1959, p.150

60. A. C. Egerton, Melchett lecture for 1956, J. Inst. Fuel, Jan. 1957

61. E. W. R. Steacie, "Atomic and Free Radical Reactions", 2nd Ed., Reinhold, 1954

62. V. N. Kondratiev, "Kinetics of Chemical Gas Reactions", Ac. Sci. U.S.S.R., Moscow, 1958, (In Russian)

63. A. J. Everett and G. J. Minkoff, "Third Symposium on Combustion", Williams and Wilkins, Baltimore, 1949, p.390

64. C. N. Satterfield and R. C. Reid, "Fifth Symposium on Combustion", Reinhold, New York, 1955, p.511

65. C. F. Cullis and E. J. Newitt, Proc. Roy. Soc., A242, 516 (1957)

66. M. D. Scheer, "Fifth Symposium on Combustion, Reinhold, New York, 1955, p.435

67. D. W. E. Axford and R. G. W. Norrish, Proc. Roy. Soc., A192, 518 (1948)

68. K. U. Ingold and W. A. Bryce, Informal Symposium on CO oxidation, Imperial College, 27th March, 1953

69. F. H. Dorman and A. S. Buchanan, Australian J. Chem., 9, 34 (1956)

70 D. W. G. Style and D. Summers, Trans. Far. Soc., 42, 388 (1946)

71. L. I. Avramenko and R. V. Lorentso, Zhur.Fiz.Khim., 24, 207 (1950)

72. A. D. Walsh, Informal Symposium on CO oxidation, Imperial College, 27th March, 1953

73. A. S. Gordon, ibid.

74. A. G. Gaydon, N. P. W. Moore and J. R. Simonson, Proc. Roy. Soc., A230, 1 (1955)

75. K. E. Shuler, "Fifth Symposium on Combustion", Reinhold, New York, 1955, p.56

76. M. A. Mardi, Ph. D. Thesis, London, 1959

77. A. Levy, Ph. D. Thesis, London, 1958

78. A. G. Gaydon, "The Spectroscopy of flames", Chapman and Hall, London, 1957

79. E. Ower, "The measurement of air flow", 3rd Ed., Chapman and Hall, London, 1949

80. K. C. Salooja, Ph. D. Thesis, London, 1954

81. See for instance J. Crank, "Mathematics of Diffusion", Clarendon Press, Oxford, 1956

82. H. S. Carslaw and J. C. Jaeger, "Conduction of Heat in Solids", O.U.P., 1947, p.216

83. J. O. Hirschfelder, C. F. Curtiss and R. B. Bird, "Molecular Theory of Gases and Liquids", Wiley, New York, 1954

84. R. E. Walker and A. A. Westenberg, J. Chem. Phys., 32, 436 (1960)

85. J. P. Longwell and M. A. Weiss, Ind. Eng. Chem., 45, 667 (1953)

86. R. M. Fristrom, W. H. Avery and C. Grunfelder, "Seventh Symposium on Combustion", Butterworths, London, 1959, p.304

87. R. M. Fristrom and A. A. Westenberg, Combustion and Flame, 1, 217 (1957)

88. J. D. Lewis and D. Harrison, "Eighth Symposium on Combustion", Williams and Wilkins, New York, 1962 p.366

89. B. P. Mullins, N.G.T.E., unpublished report, 1950

90. P. F. Knewstubb and T. M. Sugden, "Seventh Symposium on Combustion", Butterworths, London, 1959, p.247

91. J. Deckers and A. van Tiggelen, ibid., p.254

92. R. M. Fristrom, R. Prescott and C. Grunfelder, Combustion and Flame, 1, 102 (1957)

93. A. A. Westenberg, S. D. Raezer and R. M. Fristrom, ibid., p.467

94. G. Tiné, "Gas sampling and chemical analysis in combustion processes", Pergamon, 1961

95. P. Rosen, Johns Hopkins University, APL Report No. CF-2248 (1954)

96. Yumlu, Ph. D. Thesis, London, 1958

97. A. S. Leah, Leeds University, private communication, 1958

98. F. S. Simmons and G. E. Glawe, NACA TN 3893 (1957)

99. J. C. Ascough, Unpublished work at N.G.T.E., December, 1957

100. J. C. McCoubrey, Imperial College, private communication, 1960

101. Coulson and Richardson, "Chemical Engineering", Vol. I

102. International Critical Tables

103. A. J. Everett, Ph. D. Thesis, London, 1953

104. C. E. Bricker and A. R. Johnson, Ind. Eng. Chem. (Anal. Ed.), 17, 400 (1945)

105. D. A. Pantony, Royal Inst. of Chem., Lecture Series 1961, No. 2

106. J. Hilsenrath et al., "Tables of Thermal properties of Gases", N.B.S. Circular 564, 1955

107. F. D. Rossini et al., "Selected values of the properties of hydrocarbons", American Petroleum Inst., New York, 1956

108. C. C. Lin (Ed), "Turbulent Flows and Heat Transfer", Vol. V, High Speed Aerodynamics and Jet Propulsion, Princeton, New Jersey, 1959

109. S. I. Pai, "Fluid Dynamics of Jets", Van Nostrand, 1954

110. M. Sibulkin, Phys. of Fluids, 5, 280 (1962)

111. A. A. Townsend, Proc. Roy. Soc., A190, 551 (1947)

112. H. B. Squire and J. Trouncer, A.R.C. Report and Memorandum, 1974 (1944)

113. G. B. Schubauer and C. M. Tchen, Ref. 108, p.160-

114. S. Corrsin and M. S. Uberoi, NACA Report 1040 (1951)

115. A. M. Kuethe, J. Appl. Mech., 2, (3), (1935)

116. G. B. Schubauer and C. M Tchen, Ref. 108, p.168-

117. A. A. Townsend, "Structure of Turbulent Shear Flow", C.U.P., 1956

118. O. Kubaschewski and E. Ll. Evans, "Metallurgical Thermochemistry", Butterworth-Springer, 1951

119. F. D. Rossini et al., "Selected values of chemical thermodynamic properties", N.B.S. Circular 500 (1952)

120. A. A. Westenberg and N. de Haas, Phys. of Fluids, 5, 266 (1962)

121. N. S. Enikolopyan, "Seventh Symposium on Combustion", Butterworths, London, 1959, p.157

122. L. V. Karmilova, N. S. Enikolopyan, A. B. Nalbandyan and N. N. Semenov, Russian J. Phys. Chem., 34, 562 (1960) (English trans.)

123. R. M. Fristrom, C. Grunfelder and S. Favin, J. Phys. Chem., 65, 587 (1961)

124. R. Friedman and R. G. Nugent, "Seventh Symposium on Combustion", Butterworths, London, 1959, p.311

125. C. P. Fenimore and G. W. Jones, J. Phys. Chem., 61, 651 (1957)

126. J. P. Longwell and M. A. Weiss, Ind. Eng. Chem., 47, 1634 (1955)

127. R. Freidman and E. Burke, J. Chem. Phys., 22, 824 (1954)

128. M. Vanpée and H. G. Wolfhard, Conf. of Directors of Safety in Mines Research, Pittsburgh, September, 1959, and Jet Propulsion, 28, 798 (1958)

129. A. G. Gaydon and N. P. W. Moore, Proc. Roy. Soc., A233, 184 (1955)

130. G. B. Kistiakowsky and L. Willard Richards, J. Chem. Phys., 36, 1707 (1962)

131. W. E. Kaskan, Combustion and Flame, 3, 49 (1959)

132. R. R. Baldwin, P. Doran and L. Mayor, "Eighth Symposium on Combustion", Williams and Wilkins, 1962, p.103

133. R. R. Baldwin and D. Brattan, ibid., p.110

134. S. H. Bauer, G. L. Schott and R. E. Duff, J. Chem. Phys., 28, 1089 (1958)

135. P. Laffitte, C.R. Acad. Sci. (Paris), 241, 1306 (1955)

136. U. Bonne, Th. Grewer and H. Gg. Wagner, Z. Phys. Chem., 26, 93 (1960)

137. W. E. Kaskan, Combustion and Flame, 2, 286 (1958)

138. E. M. Bulewicz, C. G. James and T. M. Sugden, Proc. Roy. Soc., A235, 89 (1956)

139. F. Kaufman and F. P. del Greco, J. Chem. Phys., 35, 1895 (1961)

140. R. E. Duff, J. Chem. Phys., 28, 1193 (1958)

141. E. M. Bulewicz and T. M. Sugden, Trans. Far. Soc., 54, 1855 (1958)

142. H. Wise and C. M. Ablow, J. Chem. Phys., 29, 634 (1958) and 35, 10 (1961)

143. F. Kaufman in "Progress in Reaction Kinetics I", Ed. G. Porter, Pergamon, 1961, p.11-

144. J. Menkes, "Eighth Symposium on Combustion", Williams and Wilkins, Baltimore, 1962, p.426

145. K. Yamazaki and H. Tsuji, "Eighth Symposium on Combustion", Williams and Wilkins, Baltimore, 1962, p.543